EFFECTS OF HYDRODYNAMICS AND SEDIMENT TRANSPORT PROCESSES ON NUTRIENT DYNAMICS IN SHALLOW LAKES AND ESTUARIES

By

Xinjian Chen

A DISSERTATION PRESENTED TO THE GRADUATE SCHOOL
OF THE UNIVERSITY OF FLORIDA IN
PARTIAL FULFILLMENT OF THE REQUIREMENTS
FOR THE DEGREE OF DOCTOR OF PHILOSOPHY

UNIVERSITY OF FLORIDA

1994

ACKNOWLEDGEMENTS

First of all, I would like to express my very deep appreciation to the chairman of my advisory committee, Professor Peter Y. Sheng, for his advice, encouragement, and financial support.

Special thanks are extended to Professors Ashish J. Mehta, D. Max Sheppard, Robert J. Thieke, and K. Ramesh Reddy for serving as the members of my doctoral advisory committee, revising the dissertation and attending the final exam. Thanks are also due to Professors Robert G. Dean, Hsiang Wang, Michel K. Ochi, and Daniel M. Hanes for their teaching efforts during my study in Gainesville. Countless pieces of help provided by Mr. Subarna Malakar and Mr. Sidney Schofield in solving my computer problems are appreciated.

I am also grateful to Professors Werner Zielke and Mark Markofsky of the Institut für Strömungsmechanik der Universität Hannover for introducing me to the field of sediment transport and water quality modeling and providing financial support during my stay in Germany.

Finally, I would like to thank my wife, parents, and parents-in-law for their love, support and patience during this study.

TABLE OF CONTENTS

ACKNOWLEDGEMENTS ii

LIST OF FIGURES vi

LIST OF TABLES xiv

ABSTRACT xvi

CHAPTERS

1 INTRODUCTION 1
  1.1 Study Background 1
  1.2 Study Objectives 4
  1.3 Outline of Presentation 8

2 NUTRIENT DYNAMICS IN LAKES AND ESTUARIES 11
  2.1 Introduction 11
  2.2 Phosphorus Dynamics in Lakes and Estuaries 13
  2.3 Nitrogen Dynamics in Lakes and Estuaries 20
  2.4 Algal and Zooplankton Growth 29
  2.5 Effects of Temperature and Light Intensity on Nutrient Dynamics . . 35
  2.6 Effects of Hydrodynamics and Sediment Processes on Nutrient Dynamics 37
  2.7 Conclusions 42

3 HYDRODYNAMICS AND SEDIMENT DYNAMICS IN LAKES AND ESTUARIES 44
  3.1 Circulation 44
  3.2 Wave Boundary Layer 49
  3.3 Turbulent Mixing 55
  3.4 Sediment Dynamics 64

4 MODELING THE HYDRODYNAMICS AND SEDIMENT TRANSPORT PROCESSES 84
  4.1 Governing Equations 84
  4.2 Boundary and Initial Conditions 88
  4.3 Model Parameters 91
  4.4 Numerical Solution Algorithm 98

5 MODELING NUTRIENT DYNAMICS 99
  5.1 Governing Equations 99
  5.2 Boundary and Initial Conditions 104
  5.3 Modeling Nutrient Transformation Processes 107
  5.4 Model Parameters 113
  5.5 Numerical Solution Algorithm 121

6 FIELD DATA COLLECTED IN LAKE OKEECHOBEE 126
  6.1 Physical Setting 126
  6.2 Field Measurements 127
  6.3 1989 Spring Survey 134
  6.4 1993 Spring Short-Term Survey 139

7 MODEL APPLICATIONS TO LAKE OKEECHOBEE 143
  7.1 Modeling of the 1993 Storm Event 143
  7.2 1-D Simulations of 1989 Spring Survey 150
  7.3 3-D Simulations of 1989 Spring Survey 164
  7.4 Summary 200

8 FIELD DATA COLLECTED IN TAMPA BAY 204
  8.1 Physical Setting 204
  8.2 Field Measurements 207
  8.3 A Storm Event in February, 1992 208
  8.4 A Storm Event in March, 1993 210

9 MODEL APPLICATIONS TO TAMPA BAY 212
  9.1 Modeling the 1992 Storm Event 212
  9.2 Modeling the 1993 Storm Event 216
  9.3 Conclusions 219

10 CONCLUSIONS AND RECOMMENDATIONS 225
  10.1 Conclusions 225
  10.2 Recommendations 228

BIBLIOGRAPHY 229

APPENDICES

A COMPUTING PRESSURE GRADIENTS FROM CURRENT DATA . . 246

B FLOW CHARTS OF THE 3-D MODEL SYSTEM 248

C NUMERICAL SOLUTION ALGORITHMS IN HYDRODYNAMIC AND SEDIMENT TRANSPORT MODELS 250
  C.1 3-D Hydrodynamics Model 250
  C.2 1-D Hydrodynamics Model 252
  C.3 3-D Sediment Transport Model 253
  C.4 Numerical Stability 254

D FIELD DATA OF 1989 SPRING SURVEY IN LAKE OKEECHOBEE . . 256

E FIELD DATA OF 1993 SPRING STORM EVENT IN LAKE OKEECHOBEE 282

F 3 RUNS FOR 1993 SPRING STORM EVENT IN LAKE OKEECHOBEE 286

G FIELD DATA COLLECTED IN TAMPA BAY 295

H DETERMINING MODEL COEFFICIENTS 307
H.1 1-D Simulation of Lake Okeechobee Phosphorus Dynamics 307
H.2 3-D Simulation of Lake Okeechobee Phosphorus Dynamics 308
H.3 1-D Simulation of Tampa Bay Nitrogen Dynamics 308

BIOGRAPHICAL SKETCH 310

LIST OF FIGURES

2.1 Nutrient dynamics and the relevant hydrodynamics and sediment transport processes in lakes and estuaries 12

2.2 The two-film model for the volatilization. 29

2.3 Relative growth rate of algae in a phosphorus limiting aquatic system. 31

3.1 Critical shear stresses for erosion with and without wave action (from Maa, 1986). 50

3.2 Settling velocity as a function of suspended sediment concentration, with flocculation occurring at high concentrations (after Hwang and Mehta, 1989). 71

3.3 Erosion rate versus bottom shear stress (after Lavelle *et al.*, 1984; the numbers are for different sediments and are explained in Lavelle *et al.*, 1984). 78

4.1 A typical bed density profile from Lake Okeechobee in the vicinity of Station C (after Hwang and Mehta, 1989). 96

6.1 Major features of Lake Okeechobee (after Sheng *et al.*, 1989a). . 128

6.2 Bathymetry of Lake Okeechobee (after Sheng *et al.*, 1989a). . . . 129

6.3 Bottom sediment types of Lake Okeechobee (after Reddy and Graetz, 1989). 130

6.4 Mud Thickness in Lake Okeechobee (after Hwang and Mehta, 1989).131

6.5 A portable platform for field measurements 133

6.6 Locations of synoptic stations in Lake Okeechobee during the 1989 Spring Survey. 136

6.7 Spectra of measured current, wind speed, and SSC at Station C in Lake Okeechobee. 140

7.1 Model results of u-velocities, v-velocities, and suspended sediment concentrations at the middle layer (Layer 2) and the top layer (Layer 3) at Station L002 in Lake Okeechobee during the storm event in February, 1993. 145

7.2 Correlation coefficients between DO and SRP, DO and TDP, and DO and TP measured at Station L002 in Lake Okeechobee during the storm event in February, 1993. 148

7.3 Measured and simulated SRP of a run with adjusted pH at the top layer at Station L002 in Lake Okeechobee during the storm event in February, 1993. 151

7.4 Measured and simulated TDP of a run with adjusted pH at the top layer at Station L002 in Lake Okeechobee during the storm event in February, 1993. 152

7.5 Measured and simulated TP of a run with adjusted pH at the top layer at Station L002 in Lake Okeechobee during the storm event in February, 1993. 153

7.6 Measured and simulated SSC at Station C during week 2 of the 1989 Spring Survey in Lake Okeechobee. 155

7.7 Measured and simulated SSC at Station D during week 2 of the 1989 Spring Survey in Lake Okeechobee. 156

7.8 Measured and simulated SSC at Station E during week 2 of the 1989 Spring Survey in Lake Okeechobee. 157

7.9 Settling velocity obtained from laboratory by Hwang and Mehta (1989) and the modified settling velocity considering the shear stress effect. 160

7.10 Comparison of model results of suspended sediment concentration using two different settling velocity formula. 161

7.11 Results of Monte Carlo simulations of SSC at Station C during Week 2 of the 1989 Spring Survey in Lake Okeechobee. 163

7.12 Contours of the root-mean-square error of the Monte Carlo simulations of SSC at Station C during week 2 of the 1989 Spring Survey in Lake Okeechobee. 164

7.13 Results of the lutocline simulation at Station C during a three-day event in the 1989 Spring Survey in Lake Okeechobee. 165

7.14 SSC profiles in the lutocline simulation at Station C during a 3-day event in Week 2 of the 1989 Spring Survey in Lake Okeechobee. . 166

7.15 A Cartesian grid system for the 3-D simulation of Lake Okeechobee hydrodynamics, sediment, and nutrient dynamics. 167

7.16 Measured and predicted significant wave height and period at Station C in Lake Okeechobee. Model parameters in SMB model has been adjusted. 170

7.17 Contours of wave-induced bottom shear stress from the 1-D TKE model. 172

7.18 Comparison of model (1-D TKE) results of bottom shear stresses induced by a single wave to those induced by group waves. . . . 174

7.19 Simulated u-velocities, v-velocities, and suspended sediment concentrations at Station C of Lake Okeechobee form May 21 to June 16, 1989. 176

7.20 Simulated u-velocities, v-velocities, and suspended sediment concentrations at Station D of Lake Okeechobee form May 21 to June 16, 1989. 177

7.21 Simulated u-velocities, v-velocities, and suspended sediment concentrations at Station E of Lake Okeechobee form May 21 to June 16, 1989. 178

7.22 Spatial distribution of simulated suspended sediment concentration at the top and the bottom layers of Lake Okeechobee at noon of May 27, 1989. 179

7.23 Spatial distribution of simulated suspended sediment concentration at the top and the bottom layers of Lake Okeechobee at noon of June 3, 1989. 180

7.24 Spatial distribution of simulated suspended sediment concentration at the top and the bottom layers of Lake Okeechobee at noon of June 10, 1989. 181

7.25 Spatial distribution of simulated suspended sediment concentration at the top and the bottom layers of Lake Okeechobee at noon of June 16, 1989. 182

7.26 Spatial distribution of simulated SRP concentration at the top and the bottom layers of Lake Okeechobee at noon of May 27, 1989. . 183

7.27 Spatial distribution of simulated SRP concentration at the top and the bottom layers of Lake Okeechobee at noon of June 3, 1989. . 184

7.28 Spatial distribution of simulated SRP concentration at the top and the bottom layers of Lake Okeechobee at noon of June 10, 1989. 185

7.29 Spatial distribution of simulated SRP concentration at the top and the bottom layers of Lake Okeechobee at noon of June 16, 1989. 186

7.30 Spatial distribution of simulated TP concentration at the top and the bottom layers of Lake Okeechobee at noon of May 27, 1989. . 187

7.31 Spatial distribution of simulated TP concentration at the top and the bottom layers of Lake Okeechobee at noon of June 3, 1989. . 188

7.32 Spatial distribution of simulated TP concentration at the top and the bottom layers of Lake Okeechobee at noon of June 10, 1989. 189

7.33 Spatial distribution of simulated TP concentration at the top and the bottom layers of Lake Okeechobee at noon of June 16, 1989. 190

7.34 Correlations among SSC, SRP, and TP in the synoptic data and the 3-D model results for the 1989 synoptic survey in Lake Okeechobee. 193

7.35 Time series of simulated SSC, SRP, and TP at Station C of Lake Okeechobee during the 1989 Spring Survey. 195

7.36 Model results of time series of sediment and PIP resuspension/deposition fluxes and SRP mass in Lake Okeechobee during the 1989 Spring Survey. 196

7.37 Spatial distribution of simulated (with the WASP transformations) SRP concentration at the top and the bottom layers of Lake Okeechobee at noon of May 27, 1989. 199

7.38 Spatial distribution of simulated SRP concentration (by the 3-D model developed by Dickinson *et al*, 1992) at the top and the bottom layers of Lake Okeechobee at noon of May 27, 1989. . . . 201

8.1 Location of Tampa Bay and the experiment stations (after Sheng *et al.*, 1993b) 205

9.1 Significant wave heights calculated from SMB model for the time period of the 1992 storm event. 213

9.2 Model results of u-velocity, v-velocity, and sediment concentration at Station A during the storm event of 1992. 215

9.3 Comparison of model results of NH_4^+–N and measured data during the storm event of 1992 at Station A. 217

9.4 Model results of resuspension fluxes of (a) sediments and (b) NH_4^+–N during the storm event of 1992 at Station A. 218

9.5 Model results of u-velocity, v-velocity, and sediment concentration at Station A during the storm event of 1993. 220

9.6 Model results of u-velocity, v-velocity, and sediment concentration at Station B during the storm event of 1993. 221

9.7 Comparison of model results of NH_4^+–N and measured data during the storm event of 1993 at Station A. 222

9.8 Model results of resuspension fluxes of (a) sediments and (b) NH_4^+–N during the storm event of 1993 at Station A. 223

9.9 A test run with zero desorption rate of ammonium N at Station A during the storm event of 1992. 224

B.1 Flow chart of the 3-D model system of hydrodynamics, sediment transport, and nutrient dynamics in lakes and estuaries. 248

B.2 Flow chart of the 3-D submodel for nutrient dynamics. 249

D.1 Measured wind at Station A in Lake Okeechobee from May 21 to June 16, 1989. 256

D.2 Measured wind at Station B in Lake Okeechobee from May 21 to June 16, 1989. 257

D.3 Measured wind at Station C in Lake Okeechobee from May 21 to June 16, 1989. 258

D.4 Measured wind at Station D in Lake Okeechobee from May 21 to June 16, 1989. 259

D.5 Measured wind at Station E in Lake Okeechobee from May 21 to June 16, 1989. 260

D.6 Measured u-velocities, v-velocities, and suspended sediment concentrations at Station A from May 21 to June 16, 1989. 261

D.7 Measured u-velocities, v-velocities, and suspended sediment concentrations at Station B from May 21 to June 16, 1989. 262

D.8 Measured u-velocities, v-velocities, and suspended sediment concentrations at Station C from May 21 to June 16, 1989. 263

D.9 Measured u-velocities, v-velocities, and suspended sediment concentrations at Station D from May 21 to June 16, 1989. 264

D.10 Measured u-velocities, v-velocities, and suspended sediment concentrations at Station E from May 21 to June 16, 1989. 265

D.11 Measured u-velocities, v-velocities, and suspended sediment concentrations at Station F from May 21 to June 16, 1989. 266

D.12 Contours of synoptic data of suspended sediment concentrations at the top and the bottom layers of Lake Okeechobee at noon of May 21, 1989. 267

D.13 Contours of synoptic data of suspended sediment concentrations at the top and the bottom layers of Lake Okeechobee at noon of May 27, 1989. 268

D.14 Contours of synoptic data of suspended sediment concentrations at the top and the bottom layers of Lake Okeechobee at noon of June 3, 1989. 269

D.15 Contours of synoptic data of suspended sediment concentrations at the top and the bottom layers of Lake Okeechobee at noon of June 10, 1989. 270

D.16 Contours of synoptic data of suspended sediment concentrations at the top and the bottom layers of Lake Okeechobee at noon of June 16, 1989. 271

D.17 Contours of synoptic data of SRP concentrations at the top and the bottom layers of Lake Okeechobee at noon of May 21, 1989. . 272

D.18 Contours of synoptic data of SRP concentrations at the top and the bottom layers of Lake Okeechobee at noon of May 27, 1989. . 273

D.19 Contours of synoptic data of SRP concentrations at the top and the bottom layers of Lake Okeechobee at noon of June 3, 1989. . 274

D.20 Contours of synoptic data of SRP concentrations at the top and the bottom layers of Lake Okeechobee at noon of June 10, 1989. 275

D.21 Contours of synoptic data of SRP concentrations at the top and the bottom layers of Lake Okeechobee at noon of June 16, 1989. 276

D.22 Contours of synoptic data of TP concentrations at the top and the bottom layers of Lake Okeechobee at noon of May 21, 1989. . . . 277

D.23 Contours of synoptic data of TP concentrations at the top and the bottom layers of Lake Okeechobee at noon of May 27, 1989. . . . 278

D.24 Contours of synoptic data of TP concentrations at the top and the bottom layers of Lake Okeechobee at noon of June 3, 1989. . . . 279

D.25 Contours of synoptic data of TP concentrations at the top and the bottom layers of Lake Okeechobee at noon of June 10, 1989. . . . 280

D.26 Contours of synoptic data of TP concentrations at the top and the bottom layers of Lake Okeechobee at noon of June 16, 1989. . . . 281

E.1 Measured wind during a storm event at Station L002 in Lake Okeechobee in February, 1993. 282

E.2 Measured u-velocities, v-velocities, and suspended sediment concentrations at the middle and the bottom arms at Station L002 in Lake Okeechobee in February, 1993. 283

E.3 Measured total phosphorus (TP), total dissolved phosphorus (TDP), and soluble reactive phosphorus (SRP) at Station L002 in Lake Okeechobee in February, 1993. 284

E.4 Measured DO and pH at the bottom layer at Station L002 in Lake Okeechobee in February, 1993. 285

F.1 Measured and simulated SRP of the first run at Station L002 in Lake Okeechohee during the storm event in February, 1993. . . . 286

F.2 Measured and simulated TDP of the first run at Station L002 in Lake Okeechobee during the storm event in February, 1993. . . . 287

F.3 Measured and simulated TP of the first run at Station L002 in Lake Okeechohee during the storm event in February, 1993. . . . 288

F.4 Measured and simulated SRP of the second run at Station L002 in Lake Okeechohee during the storm event in February, 1993. . . 289

F.5 Measured and simulated TDP of the second run at Station L002 in Lake Okeechohee during the storm event in February, 1993. . . 290

F.6 Measured and simulated TP of the second run at Station L002 in Lake Okeechohee during the storm event in February, 1993. . . . 291

F.7 Measured and simulated SRP of the third run at Station L002 in Lake Okeechohee during the storm event in February, 1993. . . . 292

F.8 Measured and simulated TDP of the third run at Station L002 in Lake Okeechohee during the storm event in February, 1993. . . . 293

F.9 Measured and simulated TP of the third run at Station L002 in Lake Okeechohee during the storm event in February, 1993. . . . 294

G.1 Measured u-velocites and v-velocities at Station A in Tampa Bay during Julian days 30 to 40, 1992. 295

G.2 Measured wind at Station A in Tampa Bay during Julian days 30 to 40, 1992. 296

G.3 Measured free surface variation about the mean water level, salinity, and temperature at Station A in Tampa Bay during Julian days 30 to 40, 1992. 297

G.4 Measured u-velocity, v-velocity, and suspended sediment on the storm day at Station A of Tampa Bay during Julian day 35.6 to 36.6, 1992. 298

G.5 Measured SRP, TP, and ammonium N concentrations at Station A in Tampa Bay during Julian days 35.6 to 36.6, 1992. 299

G.6 Measured SRP, NH_4^+-N, and redox profiles in Tampa Bay. . . . 300

G.7 Measured salinity, temperature, pH, and dissolved oxygen concentration at Station A in Tampa Bay during Julian days 70.59 to 71.1, 1993. 301

G.8 Measured wind at Station A in Tampa Bay during Julian days 70.59 to 71.1, 1993. 302

G.9 Measured u-velocity, v-velocity, and suspended sediment concentration at Station A in Tampa Bay during Julian days 70.59 to 71.1, 1993. 303

G.10 Measured wind at Station A in Tampa Bay during Julian days 70.5 to 76.3, 1993. 304

G.11 Measured u-velocity, v-velocity, and suspended sediment concentration at Station B in Tampa Bay during Julian days 70.5 to 76.3, 1993. 305

G.12 Measured ammonium N and SRP concentrations at Station A in Tampa Bay during Julian days 70.5 to 71.1, 1993. 306

LIST OF TABLES

3.1 Measured exponents m in Krone's Equation. 69

4.1 Values of ρ_B, ε_M, and τ_{ce} determined by Hwang and Mehta (1989). * indicates that these values were obtained by combining the erosion rate data resulting from tests 1, 2 and 3. 95

5.1 Literature values for H_p and H_n. 116

5.2 Literature values for H_a. 116

5.3 Literature values for w_s^a. 117

5.4 Literature values for DOP mineralization rate. 118

5.5 Literature values for K_2, K_3, and K_4. 120

6.1 The synoptic surveys conducted in the spring of 1989 in Lake Okeechobee. 135

6.2 Locations and depths of the stations in Lake Okeechobee. 135

6.3 Elevations (above lake bottom) of the instruments arms at the six stations. 137

7.1 τ_{ce} and E_o values determined by the 1-D sediment model. 154

7.2 Correlation coefficients between measured and simulated SSC, SRP, and TP. The effect of water depth variation with time on wave-induced bottom shear stress was considered. 192

7.3 Correlation coefficients between measured and simulated SSC, SRP, and TP. The effect of water depth variation with time on wave-induced bottom shear stress was not considered. 192

7.4 Results of some sensitivity runs of the 3-D nutrient model. 197

H.1 Results of some sensitivity tests for Lake Okeechobee phosphorus dynamics. 308

H.2 Model coefficients used in the 3-D simulations of Lake Okeechobee phosphorus dynamics. 309

H.3 Model coefficients used in the 1-D simulations of Tampa Bay nitrogen dynamics. 309

Abstract of Dissertation Presented to the Graduate School
of the University of Florida in Partial Fulfillment of the
Requirements for the Degree of Doctor of Philosophy

EFFECTS OF HYDRODYNAMICS AND SEDIMENT TRANSPORT PROCESSES ON NUTRIENT DYNAMICS IN SHALLOW LAKES AND ESTUARIES

By

Xinjian Chen

April 1994

Chairman: Dr. Y. Peter Sheng
Major Department: Coastal and Oceanographic Engineering

Hydrodynamic processes (turbulent mixing, wave action, circulation, etc.) and sediment transport processes (settling, resuspension, deposition, flocculation, etc.) can significantly affect the nutrient dynamics in lakes and estuaries. Previous water quality models (e.g., WASP model) did not use sophisticated models for hydrodynamics and sediment dynamics and therefore lack the ability of quantitatively modeling the complex nutrient dynamics in lakes and estuaries. In addition, most of the previous water quality models used very large grid (box) size and time step (much larger than the time and length scales of hydrodynamics and sediment transport processes) which could result in totally incorrect model predictions.

Because of the dependence of nutrient dynamics on hydrodynamics and sediment dynamics, it is essential that a water quality model should be able to quantify hydrodynamic and sediment transport quantities in lakes and estuaries and that the grid size and the time step in model applications should be smaller than the length and time scales of hydrodynamics and sediment transport. This study developed 1-D and 3-D nutrient models and aggregated these nutrient models with models for hydrodynamics and sediment transport originally developed by Sheng *et al.* to study effects of hydrodynamics and sediment transport processes on nutrient cycles in shallow lakes and estuaries. The integrated 1-D and 3-D models for hydrodynamics, sediment transport, and nutrient dynamics were applied to Lake Okeechobee and Tampa Bay. From field data and model applications, this study obtained four major conclusions: (1) resuspensions of sediments and nutrients in Lake Okeechobee and Tampa Bay were mainly caused by wind-induced waves, (2) the resuspension flux of nutrients is about 2 to 3 orders of magnitude larger than the diffusive flux, (3) the release of nutrients from suspended sediments is affected by pH and dissolved oxygen levels in Lake Okeechobee and Tampa Bay, and (4) because the time step of a real-time simulation (10-15 min.) is generally much smaller than the time scale of desorption-adsorption reactions of nutrients, equilibrium models for desorption-adsorption reactions often overpredict the release of nutrients from resuspended sediments.

CHAPTER 1
INTRODUCTION

1.1 Study Background

Excess loadings of nutrients into lakes and estuaries around the world has resulted in augmented growth of various autotrophs (an autotroph is an organism which can supply its own food without requiring a specified exogenous factor for normal metabolism), of which some may in turn reach high trophic levels. Both the growth and the mortality of autotrophs (such as algae) require oxygen for respiration and for decomposition. In a stratified system, due to weak mixing process in the water column, oxygen is hardly transported downward and the dissolved oxygen (DO) level near the bottom of the water column can be very low. In this case, if the biological oxygen demand (BOD) at the bed is still high, a very stressed ecosystem (noxious condition) may be the consequence. For example, about 66 million kilograms of nitrogen and 6.5 million kilograms of phosphorus enter into Chesapeake Bay in an average year. As a result, the bay has become eutrophic with increasing anoxia, decline in submerged vegetation, severe reductions in harvests of rockfish and oysters, and contaminated sediments where marine organisms feed. In Tampa Bay, increased nutrient loading has resulted in hypoxia and decline in seagrass and fisheries, particularly in Hillsborough Bay where sediment oxygen demand becomes higher (Spaulding *et al.*, 1989). Lewis and Estevez (1988) report that dissolved oxygen (DO) levels in Hillsborough Bay are below Florida state water quality criteria for DO levels for about 60-90 days per year. In Lake Okeechobee, the annual external loading of phosphorus varied more than fivefold in less than three years (Schelske, 1989). In 1980, the phosphorus loading into the lake was about 0.22 million kilograms. It increased to 1.16 million kilograms in 1982. The annual average of orthophosphorus was as high as 45 μg/l, indicating that orthophosphorus supplies could be greater than could be utilized for algal growth.

In order to effectively manage the loading of pollutants such as nutrients in a lake or an estuary and control the eutrophication, it is necessary to have a quantitative understanding of the transport and transformation processes of nutrients such as nitrogen and phosphorus in the aquatic system. The nutrient dynamics in lakes and estuaries are not only determined by biological and chemical processes, but are also strongly affected by climate (wind, air temperature, etc.), hydrodynamics (wave, tide, current, turbulence mixing, etc.) and sediment transport processes (resuspension, deposition, flocculation, etc.). It is apparent that there exist interactions among all these processes. For example, wind can generate waves and create circulation in lakes or estuaries. Waves and currents can not only transport pollutants through advective/diffusive processes, but can also cause resuspension of the bottom sediments, which is strongly coupled with the food chain of organisms and nutrient dynamics. The major connections among hydrodynamics, sediment transport dynamics, and nutrient dynamics in lakes and estuaries are shown schematically in Figure 2.1.

Because a physical process usually occurs more quickly than a biochemical one, hydrodynamics and sediment transport processes are often the dominant controlling factors of a marine ecosystem. It is now widely recognized (Kemp *et al.*, 1982; Simon, 1989; Sheng *et al.*, 1989a) that a thorough understanding of the ecology of lakes and estuaries requires a comprehensive knowledge on the interactions among biochemical and physical processes affecting the system.

Numerous water quality models (e.g., Chen and Orlob, 1975; Di Toro *et al.*, 1977; Harleman, 1977; Voinov and Akhremenkov, 1990; Ambrose *et al.*, 1991) have been developed since the primary work of Streeter and Phelps (1925). However, most of these models lacked the coupling of hydrodynamics and sediment transport processes with biochemical processes. Although some of the recent models (e.g., Lam *et al.*, 1983; Ambrose *et al.*, 1991) did consider physical processes such as the benthic flux of nutrients due to the sediment resuspension, they can not be used to simulate real-time nutrient variations caused by a short-term physical process such as an episodic storm event because these models are unable to resolve such a short-term event.

Most of the previous water quality models (e.g., Chen and Orlob, 1975; Ambrose *et al.*, 1991) have been used to simulate long-term variations of nutrient dynamics in lakes and estuaries. In these applications, because the time step (usually a few hours to one day) was larger than the time scale of hydrodynamics and sediment transport (a few minutes to a few hours), a lot of hydrodynamic processes (e.g., circulations, wave actions etc.) and sediment transport processes (e.g., deposition, resuspension, etc.) which can have significant effects on nutrient cycles have not been accurately considered. For example, the internal loading of nutrients from bottom sediments in Lake Okeechobee can not be accurately calculated in a water quality model if a time step of 6 hours is used to simulate nutrient dynamics in the lake because the resuspension event can be shorter than 6 hours and the net flux of sediments at the water-sediment interface can alter direction. During one time step (6 hours), the bottom sediments can be eroded in the first 3 hours due to an increase of wind speed and the suspended sediments can be deposited to the bottom in the second 3 hours when the wind becomes calm. In this case, the internal loading of nutrients from bottom sediments calculated by a conventional water quality model may be zero because the average of net flux of bottom sediments in 6 hours may be zero. Apparently, the internal loading of nutrients from bottom sediment so calculated is not correct, because it is not different from that of no resuspension/deposition in 6 hours. In reality, even the net loading of sediments from the lake bottom is zero in 6 hours, the net loading of nutrients due to resuspension may not be zero because of the desorption of nutrients from sediments after the resuspension.

Problems with these previous water quality models are beyond the time step and grid size used by them. Even with small time step and grid size, most of these models still can not be used to simulate short-term nutrient dynamics in shallow lakes and estuaries because of the following reasons:

1. Wave boundary layer dynamics and wave-current interactions are simulated in none of the previous water quality models.
2. It is assumed that the water column is well mixed, and a spatial- and time-independent eddy diffusivity is used in most previous water quality models (e.g., Chen and Orlob, 1975; Ambrose *et al.*, 1991).
3. Because most previous water quality models were not coupled with a 3-D time-dependent free surface model of hydrodynamics, they could not accurately simulate the horizontal and vertical transport of different water quality components due to advective and diffusive motions.
4. Because most previous water quality models were not coupled with a sophisticated model for sediment dynamics (e.g., constant settling velocities were often used in previous water quality models even for fine sediments), they could not accurately consider effects of sediment processes such as resuspension, deposition, flocculation, and settling on nutrient dynamics in lakes and estuaries.
5. If a small time step (e.g., 15 minutes) is used, the assumption that the desorption/adsorption reactions reach equilibrium instantaneous may be not correct because the time scale of desorption/adsorption reactions can be much larger than the time step used in the model. However, most previous water quality models used the instantaneous model for desorption/adsorption reactions.

1.2 Study Objectives

Because nutrient concentrations in the sediment column are usually 2 to 3 orders of magnitude higher than these in the water column (Simon, 1989; Sheng *et al.*, 1989a), the resuspension of bottom sediments and the desorption/adsorption of nutrients from/onto sediments are two important processes controlling nutrient budget in the water column. The resuspension of nutrients is especially significant in shallow lakes and estuaries because it is mainly caused by wind-induced waves which can be very large under servere storm conditions. However, the resuspension of nutrients during a storm event does not necessarily mean an increase of nutrient concentration in the water column after the storm is gone because the deposition of sediments can bring the resuspended nutrient back to the bottom. An increase of nutrient concentration occurs when the desorption process takes place during the sediment resuspension. Recently, some researchers have studied the adsorption/desorption kinetics of chemical species in the presence of solid particles (e.g., Gschwend *et al.*, 1987; Gibbs, 1983). However, little has been done to quantify the influence of various sediment transport processes (erosion, deposition, turbulent mixing, settling) on the distribution and cycling of pollutants or nutrients, particularly in the near-bed region.

Hydrodynamics, sediment dynamics, and nutrient dynamics in shallow lakes and estuaries may be different from those in deep ones. For example, because of the shallowness and the turbulent mixing induced by wind, a shallow lake is often well-mixed (Harleman and Shanahan, 1983), while a deep lake can have a significant density stratification. Another important hydrodynamic characteristic in a shallow lake is the water surface set-up wherein the free surface at the downwind side of the lake is superelevated by the wind force above the elevation of the upwind side. Compared to deep lakes, set-up in shallow lakes is enhanced (Harleman and Shanahan, 1983). Because of the set-up, a decrease in wind speed often causes a seiche motion in a shallow lake. Sheng *et al.* (1989a) recorded strong seiche motion in Lake Okeechohee (a shallow lake in South Florida with a mean depth of about 3 meters). Their data show that the peak value of water current was associated with seiche motion in the lake.

Because of the shallowness, wave-induced bottom shear stress in shallow lakes and estuaries is usually much higher than in deep ones (for the same wave height and wave period). As a result, wave action in shallow lakes and estuaries plays an important role in sediment dynamics. Therefore, it is essential that modeling sediment dynamics in shallow lakes and estuaries requires a sophisticated model for wave boundary layer dynamics and wave-current interaction.

Biochemical transformations in nutrient cycles in shallow lakes and estuaries can also be different from deep ones. In shallow lakes and estuaries, the water column is usually well-aerated because of the shallowness and the turbulent mixing induced by wind (Somlyody, 1983). Because the depth-intergal light intensity in shallow lakes and estuaries is higher than in deep ones, photosynthesis in the water column of shallow lakes and estuaries is quicker than that of deep ones. On the other hand, wave-induced sediment resuspension in shallow lakes and estuaries can affect nutrient cycles by causing the reduction of light intensity and loading nutrient from the sediment column to the water column.

Because of the importance of hydrodynamics and sediment transport processes to nutrient dynamics in shallow lakes and estuaries, this study intended to develop a coupled numerical model of hydrodynamics, sediment transport, and nutrient dynamics. By using the numerical model and some field data collected in Lake Okeechobee and in the shallow region of Tampa Bay (Hillsborough Bay), this study investigated effects of hydrodynamics and sediment transport processes on nutrient dynamics in shallow lakes and estuaries. In detail, this study would like to answer the following questions:

1. What is the relationship among wind, current, and suspended sediment concentration in Lake Okeechobee?
2. How important is horizontal transport in affecting the distributions of suspended sediment and phosphorus components in Lake Okeechobee?

3. How important are wave actions in affecting sediment resuspension process in Lake Okeechobee and Tampa Bay?
4. How lutocline, if there is, is built up in the muddy zones of Lake Okeechobee and Tampa Bay?
5. How important is sediment resuspension to nutrient dynamics in the water column?
6. Is the release of SRP from sediments affected by pH, temperature, and dissolved oxygen concentration in Lake Okeechobee?
7. Is the instantaneous equilibrium model for adsorption/desorption reactions applicable in a real-time simulation?
8. How important are adsorption/desorption kinetics in affecting nutrient dynamics in lakes and estuaries?
9. How important is settling of particulate nutrients in affecting short-term and long-term nutrient dynamics in lakes and estuaries?
10. How large can resuspension fluxes of nutrients be in Lake Okeechobee and Tampa Bay during episodic events?

In order to accomplish these objectives, the following steps have been taken:

1. Field data on wind, waves, suspended sediment concentration, current, tide, dissolved oxygen (DO), and various nitrogen and phosphorus species of nutrients were collected in Tampa Bay and Lake Okeechobee,
2. Field data were analyzed,
3. Numerical models of hydrodynamics and sediment transport originally developed by Sheng (e.g. Sheng and Chen, 1992) were used to compute currents and sediment concentrations in Lake Okeechobee and Tampa Bay.

4. Numerical models of nutrient dynamics were developed and used to study phosphorus dynamics in Lake Okeechobee and nitrogen dynamics in Tampa Bay.
5. Some important factors controlling nutrient concentrations in the water column (e.g. advections, wave actions, sediment resuspension, the adsorption/desorption kinetics of phosphorus and nitrogen, algal uptake of nutrients) were studied using the nutrient models.
6. Model results of current, suspended sediment concentration, and nutrient concentrations in Lake Okeechobee and Tampa Bay were analyzed and compared to the data.
7. Based on model results and field data on currents, suspended sediment concentrations, and nutrient concentrations, some conclusions were drawn.

1.3 Outline of Presentation

Chapter 2 discusses phosphorus and nitrogen dynamics in lakes and estuaries. Effects of temperature, light intensity, hydrodynamics and sediment transport processes on nutrient dynamics are also discussed in this chapter.

Chapter 3 discusses the general hydrodynamics of circulation, waves, and wave-current interaction in shallow lakes and estuaries, followed by a discussion of sediment transport processes in these water bodies. Previous studies on the relevant subjects are reviewed.

Chapter 4 describes a 3-D model and a 1-D model for hydrodynamics and sediment transport. This chapter contains (1) assumptions used in the 3-D and 1-D models for hydrodynamics and sediment dynamics in shallow lakes and estuaries, (2) governing equations for current and suspended sediment concentration, (3) specification of boundary and initial conditions for current and suspended sediment concentration in the models, (4) determination of model parameters, and (5) solution algorithms used in the models.

Chapter 5 describes a 3-D model and a 1-D model for nutrient dynamics in shallow lakes and estuaries. Similar to Chapter 4, this chapter contains (1) assumptions used in the models for phosphorus dynamics and nitrogen dynamics, (2) governing equations for phosphorus and nitrogen species, (3) specification of boundary and initial conditions for different phosphorus and nitrogen species, (4) models for kinetic pathways in phosphorus and nitrogen cycles, (5) determination of model parameters, and (6) solution algorithms.

Chapter 6 presents field data collected in Lake Okeechobee. These data include a four-week survey in the spring of 1989 and a three-day storm event survey in February, 1993. Measured wind, current, suspended sediment concentration, and nutrient concentrations are analyzed in this chapter.

Chapter 7 presents model simulations of hydrodynamics, sediment dynamics, and nutrient dynamics presented in Lake Okeechobee. These model simulations include the following: 1-D simulations of sediment and phosphorus dynamics at L002 (a station) during a three-day storm event in February 1993, 1-D simulations of sediment dynamics at several stations during the 1989 Spring Survey, and 3-D simulations of hydrodynamics, sediment transport, and phosphorus dynamics of the four-week survey in spring of 1989.

Chapter 8 presents field data collected in Tampa Bay. Measured wind, suspended sediment concentration, nutrient concentrations during two storm events in February 1992 and March 1993 are analyzed in this chapter.

Chapter 9 presents applications of the 1-D model of hydrodynamics, sediment transport, and nutrient dynamics to Tampa Bay. These applications include (1) a one-day storm event observed in February 1992, (2) a one-day storm event observed in March 1993, and (3) a one-week event observed in March 1993.

Chapter 10 summarizes this study. Some conclusions are drawn from the applications of the numerical models to Lake Okeechobee and Tampa Bay. Limitations and shortcomings of the numerical models for hydrodynamics, sediment dynamics, and nutrient dynamics used or developed for this study have been discussed. Recommendations are provided for further modifications of the models and further research on modeling hydrodynamics, sediment transport processes, and nutrient dynamics in shallow lakes and estuaries.

CHAPTER 2
NUTRIENT DYNAMICS IN LAKES AND ESTUARIES

2.1 Introduction

Nutrients serve as raw materials for primary production of organic matter in lakes and estuaries. The importance of nutrient dynamics in controlling the primary and secondary production in lakes and estuaries is becoming increasingly apparent. As more and more information on nutrient dynamics in lakes and estuaries is developed, our understanding of the roles of various transformation pathways continues to be refined. Excess nutrient loading into a lake or an estuary can result in increased growth of various autotrophs. Algae and other autotrophs require numerous nutrients, including nitrogen, phosphorus, carbon, silicon, and sulfur, etc. Among these nutrients, the first three are utilized most heavily by algae. Since carbon is generally abundant in lakes and estuaries, nitrogen and phosphorus are the two major nutrients regulating the ecological balance.

Nutrient concentrations in lakes and estuaries are constantly changing in time and space due to loadings from rivers, exchanges with ocean, seasonal climatic changes, biochemical transformations, as well as hydrodynamics and sediment dynamics. Figure 2.1 presents a conceptional picture of the major phosphorus and nitrogen pathways and the relevant hydrodynamic and sediment transport processes in lakes and estuaries. Although somewhat simplified, this figure shows how various phosphorus and nitrogen components are transformed and how phosphorus and nitrogen cycles in lakes and estuaries are connected with hydrodynamics and sediment transport processes.

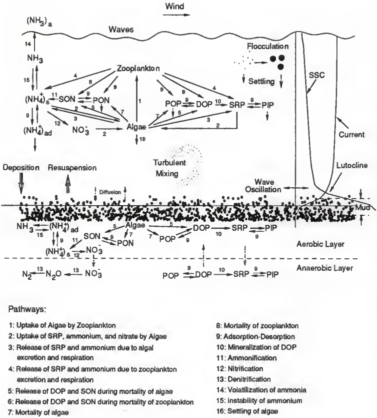
Wind
$(NH_3)_a$
Waves
14
NH_3
15
Zooplankton
Flocculation
Settling
SSC
$(NH_4^+)_s$
SON
PON
POP
DOP
SRP
PIP
Algae
$(NH_4^+)_{ad}$
NO_3^-
16
Current
Deposition
Resuspension
Turbulent Mixing
Lutocline
Diffusion
Wave Oscillation
Mud
Aerobic Layer
Anaerobic Layer
N_2
N_2O
Pathways:
1: Uptake of Algae by Zooplankton
2: Uptake of SRP, ammonium, and nitrate by Algae
3: Release of SRP and ammonium due to algal excretion and respiration
4: Release of SRP and ammonium due to zooplankton excretion and respiration
5: Release of DOP and SON during mortality of algae
6: Release of DOP and SON during mortality of zooplankton
7: Mortality of algae
8: Mortality of zooplankton
9: Adsorption-Desorption
10: Mineralization of DOP
11: Ammonification
12: Nitrification
13: Denitrification
14: Volatilization of ammonia
15: Instability of ammonium
16: Settling of algae

Figure 2.1: Nutrient dynamics and the relevant hydrodynamics and sediment transport processes in lakes and estuaries

2.2 Phosphorus Dynamics in Lakes and Estuaries

Phosphorus enters lakes or estuaries from weathering of soil and rock and subsequent runoff, point source discharge such as sewage treatment plants, and from dairy farms and agricultural fertilizers. The magnitude of these pathways and their constituent makeups ultimately determine phosphorus availability. However, phosphorus concentration in the water column of a lake or an estuary is not merely determined by these external sources. Internal sources such as resuspended bottom sediments containing inorganic and organic phosphorus are also very important.

Phosphorus can be classified into two groups: dissolved phosphorus and particulate phosphorus. The criterion for this classification of phosphorus species is to use a 0.45 μm membrane filter to separate the two fractions. Typically, dissolved (or soluble) phosphorus in lakes and estuaries includes soluble reactive phosphorus (SRP), dissolved organic phosphorus (DOP), and dissolved inorganic phosphorus (DIP). Particulate phosphorus includes alga particulate phosphorus (green, blue-green, and diatom), bacteria particulate phosphorus, zooplankton particulate phosphorus, particulate inorganic phosphorus (PIP), and particulate organic phosphorus (POP). Individual lakes or estuaries can have very different compositions of particulate phosphorus. For example, a lake with high external loading of organic matter can have a bacterial biomass greater than the phytoplankton biomass (Grobbelaar, 1985). Algae associated particulate phosphorus seldom dominates in lakes unless the lake system is very eutrophic or an algal bloom is occurring. Bacterial phosphorus is usually not simulated in a water quality model because once bacteria are saturated with phosphorus their excretion of internal phosphorus molecules will be equal to the phosphorus molecules they have actively taken up from the external pool (Jansson, 1988).

The cycle of phosphorus in lakes and estuaries is in dynamic flux with continuous movement among the different forms of phosphorus mentioned above. In most lakes and estuaries particulate phosphorus (PP) concentration is much higher than dissolved organic phosphorus concentration, which in turn is higher than dissolved inorganic phosphorus concentration (DIP). Generally, phosphorus in lakes is partitioned into about 60 to 70 percent PP, 20 to 30 percent DOP, and 5 to 10 percent DIP (Valiela, 1984). However, the relative proportions of the different forms of phosphorus vary from one aquatic system to another. The Organization for Economic Cooperation and Development (OECD, 1982) found that the percentage of orthophosphorus ranges from 20 percent to 45 percent in many of the European and U.S. lakes. Schnoor and O'Connor (1980) found dissolved phosphorus to range from 35 to 75 percent in 81 northern U.S. lakes, and phytoplankton phosphorus to account for 10 to 40 percent of the total phosphorus. In seawater, because algal concentrations are usually lower than those in lakes, dissolved organic phosphorus concentration may be lower than dissolved inorganic phosphorus concentration. In the English Channel, most of the phosphorus present is DIP in winter and DOP in summer when algae are abundant (Valiela, 1984).

As shown in Figure 2.1, biochemical transformation processes in the phosphorus cycle include (1) mineralization of organic phosphorus, (2) uptake of soluble reactive phosphorus by algae, (3) conversion of algal particulate phosphorus to zooplankton particulate phosphorus due to the uptake of algae by zooplankton, (4) excretion of SRP by algae and zooplankton, and (5) sorption-desorption reaction of inorganic and organic phosphorus.

2.2.1 Mineralization of DOP

The mineralization process of DOP is a biological decomposition process, which is mediated by bacteria. Since dissolved organic phosphorus comprises a major portion of phosphorus in many lakes and estuaries, the speed of mineralization of DOP directly influences the SRP level in lakes and estuaries and further influences the growth rate of algae. The mineralization of DOP is a relatively fast process, it can take place in a few hours (compared to the mineralization of carbon and nitrogen, which takes place in a few days. See, for example, Golterman, 1973).

The decomposition of dissolved organic phosphorus has been studied extensively. Thompson *et al.* (1954) found that the mineralization of dissolved organic phosphorus is influenced by pH. An increase in pH causes a temporary increase in the rate of mineralization of dissolved organic phosphorus. Temperature can also affect the speed of the mineralization of DOP. High temperature can stimulate the mineralization process of DOP and thereby liberate organic-bound phosphorus (Jensen and Andersen, 1992).

The mineralization rate of DOP is usually modeled by a first-order equation as follows (Jørgensen, 1983b):

$$\frac{\partial P_2}{\partial t} = -K_D P_2 \tag{2.1}$$

wherein, P_2 is the DOP concentration and K_D is a rate constant for the mineralization of DOP. K_D is a function of pH and temperature.

2.2.2 Uptake of SRP by Algae

Soluble reactive phosphorus (SRP), sometimes also called dissolved reactive phosphorus (DRP), can be taken up by algae as a nutrient. In a phosphorus limiting system, algal growth is dependent on the available SRP in the water column.

Soluble reactive phosphorus is a combination of orthophosphorus and low molecular weight organic phosphorus (Barica and Allen, 1988). Since the low molecular weight organic phosphorus can be rapidly cycled and ultimately taken up by algae, SRP is an acceptable measure of dissolved bioavailable phosphorus (Barica and Allen, 1988).

Bioavailable phosphorus is commonly defined as the sum of immediately available phosphorus and that which will become available by a naturally occurring process (Bostrom *et al.*, 1988). NaOH-Extractable P, commonly assumed to correspond to aluminum- and iron-bound phosphorus, is the sediment form most readily available to algae (Bostrom *et al.*, 1988). HCl-Extractable P, corresponding to calcium-bound phosphorus, and particulate organic P (POP) were found not to support algal growth.

Through the uptake of SRP by algae, SRP is converted to algal particulate phosphorus as shown in Figure 2.1. The uptake rate of SRP by algae is proportional to the growth rate of algae. This can be seen from the mass conservation of SRP (excluding other processes):

$$\frac{\partial P_1}{\partial t} = -\frac{\partial (p_3 c_a)}{\partial t} \tag{2.2}$$

or

$$\frac{\partial P_1}{\partial t} = -p_3 \frac{\partial c_a}{\partial t} - c_a \frac{\partial p_3}{\partial t} \tag{2.3}$$

where P_1 is the SRP concentration, p_3 is phosphorus per unit biomass of algae, and c_a is the algal biomass concentration.

Because p_3 varies only slowly within a narrow range (0.01 to 0.02), the second term on the right-hand side of Equation (2.3) is negligible compared to the first term, and the uptake rate $\partial P_1/\partial t$ becomes

$$\frac{\partial P_1}{\partial t} = -p_3 \frac{\partial c_a}{\partial t} = -P_3 \mu_a \tag{2.4}$$

where $P_3 (= p_3 c_a)$ is the concentration of algal particulate phosphorus and μ_a is the growth rate of algae due to the uptake of SRP (see Section 2.4).

2.2.3 Conversion of Algal P to Zooplankton P

While the uptake of SRP by algae converts the dissolved inorganic phosphorus to algal particulate phosphorus, the uptake of algae by zooplankton converts the algal particulate phosphorus to zooplankton particulate phosphorus. As will be seen in Section 2.4, different zooplankton species use different mechanisms to eat algae at different speeds. The conversion rate of algal P to zooplankton P is related to the uptake rate of algae by zooplankton.

Let p_4 be the phosphorus per unit biomass of zooplankton, P_4 the concentration of zooplankton particulate phosphorus, and c_z the concentration of zooplankton biomass, then

$$\frac{\partial P_4}{\partial t} = p_4 \frac{\partial c_z}{\partial t} + c_z \frac{\partial p_4}{\partial t} \qquad (2.5)$$

Because p_4 is almost constant during the grazing of algae, the second term on the right hand side can be neglected. Therefore, the rate of increase of zooplankton particulate phosphorus (P_4) during the grazing of algae by zooplankton becomes

$$\frac{\partial P_4}{\partial t} = p_4 \frac{\partial c_z}{\partial t} = p_4 \mu_z c_z = \mu_z P_4 \qquad (2.6)$$

wherein μ_z is the growth rate of zooplankton due to the grazing of algae (see Section 2.4).

2.2.4 Excretion of Algae and Zooplankton

The excretion process of dissolved phosphorus by algae and zooplankton is a regeneration process of phosphorus from organic phosphorus. Although there are little or no data on the excretion of algae and zooplankton under field conditions, there are some excretion data from laboratory studies and *in situ* field measurements within enclosed systems. The excretion process is dependent of the feeding rate, density of algae or zooplankton, density and quality of the food, temperature, etc. (Hooper, 1972). For example, it was found (Martin, 1968) that the excretion of phosphorus by zooplankton is minimal when phytoplankton are abundant and *vice versa.* The reason for it is because phospholipids are being stored and/or used in egg production when food is abundant. When food is scarce, the stored lipids are used as energy source and phosphorus is then excreted.

If excretion rates are constant, the SRP increase due to excretion of algae and zooplankton will be proportional to the biomass of algae and zooplankton (Jørgensen, 1983a):

$$\frac{\partial P_1}{\partial t} = K_{ax} c_a + K_{zx} c_z \qquad (2.7)$$

wherein K_{ax} and K_{zx} are rate constants of excretion of SRP by algae and zooplankton, respectively.

2.2.5 Sorption-Desorption Reactions

Sorption-desorption processes play important roles in phosphorus dynamics in lakes and estuaries. Due to the fact that adsorbed phosphorus in sediments is generally two to three orders of magnitude higher than the phosphorus concentration in the water column, desorption of adsorbed phosphorus during a resuspension event can cause a significant increase of phosphorus concentration in the water column. On the other hand, sorption of phosphorus ions by sediment particles implies the removal of phosphorus from solution, an often used method in wastewater treatment.

The term *sorption* means either the process of *adsorption*, or the process of *absorption*, or both. If the conversion of phosphorus from soluble phase to solid phase is restricted to the surface, it is regarded as an adsorption reaction. An absorption reaction, on the other hand is the penetration of phosphorus into the solid phase. Since it is generally very difficult to distinguish these two reactions, the less specific term *sorption* is frequently used.

Sorption-desorption reactions of inorganic and organic phosphorus are influenced by temperature, pH value, and the concentration of dissolved oxygen (Berkheiser *et al.*, 1980). Sorption isotherms have been used to described the relationship between the amount of P sorbed and that remaining in water at a constant temperature in equilibrium conditions. The Freundlich and Langmuir equations (Berkheiser *et al.*, 1980) below are frequently used to represent sorption isotherms.

The Freundlich equation reads as

$$P_{ad} = K P_{dis}^{n} \tag{2.8}$$

where P_{ad} is the phosphorus sorbed per unit sediment particles, P_{dis} is the dissolved phosphorus concentration, and K and n are constants. This equation shows a linear relationship between adsorbed phosphorus (P_{ad}) and dissolved phosphorus (P_{dis}) in a log-log plot,

$$\log P_{ad} = n \log P_{dis} + \log K \tag{2.9}$$

On the other hand, the Langmuir equation shows a linear relationship between the reciprocal values of adsorbed and dissolved phosphorus:

$$\frac{1}{P_{ad}} = \frac{a}{P_{dis}} + \frac{1}{P_s}, \tag{2.10}$$

or

$$P_{ad} = \frac{P_s P_{dis}}{aP_s + P_{dis}} \tag{2.11}$$

where a is a constant related to the sorption energy and P_s is the maximum value of adsorbed phosphorus when P_{dis} goes to positive infinity. P_s is dependent on temperature and pH value.

Most water quality models assume that sorption-desorption reactions take place so quickly that the adsorbed and the dissolved phosphorus reach equilibrium instantaneously (e.g. Ambrose *et al.*, 1991; Dickinson and Huber, 1992). This may be a reasonable assumption when the time step of the water quality simulation is large compared to the time it takes to reach equilibrium. However, sometimes a water quality model may use a small time step during which the adsorbed and the dissolved phosphorus may not achieve equilibrium. In this case a kinetics model which describes the process rate is needed. As pointed out by Witkowski and Jaffe (1987), analytical chemists have repeatedly found that complete recovery of contaminants from soil/sediments frequently requires lengthy extraction periods, abrasive mixing, and strong solvents. These observations are in contradiction with the equilibrium models which assume that sorption-desorption reactions are accomplished instantaneously.

The frequently used kinetics models for sorption-desorption reactions are the first-order models (e.g., Berkheiser *et al.*, 1980):

$$\frac{\partial P_{ad}}{\partial t} = -D_r P_{ad} + S_r P_{dis} \tag{2.12}$$

where D_r is the desorption rate of adsorbed phosphorus and S_r is the sorption rate of dissolved phosphorus.

Because at equilibrium $\partial P_{ad}/\partial t = 0$, we have

$$\frac{S_r}{D_r} = \frac{P^o_{ad}}{P^o_{dis}} = P_c \tag{2.13}$$

where P^o_{ad} and P^o_{dis} are the adsorbed and dissolved phosphorus, respectively, at the equilibrium condition and P_c is the partition coefficient. Therefore, Equation (2.12) becomes

$$\frac{\partial P_{ad}}{\partial t} = -D_r(P_{ad} - P_c P_{dis}) \tag{2.14}$$

Wu and Gschwend (1988) developed a retarded intraparticle-diffusion model to simulate sorption-desorption kinetics of organic compounds. In their model, sediment particles making up of natural soils or sediments were viewed as porous spherical aggregates of finer grains in which macroscopically sorbed chemicals occur microscopically either sorbed to the natural organic matter on the solid matrices or freely dissolved in the intraparticle pore water. The diffusive penetration of hydrophobic compounds into or out of such particles is retarded by microscopic scale linear reversible sorption exchange between intraparticle pore water and adjacent solids. Wu and Geschwend's model seems to have a more solid theoretical background than the widely used first-order models. However, Wu and Geschwend's model for sorption-desorption is complicated to use in a water quality model. Furthermore, their model has no validation at all. They compared their model results to the results of the first order model. If the size distribution is not very wide, the retarded intraparticle diffusion model gives almost the same results as the first-order model (Wu and Geschwend, 1988).

2.3 Nitrogen Dynamics in Lakes and Estuaries

Nitrogen enters into lakes or estuaries from point and diffuse sources on the land, atmospheric diffusion, upwelling deep ocean, and biological fixation. The gaseous form of elemental nitrogen N_2 comprises about 78% of the atmosphere. Nitrogen is the major part of the atmospheric air. Although the gaseous form of nitrogen is relatively insoluble in water, it dissolves sufficiently so that nitrogen deficiences would never limit photosynthesis if N_2 were available for photoplankton assimilation.

Similar to phosphorus, nitrogen components in lakes or estuaries also include adsorbed organic nitrogen, soluble organic nitrogen (SON), ammonium nitrogen NH_4^+, adsorbed ammonium nitrogen, ammonia nitrogen NH_3, nitrate NO_3^-, and nitrite NO_2. As shown in Figure 2.1, kinetic pathways in the nitrogen cycle in lakes and estuaries are also shown, together with the relevant processes of hydrodynamics and sediment dynamics. This figure indicates that nitrogen in lakes and estuaries can undergo the following biological, chemical, and physical processes:

1. mineralization of organic nitrogen, i.e., ammonification of soluble organic nitrogen to ammonium-nitrogen,
2. nitrification of ammonium-nitrogen in the presence of oxygen; in this process, ammonium is first converted to nitrite and then converted to nitrate,
3. volatilization of ammonia-nitrogen,
4. denitrification of nitrate to gaseous nitrogen N_2 in the anaerobic sediment layer,
5. fixation of nitrogen N_2 by aquatic phytoplankton,
6. uptake of nitrate and ammonia by algae, and
7. conversion of algal particulate nitrogen to zooplankton particulate nitrogen due to grazing of algae by zooplankton.

Like the phosphorus cycle, the nitrogen cycle is influenced by the hydrodynamics and sediment dynamics in lakes and estuaries. For example, the resuspension of sediments from the bottom and the desorption process afterwards provide a significant pathway for nitrogen nutrient to enter into the water column, while the adsorption process and the deposition of sediment particles are major sinks for nitrogen in the water column. The vertical turbulent mixing not only transports the resuspended nitrogen from the near bottom layer to the top layer of the water column, but also influences the desorption/adsorption reactions of nutrients from/onto suspended sediments because of the flocculation and breaking of sediments caused by the turbulence. The following is a brief review of nitrogen dynamics in lakes and estuaries. Because of the similarity to those in the phosphorus cycle, nitrogen kinetic pathways associated with algae and zooplankton are omitted in the discussion.

2.3.1 Ammonification

Ammonification is the biological process of formation of ammonium from soluble organic nitrogen. It is the first step of nitrogen mineralization, in which organic nitrogen is converted to the more mobile, inorganic state. The mineralization process is a pathway of regenerating the nutrient in a form usable by plants.

Ammonification is actually the decomposition process of soluble and particulate nitrogen compounds of dead organisms and those excreted by plants and animals. This decomposition process is brought about by the various species of proteolytic bacteria. Generally, the decomposition is quite efficient, and at no time does any substantial concentration of free or combined dissolved amino acids build up. However, some particularly stable organic nitrogen compounds resist attack by bacteria and eventually sink to the bottom where they are incorporated into the sediments.

The rate of ammonification is often expressed as a first-order reaction (Rao *et al.*, 1984):

$$\frac{\partial N_1}{\partial t} = -K_4 N_1 \tag{2.15}$$

wherein, K_4 is the rate constant of ammonification which is a function of water temperature, pH, and C/N ratio of the residue (Reddy and Patrick, 1984).

2.3.2 Nitrification

The second step of mineralization of organic nitrogen is nitrification, in which nitrite is formed by the oxidation of ammonium and is further oxidized to nitrate:

$$NH_3 + 3/2O_2 \rightarrow HNO_2 + H_2O \tag{2.16}$$

$$HNO_2 + 1/2O_2 \rightarrow HNO_3 \tag{2.17}$$

Nitrification requires oxygen as the electron acceptor and thus can only occur in an aerobic condition, i.e. in the water column and in the aerobic layer of the sediment column. This pathway is typically associated with the metabolism of certain bacteria. Two groups of bacteria are distinguished: one derives its energy for cell synthesis by the oxidation of ammonium, the other by the oxidation of nitrite. The dominant species of the former group is *Nitrosomonas*, while the latter group is *Nitrobacter*. In most cases, species of *Nitrosomonas* and *Nitrobacter* are found together; otherwise nitrite might accumulate to phototoxic levels.

Several models for the nitrification have been proposed: (1) zero-order equation, (2) first-order equation, and (3) Monod equation of population dynamics. Some researchers (e.g. Srinath *et al.*, 1976) found that the nitrification rate is independent of the substrate concentration N_{ii}:

$$\frac{\partial N_{ii}}{\partial t} = -K_3 \tag{2.18}$$

where N_{ii} is the concentration of soluble NH_4^+-N and K_3 is the nitrification rate coefficient. Others (e.g. Broadbent and Clark, 1965) showed that the nitrification rate is indeed a linear function of the substrate concentration:

$$\frac{\partial N_{ii}}{\partial t} = -K_3 N_{ii} \tag{2.19}$$

Because the rate of nitrification is determined by the growth rate of nitrifying bacteria,

$$\frac{\partial N_{ii}}{\partial t} = -\alpha_n \mu_n \tag{2.20}$$

where α_n is a constant and μ_n is the growth rate of nitrifying bacteria, Stratton and McCarty (1969) and Garland (1978) used the Monod expression for the rate of nitrifying bacterial growth in natural streams such as the Clinton River and Trent River,

$$\mu_n = \mu_{n_{max}} \frac{N_{ii}}{H_{n_2} + N_{ii}}. \tag{2.21}$$

where $\mu_{n_{max}}$ is the maximum growth rate of nitrifying bacteria and H_{n_2} is the half-saturation constant for the bacterial growth. The nitrification rate is therefore

$$\frac{\partial N_{ii}}{\partial t} = -\alpha_n \mu_{n_{max}} \frac{N_{ii}}{H_{n_2} + N_{ii}}. \tag{2.22}$$

The Monod equation gives a continuous transition between zero-order kinetics and the first-order kinetics based on the substrate concentration of ammonium. For N_{ii} much lower than H_{n_2}, it approaches the first-order equation; and for N_{ii} much higher than H_{n_2}, it approaches the zero-order equation. Since the H_{n_2} value is typically smaller than N_{ii} in natural aquatic systems, zero-order kinetics were often used in the previous studies (e.g. Hall and Murphy, 1980; Watanabe *et al.*, 1980).

2.3.3 Denitrification

The microbial reduction of nitrite and nitrate with the liberation of molecular nitrogen and nitrous oxide is called denitrification. Denitrification is essentially a respiratory mechanism in which nitrate replaces molecular oxygen, i.e., nitrate respiration. The end product of denitrification is the gaseous form of elemental nitrogen N_2, which can escape to the atmosphere. Therefore, this process is a sink for nitrate. However, denitrification is not the sole sink of nitrate. Another sink is the utilization of nitrate as a nutrient source of plants (this may be termed nitrate assimilation). Both transformations involve reductive pathways, but the end products of nitrate respiration are volatilized while the products of nitrate assimilation are incorporated into the cell material.

Denitrification process in lakes and estuaries is associated with denitrifying bacteria such as *Pseudomonas denitrificans*, which use NO_3^- as an electron acceptor to oxidize organic matter anaerobically, releasing N_2 gas by the following reaction (Day *et al.*, 1989):

$$5C_6H_{12}O_6 + 24HNO_3 \rightarrow 30CO_2 + 42H_2O + 12N_2 \tag{2.23}$$

In fact, this reaction consists two steps. In the first step of denitrification, nitrous oxide N_2O is produced from NO_3^- by denitrifers:

$$C_6H_{12}O_6 + 6HNO_3 \rightarrow 6CO_2 + 9H_2O + 3N_2O \tag{2.24}$$

Nitrous oxide, which is produced as an intermediate product in denitrification, is unavailable for phytoplankton assimilation. Anthropogenic acceleration of N_2O production could result in a general heating of earth's atmosphere because N_2O reacts with and breaks down atmospheric ozone O_3 which normally helps maintain the earth's heat balance (McElroy *et al.*, 1978).

While nitrification occurs in the water column and the aerobic layer of the sediment column, denitrification occurs only in the anaerobic layer of the sediment column. The nitrate used in the denitrification process comes from the water column and the aerobic layer by diffusion between the aerobic and anaerobic layers. Seitzinger (1988) reviewed various studies on the denitrification process in freshwater and coastal marine ecosystems. He found that the major source of nitrate for denitrification in most river, lake, and marine sediments comes from the nitrification process in the sediments, not the diffusion of nitrate from overlying water into the sediments. Denitrification accounts for a major portion of loss of mineralized nitrogen during the mineralization of SON in sediments. In rivers and lakes, 76-100% of nitrogen flux across the sediment-water interface is N_2, but only 5-70% in estuarine and coastal marine sediments because of the presence of salinity (Heath, 1992).

Denitrification can be measured directly as total N_2 production from degassed sediments. However, because N_2 is very abundant in the atmosphere, long incubations (about one week) are needed to obtain significant N_2 concentration changes. The process can also be measured indirectly as N_2O production in the presence of acetylene which inhibits the reduction of N_2O to N_2.

The denitrification process can be described by a zeroth-order rate equation, a first-order rate equation, or the standard Michaelis-Menten equation. Dawson and

Murphy (1972) found that the denitrification is of zeroth-order

$$\frac{\partial N_3}{\partial t} = -K_2 \tag{2.25}$$

wherein N_3 is the concentration of nitrate and K_2 is the denitrification rate constant.

Stanford *et al.* (1975) found the denitrification to be first-order at low nitrate nitrogen concentration. Reddy *et al.* (1978) also showed that under carbon-limiting conditions the denitrification followed the first-order kinetics:

$$\frac{\partial N_3}{\partial t} = -K_2 N_3 \tag{2.26}$$

Bowman and Focht (1974) showed that the denitrification followed the Michaelis-Menten kinetics:

$$\frac{\partial N_3}{\partial t} = -K_{2_{max}} \frac{N_3}{H_{n_3} + N_3} \tag{2.27}$$

where $K_{2_{max}}$ is the maximum denitrification rate and H_{n_3} is the half-saturation constant for denitrification.

2.3.4 Nitrogen Fixation

Nitrogen fixation is a biological process by which organisms reduce N_2 gas to ammonia. This process is brought about by free-living bacteria or blue-green algae. It is an energy-intensive anaerobic reaction:

$$N_2 + 3H_2 \rightarrow 2NH_3 \tag{2.28}$$

Quantitative estimation of the flux rate of nitrogen fixation in the nitrogen cycling is quite uncertain, because this process is governed by a number of physical and chemical factors. For example, if ammonium is abundant in the system fixation can be inhibited because bacteria and algae use the nitrogen salt rather than N_2. pH value can affect nitrogen fixation because the abundance of certain organisms such as *Azotobacter* is characteristically sensitive to pH value. Temperature also has a profound influence on N_2 fixation. There is little activity at low temperature and warming promotes the microbial uptake of N_2.

In lakes and other fresh water systems, N_2 fixation may represent a major component in the overall nitrogen budget and this pathway commonly contributes 30 to 80 percent of the total annual nitrogen income for an entire water body (Horne, 1978). However, in estuarine waters, N_2 fixation tends to be relatively unimportant for overall nitrogen budgets except in specialized environments. The reason why the N_2 fixation in estuaries is commonly less important than in lakes is uncertain. One possible reason may be because of the relative high ammonium concentration. However, coastal waters containing low ammonium concentration still have little N_2 fixation. There has been some suggestion that turbulent mixing may cause sufficient stress to destroy the structure of delicate heterocysts (Fogg, 1978). Another possibility suggested by Howarth and Cole (1985) is that the high sulfate concentration in sea-water compared to freshwater may inhibit the ability of nitrogen-fixers to obtain sufficient quantities of molybdenum needed for synthesis of nitrogenase.

2.3.5 Nitrogen Volatilization

The dissolved form of ammonium in water is generally not stable and can exist in its gaseous form or ammonia (NH_3). Because the ammonia concentration in the atmosphere is very low, ammonia in the water column can escape to the air. This is the volatilization process of ammonia. The volatilization of ammonia is a sink for nitrogen in an aquatic system. This process is dependent on the pH value, as can be seen from the following reaction:

$$NH_4^+ \rightarrow NH_3 + H^+ \tag{2.29}$$

$$\frac{[NH_3]}{[NH_4^+]} = \frac{K_a}{[H^+]} \tag{2.30}$$

or

$$\log_{10}(\frac{[NH_3]}{[NH_4^+]}) = pH - pK_a \tag{2.31}$$

where K_a is the dissociation constant for ammonium ion and $pK_a = -\log_{10} K_a$ is 9.3.

It can be seen from Equation (2.31) that ammonia only consists a small portion of the total ammonia and ammonium at neutral pH and that ammonia concentration equals ammonium concentration at $pH = pK_a$=9.3.

During the summer months, a pH value higher than 9.0 can be found in some very eutrophic lakes. For example, a pH of 11.0 has been reported in the shallow Sollerod Lake of Denmark (Jørgensen, 1989). In this case, the volatilization of ammonia can be very significant.

A first order rate equation can be used to describe the kinetics of the ammonia volatilization process:

$$V_{N_4} = v_{an}(h_v N_4 - N_4^a) \tag{2.32}$$

where N_4 is the concentration of ammonia nitrogen at the top layer of the water column, N_4^a is the ammonia concentration in the air, v_{an} is the rate constant of volatilization, and h_v is Henry's constant.

Equation (2.32) can be derived from the so-called *two-film* model (Jørgensen, 1983c), which is often used in chemical engineering. The basic idea of a two-film model assumes that a stagnant liquid film of thickness dL and a stagnant gas film of thickness dG exist at the water-air interface (Figure 2.2). The transport of a volatile component through these films is due to the diffusion

$$V_w = K_w(N_4^w - N_{4i}^w) \tag{2.33}$$

$$V_g = \frac{K_g}{RT}(N_{4i}^a - N_4^a) \tag{2.34}$$

wherein V_w and V_g are the rates at which ammonia is transported across the water film and the air film, respectively, K_w and K_g are transfer coefficients of water film and air film, respectively, T is the absolute air temperature, and R is the gas constant.

V_w and V_g should be equal because of the mass conservation across the two films. By using Henry's law,

$$N_{4i}^a = h_v N_{4i}^w \tag{2.35}$$

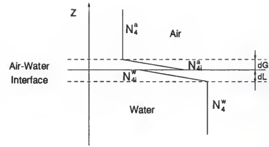

Figure 2.2: The two-film model for the volatilization.

we get

$$V_{N_4} = V_w = V_g = \frac{K_w K_g}{RTK_w + h_v K_g}(h_v N_4^w - N_4^a) \tag{2.36}$$

or

$$v_{an} = \frac{K_w K_g}{RTK_w + h_v K_g} \tag{2.37}$$

in Equation (2.32).

2.4 Algal and Zooplankton Growth

2.4.1 Algal Growth

For an aquatic system with steady nutrient, temperature, and light intensity, the growth of algae is exponential: one single cell gives two, and two cells give four cells, etc. In other words, the rate of growth is proportional to the number of cells at any time:

$$\frac{dM}{dt} = \mu_a M \tag{2.38}$$

where M is the number of algal cells and μ_a is the growth rate constant, which is a function of temperature, light intensity, and nutrient concentration. In a phosphorus-limiting aquatic system, the growth rate constant μ_a of algae may be described by an empirical equation as e.g. of Monod (1949)

$$\mu_a = \mu_{a_{max}} \frac{P_1}{H_p + P_1} \tag{2.39}$$

where H_p is the half-saturation concentration of SRP for algal growth and $\mu_{a_{max}}$ is the maximum growth rate of algae. $\mu_{a_{max}}$ is dependent on temperature and light intensity. An example of Equation (2.39) is shown in Figure 2.3 (Golterman, 1975).

If nitrogen is also limiting in the system, Equation (2.39) becomes

$$\mu_a = \mu_{a_{max}} \frac{P_1}{H_p + P_1} \frac{N_3 + N_4}{H_n + N_3 + N_4} \tag{2.40}$$

where H_n is the half-saturation concentration of nitrogen for algal growth.

The growth rate of freshwater algae (e.g., *Cyanobacteria*) can be affected by salinity toxicity. Cerco and Cole (1992) used an empirical equation to represent the effect of salinity on freshwater Cyanobacteria growth:

$$f(S) = \frac{S_t^2}{S_t^2 + S^2} \tag{2.41}$$

where S is salinity (*ppt*) and S_t is the salinity at which Microcystis growth is halved.

Some researchers (e.g., Jørgensen, 1976) argued that the growth rate of algae is more likely dependent on the internal nutrient content of the cell as defined by the cell quota concept (Equation (2.42)). According to the cell quota model, external nutrients is taken up by the cell and stored; subsequent cell growth is dependent on the internal nutrient concentrations in the cell. The advantage of this model over Monod kinetics is that the uptake of nutrients and cell growth are decoupled. Here,

$$\mu_a = \mu_{a_{max}} \frac{Q_c - q_o}{Q_c} \tag{2.42}$$

where Q_c is the cell quota and q_o is the minimum cell quota, or the subsistence cell quota at zero growth rate.

The external nutrients and cell quota formulations are equivalent if the internal cell concentration is assumed to be in dynamic equilibrium with the external concentration (Di Toro, 1980). Di Toro (1980) estimated that the uptake of internal cell

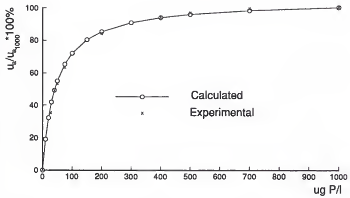

Figure 2.3: Relative growth rate of algae in a phosphorus limiting aquatic system.

storage occurs in 0.125 – 0.5 of the time required for the uptake of external nutrients. The internal cell concentrations are thus in dynamic equilibrium with the external concentration. Equation (2.42) is difficult to use directly since the cell quotas and minimum cell quotas are species specific. However, this difficulty can be avoided by expressing μ_a as a function of internal phosphorus, nitrogen, and chlorophyll *a* concentrations (Riley and Stefan, 1988):

$$\mu_a = \mu_{a_{max}} \frac{P_c - C_a P_{min}}{P_c} \frac{N_c - C_a N_{min}}{N_c} \tag{2.43}$$

where P_c and N_c are internal concentrations of phosphorus and nitrogen, respectively; P_{min} and N_{min} are the minimum ratios of phosphorus to chlorophyll *a* and nitrogen to chlorophyll *a*, respectively, for algal growth; and C_a is the concentration of chlorophyll *a*.

Algal biomass is typically represented by chlorophyll *a*, which can be measured fluorometrically. The ratio of chlorophyll *a* to carbon in algal cell is about 0.01 to 0.02, which is almost the same as the ratio of phosphorus to carbon in algal cell

(OECD, 1982). The final concentration of algal biomass c_a is dependent on the algal growth rate μ_a, the respiration rate r_a, the mortality of algae K_{as}, the grazing rate g_z by zooplankton, and the settling rate of algae w_s^a:

$$\frac{\partial c_a}{\partial t} = \mu_a c_a - r_a c_a - K_{as} c_a - g_z + \frac{\partial w_s^a c_a}{\partial z} \tag{2.44}$$

2.4.2 Growth of Zooplankton

Zooplankton play an important role in the recycling of phosphorus and nitrogen in lakes and estuaries by uptaking algae and excreting phosphorus and nitrogen after ingesting algae. Zooplankton grazing of algae enhances the cycling speed of phosphorus and nitrogen. Devol (1979) found that zooplankton can be a major supply of SRP to algae during periods of low SRP concentrations. Additionally, the selective zooplankton grazing of green algal cells shifts the algal population towards blue-green algal domination in the summer.

The growth of zooplankton in lakes and estuaries is determined by its present abundance, its grazing rate, and the efficiency with which it converts algal carbon into zooplankton carbon. The eating mechanism of zooplankton differs greatly among zooplankton species (nonselective filters, selective filters, and raptors). Nonselective filters eat algae by grazing with a constant rate, regardless of algae concentration. Selective filters eat algae by grazing, but have developed an ability to vary their filtering rate. The filtering rate increases as the concentration of algal biomass decreases, but approaches a fixed filtering rate which is determined by the physical characteristics of selective filters. If the algal concentration is high, selective filters can alter their particle-size selectivity and lower their filtering rate, and thus make more efficient use of algae and conserve energy. A formulation for the filtering rate μ_S has been proposed by Canal *et al.* (1976):

$$\mu_S = \mu_{S_{max}} \frac{S_m c_a + A_h}{c_a + A_h} \tag{2.45}$$

where $\mu_{S_{max}}$ is the maximum filtering rate of selective filters (dependent on temperature), S_m is the minimum filtering rate multiplier, A_h is the algal concentration when the multiplier is $(1 + S_m)/2$, and c_a is the concentration of algal biomass.

The growth rate of selective filters is then

$$\frac{\partial C_S}{\partial t} = \mu_S C_S \tag{2.46}$$

where C_S is the concentration of selective filters.

Raptorial species eat algae by selecting, snatching, and devouring. The eating rate of raptorial species increase with the concentration of algal biomass but reaches a saturation level. The mathematical formulation for the eating rate μ_R of raptors can be expressed in a Monod form (Canal *et al.*, 1976):

$$\mu_R = \mu_{R_{max}} \frac{c_a}{c_a + H_a} \tag{2.47}$$

where H_a is the half-saturation algal level for raptors and $\mu_{R_{max}}$ is the maximum snatching rate of raptors. $\mu_{R_{max}}$ is a function of temperature.

2.4.3 Algal Non-Predatory Mortality

Algal mortality involves the conversion of algal phosphorus and nitrogen to biologically available nutrients. This can be conceived as a two step process (DePinto *et al.*, 1986). First, algal death and lysis of the cell membrane releases any stored excess inorganic phosphorus and nitrogen. DePinto *et al.* (1986) found that cellular phosphorus exceeding the minimum cell quota was released in an available form rapidly after cell death and lysis. Lysed material is usually 20-50 percent of the cell's organic content (Cole, 1982), and this excess inorganic phosphorus is immediately available for algal uptake. Secondly, bacteria mineralize the remainder of the cell organic phosphorus to available phosphorus.

The non-predatory mortality of algae can be modeled by a first-order equation (Gargas, 1976):

$$\frac{\partial c_a}{\partial t} = -K_{as} c_a \tag{2.48}$$

where K_{as} is the mortality rate of algae and is temperature-dependent.

2.4.4 Algal Settling

Nutrient loss to sediments is a significant fraction of the total incoming nutrient load from rivers or oceans in lakes and estuaries. The loss to sediments is via two main mechanisms: (1) algal sedimentation and (2) non-algal nutrient sedimentation. Some of the nutrients are regenerated and later mixed with the water column due to biologic movement and sediment resuspension.

Different algal classes may have different settling velocities. Takamura and Yasuno (1988) measured algal sinking rates in a shallow hypereutrophic lake and found blue-greens to settle much slower than green and diatom algae. The sinking rate of senescent algae was much higher than algae in exponential growth. Diatoms sank as living cells and blue-greens sank as detritus. The cell structure of the blue-green algae *Microcystis* collapsed rapidly after losing its function of carbon fixation (Takamura and Yasuno, 1988).

Since algal radius is generally in the order of μm's, algae can undergo flocculation, just like normal sediment particles (Section 3.4). Alldredge and Gotschalk (1988) reported the formation of flocs, known as marine snow or aggregates, after diatom blooms in marine water. Riehesell's (1991) studies in the North Sea show that flocculation is an important mechanism for determining the fate of organic matter produced after the algal bloom. Recently, Jackson and Lochmann (1992) studied the effect of coagulation on nutrient and light limitation of an algal bloom. Their major conclusions are (1) loss of algal cells to coagulating particles can occur when algal cells are growing at a fairly constant rate, placing a cap on the concentrations that algae can achieve and (2) the vertical flux of algae from the top layer is enhanced when flocculation occurs.

In contrast to the settling, algae can also have buoyancy. The mechanisms an algal cell uses to control buoyancy are very complicated. Blue-green algae use three mechanisms to control buoyancy: (1) cell pressure increases at high light intensities causing the collapse of cell gas vacuoles and decreased buoyancy; (2) algae alter the rate of gas vacuole synthesis in response to the cell C/N internal ratio (a low C/N ratio increases gas vacuole synthesis); and (3) the cell may accumulate high-density storage products that act as ballast and affect cell buoyancy (Spencer and King, 1989). Some blue-green algae that use one or more of these mechanisms are ***Anabaena sp.***, ***Aphanizomenon flos-aque***, ***Microcystis***, ***Oscillatoria***, and ***Nostoc muscorum***.

2.5 Effects of Temperature and Light Intensity on Nutrient Dynamics

2.5.1 Temperature

In the nutrient cycles shown in Figure 2.1, almost all of the transformation processes are affected by temperature. Generally speaking, temperature will accelerate the processes. For example, the desorption rate of inorganic phosphorus from sediment particles increases as temperature increases. However, exception also exist. For example, many investigations have confirmed that the nitrification rate below $5°C$ and above $40°C$ is very slow. The maximum rate of nitrification lies between 30 and $35°C$. The reason for this is presumably because of physiological differences in dominant bacterial strains (Alexander, 1965).

The effect of temperature on reaction rates can be explained by the Van't Hoff-Arrhenius equation as follows:

$$\frac{d(lnK)}{dT} = \frac{\Delta H}{RT^2} \tag{2.49}$$

where K is the reaction rate at temperature T, ΔH is the amount of heat required to bring the molecules of the reactant to the energy state required for the reaction, and R is the universal gas constant.

Integrating Equation (2.49) from temperature T_1 to T_2 gives:

$$\frac{K_2}{K_1} = \exp[\frac{\Delta H}{RT_1T_2}(T_2 - T_1)] \tag{2.50}$$

Since $\exp(\frac{\Delta H}{RT_1T_2})$ is almost constant at the temperature range of interest (0 – 30 ^0C), we have (Chen and Orlob, 1975)

$$K(T) = K_{20}\theta^{T-20} \tag{2.51}$$

wherein $K(T)$ is the rate constant at temperature T, K_{20} is the rate constant at $20C^o$, and θ is a unitless temperature coefficient ranging from 1.0 to 1.1.

For some biological processes, Equation (2.51) can not appropriately describe the temperature-dependency because the growth of organisms may stop below or above certain temperature but reaches maximum at an optimum temperature. This phenomenon has been studied by some researchers. For example, Lassiter and Kearns (1974) proposed a formula as follows:

$$K(T) = K_{opt}exp[a(T - T_{opt})](\frac{T_{max} - T}{T_{max} - T_{opt}})^{a(T_{max}-T_{opt})} \tag{2.52}$$

wherein K_{opt} is the rate constant at optimum temperature, T_{opt} is the optimum temperature, T_{max} is the maximum temperature at which the rate constant is zero, and a is a coefficient with the unit $^oC^{-1}$.

2.5.2 Light Intensity

Light Intensity affects the photosynthesis process and thus the algal growth rate. As will be discussed later, one of the effects of sediment resuspension on nutrient cycling is that resuspended sediment will reduce the light penetration and weaken the photosynthesis process in the water column.

The effects of light intensity on nutrient cycling is often modeled by a light intensity limiting function as follows (Steele, 1974):

$$f_2(I) = \frac{I}{I_s} e^{1-\frac{I}{I_s}} \tag{2.53}$$

where I is the light intensity and I_s is the optimum light intensity for algal growth.

According to Beer-Lambert's law light adsorbed as it passes through a solute or solution is proportional to the light intensity and the optical path length:

$$-\Delta I = \varepsilon \Delta z I \tag{2.54}$$

where the extinction coefficient ε is a function of suspended sediment concentration and algal concentration in the water column:

$$\varepsilon = f(c, c_a) \tag{2.55}$$

If ε is constant over the water depth, then the light intensity over the water depth is

$$I(z) = I_o e^{-\varepsilon z} \tag{2.56}$$

where $I(z)$ is the light intensity at depth z and I_o is the light intensity at the water surface.

2.6 Effects of Hydrodynamics and Sediment Processes on Nutrient Dynamics

Water and sediment particles are carriers of nutrient species in lakes and estuaries. Thus the transport and transformation processes of nutrients as discussed in Section 2.2 and 2.3 are thus closely linked with the dynamics of the water movement and the sediment transport processes. For example, as shown in Figure 2.1, nitrogen cycling is connected to hydrodynamics and sediment dynamics as follows:

- Organic nitrogen contained in the soil particle is hrought from the soil surface to the water column due to the excess of bottom shear stress over the critical shear stress of the bed.
- In the water column, part of the organic nitrogen on particles can change into dissolved form due to desorption because the resuspended sediment particles

contain a large amount of organic nitrogen. This process will not stop until the concentration of organic nitrogen on sediment particles and the soluble organic nitrogen (SON) in water reaches equilibrium.

- Ammonium NH_4^+ can be adsorbed onto the clay particle due to electrical attraction and be nitrified to nitrate NO_3^- due to the presence of O_2 in the water column.
- In the water column, nitrogen species are mixed due to the turbulence mixing process. As a result, the vertical distributions of dissolved nitrogen components become more uniform.
- If adsorbed nitrogen concentrations are lower than their equilibrium values, sediment particles will adsorb nitrogen species in dissolved form.
- Through the settling of sediment particles, nitrogen will fall back to the bottom. In this case sediment particles act like a sink.

Another important effect of hydrodynamics and sediment transport on nutrient budget in lakes and estuaries is the horizontal transport due to advection and diffusion. Adsorbed and dissolved forms of nutrient species are transported by currents from one part of a lake or an estuary to another part. During this process, dissolved nutrients can generally follow the the current circulation, while nutrients in adsorbed (particulate) form can be transported and deposited to the bottom with sediment.

The resuspension of bottom sediments is an important mechanism controlling the nutrient regeneration in lakes and estuaries. It is often found that the nutrient concentration in the bottom sediments is one or two orders of magnitude higher than that in the water column (Simon, 1988 and 1989). McClelland (1984) produced a nutrient box model for Tampa Bay and found that all point and non-point sources accounted for only one-third of the nitrogen released from the sediments. Adding inputs from the point and non-point sources to the diffusive benthic flux still only accounted for about 50% of the nitrogen needed to support the observed primary production. McClelland suggested that other sources supply the nitrogen via sediment resuspension and *in-situ* water column regeneration. Johansson and Squires (1989) computed a preliminary nutrient budget for Tampa Bay and concluded that internal loading of nitrogen associated with sediment resuspension events can be quite significant.

In an episodic storm event, large amount of nutrients can be brought into the water column with sediment due to large current or wave induced bottom shear stress. In the water column, because of the relatively higher redox potential, stronger mixing, and sufficient light, some transformation (e.g., nitrification) processes of nutrients can occur faster than those in the bed. Therefore, the resuspension of sediment from bottom not only increases the nutrient concentration in the water column, but may also accelerate the nutrient cycling. Because the time scale of sediment dynamics is much smaller than that of the transformation processes, the effect of resuspension of bottom sediment on nutrient cycling is very significant. On the other hand, since the food chain in lakes and estuaries is built by the constant nutrient cycling between water column and benthic sediment, it is very important to clarify the role of benthic sediment fluxes in the cycling of nutrients.

It is problematic to quantify the benthic flux due to the competing influences of molecular diffusion, resuspension, and ground water seepage, and difficulties in quantifying each one of them. Some past water quality modeling studies (e.g., HydroQual, 1987) treated the net benthic flux as an adjustable parameter in the model, which was adjusted to achieve a reasonable fit between model results and limited data. Thus, the conventional empirical treatment does not lead to a robust estimate of the benthic flux and introduces major uncertainty in the use of the water quality model as a predictive and management tool. A definitive model of benthic flux is needed to significantly reduce the uncertainty of water quality models. Harleman (1977) simply ignored the exchange of nitrogen between sediment and water. Lam and Jaquet

(1976) proposed an empirical formula for computing the upward flux of phosphorus due to the wind-wave induced sediment resuspension in Lake Erie,

$$J = k\rho_w \frac{\rho_w}{\rho_s - \rho_w} w_e \tag{2.57}$$

where k is a constant, ρ_w and ρ_s are water density and dry sediment density, respectively, and w_e is the excess wave orbital velocity. Beck and Somlyody (1982) assumed a simple relationship between wind speed W and w_e, and proposed

$$J = k_1\rho_w \frac{\rho_w}{\rho_s - \rho_w} W^m \tag{2.58}$$

for Lake Balaton, where k_1 and m are constants. Lam *et al.* (1983) used Equation (2.57) in a simplified Lake Erie phosphorus model for the Western Basin.

There have been a limited number of studies of nutrient cycling between benthic sediments and water column in estuaries (Simon, 1988 and 1989; Kemp *et al.*, 1982) and lakes (Sheng *et al.*, 1989a; Sheng, 1993; Reddy and Graetz,1989). Simon's studies strongly suggested that during periods of sediment resuspension, desorption of ammonium from sediment solids can be the major pathway for enriching the water column in a shallow estuary. However, Simon's resuspension experiment was conducted in laboratory rather than in the field. The field studies of Sheng *et al.* (1989a and 1989b). and Reddy and Graetz (1989) confirmed that particulate phosphorus in water column increased significantly during sediment resuspension events in a shallow lake. Recent studies by Simon (1989) and Sheng (1993) show that the resuspension flux of nutrient in shallow water is typically 2 to 3 orders of magnitude larger than the diffusive flux from the bottom. Simon's study in the Potomac estuary found that particulate forms of nutrient deposited onto the bottom sediments in the upper reaches became resuspended and released into the water column a season later.

In addition to generating benthic flux of nutrients, sediment resuspension can also affect algal populations by adsorbing the incoming light from the water surface and reducing light penetration through the water column. High sediment resuspension may result in dramatic reduction of light intensity and thus affect the rate of photosynthesis.

Because hydrodynamics and sediment dynamics can directly contribute to nutrient transport and nutrient regeneration in lakes and estuaries, the study of nutrient dynamics should be coupled with the study of hydrodynamics and sediment dynamics. The U.S. E.P.A. developed a water quality model called WASP5 (Ambrose *et al.*, 1991), which assumed that lakes or estuaries consist of a few boxes and solved the nutrient equations for each box. However, the coupling of nutrient dynamics with hydrodynamics and sediment dynamics in this model is rather poor because a few box can not give a good resolution to hydrodynamics and sediment dynamics in lakes and estuaries. In addition, WASP5 generally uses a large time step (a few hours to a day), which can be larger than the time scale of hydrodynamics and sediment transport processes. Because of the poor resolution of hydrodynamics and sediment dynamics, the prediction ability of WASP5 model is questionable. Harleman (1977) used a one-dimensional model to simulate ammonia concentrations in an idealized estuary. Two cases were studied: one with the real-time tidal current, and the other with through-flow velocity due to freshwater inflow. He found that ammonia concentrations predicted in the latter case (through-flow) differ by as much as 100 percent from the real-time tidal averages even though the same biochemical model is used. This indicates that the consideration of short-term hydrodynamics and sediment transport processes is very important in a water quality model.

To study phosphorus dynamics in Lake Okeechobee with real-time hydrodynamic and sediment transport processes, Dickinson *et al.* (1992) developed a 3-D phosphorus model, which coupled with a 3-D model of hydrodynamics and sediment dynamics developed by Sheng *et al.* (1991). The time step used in the 3-D phosphorus model was the same as that in the 3-D model of hydrodynamics and sediment transport processes. The transformation processes considered in their model were similar to the WASP5 model except for that Dickinson *et al.* differentiated algae into three groups (green, blue-green, and diatom). However, since no data exists for each of the algal groups thus differentiation has not been validated yet. Same as WASP5, Dickinson *et al.* assumed instantaneous equilibrium between dissolved and adsorbed nutrients, which is not necessary true in many cases (Witkowski and Jaffe, 1987).

2.7 Conclusions

It is very difficult to study the transport/transformation processes of nutrients in lakes or estuaries for the following reasons:

- The measurement and analysis of nutrient species generally takes a very long time and sometimes can only be done in laboratories. To date, there is still no method available to measure the instantaneous variations of different nutrient concentrations in lakes or estuaries. As a result, the measured data may lack dynamics.
- Nutrient cycles in lakes or estuaries are influenced by hydrodynamics and sediment transport processes. Hydrodynamics and sediment dynamics in lakes and estuaries are very complicated.
- Transformation processes are affected by algal activities, aquatic plants, microbial communities and other biochemical factors. Quantitative relationships between many of these factors and the nutrient cycles are still unknown.
- Nutrient cycles are also affected by geological factors such as soil texture and cation exchange capacity (CEC) of soil. For example, CEC affects not only particle aggregation, but also the kinetics of NH_4^+ and the volatilization process of NH_3.
- Nutrient transformations in lakes and estuaries are generally mediated by different bacteria. The activities of these bacteria are often determined by the partial pressures of other species such as oxygen and carbon.

- Meteorological factors (wind, humidity, temperature, sunshine etc.) can also alter nitrogen cycling either directly or indirectly. There is not enough data to quantify these complicated effects.

Because of the these difficulties, numerical modeling for nutrient dynamics in lakes and estuaries is still in its infancy, although a lot of models have been developed (see, for example, the book edited by Jørgensen and Gromiec in 1989). None of the existing numerical models for nutrient dynamics has the real ability of predicting an event, particularly a short-term event. Some models may fit field data well, but are generally site-specific because of the assumptions contained in these models may not be correct for other aquatic systems. Moreover, because of the lack of complete understanding of all the processes involved in nutrient cycles, many model parameters have to be tuned to fit field data.

CHAPTER 3
HYDRODYNAMICS AND SEDIMENT DYNAMICS IN LAKES AND ESTUARIES

As mentioned previously, biological processes in an ecosystem such as a lake or an estuary are strongly affected by hydrodynamics and sediment transport processes. For example, the amount of nutrient resuspended during an episodic event could be as high as the total amount of dissolved nutrient diffused from the bottom due to molecular diffusion over a period of a few months or even a few years (Simon, 1989). The resuspension of sediments was found to be a dominant factor controlling the nutrient budget in an estuary or a lake. Therefore, as the first step to study nutrient cycling in an estuary or a lake, hydrodynamics and sediment transport processes should be investigated and understood. Important hydrodynamics and sediment transport processes affecting nutrient dynamics in lakes and estuaries include circulation, wave action, wave-current interaction, erosion, deposition, settling, flocculation, and consolidation. This chapter reviews all these processes.

3.1 Circulation

Circulation is the physical process of water movement in a lake or an estuary. Circulation in a lake is generally wind-driven. In a large lake, differential heating over the lake can sometimes result in horizontal density-driven circulation. Circulation in an estuary could be driven by tide, wind, and density gradients.

Estuarine circulation induced by the horizontal density gradient between fresh water and salt water is often refered to as gravitational circulation (Hansen and Rattray, 1966). Fresh water runoff, which is less dense than salt water in the ocean side of the estuary, tends to stay at the surface layer of the estuary and flows towards the ocean. The salt water remains at the bottom layer of the estuary and has the tendency of flowing upstream because of the horizontal density gradient. The stratification in an estuary can be described by Harleman's estuary number which is defined as: PFr^2/RT, where P = tidal prism = amount of ocean and river water entered into the estuary in one tidal cycle, Fr^2 is the Froude number defined as $\frac{U_o}{\sqrt{gh}}$, R is the river discharge rate, T is the tidal period, U_o is the maximum flood velocity, and h is the mean water depth. For well-mixed estuary, tidal range is generally large and the river discharge is generally low. Therefore, a well-mixed estuary has large Harleman's estuary number. Detailed discussion and study of this "gravitational circulation" can be found in Pritchard (1956), Hansen and Rattray (1966), and Dyer (1973).

Tidal circulation is the water movement driven by tides at the mouth of the estuary. If the tidal range is large and the river flow is low, tide is the most important force driving the current, especially for a shallow estuary such as Tampa Bay, which has an averaged water depth of 3.7 meters. Tidal force generally consists of more than one astronomic component. In Tampa Bay, the predominant astronomic constituents are the lunar semi-diurnal M_2 and solar diurnal O_1 (Goodwin, 1987). Because of the complexity of the geometry and bathymetry of an estuary, tidal circulations are often very complex. For example, the interaction between tidal currents and estuary boundary can sometimes cause a residual circulation pattern in which the time-averaged tidal currents are ebb-directed on one side of an estuary cross section and flood-directed on the other side (Kjerfv and Proehl, 1979). Tee (1976) studied the tidal circulation in the Minas Basin of the Bay of Fundy. Results of his numerical model showed that the time-averaged tidal circulation manifested itself as large horizontal eddies with diameters on the order of the width of the estuary. The rotation of these eddies indicated that they were not caused by the Coriolis force but by the interaction between tidal force and coastal boundary.

Wind-driven circulation can be found in both lakes and estuaries. It is the current induced by the wind action on the free surface of the lake or the estuary. Wind-driven circulation is particularly pronounced in shallow lakes and lagoons. Depending on the wind and the water body, wind-driven circulation can be very important even when gravitational and tidal circulations are important in an estuary. For example, in the event of an oil-spill, the movement of oil at the water surface is primarily driven by the wind. Since oil is generally less dense than water, the velocity of the thin oil layer on the water surface can be very large.

Because wind and other meteorological factors can be highly variable both temporally and spatially, wind-driven circulation is very complicated. Sheng and Lick (1979) developed a three-dimensional model for simulating wind-driven circulation in Lake Erie. Sheng *et. al* (1991) developed Cartesian-gird and curvilinear grid three-dimensional models to study wind-driven circulation in Lake Okeechobee. Their study showed that wind-driven circulation in Lake Okeechobee is often associated with seiche oscillations due to the sudden increase of wind over the lake in the afternoons. A recent study by Lee and Sheng (1993) indicated that wind-driven current in Lake Okeechobee is affected by the vertical variation of lake temperature. In order to successfully simulate strong near surface current in the lake during seiches, it was necessary to include temperature in their model simulation.

The development of numerical models for circulations in lakes and estuaries has advanced significantly during the last two decades due to increased demand for quantitative assessment of the human impact on water quality and the rapid improvement of the computer resources and numerical methods. The fast development of high-speed computers has facilitated remarkable progress in three-dimensional free-surface time-dependent circulation models.

Earlier free-surface three-dimensional models (e.g., Leenderste and Liu, 1975) used explicit finite-difference methods to solve the three-dimensional equations (Equations (4.1) – (4.4)). The explicit algorithm is simple and has relatively little numerical diffusion but requires a very small time step to resolve the gravity wave propagation, hence is very time-consuming. Leenderste and Liu (1975) used a time step of 10 seconds for modeling circulation in Chesapeake Bay and San Francisco Bay. The three-dimensional model system developed by Markofsky *et al.* (1986) was basically the same as Leenderste and Liu's model. They also used a very small time step (15 seconds) for Weser Estuary, Germany.

To overcome the shortcoming of small time step in explicit 3-D free-surface time-dependent models, Simons (1974) and Sheng *et al.* (1978) applied the time-splitting technique to models of Lake Ontario and Lake Erie, respectively. The time-splitting technique is based on the fact that while the surface gravity wave propagates rapidly, the rate of change of internal flow (vertical flow structure) is much slower so that for the computation of the vertical flow structure it is possible to use a much larger time step than that for the external flow (water levels and the vertically-integrated flow). Using the time-splitting technique, Simons was able to use a time step of 100 seconds for the external mode (flow) and a time step of 15 minutes for the internal mode with a horizontal grid of 5 km. However, using different Δt's for external and internal steps could lead to inaccurate results, due to inconsistency between the external and internal solutions. Thus, Sheng and Butler (1982) developed a 3-D model which generally uses the same large steps for the external and internal modes. For the external mode, they treated all terms in the continuity equation and the surface slopes in the vertically-integrated momentum equations implicitly and all other terms explicitly so that a larger time step is allowed for the external computation. By using the factorized implicit method for the external computation, the computing time for each time step was significantly reduced.

Two types of vertical grid systems have been used in three-dimensional free-surface models. One is the z-grid and the other is the σ-grid. In z-grid 3-D models, the vertical grid system is composed of fixed straight lines (layers), while in σ-grid

3-D models, grids are vertically stretched through the following transformation:

$$\sigma = \frac{z - \zeta(x,y,t)}{H(x,y,t)} \tag{3.1}$$

where σ is the new vertical coordinate, z is the old vertical coordinate, $H(x,y,t)$ is the total water depth, and $\zeta(x,y,t)$ is the surface elevation (measured from the mean water).

The advantage of using the σ-grid is that the same vertical resolution can be obtained in both the shallow water region and the deep water region. However, it has the disadvantage of creating larger numerical diffusion than the z-grid does, because the σ-grid enables the communication between gird points in the shallow and deep regions, which is not necessarily physically correct.

The z-grid was used in the three-dimensional models of Leenderste and Liu (1975), Lang *et al.* (1989), and Casulli and Cheng (1992). The σ-grid has been used in the 3-D models of Blumherg and Meller (1987), Sheng and Butler (1982), and Sheng *et al.* (1990 and 1991). In order to significantly reduce the numerical error due to the use of σ-grid, Sheng *et al.* (1989c) modified Sheng's σ-grid model to solve the salinity equation on the z-plane (the horizontal gradient terms were calculated by first finding the salinity values at the z-plane using linear interpolation from the salinity values at σ points and then solving the difference equation on the z-plane) in the 3-D simulation of circulation in Chesapeake Bay. They were able to significantly reduce the numerical error of the σ-grid model and successfully simulate the stratification-destratification cycle of salinity in the mid bay. Lee and Sheng (1993) and Choi and Sheng (1992) used the curvilinear grid 3-D model (CH3D) originally developed by Sheng to simulate the circulations in Lake Okeechobee and James River, respectively. The present study uses a Cartisian-grid 3-D model (EHSM3D) originally developed by Sheng to simulate the wind-driven circulation in Lake Okeechobee.

3.2 Wave Boundary Layer

3.2.1 Pure Wave Motion

Waves in lakes and estuaries are primarily generated by wind. High frequency oscillatory currents are usually associated with wind waves. Slowly varying currents are the result of tides, density gradients, or wind.

Because of its high frequency oscillatory behavior, the wave boundary layer is much thinner than the current boundary layer. The thickness of a fully developed wave boundary layer is on the order of $\sqrt{A_v T/(2\pi)}$, where T is the wave period and A_v is the vertical eddy viscosity near the bottom. If A_v is 1 cm^2/s and T is 2 seconds, the thickness is less than 2 cm. Consequently, the bottom shear stress induced by wind wave motion is much larger than that induced by slowly varying current.

Waves can significantly affect the resuspension of bottom sediment in shallow lakes and estuaries (Sheng *et al.*, 1989b). This is not only because a wave is capable of inducing a higher bottom shear stress than that by a comparable current, but also because the bed can undergo fluidization process under wave action. Various studies (e.g., Maa, 1986) indicated that waves are primarily responsible for the fluidization of bottom sediments. The erosional strength of the bed is weakened by the dynamic loading of waves which transmits normal and shear stresses downward to buildup excess pore pressure in the bed and thereby results in the rupture of interparticle bonds. As shown in Figure 3.1, the critical shear stress for erosion under wave action is much smaller than that without wave action.

Because of the significant effect of waves on sediment dynamics in lakes, estuaries, and ocean, many researchers have investigated wave boundary layer dynamics. For example, a series of laboratory experiments of oscillatory flows were conducted by Jonsson (1966) and Jonsson and Carlsen (1976). By assuming that the velocity distribution is logarithmic, Jonsson and Carlsen (1976) calculated the bottom shear stress near a rough wall by integrating the momentum equation from the bottom to

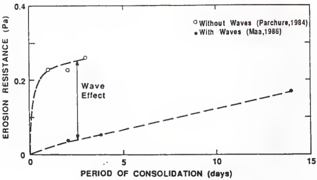

Figure 3.1: Critical shear stresses for erosion with and without wave action (from Maa, 1986).

the top of the wave boundary layer. The friction factor, f_w, was then calculated from the of the quadratic shear stress law:

$$\tau_b = \frac{1}{2}\rho f_w U_{\infty m}^2 \tag{3.2}$$

where ρ is water density and $U_{\infty m}$ is the maximum bottom orbital velocity computed from the linear wave theory. For an oscillatory motion with 2 m/sec amplitude and 8.39 sec period, they reported the logarithmic layer thickness to be approximately 6 cm, and the maximum bottom shear stress to be on the order of 400 dynes/cm^2. Based on the experiments, they derived a semi-empirical formulation for f_w. Kampbuis (1975) also did extensive laboratory measurements of the maximum bottom shear stress induced by waves. He produced a diagram of the friction factor for different values of bottom roughness and Reynolds' number.

Kajiura (1968) solved the vertically one-dimensional time-dependent wave boundary layer equation using a three-layer eddy viscosity formulation. He assumed a time-invariant eddy viscosity in studying the turbulent boundary layer dynamics: constant eddy viscosity in the small inner layer ($z < k_s/2$, where k_s is the Nikuradse roughness height), linearly increasing eddy viscosity in an overlap layer ($k_s/2 < z < \delta$, where $\delta = U_{*m}/(20\omega)$, $U_{*m}(= \sqrt{\tau_{max}/\rho})$ is the maximum shear velocity, and ω is the angular frequency), and another constant eddy viscosity for the region outside δ. From this assumed profile of eddy viscosity and by using the equation of motion, Kajiura obtained a theoretical solution and developed a theoretical-numerical method to calculate the friction factor in equation (3.2). Brevik (1981) simplified Kajiura's eddy viscosity concept by avoiding the inner layer to reduce the calculation in Kajiura's model. His results were very similar to Kajiura's.

One common weakness in the Kajiura and Brevik models is the assumption of time-independent eddy viscosity. Studies by Horikawa and Watanabe (1968) showed that eddy viscosity is a function of time and can vary significantly during the wave period. Bakker (1974) adopted a mixing length model similar to that of Prandtl to take into account the time dependence of eddy viscosity. He combined the mixing length model with the equation of motion to obtain an equation for frictional velocity ($\sqrt{\tau/\rho}$). However, his model did not show much improvement over Kajiura's or Brevik's model, because his mixing length assumption is questionable for oscillatory flow. To represent the temporal and spatial dependence of eddy viscosity in the wave boundary layer more precisely, Sheng (1982) used a Reynolds stress model to calculate the turbulence and the eddy viscosity. His results for currents and shear stresses compared well with the measurements of Jonsson and Carlsen. More recently, Sheng and Villaret (1989) used a turbulent kinetic energy (TKE) model to calculate the turbulence and the eddy viscosity. They also achieved good agreement with Jonsson and Carlsen's experiment.

3.2.2 Wave-Current Interactions

Wind generated waves in lakes and estuaries typically have a wave period ranging from 2 to 10 seconds. Such short period waves can feel the influence of the bottom in approximately 10 – 30 meters of water, where wave-induced near-bottom orbital velocities are of the same order of magnitude as those due to wind-driven and/or tide-driven currents in lakes and estuaries. For example, in Lake Okeechobee, the maximum wind-driven current is on the order of 25 cm/sec, while the near-bottom orbital current can be equally strong. However, as discussed in the previous section, because of the high frequency oscillatory nature of wave-induced current, the wave boundary layer is much thinner and wave-induced bottom shear stress is much higher than those associated with a slowly varying current of comparable magnitude. Therefore, waves are more capable of causing sediment resuspension when a current of comparable magnitude may be too weak to initiate sediment motion.

Although waves can induce strong bottom shear stresses, their ability to transport sediments is very weak. Because the wave boundary layer is very thin, resuspended sediments near the bed may not be easily transported upward. Horizontally, because the oscillatory wave motion produces little net flow over a wave cycle, the net transport of sediments is only of second order importance. However, the combined presence of a current and a wave can cause significant sediment transport in both the vertical and horizontal directions. The upward transport of resuspended sediment is mainly due to the turbulent mixing processes in the current boundary layer which is generally quite thick (sometimes the current boundary layer extends throughout the entire water column).

In order to consider the combined effects of waves and currents on sediment transport processes, it is necessary to first study the combined flow motion of waves and currents and quantify their interactions. Because the bottom shear stress and the eddy viscosity inside the wave boundary layer are associated with both the wave and the current, the combination of waves and current is nonlinear. The bottom shear stress for the combination of a wave and a current is not the linear addition of that due to the pure wave action and that due to pure current action. It is known that a slowly varying current will experience more resistance if a wave is added to the flow (Grant and Madsen, 1979). In addition, current inside the wave boundary layer will change direction if the current is not in the same or opposite direction as that of the wave propagation (Davies *et al.*, 1988). This is because the mean bottom shear stress over the wave period should always be in balance with the force driving the motion of the current outside the wave boundary layer.

The governing equations for the combined wave and current motion are the vertically one-dimension equations of motion:

$$\frac{\partial u}{\partial t} = -\frac{1}{\rho_0}\frac{\partial p}{\partial x} + \frac{\partial}{\partial z}(\frac{\tau_{zx}}{\rho}) \tag{3.3}$$

$$\frac{\partial v}{\partial t} = -\frac{1}{\rho_0}\frac{\partial p}{\partial y} + \frac{\partial}{\partial z}(\frac{\tau_{zy}}{\rho}) \tag{3.4}$$

where u and v include the wave orbital velocities u_w and v_w as well as the slowly varying current velocities u_c and v_c, the pressure p includes p_w and p_c, and τ_{zx} and τ_{zy} are turbulent shear stresses in x- and y-directions. The turbulent shear stresses τ_{zx} and τ_{zy} are related to the vertical shear:

$$(\tau_{zx}, \tau_{zy}) = A_v\frac{\partial}{\partial z}(u, v) \tag{3.5}$$

where A_v is the vertical turbulent eddy viscosity.

Grant and Madsen (1979) assumed the turbulent eddy viscosities (A_v) inside and outside the wave boundary layer as linear functions of the distance from the bed. By defining the characteristic shear velocities of respective current and wave boundary layers using a combined wave-current friction factor, the turbulent eddy viscosities were assumed to be

$$A_v = \kappa u_{cw}^* z \qquad z < \delta_w \tag{3.6}$$

$$A_v = \kappa u_c^* z \qquad z > \delta_w \tag{3.7}$$

where κ is the von Karman constant, δ_w is the wave boundary layer thickness, and u_{cw}^* and u_c^* are the characteristic shear velocities of wave and current boundary layers, respectively:

$$u_c^* = \sqrt{\frac{\tau_c}{\rho}} = (\frac{1}{2} f_{cw} V_2)^{1/2} |u_b| \tag{3.8}$$

$$u_{cw}^* = \sqrt{\frac{\tau_{b,max}}{\rho}} = (\frac{1}{2} f_{cw} \alpha)^{1/2} |u_b| \tag{3.9}$$

where u_b is the maximum bottom orbital velocity computed from linear wave theory, f_{cw} is the combined wave-current friction factor, τ_c is the time-averaged shear stress over the wave cycle, $\tau_{b,max}$ is the maximum boundary shear stress due to the combined wave and current, and V_2 and α are functions of current velocity, wave orbital velocity, and the angle between the current and the wave.

In Grant and Madsen's model, it was assumed that the thickness of the logarithmic layer is constant and the eddy viscosity is time-invariant. As already pointed out by Sheng (1984), the thickness of the logarithmic layer and the eddy viscosity change significantly with time during a wave cycle. Because of the time-invariant eddy viscosity, Grant and Madsen's model can not predict the phase shift in the wave boundary layer correctly (Sheng, 1982).

Davies *et al.* (1988) used a turbulent closure scheme to estimate the eddy viscosity shown in Equation (3.5). The eddy viscosity calculated is time-dependent, but may not be accurate for the surface layer of the water column because they assumed a linear increase of mixing length with the distance above the bed, which is not correct (Nezu and Rodi, 1986). Although some model results were shown in their paper, no comparison between model results and measured data was made.

Wave-current models that compare well with laboratory data were developed by Eidsvik (1990) and by Sleath (1991). Eidsvik used Prandtl's turbulent closure model for the region far above the wave boundary layer (δ_w) and a one-equation turbulent closure model for the region significantly below δ_w. The effect of the oscillatory motion on the current is considered solely by a scalar valued bottom roughness (z_{0w}), which is on the order of the wave boundary layer thickness. z_{0w} is estimated by matching the current calculated from above and below δ_w at a height ($\alpha_4 \delta_w$) above the bed, where the coefficient α_4 should be determined by fitting the model results with measured data. Eidsvik's model is relatively simple, but requires very fine vertical resolution ($\Delta z \le \frac{H}{100}$) and a very small time step ($\Delta t \le \frac{T}{300}$) because of the explicit treatment of the turbulent closure. The coefficient α_4 may depend on the characteristics of the wave and the current, as well as the angle between them.

In conclusion, numerous models for wave-current interaction have been developed in the last two decades. Most simple models contain simplifying assumptions and hence some limitations. For example, Grant and Madsen's model is only applicable for weak current situations. Onishi *et al.* (1993) pointed out that for strong current situations, Grant and Madsen's model results of bottom drag coefficient and bottom shear stress under wave-current interaction are smaller than those under pure current action. Eidsvik's model requires a lot of measured data to determine model parameters and is thus limited in its ability for prediction. On the other hand, numerical models with a sophisticated turbulent closure model are more robust because of their ability to accurately estimate the eddy viscosity. This study uses the TKE model developed by Sheng and Villart (1989) to calculate the the bottom shear stresses induced by the combined wave and current action (see Section 4.3 for detail).

3.3 Turbulent Mixing

Turbulent mixing is a very important physical process which can affect the flow pattern and the horizontal and vertical distributions of sediments and nutrients. The eddy viscosity mentioned in the last section represents the vertical mixing produced by the turbulent motion. As can be seen, the basic differences among different wave boundary layer or wave-current interaction models are the different methods for parameterization of the eddy viscosity.

The concept of eddy viscosity and eddy diffusivity has been widely used in modeling the turbulent mixing of momentum, heat, and mass (salinity and other species). The basic assumption of the eddy viscosity/diffusivity model is that the turbulent flux of momentum $\overline{u_i'u_j'}$ (correlations of velocity fluctuations) is the product of mean velocity gradients and "eddy viscosities," and the turbulent mass flux is the products of mean mass concentration gradients and "eddy diffusivities":

$$-\overline{u_i'u_j'} = A_t\left(\frac{\partial u_i}{\partial x_j} + \frac{\partial u_j}{\partial x_i}\right) - \frac{q^2}{3}\delta_{ij} \tag{3.10}$$

$$-\overline{u_i'\phi'} = B_t\frac{\partial \phi}{\partial x_i} \tag{3.11}$$

where i, j can be $1, 2$, and 3, u_i and u_j are the mean velocity components, u_i' and u_j' are the fluctuations of u_i and u_j, respectively, ϕ represents the mean concentration of suspended sediment or nutrients, ϕ' is the fluctuation part of ϕ, δ_{ij} is the Kronecker delta function, $q^2 = \overline{u_iu_i}$ = twice of turbulence energy, and A_t and B_t are turbulent eddy viscosity and diffusivity, respectively.

The horizontal turbulent eddy coefficients represent the mixing due to small scale sub-grid scale variations of velocity and concentration which can not be resolved by the large grid size. Therefore, the values of horizontal eddy viscosities/diffusivities in a 3-D model are dependent on the grid size used for a particular simulation. Generally, constant values can be used in a three-dimensional simulation (e.g., Sheng *et al.*, 1991; Lang *et al.*, 1989).

For vertical turbulent mixing, Lehfeldt and Bloss (1988) used a mixing-length-based algebraic model:

$$A_{v_o} = \rho_o\Lambda_o^2\sqrt{(\frac{\partial u}{\partial z})^2 + (\frac{\partial v}{\partial z})^2} \tag{3.12}$$

$$A_v = f(Ri)A_{v_o} \tag{3.13}$$

$$B_v = g(Ri)A_{v_o} \tag{3.14}$$

where A_{v_o} is the eddy viscosity/diffusivity in non-stratified flow situation, Λ_o is the mixing length and is assumed to be a linear function of z, increasing with distance above the bottom or below the free surface with its peak value at mid-depth not exceeding a certain fraction of the local depth (in the presence of strong waves, turbulent mixing in the upper layers may be significantly enhanced. In such a case, the length scale Λ_o throughout the upper layers may be assumed to be equal to the maximum value at mid-depth) and $f(Ri)$ and $g(Ri)$ are stability functions dependent on the Richardson number Ri defined as:

$$Ri = \frac{-g}{\rho_0} \frac{\partial\rho/\partial z}{(\partial u/\partial z)^2 + (\partial v/\partial z)^2} \tag{3.15}$$

The stability functions $f(Ri)$ and $g(Ri)$ are traditionally assumed to have the following forms:

$$f(Ri) = (1 + \alpha_1 \, Ri)^{\beta_1} \tag{3.16}$$

$$g(Ri) = (1 + \alpha_2 \, Ri)^{\beta_2} \tag{3.17}$$

As discussed by Sheng (1983), there exist great discrepancies among the many existing empirical forms of the stability functions. To determine the coefficients in these stability functions, one needs sufficient data to achieve the "best fit" between modeled and measured results. Therefore, specific formulae and coefficients will vary with the problem, the environment, and the available data. Munk and Anderson (1948) used the following formula in a study on the marine thermocline:

$$f(Ri) = (1 + 10Ri)^{-1/2} \tag{3.18}$$

$$g(Ri) = (1 + 33.3Ri)^{-3/2} \tag{3.19}$$

Others (Kent and Pritchard, 1959; Blumberg, 1975; Bowden and Hamilton, 1975) used $f(Ri)$ and $g(Ri)$ in the form of Equations (3.16) and (3.17) but with coefficients significantly different from those in Equations (3.18) and (3.19).

The second-order closure models, on the other hand, resolve the dynamics of turbulence by including the differential transport equations for the turbulence variables; i.e., the second-order correlations ($-\overline{u_i'u_j'}$, $-\overline{u_i'}$, ϕ' and $\overline{\phi'\phi'}$). In the most complicated case, i.e., the Reynolds stress model, differential transport equations of the following forms are solved (Lewellen, 1977; Sheng, 1982; Sheng and Villaret, 1989)

$$
\begin{aligned}
\frac{\partial \overline{u_i'u_j'}}{\partial t} + u_k \frac{\partial \overline{u_i'u_j'}}{\partial x_k} &= -\overline{u_i'u_k'}\frac{\partial u_j}{\partial x_k} - \overline{u_j'u_k'}\frac{\partial u_i}{\partial x_k} + g_i \frac{\overline{u*_j'\,\phi'}}{\phi_o} + g_j \frac{\overline{u_i'\phi'}}{\phi_o} \\
&- 2\varepsilon_{ikl}\Omega_k \overline{u_l'u_j'} - 2\varepsilon_{jlk}\Omega_l \overline{u_k'u_i'} + v_c \frac{\partial}{\partial x_k}\left(q\Lambda \frac{\partial \overline{u_i'u_j'}}{\partial x_k}\right) \\
&- \frac{q}{\Lambda}\left(\overline{u_i'u_j'} - \delta_{ij}\frac{q^2}{3}\right) - \delta_{ij}\frac{2bq^3}{12\Lambda} - \frac{2a\nu\overline{u_i'u_j'}}{\Lambda^2}
\end{aligned}
\tag{3.20}
$$

$$
\begin{aligned}
\frac{\partial \overline{u_i'\phi'}}{\partial t} + u_j \frac{\partial \overline{u_i'\phi'}}{\partial x_j} &= -\overline{u_i'u_j'}\frac{\partial \phi}{\partial x_j} - \overline{\phi' u_j'}\frac{\partial u_i}{\partial x_j} + g_i \frac{\overline{\phi'\phi'}}{\phi_o} \\
&- 2\varepsilon_{ijk}\Omega_j \overline{u_k'\phi'} + v_c \frac{\partial}{\partial x_j}\left(q\Lambda \frac{\partial \overline{u_i'\phi'}}{\partial x_j}\right) \\
&- \frac{Aq}{\Lambda}\overline{u_i'\phi'} - \frac{2a\nu}{\Lambda^2}\overline{u_i'\phi'}
\end{aligned}
\tag{3.21}
$$

$$
\begin{aligned}
\frac{\partial \overline{\phi'\phi'}}{\partial t} + u_j \frac{\partial \overline{\phi'\phi'}}{\partial x_j} &= -2\overline{u_j'\phi'}\frac{\partial \phi}{\partial x_j} + v_c \frac{\partial}{\partial x_j}\left(q\Lambda \frac{\partial \overline{\phi'\phi'}}{\partial x_j}\right) \\
&- \frac{2bsq}{\Lambda}\overline{\phi'\phi'} - \frac{2as\nu}{\Lambda}\overline{\phi'\phi'}
\end{aligned}
\tag{3.22}
$$

where x_i are coordinate axes, t is time, (u_i, u_j, u_k) are the mean velocity components, (u_i', u_j', u_k') are the fluctuating velocity components, ϕ and ϕ' are the mean and fluctuating values of density or temperature or salinity, ε_{ijk} is the alternating tensor, Ω is earth rotation, δ_{ij} is Kronecker delta, $q = (\overline{u_i'u_i'})^{1/2}$ is the total root-mean-square fluctuating velocity, and Λ is the turbulence macroscale which is a measure of the average turbulent eddy size. A total of five model coefficients: a, A, b, v_c, and s are contained in the above equations. By matching model results to data from critical laboratory experiments where only one or two of the turbulent transport processes are important, these model constants were found to be (Lewellen, 1977) $a = 2.5, A = 0.75, b = 0.125, v_c = 0.3$ and $s = 1.8$. An additional equation for Λ is needed to close the system.

Despite the complexity of the Reynolds stress models, such models do contain more physics and hence the model constants remain unchanged for all model applications. The above Reynolds stress model was used to produce successful simulations of wave boundary layer (Sheng 1982; Sheng 1984; Sheng 1986; Sheng and Villaret, 1989), wave-current boundary layer (Sheng 1984), and vegetated boundary layer (Sheng 1982).

Because of the complexity of Reynolds stress models, simplified second-order closure models have been developed. These include the turbulent kinetic energy (TKE) closure model (Sheng and Villaret, 1989) and the equilibrium closure model. Both of these models contain the assumption that the turbulence time scale is much less than the mean flow time scale. The TKE closure model resolves the turbulent dynamics by including the differential transport equation for $q^2 \left(= \overline{u'u'} + \overline{v'v'} + \overline{w'w'}\right)$, while the other second-order correlation equations are simplified to algebraic equations. The TKE closure model is similar to the Level-3 model of Mellor and Yamada (1982) and the $k-\varepsilon$ model of Rodi (1980), although both models favor the solution of turbulence dissipation (ε) instead of length scale (Λ). The equilibrium closure model (Sheng, 1985; Sheng and Chiu, 1986; Sheng *et al.*, 1989d) is slightly more simplified than the TKE closure model, since only algebraic equations are used to resolve the second-order correlations. The equilibrium closure model is similar to Mellor and Yamada's Level-2 model. Instead of solving the differential transport equations for Λ which consists completely of modeled terms, simplified second-order closure models often solve a set of integral constraints for Λ (Sheng 1985; Sheng and Chiu 1986).

The equilibrium closure model computes the vertical turbulence based on the assumption that the local equilibrium condition is valid when the time scale of mean flow is much larger than that for turbulence and when turbulence varies little over the turbulence macroscale. The equilibrium closure model is significantly simpler than the complete second-order closure model (Reynolds stress model) and has been found to give very good results for mean flow, salinity and temperature with little or no tuning on model coefficients.

In the equilibrium model, a set of algebraic equations are solved for the second-order correlation quantities to obtain the stability functions $f(Ri)$ and $g(Ri)$ in terms of the mean flow variables. These equations, when written in dimensional and tensor forms, are (Sheng *et al.*, 1989d)

$$\begin{aligned} 0 &= -\overline{u_i'u_k'}\frac{\partial u_j}{\partial x_k} - \overline{u_j'u_k'}\frac{\partial u_i}{\partial x_k} - g_i\frac{\overline{u_j'\rho'}}{\rho_o} - g_j\frac{\overline{u_i'\rho}}{\rho_o} \\ &- 2\varepsilon_{ik\ell}\Omega_k\overline{u_\ell'u_j'} - \varepsilon_{j\ell k}\Omega_\ell\overline{u_k'u_i'} \\ &- \frac{q}{\Lambda}\left(\overline{u_i'u_j'} - \delta_{ij}\frac{q^2}{3}\right) - \delta_{ij}\frac{q^3}{12\Lambda} \end{aligned} \tag{3.23}$$

$$\begin{aligned} 0 &= -\overline{u_i'u_j'}\frac{\partial \rho}{\partial x_j} - \overline{u_j'\rho'}\frac{\partial u_i}{\partial x_j} - \frac{g_i\overline{\rho'\rho'}}{\rho_o} \\ &- 2\varepsilon_{ijk}\Omega_j\overline{u_k'\rho'} - 0.75q\frac{\overline{u_i'\rho'}}{\Lambda} \end{aligned} \tag{3.24}$$

$$0 = 2\overline{u_j'\rho'}\frac{\partial \rho}{\partial x_j} + \frac{0.45q\overline{\rho'\rho'}}{\Lambda} \tag{3.25}$$

where the subscripts i, j, k can be 1, 2, or 3. Hence Equation (3.23) represents six equations and Equation (3.24) represents three equations in general. A total of five model coefficients are contained in the above equations. These coefficients were determined from comparing model results with data from critical laboratory experiments where only one or two of the turbulent transport processes are dominant. These coefficients remained "invariant" in application of the equilibrium closure model, the kinetic energy closure model (Sheng and Villaret, 1989) and the Reynolds stress model (Sheng, 1982; Sheng, 1984; Sheng and Villaret, 1989).

As shown in Sheng *et al.* (1989d), q^2 can be determined from the following dimensional equations when mean flow variables are known:

$$\begin{aligned} 3A^2b^2sQ^4 \; &+ \; A[(bs + 3b + 7b^2s)\,Ri - Abs(1-2b)]Q^2 && (3.26) \\ &+ \; b(s + 3 + 4bs)\,Ri^2 + (bs - A)(1-2b)\,Ri = 0 \end{aligned}$$

where the model constants A, b, and s are "invariant" and have the values 0.75, 0.125, and 1.8, respectively, and

$$Q = \frac{q}{\Lambda\sqrt{\left(\frac{\partial u}{\partial z}\right)^2 + \left(\frac{\partial v}{\partial z}\right)^2}} \qquad (3.27)$$

$$Ri = -\frac{\frac{g}{\rho_o}\frac{\partial \rho}{\partial z}}{\left(\frac{\partial u}{\partial z}\right)^2 + \left(\frac{\partial v}{\partial z}\right)^2} \qquad (3.28)$$

The total root-mean-square turbulent velocity q can then be obtained from the above equations after the mean flow variables are determined at each time step:

$$q = Q\Lambda\sqrt{\left(\frac{\partial u}{\partial z}\right)^2 + \left(\frac{\partial v}{\partial z}\right)^2} \qquad (3.29)$$

Once q^2 is computed, the vertical eddy coefficients can be computed from

$$A_v = \frac{A + \bar{w}\overline{w'w'}}{A - wq^2}\,\Lambda \cdot q \qquad (3.30)$$

$$B_v = \frac{bs}{(bs - w)A}\frac{\overline{w'w'}}{q^2}\,\Lambda \cdot q \qquad (3.31)$$

where

$$w = Ri/(AQ^2) \qquad (3.32)$$

$$\bar{w} = w/(1 - w/bs) \qquad (3.33)$$

$$\overline{w'w'} = \frac{1-2b}{3(1-2\bar{w})}q^2 \qquad (3.34)$$

In the complete second-order closure model, a differential transport equation for the turbulent macroscale Λ is derived. However, the Λ equation contains four model coefficients that must be calibrated with experimental data. For ease of application, the turbulent macroscale Λ is assumed to satisfy a number of integral constraints. First of all, Λ is assumed to be a linear function of vertical distance immediately above the bottom or below the free surface. In addition, the turbulent macroscale Λ must satisfy the following relationships (Sheng *et al.*, 1989d):

$$\left|\frac{d\Lambda}{dz}\right| \leq 0.65 \tag{3.35}$$

$$\Lambda \leq C_1 \cdot H \tag{3.36}$$

$$\Lambda \leq C_1 \cdot H_p \tag{3.37}$$

$$\Lambda \leq C_2 \cdot \delta_{q^2} \tag{3.38}$$

$$\Lambda \leq \frac{q}{N} \tag{3.39}$$

where C_1 is a number usually within the range of 0.1 to 0.25; H is the total depth; H_p is the depth of the pynocline; C_2, which is between 0.1 and 0.25, is the fractional cut-off limitation of turbulent macroscale based on δ_{q^2}, the spread of turbulence determined from the turbulent kinetic energy (q^2) profile; and N is the Brunt-Väisäla frequency defined as:

$$N = \left(-\frac{g}{\rho}\frac{\partial\rho}{\partial z}\right)^{1/2} \tag{3.40}$$

Although the simplified second-order closure model presented above is strictly valid when the turbulence time scale (Λ/q) is much less than the mean flow time scale and when turbulence does not change rapidly over Λ, it has been found to be quite successful in simulating vertical flow structures in estuarine and coastal waters. Recent simulations of wind-induced mixing of salinity in Chesapeake Bay (Sheng *et* *al.*, 1989c; Johnson *et al.*, 1989) and wind-driven circulation and sediment transport in Lake Okeechobee (Sheng *et al.*, 1989b) gave good results with little or no tuning of model coefficients.

Compared to the equilibrium closure model, the kinetic energy closure model does not assume that the turbulence created at any second is in equilibrium with the turbulence disappearance due to the advection, diffusion and dissipation. It contains an extra equation for the turbulent kinetic energy, q^2, which can be obtained directly (let $i = j$) from Equation (3.20):

$$\frac{\partial q^2}{\partial t} + u_k \frac{\partial q^2}{\partial x_k} = -2\overline{u_i' u_k'} \frac{\partial u_i}{\partial x_k} + 2 g_i \frac{\overline{u_i \phi'}}{\phi_o} + 0.3 \frac{\partial}{\partial x_k}(q \Lambda \frac{\partial q^2}{\partial x_k}) - \frac{q^3}{4\Lambda} \tag{3.41}$$

The vertically one-dimensional version of this equation reads

$$\frac{\partial q^2}{\partial t} = -2\overline{u_i' u_k'} \frac{\partial u_i}{\partial x_k} + 2 g_i \frac{\overline{u_i' \phi'}}{\phi_o} + 0.3 \frac{\partial}{\partial x_3}(q \Lambda \frac{\partial q^2}{\partial x_3}) - \frac{q^3}{4\Lambda} \tag{3.42}$$

or

$$\frac{\partial q^2}{\partial t} = -2\overline{u'w'} \frac{\partial u}{\partial z} - 2\overline{v'w'} \frac{\partial v}{\partial z} + 2g \frac{\overline{w'\rho'}}{\rho_o} + 0.3 \frac{\partial}{\partial z}(q \Lambda \frac{\partial q^2}{\partial z}) - \frac{q^3}{4\Lambda} \tag{3.43}$$

The second-order correlation terms of fluctuating velocities and density, $\overline{u'w'}$, $\overline{v'w'}$, and $\overline{w'\phi'}$, can be calculated from Equations (3.23), (3.24), and (3.25), or the solutions of the equilibrium closure model discussed above. They have the following forms:

$$\overline{u'w'} = \frac{-81\Gamma + 336\Psi}{4\Delta} \frac{q^3}{\Lambda} \frac{\partial u}{\partial z} \tag{3.44}$$

$$\overline{v'w'} = \frac{-81\Gamma + 336\Psi}{4\Delta} \frac{q^3}{\Lambda} \frac{\partial v}{\partial z} \tag{3.45}$$

$$\overline{w'\rho'} = \frac{-108\Gamma + 144\Psi}{4\Delta} \frac{q^3}{\Lambda} \frac{\partial \rho}{\partial z} \tag{3.46}$$

where

$$\Gamma = \left(\frac{q}{\Lambda}\right)^2 \tag{3.47}$$

$$\Psi = \frac{\partial \rho}{\partial z}\frac{g}{\rho} \tag{3.48}$$

$$\Delta = 81(\frac{q}{\Lambda})^4 - 804\frac{\partial \rho}{\partial z}(\frac{q}{\Lambda})^2 q^2 + 928(\frac{\partial \rho}{\partial z})^2 q^4 \tag{3.49}$$

Substitute the second-order correlation terms in Equation (3.43) with Equations (3.44) – (3.45), the q^2 equation can be solved with a finite difference method. Once q^2 is solved from Equation (3.43), the vertical eddy viscosity (A_v) and diffusivity (B_v) can be calculated by Equations (3.30) and (3.31), where Q is calculated by Equation (3.27) and the turbulent macroscale Λ is also determined by the constraints mentioned above.

Sheng and Villaret (1989) used the TKE closure model to simulate a wave boundary layer, a thermally stratified boundary layer and a sediment-laden boundary layer. Mellor and Yamada (1982) generally favor the use of their Level-3 model or Level-2.5 model. The $k - \varepsilon$ models used by Rodi (1980) and others have also been quite successful. On the other hand, the equilibrium closure model has also been found to be very successful for simulating the vertical mixing in estuaries (Sheng *et al.*, 1989c; Sheng *et al.*, 1989d), despite the slightly further simplification. In this study, the TKE closure model is chosen to calculate the vertical eddy coefficients A_v and B_v, while the horizontal eddy coefficients A_H and B_H are assumed to be constant (both spatially and temporally).

3.4 Sediment Dynamics

3.4.1 Settling and Flocculation

Settling is a process by which sediment particles fall through the water column because of density differences between sediment particles and water. This process is closely related to the flocculation process in the water column. In the flocculation process, sediment particles are flocculated together due to the turbulent shearing of water, differential settling of sediment particles, Brownian motion, and electrochemical/biochemical attraction. The flocculation process results in the formation of flocs, which can generally fall through the water column faster than the primary sediment particles.

The simplest parameterization of settling is the use of a constant settling velocity. For a single spherical sediment particle in the laminar flow, the settling velocity is described the Stoke's formula:

$$w_s = \frac{1}{18} \frac{g(\rho_s - \rho_w) d_s^2}{\eta} \tag{3.50}$$

where ρ_w and ρ_s are densities of water and the sediment particle and d_s is the diameter of the particle.

Stoke's formula is a analytical solution for a very idealized case. In practice, sediment particles are not necessary spherical. Furthermore, instead of a single sediment particle, many particles are settling to the bottom at the same time. The fact that many particles are present in the water column not only suggests the influence of the settling behavior of one particle on the settling of other particles around it, but also the aggregation and flocculation of fine sediment particles ($d \leq 60 \mu m$) because of the significant electrostatic forces (cohesion) and the collision among them. The end product of the flocculation, flocs, can fall faster to the bottom than the primary sediment particles due to the relatively large size. However, if the sediment concentration is too higher ($\geq$ 10 g/l), collisions among sediment particles will actually retard the particle settling. This is the so-called "hindered settling".

The cohesion of sediment particles depends on the type of clay minerals, cation exchange capacity (CEC), sodium adsorption ratio (SAR), and the salinity and pH of water. Gibbs (1983) studied the flocculation rates of clay minerals, and found that flocculation begins at low salinities of 0.05 to 1 *ppt*. Hunt (1982) performed laboratory experiments on flocculation of kaolinite and illite induced by Brownian motion and laminar shear, and obtained an equilibrium particle size distribution within a few minutes. However, the equilibrium condition may not be valid for sediments in turbulent estuaries and lakes, where the flocculation time scale is typically on the order of a few hours.

Most of flocculation models developed so far followed the basic theory proposed by Smoluchowski in 1918. Smoluchowski determined the rate of collisions among two particle groups due to Brownian motion (β_b), differential settling (β_d), and turbulent shearing (β_t) to be as

$$\beta_b = \frac{2BT}{3\mu}\frac{(r_i + r_j)^2}{r_i r_j} n_i n_j \tag{3.51}$$

$$\beta_d = \pi(r_i + r_j)^3 |w_i - w_j| n_i n_j \tag{3.52}$$

$$\beta_t = \frac{4G}{3}(r_i + r_j)^3 n_i n_j \tag{3.53}$$

wherein μ is the molecular viscosity, B is the Boltzman constant, T is the absolute temperature, r_i and r_j are radii of particles of size i and j, respectively, n_i and n_j are number densities of size i and j, respectively, w_i and w_j are settling velocities of size i and j, respectively, and G is the micro-shear which the particles experience. G is assumed uniform with a constant velocity gradient du/dz in Equation (3.53). In general, it is impossible to represent G by du/dz because there are turbulent velocity gradient superimposed upon the mean velocity gradient. Instead, a so-called 'absolute velocity gradient' defined as follows should be used for G:

$$G = \sqrt{\frac{\epsilon}{\nu}} \tag{3.54}$$

wherein ϵ is the total energy dissipation and ν is the kinematic viscosity of water.

Farley and Morel (1986) solved the particle size distribution equation following the basic work of Smoluchowski (1918). However, their studies treat the entire particle size distribution, and are too cumbersome for practical applications in a multi-dimensional model. In addition, explicit accounting of the effect of turbulent motion on flocculation was not included. Tsai *et al.* (1987) demonstrated the effect of fluid shear on flocculation. However, only shear stress, but not turbulence level or shearing rate, was measured in their study.

Using Smoluchowski's equations for collision, Burhan *et al.* (1989) developed a flocculation model with an additional break-up term induced by turbulent shearing. However, they could not fit their model results to their measured equilibrium particle size distribution in a laboratory device without modifying the break-up term and adjusting several model coefficients. Thus, the laboratory data of Burban *et al.* were used primarily for calibration of their flocculation-breakup model. Due to the lack of comprehensive data, the detailed dynamics of flocculation are still not well understood particularly in field conditions. Moreover, since their model is primarily a box-model, work is needed to extend it to multi-dimensional models for simulating field situations. In another study, Farley and Morel (1986) performed laboratory experiments on flocculation-induced mass removal in high sediment concentration environments ($c > 10g/\ell$). They produced an empirical equation for the removal rate which depends on differential settling, fluid shear and Brownian motion:

$$\frac{dc}{dt} = -B_d\, c^{2.3} - B_t\, c^{1.9} - B_b\, c^{1.3} \tag{3.55}$$

where c is the volume-averaged sediment concentration in the device, B_d, B_t and B_b are contributions of differential settling, fluid shear and Brownian motion on the collision frequency of particles, respectively. The empirical coefficients of 2.3, 1.9 and 1.3 may require site-specific parameter tuning. To apply their results to multi-dimensional modeling, one can derive an expression for the settling velocity in the following:

$$w_s = \frac{1}{\partial c/\partial z}(B_d c^{2.3} + B_t c^{1.9} + B_b c^{1.3}) \tag{3.56}$$

The above equation for w_s, however, is only valid for high concentration situations where c is on the order of $10g/l$ or higher. Moreover, it does not contain any effect of particle breakup on settling. This formula requires sufficient data to allow tuning of the model coefficients.

Krone (1962) considered the flocculation at a constant collision rate and derived an analytical equation relating the settling velocity with the sediment concentration:

$$w_s = \alpha c^m \tag{3.57}$$

where α is an empirical constant and $m = 4/3$.

Such a power law of settling velocity has been supported by numerous field and laboratory measurements, but with slightly different exponent values (Table 3.1). For example, Thorn (1981) obtained the following settling velocity for mud from Severn Estuary, England:

$$w_s = 0.513c^{1.28} \qquad c \leq 2g/l \tag{3.58}$$

For $c > 2$ g/l, he found that hindered settling dominated, and the settling velocity decreased with the increasing sediment concentration:

$$w_s = 2.6(1 - 0.008c)^{4.65} \tag{3.59}$$

Sheng and Lick (1979) measured the settling velocity for sediments collected in Lake Erie in laboratory and used the measured settling velocity in a three-dimensional simulation of sediment transport in Lake Erie. Gibbs (1985) measured the settling velocity of freshly formed flocs of illite, kaolinite and smectite in a laboratory and found that the settling velocity is related to the floc diameter through a non-Stokesian relation which indicated that the floc density decreased and the drag increased as the flocs increased in size. Toorman and Berlamont (1993) measured the settling rate in a settling column, while considering the combined problem of settling and consolidation. He found two distinct settling modes in all his experiments: one corresponds to the hindered settling and the other corresponds to the consolidation. van Leussen *et al.* (1993) measured the settling velocity in the Ems Estuary in The Netherlands. Their

Table 3.1: Measured exponents m in Krone's Equation.

Exponent m	Water body	Reference
1.33	San Francisco Bay (lab measurement)	Krone (1962)
1.2–1.3	Chao Phya Estuary	NEDECO (1965)
1.1	Thames (spring tide)	Owen (1970)
2.2	Thames (neap tide)	Owen (1970)
1.0	Thames (lab measurement)	Owen (1970)
1.29	Severn Estuary	Thorn (1981)
1.37	Thames	Burt (1986)
2.92	Elbe Estuary (limnetic zone)	Puls and Kuehl (1986)
2.55	Elbe Estuary (brackish zone)	Puls and Kuehl (1986)
2.07	Elbe Estuary (limnetic zone)	Puls *et al.* (1988)
1.97	Elbe Estuary (brackish zone)	Puls *et al.* (1988)
2.5 - 3.6	Ems Estuary (The Netherlands)	van Leussen *et al.* (1993)

measurements showed that there exists no unique relationship between the settling velocity, w_s, and the suspended sediment concentration, c, over the entire estuary, although for a specific location there seems to be an unique relation between them. They used Equation (3.57) to fit their data with an exponent ranging from 2.5 at the mouth of the estuary to 3.6 at the upper stream of the estuary due to the different tidal, salinity, and flow conditions. They suggested that a location-dependent relation between the settling velocity and the suspended sediment concentration should be used in studying fine sediment transport in estuaries.

Hwang and Mehta (1989) measured the settling velocity for sediments collected in Lake Okeechobee. They empirically parameterized the effects of flocculation and hindered settling on the settling velocity by a formulation proposed by Wolanski *et al.* (1989):

$$w_s = \frac{ac^n}{(c^2 + b^2)^m} \tag{3.60}$$

where c is the sediment concentration and $a, b, m,$ and n are empirical constants determined from laboratory experiments. The shape of w_s as a function of c is shown in Figure 3.2 (Hwang and Mehta, 1989). As the sediment concentration increases, flocculation occurs as the result of increased collision among particles, thus leading to the increase of the settling velocity w_s. As c exceeds $3000\,mg/\ell$, w_s starts to decrease due to hindered settling, i.e., interference on settling due to the presence of other particles.

It should be pointed out that such w_s formulations expressed as functions of the sediment concentration c do allow the empirical parameterization of flocculation due to Brownian motion and differential settling. However, because of the use of the settling tube in the measurements, the real settling velocity in the field may be different from that obtained in the settling tube. Three factors may cause the deviation of measured settling velocity from the real one: (1) the lower turbulence level in the tube, (2) the small dimensions of the tube, and (3) the breakup of flocs during

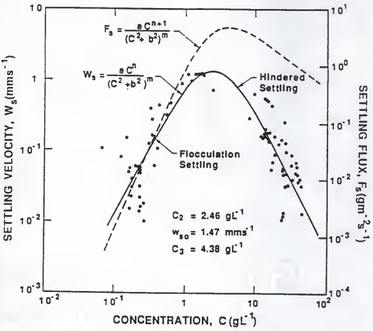

Figure 3.2: Settling velocity as a function of suspended sediment concentration, with flocculation occurring at high concentrations (after Hwang and Mehta, 1989).

the sampling process in the field. Therefore, the measured empirical relationship between settling velocity and sediment concentration may require some adjustments if used in the numerical model.

3.4.2 Deposition

Deposition is the process that governs the removal of sediment particles from the water column. The speed with which particles are deposited onto the bottom from the water column is the deposition velocity. Once the sediments are brought near the bottom by settling, deposition determines their removal from the water column. Deposition in estuaries and lakes are determined by the settling velocity, shear strength, and concentration of depositing aggregates as they encounter the higher velocity gradients near the bed (Krone, 1993). Many past studies (Lavelle *et al.*, 1984; Bedford *et al.*, 1987) assumed that the deposition velocity is the same as the settling velocity, which can be a constant or determined by Stoke's settling formula (Equation (3.50)).

Krone (1962) observed that the occurrence of the final deposition of sediments is related to the flow condition just above the bed. Under calm flow conditions, most of the sediment particles in the bottom layer will deposit onto the bed. While the flow becomes stronger and stronger, however, more and more sediment particles will refuse to settle onto the bed. He introduced a probability function for deposition as followed:

$$p = \frac{1}{2}(1 - \frac{\tau_b}{\tau_{cd}} + \left|1 - \frac{\tau_b}{\tau_{cd}}\right|) \qquad (3.61)$$

where p is the probability of deposition, τ_b is the bottom shear stress, and τ_{cd} is the critical shear stress for the deposition.

Equation (3.61) shows that when $\tau_b = 0$, the probability of deposition is 1, and when $\tau_b \geq \tau_{cd}$, there is no deposition. The probability of deposition of sediment particles in the bottom layer increases linearly as the bottom shear stress decreases. The deposition velocity, which is defined as the deposition rate D divided by the sediment concentration near the bed c_1, is then $w_s p$, or

$$v_d = \frac{w_s}{2}(1 - \frac{\tau_b}{\tau_{cd}} + \left|1 - \frac{\tau_b}{\tau_{cd}}\right|) \tag{3.62}$$

The advantage of Krone's model lies in its simplicity. Laboratory experiments using sediments collected from the harbor at Redwood City, on South San Francisco Bay showed that results of Krone's model agree well with the experimental data (Krone, 1993). However, Krone's model lacks rigorous theoretical foundation. The empirical constant, τ_{cd}, incorporates many processes (such as the strength of aggregates, the flow condition near the bed etc.) associated with the deposition. Because of the empirical nature of the model, there is no guideline as to how τ_{cd} can be estimated.

Based on rigorous theoretical consideration of the deposition process, Sheng (1986) considered the flow over a surface covered with several layers with the possible presence of vegetation, by expressing the deposition velocity as

$$-(\overline{w'c'})_o/c_1 \equiv v_d = \frac{1}{(v_{dh})^{-1} + (v_{ds})^{-1} + (v_{dc})^{-1}} \tag{3.63}$$

where $-(\overline{w'c'})_o$ represents the deposition flux at the bed, c_l is the concentration at the first grid point above the bottom, and v_{dh}, v_{ds}, and v_{dc} represent the deposition velocity within the hydrodynamic layer (logarithmic layer), the viscous sublayer, and the canopy layer, respectively

$$v_{dh} = \frac{\kappa u_*}{.75 ln \frac{z_1}{z_0}} \tag{3.64}$$

$$\begin{aligned} v_{ds} &= \left(\frac{4}{3}\right)^{0.3} \left(\frac{D_B}{\nu}\right)^{0.7} \frac{u_*^2}{u_\ell} \\ &+ 0.1 \frac{u_*^2}{u_\ell} \frac{\tau_r u_*^2}{\nu} [1 - \exp(-0.08 q^2 \tau_r / \nu)] + \tau_r g \end{aligned} \tag{3.65}$$

$$v_{dc} = v_{ds} \frac{1 + LAI}{1 + D_p/D_f} \tag{3.66}$$

where z_1 is the distance of the first grid point above the bottom, $D_B = 2.176 \times 10^{-9}/r_p$ is the Brownian diffusion coefficient, ν is the fluid kinematic viscosity, $u_* = \sqrt{\tau_b/\rho_f}$ is the friction velocity, τ_b is the bottom stress, $u_\ell = (u_*/k)\ell n(z_\delta/z_o)$ is the fluid velocity outside the laminar sublayer, with $z_\delta = 10z/u_*$ as the height of the viscous sublayer. $\tau_r = w_s/g$ is the relaxation time of sediment particles, $q = (32)^{1/4}u_*$ is the total turbulent fluctuating velocity, LAI is the leaf area index (total wetted leaf area per unit bottom area), and D_p/D_f is the ratio of the profile drag to the skin friction drag in the vegetation area. In the absence of a vegetation canopy, $v_{dc} = 0$.

The derivation of Sheng's deposition model is based on fundamental consideration of fluid dynamics principles and the fact that the inverse of v_d is a "resistance" which is additive through the various layers. The advantage of Sheng's model is that v_d can be explicitly computed if the turbulent and sediment parameters are known. The disadvantage, however, is that it is difficult to obtain the field data required for the validation of the model.

It can be concluded that Sheng's deposition model is more general than Krone's one, because it considers several dominant processes and does not require the ad-hoc tuning of empirical constants. There is no τ_{cd} in Sheng's model. In other words, the critical shear stress for deposition in Sheng's model is infinite. Krone's deposition model is simple and widely used, but requires the rather arbitrary choice of the empirical constant of critical shear stress for deposition (τ_{cd}), which has little theoretical foundation.

3.4.3 Erosion

Erosion is the process by which sediment is suspended from the bottom into the water column due to a large bottom shear stress induced by currents and waves. The erosion or resuspension of bottom sediment depends on the bed structure and the characteristics of the flow above the bed. The softer the bed, the more easily the bottom can be eroded. The stronger the flow above the bed, the higher the erosion rate becomes. The mechanism of erosion for fine sediments is different from that of coarse sediments. For non-cohesive sediments, erosion takes place when the lift force acting on a grain is larger than the downward force, while for cohesive sediments, the binding forces among flocs should be overcome before erosion occurs.

Most of the existing erosion models can be grouped into two catalogues: (1) critical current model and (2) critical shear stress model. Markofsky *et al.* (1986) and Wolanski *et al.* (1988) calculated the erosion rate based on the depth-averaged current as follows:

$$E = \frac{E_o}{2}\left(\frac{\overline{u}}{u_{ce}} - 1 + \left|\frac{\overline{u}}{u_{ce}} - 1\right|\right) \tag{3.67}$$

where E_o is the erosion rate constant, $\overline{u}$ is the depth-averaged velocity, and u_{ce} is the critical velocity for erosion.

Because the upward motion of sediment particles is directly related to forces acting on the particles rather than the depth-averaged velocity, the critical current model as shown in Equation (3.67) is not very reasonable, although it is always possible to adjust the u_{ce} value to fit the data. On the other hand, Partheniades (1962) proposed a critical shear stress model for the erosion rate as follows:

$$E = \frac{E_o}{2}\left(\frac{\tau_b}{\tau_{ce}} - 1 + \left|\frac{\tau_b}{\tau_{ce}} - 1\right|\right)^n \tag{3.68}$$

where E_o is the erosion rate constant, τ_b is the bottom stress, and τ_{ce} is the critical stress for erosion.

Mehta *et al.* (1982) pointed out that the above critical shear stress model is appropriate for a dense bed in which the bed properties are vertically uniform. For a partially consolidated bed, both the density and the bed strength increase with the depth. The erosion rate for this kind of soft bed should be calculated using the following equation (Parchure and Mehta, 1985):

$$E = E_f \exp[\alpha(\tau_b - \tau_e)^{1/2}] \tag{3.69}$$

wherein E_f is the floc erosion rate and τ_e is a measure of bed resistance to the shear stress. τ_e increases with the depth and has the unit of shear stress. When $\tau_b = \tau_e$, the erosion rate is the floc erosion rate.

Parchure and Mehta (1985) determined the coefficient E_f and α in Equation (3.69) by measuring the time history of the suspended sediment concentration and the known bed density variation in laboratory. They found that $\alpha = 18.4 mN^{-1/2}$ and $E_f = 5 \times 10^{-6} g\ cm^{-2} min^{-1}$ for kaolinite in tape water, and $\alpha = 17.2 mN^{-1/2}$ and $E_f = 1.4 \times 10^{-5} g\ cm^{-2} min{-}1$ for kaolinite in salt water.

The above models for the erosion rate were developed for a steady uni-directional current. Under an oscillatory wave action, Maa (1986) found that the erosion rate can be calculated by a similar expression as that for the dense bed (Equation (3.68)),

$$E = \frac{E_w}{2}\left(\frac{\tau_{b_{max}}}{\tau_{ce}} - 1 + \left|\frac{\tau_{b_{max}}}{\tau_{ce}} - 1\right|\right) \qquad (3.70)$$

where E_w is the erosion rate constant under the wave action and $\tau_{b_{max}}$ is the maximum bottom shears stress induced by the oscillatory flow in a wave cycle.

Maa (1986) determined the erosion rate constant E_w and the critical shear stress τ_{ce} for Cedar Key mud. He obtained $E_w = 1.2 \times 10^{-3} g\ cm^{-2} min^{-1}$, which is about one order of magnitude higher than the erosion rate constant ($E_o = 9.7 \times 10^{-5} g\ cm^{-2} min^{-1}$) obtained by Villarent and Paulic (1986) under steady current over mud collected at the same place. Maa (1986) also determined the critical shear stresses for erosion under wave action for kaolinite beds. Critical shear stresses were found to be smaller than those determined by Parchure and Mehta (1985) under steady current conditions. For example, a τ_{ce} of 0.25 Nm^{-2} under steady current action can become only 0.03 Nm^{-2} due to a wave action.

In considering the relative merits of the different models for computing the erosion rate, the study done by Lavelle *et al.* (1984) should be mentioned. As shown in Figure 3.3, a summary by Lavelle *et al.* (1984) of erosion versus bottom stress for several locations indicated that a power law relationship exists between E and τ_b, but no universal constants exists for the relationship. Thus, no *a priori* judgement can be made as to which formula for the erosion rate is best. The best erosion rate for a particular application must therefore be selected on an *ad hoc* basis. Field validation of the erosion model must be conducted for each new sediment transport study.

It should be clear that most of the erosion models are descriptive models which were developed with very simple concepts and calibrated with limited laboratory data and numerous *ad hoc* empirical assumptions. Although most of the erosion models did appear to reproduce the particular laboratory data with which the models were calibrated, applications of most models to field conditions have not been proven to be successful. Only a few of the models have been applied to the field successfully. In a recent study (Sheng *et al.*, 1989a), field data and a water-column sediment mixing model were used to aid the determination of the erosion rate, which was found to be an order of magnitude higher than the laboratory determined erosion rate using the same sediment. This fact and other uncertainties associated with laboratory erosion studies strongly suggest the need to develop erosion rate from comprehensive field data, rather than laboratory data which represent very different hydrodynamic and sedimentary conditions. Even in laboratory experiments, there is a need to obtain more comprehensive data, particularly within the bottom $30cm$ of the water column and the top $10cm$ of the sediment column. In high concentration ($c > 1000mg/\ell$) and low flow situations, a sharp density gradient can develop near the bottom to cause the formation of a lutocline, which is similar to the thermocline or pynocline in the water column. Although the simulation of lutocline has been attempted (Ross, 1988; Wolanski *et al.*, 1988), the paucity of data near the bottom has limited the modeling to merely qualitative calibration.

3.4.4 Fluidization and Consolidation

The erosion process is related to the sediment processes in the bed, including the fluidization process and the consolidation process. The fluidization is a process by which the bed is fluidized due to the excess pore stress induced by the flow movement

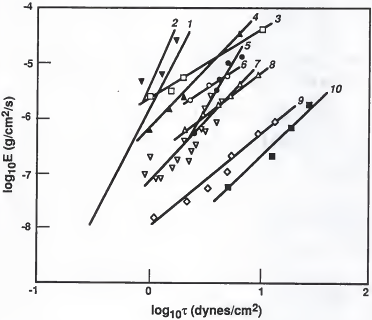

Figure 3.3: Erosion rate versus bottom shear stress (after Lavelle *et al.*, 1984; the numbers are for different sediments and are explained in Lavelle *et al.*, 1984).

in the water column (e.g., wave action). The opposite process of fluidization is the consolidation process, in which the bed is consolidated due to the overburden or self-weight.

The fluidization process is one of the interactions between waves and the mud (other interactions between waves and mud include the wave energy dissipation due to the mud movement and the internal wave dynamics along water-mud interface). It is a rheological response of fine sediments to the wave action. The basic mechanism of wave-induced fluidization is that the bed is shaken and water is pumped downward into the bed under highly oscillatory flows, so that internal pore pressure can be built up and the bed becomes fluid-like mud.

The fluidization process has not been well studied due to the complexity of the rheological property of different sediments. Mallard and Dalrymple (1977) treated the mud as a pure elastic solid in studying the wave-mud interaction. Voigt model (a linear viscoelastic model) was used by Hsiao and Shemdin (1980) and Maa and Mehta (1986) for muddy seabeds subjected to wave action. Mei and Liu (1987) used a Bingham model to simulate the response of muddy seabeds under long waves. Their model assumed that mud motion begins when the imposed shear stress is larger than the yield shear stress and stops when it is less than the yield stress. Their model results showed that mud motion is intermittent. But unfortunately, intermittent motions of mud were not observed in either the field and or laboratory (Chou *et al.*, 1993).

Maa (1986) studied the erosion process under wave action and obtained a rate expression for the erosion of fluidized mud. To study the wave-induced fluidization of a natural estuarine mud, Ross (1988) measured the pore and total pressures of Tampa Bay mud subjected to progressive, non-breaking waves. By defining a small effective stress, he tracked the fluid mud-bed interface as fluidization proceeds. His results showed that the the fluid mud thickness increased rapidly in the first 15 minutes and continued to increase afterwards with a relative slow but constant rate. During the fluidization, the upper limit of the fluid mud, the so-called lutocline (Kirby and Parker, 1984), was found to increase only in the first 15 minutes and stayed almost stable later on. Ross' experiment showed the importance of waves during the fluidization process. However, since he was not be able to control the horizontal advective transport of the fluid mud, he could not obtain the steady-state fluid mud-bed interface, which should be a function of the water depth and the wave parameters (wave height, wave period, or wave spectrum of wave group) for a given mud.

Feng *et al.* (1992) also measured the pore-water pressure under oscillatory loading in laboratory. The fluidization process measured by Feng *et al.* (1992) was subjected to a single progressive wave. They obtained some expressions for the fluidization rate for their experiment runs. However, no quantitative relations between fluidization rate and wave parameters or the final fluid mud thickness and the wave parameters were drawn.

Tzang *et al.* (1992) recorded resonant amplification of pore pressure oscillation during their laboratory experiments of fluidization subjected to wave action. Measurements by Clukey *et al.* (1983) showed that total or partial fluidization occured in a soil trench below shallow water waves.

Owing to the complexity of fluidization, most of the previous studies were limited in the laboratory experiment. Field measurements or model studies were barely done. Sakai *et al.* (1992) were among the few groups who measured the wave-induced transient porewater pressure in the field. Chou (1989) developed a fluidization model by assuming that the bed acts like an elastic solid at a low strain, a viscous fluid at a very high strain, and a viscoelastic material at an intermediate strain. His model predicted that the sediment fluidization depth increased with wave height, but did not show the effect of wave period on fluidization.

Like fluidization, the consolidation process is also a very complex one and has not been well studied. Alexis *et al.* (1992) did some *in situ* consolidation experiments for estuary mud. Some field and laboratory observations have been made by Toorman and Berlamont (1993) for dredged mud. Toorman found a hindered settling mode and a consolidation mode in all his experiments.

Most of the consolidation models were developed from the point of view of soil mechanics, i.e., solve the void ratio described by Gibson's law. Alexis *et al.* (1992) proposed a new governing equation for the void ratio which takes into account the compressibility of fluid and grains, the history of material (erosion and deposition), and non pure Darcinian flow. Toorman and Berlamont (1992) developed a soil mechanics model and a hindered settling model to simulate the consolidation process he observed in experiments. His results showed that the soil mechanics model was more or less suitable for long term prediction and the hindered settling model only gives good result in the initial stage of consolidation. He found that the soil mechanics model requires a lot of experimental data for calibration and the hindered settling model requires long-term laboratory experiment data for optimal simulations.

3.4.5 Models for Multi-dimensional Sediment Transport in Lakes and Estuaries

Although controlled laboratory experiments can be used to provide insight into certain sediment processes, sediment transport models developed from laboratory studies may not be applicable to field conditions due to scaling problems, both in terms of flow and sediment. Field data, on the other hand, are very difficult and expensive to obtain. Thus, mathematical models of fine sediment transport, in conjunction with field data, are necessary to provide quantitative understanding of sediment transport.

Since the transport of fine sediment particles involves many complicated processes, there exists no fully validated and universal sediment transport model at the present time (Sheng, 1989). The difficulty of modeling 3-D sediment transport in lakes and estuaries is additionally compounded by the complicated flow conditions, the interactions between sediment particles and flow field, the inhomogeneity of sediments over the entire bottom of the water body, the complicated geometry and bathymetry of the water body, and the boundary conditions at water-sediment interface. In addition, 3-D simulations of sediment transport require a lot of data for model calibration and validation, and data collection is very expensive.

Due to the above problems, past comprehensive models for large scale sediment transport are rather scarce. Sheng and Lick (1979) developed the framework of a comprehensive sediment transport model, and validated it with data from the western basin of Lake Erie. Transport processes considered in their model were advection, turbulent diffusion, erosion, deposition, and gravitational settling. To quantify the transport process, they applied a 3-D hydrodynamic model (Sheng *et al.*, 1978) to compute the 3-D lake circulation. To quantify the bottom stress acting on the lake bottom, they developed a wave model to compute the wave field and orbital velocity over the entire western basin of Lake Erie. Erosion and deposition rates were determined from laboratory experiments using actual lake sediments. Settling velocity of sediments was also measured in the laboratory. Even though some of the individual process models contained some empiricism, Sheng and Lick were able to successfully simulate the large scale transport of fine sediments in the western basin of Lake Erie during a two-day episodic event. Ariathurai and Krone (1976) developed a 2-D vertically integrated sediment transport model and applied it to study the dispersion of sediments in the Savannah River estuary. Despite the empiricism of their model, reasonable success was reported. Unfortunately, little data exist to validate their simulations. In addition, they considered deposition and erosion as a combined process and assumed that either net erosion or net deposition exists, depending on the bottom stress. Thus, for a certain range of bottom stress, their model predicts a zero net flux. Hayter and Pakala (1989) developed a 3-D model to simulated the contaminant transport in the Sampit River. They used the sediment removal rate obtained by Farley and Morel to calculate the settling velocity. This settling velocity may not be suitable for low sediment concentration in the water column (Sheng *et al.*, 1991). No detailed comparison between model results and measured data was given by them. Lang *et al.* (1989) applied a 3-D model developed by Markofsky *et al.* (1986) to simulate suspended sediment dynamics in Weser estuary in Germany. The model calculates eddy coefficients using a mixing-length-based algebraic model developed by Lehfeldt and Bloss (1988). Equation (3.67) was used to calculated the erosion rate. Because of the explicit treatment in the hydrodynamics part of the model, the time step used was very small (about 15 seconds). Onishi *et al.* (1993) used a 3-D model to simulate sediment transport processes during a storm event in New Bedford Harbor. They used Grant and Madsen's model to calculate bottom shear stresses due to wave-current interaction only during storm days and did not consider wave effects on sediment dynamics before and after the storm. The reason why they calculated bottom shear stresses in this way is because Mrant-Madsen's model failed to produce reasonable drag coefficients and bottom shear stresses before and after the storm. Obviously, this argument is questionable.

CHAPTER 4

MODELING THE HYDRODYNAMICS AND SEDIMENT TRANSPORT PROCESSES

Because the transport/transformation processes of nutrients in lakes and estuaries are closely related to the hydrodynamics and sediment transport processes, sophisticated models for hydrodynamics and sediment transport processes must be developed and used for better understanding the complicated nutrient processes. This study uses two model systems to quantify the hydrodynamics and sediment transport processes. One is a three-dimensional model system and the other is a one-dimensional model system. The basic difference between them is that the latter one does not include any horizontal processes, and is thus a simplified version of the former.

4.1 Governing Equations

The hydrodynamics and sediment transport processes in estuaries are very complicated, three-dimensional and time-dependent problems. Mathematical descriptions of such problems generally require some simplifying assumptions. For the flow, it is generally assumed that

1. the horizontal scale is much larger than the vertical scale such that the hydrostatic pressure distribution is valid,
2. the turbulence time scale is much less than the mean flow time scale,
3. the flow is incompressible,
4. the Boussinesq approximation can be used to simplify the treatment of the baroclinic terms,
5. the concept of eddy viscosity is acceptable, and
6. molecular viscosity is much smaller than the eddy viscosity, such that it can be neglected.

Under these assumptions, the three-dimensional governing equations for an incompressible fluid in a right-handed Cartesian coordinate system are

$$\frac{\partial u}{\partial x}+\frac{\partial v}{\partial y}+\frac{\partial w}{\partial z}=0 \tag{4.1}$$

$$\begin{aligned}\frac{\partial u}{\partial t}+\frac{\partial u^2}{\partial x}+\frac{\partial uv}{\partial y}+\frac{\partial uw}{\partial z} &= fv-\frac{1}{\rho_o}\frac{\partial p}{\partial x}+\frac{\partial}{\partial x}\left(A_H\frac{\partial u}{\partial x}\right) \\ &+ \frac{\partial}{\partial y}\left(A_H\frac{\partial u}{\partial y}\right)+\frac{\partial}{\partial z}\left(A_v\frac{\partial u}{\partial z}\right)\end{aligned} \tag{4.2}$$

$$\begin{aligned}\frac{\partial v}{\partial t}+\frac{\partial uv}{\partial x}+\frac{\partial v^2}{\partial y}+\frac{\partial vw}{\partial z} &= -fu-\frac{1}{\rho_o}\frac{\partial p}{\partial y}+\frac{\partial}{\partial x}\left(A_H\frac{\partial v}{\partial x}\right) \\ &+ \frac{\partial}{\partial y}\left(A_H\frac{\partial v}{\partial y}\right)+\frac{\partial}{\partial z}\left(A_v\frac{\partial v}{\partial z}\right)\end{aligned} \tag{4.3}$$

$$\frac{\partial p}{\partial z}=-\rho g \tag{4.4}$$

where (u, v, w) are fluid velocities in the (x, y, z) directions, f is the Coriolis parameter defined as $2\Omega\sin\phi$ where Ω is the rotational speed of the earth and ϕ is the latitude, ρ is density, p is pressure, A_H is the horizontal turbulent eddy viscosity, and A_v is the vertical turbulent eddy viscosity.

For large and shallow lakes and estuaries, if the horizontal transport of momentum is not very significant, the horizontal derivative terms in the above equations can be neglected and a set of vertical one-dimensional governing equations can be obtained:

$$\frac{\partial u}{\partial t} = fv+\frac{\partial}{\partial z}(A_v\frac{\partial u}{\partial z}) \tag{4.5}$$

$$\frac{\partial v}{\partial t} = -fu+\frac{\partial}{\partial z}(A_v\frac{\partial v}{\partial z}) \tag{4.6}$$

For the sediment transport in lakes and estuaries, the governing equation is (Sheng and Lick, 1979):

$$\begin{aligned}\frac{\partial c}{\partial t}+\frac{\partial uc}{\partial x}+\frac{\partial vc}{\partial y}+\frac{\partial(w+w_s)c}{\partial z} &= \frac{\partial}{\partial x}(B_H\frac{\partial c}{\partial x})+\frac{\partial}{\partial y}\left(B_H\frac{\partial c}{\partial y}\right) \\ &+ \frac{\partial}{\partial z}\left(B_v\frac{\partial c}{\partial z}\right)\end{aligned} \tag{4.7}$$

where w_s is the settling velocity of suspended sediment particles, c is the suspended sediment concentration, B_H is the horizontal turbulent eddy diffusivity, and B_v is the vertical turbulent eddy diffusivity.

The following assumptions were invoked when deriving Equation (4.7):

1. the sediment particles are sufficiently homogeneous in their sizes such that the suspended sediment dynamics can be represented by the concentration of a single particle size group,
2. the volumetric concentration of the sediment particles is sufficiently small such that all particles follow all turbulent eddy motions (for example, the suspended sediment concentration in Lake Okeechobee is in the order of 20 to 200 mg/l and the volumetric concentration of suspended sediments is in the order of 0.00002 to 0.0002),
3. the suspended sediment concentration is sufficiently low ($\leq 1000\,mg/\ell$) such that non-Newtonian behavior can be neglected,
4. the vertical gradient of suspended sediment concentration can affect the density field, buoyancy and turbulence,
5. measurements of such model parameters as settling velocity, mineralogical composition of sediments, and bed structure are available,
6. the concept of eddy diffusivity is valid for the turbulent mixing of suspended sediment, and
7. since the molecular diffusivity is much smaller than the eddy diffusivity, the molecular diffusivity is not considered.

The vertically one-dimensional equation for sediment transport reads

$$\frac{\partial c}{\partial t} + \frac{\partial w_s c}{\partial z} = \frac{\partial}{\partial z}(B_v \frac{\partial c}{\partial z}) \qquad (4.8)$$

In Equation (4.4), density ρ is generally a function of temperature T, salinity S, and suspended sediment concentration:

$$\rho = \rho(T, S, c) \tag{4.9}$$

which can be further decomposed into ρ_w, the density of water, plus the contribution of sediments to the mixture density ρ:

$$\rho = \rho_w + c(1 - \frac{\rho_w}{\rho_s}) \tag{4.10}$$

where ρ_s is tbe floc density of sediment and ρ_w is the water density.

The water density ρ_w can be computed by using the following equations given by Eckart (1958):

$$\begin{aligned} \rho_w &= (P+1)/(\alpha + 0.698P) \qquad (4.11) \\ P &= 5890 + 38T - 0.375T^2 + 3S \\ \alpha &= 1779.5 + 11.25T - 0.0745T^2 - (3.8 + 0.01T)S \end{aligned}$$

where T is in ^0C, S is in $^0/_{00}$, and ρ is in g/cm^3.

It should be pointed out tbat tbe assumptions made in deriving Equation (4.7) are valid in many practical applications, but are occasionally violated. For example, in the case of high sediment concentration (higher than 2-10 g/l), the particle size distribution may be quite broad and may undergo significant change in time such that several equations similar to Equation (4.7) are needed to represent the concentration of several particle size groups. However, this could lead to extreme complexity in the present three-dimensional model. Moreover, although such a multi-equation sediment model can be and has been formulated (Sbeng, 1983 and 1986), limited data and understanding on the flocculation dynamics does not allow us to specify the model coefficients quantitatively. Thus, in general, only a single equation is used to describe the dynamics of suspended sediment concentration.

4.2 Boundary and Initial Conditions

Obtaining solutions for equations given by Equations (4.1) through (4.7) requires the specification of appropriate boundary and initial conditions. For a 3-D problem, necessary boundary conditions include not only the vertical boundaries, but also the lateral boundaries.

4.2.1 Vertical Boundary Conditions

The boundary conditions at the free surface are specified as

$$A_v \frac{\partial u}{\partial z} = \tau_{wx} \tag{4.12}$$

$$A_v \frac{\partial v}{\partial z} = \tau_{wy} \tag{4.13}$$

$$-(w + w_s)c + B_v \frac{\partial c}{\partial z} = 0 \tag{4.14}$$

where τ_{wx} and τ_{wy} are wind shear stresses at the free surface and can be computed from the quadratic form

$$\tau_{wx} = \rho_a C_{da} W_x \sqrt{W_x^2 + W_y^2} \tag{4.15}$$

$$\tau_{wx} = \rho_a C_{da} W_y \sqrt{W_x^2 + W_y^2} \tag{4.16}$$

wherein $\rho_a = 1.27 \times 10^{-3}\,\mathrm{g\,cm^{-3}}$ is the density of air, W_x and W_y are the wind speeds in the x and y directions, respectively; and C_{da} is the drag coefficient of air. The drag coefficient of air was computed from Garratt's formula (1977):

$$C_{da} = 0.001\left(0.75 + 0.00067\sqrt{W_x^2 + W_y^2}\right) \tag{4.17}$$

where the wind speeds are in cgs units (cm/sec).

The boundary conditions at the bottom are (Sheng and Lick, 1979)

$$A_v \frac{\partial u}{\partial z} = \tau_{bx} \tag{4.18}$$

$$A_v \frac{\partial v}{\partial z} = \tau_{by} \tag{4.19}$$

$$-(w + w_s)c + B_v \frac{\partial c}{\partial z} = v_d c - E \tag{4.20}$$

where τ_{bx} and τ_{by} represent the bottom shear stress induced by current, v_d is a dimensional deposition velocity (see Section 3.4.2), and E is the dimensional rate of erosion (see Section 3.4.3).

The bottom shear stresses due to the current (τ_{bx} and τ_{by}) are calculated by the quadratic formula

$$\tau_{bx} = \rho C_d \sqrt{u_1^2 + v_1^2}\, u_1 \tag{4.21}$$

$$\tau_{by} = \rho C_d \sqrt{u_1^2 + v_1^2}\, v_1 \tag{4.22}$$

where u_1 and v_1 are horizontal velocities in the bottom layer at a distance z_1 above the bed and C_d is the drag coefficient. In a fully developed turbulence boundary layer, the velocity distribution is logarithmic, and C_d can be calculated as follows:

$$C_d = \left[\frac{\kappa}{\ln(z_1/z_o)}\right]^2 \tag{4.23}$$

where $\kappa = 0.4$ is the von Karman constant, $z_o = k_s/30$ and k_s is the bottom roughness.

4.2.2 Lateral Boundary Conditions

Along the shoreline where river inflow or outflow may occur, data of riverine flow should be available so that the depth-averaged velocities ($\overline{u}$ and $\overline{v}$) can be calculated. Assuming that the vertical distributions of velocities u and v are parabolic, u and v are specified as follows:

$$u = 3\overline{u}(x, y, t)\frac{z^2}{h^2} \tag{4.24}$$

$$v = 3\overline{v}(x, y, t)\frac{z^2}{h^2} \tag{4.25}$$

For suspended sediment simulation, the concentration of suspended sediments, $c(x, y, t)$, at the month of the river is needed. Because both the horizontal and vertical diffusions are much generally smaller than the horizontal advection at the month of the river, the boundary conditions for suspended sediment concentration at the river cells can be specified as follows by assuming an uniform distribution of suspended sediment concentration in the vertical direction:

$$\frac{\partial c}{\partial t} = -\frac{\partial uc}{\partial x} - \frac{\partial vc}{\partial y} \tag{4.26}$$

Along a solid boundary, zero velocity is specified for the normal velocity component and zero gradient is specified for the tangential velocity component, because the grid size used in the model is much larger than the lateral boundary layer thickness. At a solid boundary, the normal gradient of suspended sediment concentration is assumed to be zero.

4.2.3 Initial Conditions

To initiate a run, the initial spatial distributions of velocities u, v, w, and the sediment concentrations c must be specified. When initial data are unknown, one can start with zero initial fields or other "reasonable" initial fields. When initial data are known at a number of locations, a smooth initial field can be generated by a 2-D interpolation which uses distance-inverses as weighting factors. It should be kept in mind that the initial fields may not satisfy conservation of momentum and suspended sediments. In order to correct this problem, a spin-up run must be invoked.

For practical simulations, the initial condition for the flow is usually assumed as no motion all over the field if little initial data are known. This is reasonable because the spin-up time of the flow field is relatively short. In case of simulation involving suspended sediments, the spin-up time is longer and an interpolation routine is needed to produce a smooth initial field from data at a select number of points.

4.3 Model Parameters

In the governing equations, Equations (4.1) – (4.7), and boundary conditions, Equation (4.12) – (4.26), of hydrodynamics and sediment transport processes, the following model parameters need to be determined:

1. horizontal eddy viscosity A_H and horizontal eddy diffusivity B_H,
2. vertical eddy viscosity A_v and and vertical eddy diffusivity B_v,
3. settling velocity of sediment particles w_s
4. deposition velocity v_d of sediments, and
5. erosion rate E of sediment.

In the following, methods for determining these model parameters are presented.

4.3.1 Eddy Coefficients

In the governing equations for hydrodynamics and sediment transport (Equations (4.3), (4.4), and (4.7)), the terms containing the eddy coefficients (A_v, A_H, B_v and B_H) represent the horizontal and vertical turbulent mixing of momentum and suspended sediments. The general forms of turbulent mixing in the water column are $-\partial\overline{u_i'u_j'}/\partial x_j$ for momentum and $-\partial\overline{u_i'\phi_j'}/\partial x_j$ for suspended sediments, where i, j, and k can be 1, 2, and 3, u_i' is the fluctuating velocity in i-direction, ϕ represents the suspended sediment concentration, and ϕ' is the fluctuating concentration.

Assuming the length scale of horizontal turbulent mixing in lakes and estuaries is much larger than the grid size of the model and an uniform grid is used, one can use constant horizontal eddy coefficients (A_H and B_H) in the model. For this study, the uniform grid size of the Lake Okeechobee model is 2 km, and A_H and B_H are on the order of $1.0 \times 10^5 cm^2/sec$. The vertical eddy coefficients (A_v and B_v) are calculated from the equilibrium closure model or the TKE closure model contained in the hydrodynamic model because of the previous success of these two models (e.g. Sheng, 1982; Sheng *et al.*, 1991, Schoellhammer and Sheng, 1993).

4.3.2 Settling Velocity

In the sediment transport model developed by Sheng and Chen (1992), the settling velocity can be calculated by one of the following methods: (1) a constant settling velocity determined from either laboratory experiment or field data, (2) Stoke's formula for a single sediment particle (Equation (3.50)), (3) an empirical settling velocity formula which considers flocculation and hindered settling (Equation (3.60)), and (4) a settling velocity derived from Farley and Morel's formula for the removal rate of sediments (Equation (3.56)). This study uses the empirical formula described by Equation (3.60) with a minimum settling velocity cutoff:

$$w_s = \max\left[\frac{ac^n}{(c^2+b^2)^m}, w_{s_{min}}\right] \tag{4.27}$$

where the model parameters $(a, b, m$, and $n)$ are determined by Hwang (1989) using Lake Okeechobee mud.

4.3.3 Deposition Velocity

The sediment transport model of Sheng and Chen (1992) include three options for calculating deposition velocity: (1) the deposition velocity is set to the settling velocity at the bottom water layer, (2) the deposition velocity is equal to the settling velocity at the bottom water layer multiplied by Krone's probability function (Equation (3.61)), and (3) Sheng's deposition model (Equation (3.63)). Sheng's model for deposition is used in this study because it is more general. However, since Sheng's model has an infinite critical shear stress for deposition, the predicted SSC profile near the bed has no significant stratification. This may not be correct for fine sediments because many researcher have noticed that high SSC gradient exits near the bottom (e.g., Kirhy and Parker, 1984). In order to simulate the near-bed dynamics of fine sediments (i.e., the lutocline dynamics), this study modified Sheng's deposition model by introducing Krone's probability function for deposition:

$$v_d = \frac{p}{v_{dh}^{-1} + v_{ds}^{-1} + v_{dc}^{-1}} \tag{4.28}$$

where p is the probability function defined in Equation (3.61).

When using Krone's deposition velocity formulation to simulate the suspended sediment dynamics in Lake Okeechobee, it was necessary to use a critical shear stress for deposition which is about 5 times larger than the critical shear stress for erosion. Mimura (1993) also showed that the critical shear stress for deposition is larger than the critical shear stress for erosion under wave action.

4.3.4 Erosion Rate

The sediment transport model of Sheng and Chen (1992) include three erosion models: (1) power law, (2) variation of power law, and (3) exponential law. These erosion models are briefly described in the following.

(1) Power Law

$$E = \frac{E'_o}{T_d^2}\left\{\frac{1}{2}\left[(\tau_b - \tau_{ce}) + |\tau_b - \tau_{ce}|\right]\right\}^p \tag{4.29}$$

where E'_o is the erosion rate constant per unit stress (i.e., it has the same units as E divided by stress), τ_b is the bottom stress, τ_{ce} is the critical stress for erosion, and T_d is a dimensionless erosion time constant. Non-dimensionalization of the erosion time constant is by $T_d = T'_d/T_{d_o}$, where T'_d is the dimensional time constant for erosion, and T_{d_o} is the amount of time the sediment bed has been lying undisturbed. Typically, T_{d_o} is about one day, so the units of T_{d_o} and T'_d are days. E_o, T_d, τ_{ce}, and p are empirical constants which must be determined from laboratory or field experiments. The above equation is identical in form to the one described in Sheng and Lick (1979) for Lake Erie and Sheng *et al.* (1990) for Lake Okeechobee when $T_d = 1$ and $p = 1$. This form is also similar to those used by Parchure (1984) and Sheng and Villaret (1989) for a "placed bed", i.e., a bed made of sediments with uniform density in the laboratory.

(2) Variation of Power Law

$$E = \frac{E_o}{T_d^2}\left\{\frac{1}{2}\left[\left(\frac{\tau_b}{\tau_{ce}} - 1\right) + \left|\frac{\tau_b}{\tau_{ce}} - 1\right|\right]\right\}^p \tag{4.30}$$

where E_o is the erosion rate constant, which has the same units as does the erosion rate, E (i.e., $g\,cm^{-2}s^{-1}$). This erosion rate fomulation is similar to Equation (4.29), and the relationship between E_o and E_o' is: $E_o = E_o'\tau_{ce}^p$.

(3) Exponential Law

$$E = \frac{E_o}{T_d^2}\cdot \exp\left[\alpha\left\{\frac{1}{2}\left[\left(\frac{\tau_b}{\tau_{ce}} - 1\right) + \left|\frac{\tau_b}{\tau_{ce}} - 1\right|\right]\right\}^{0.5}\right] \tag{4.31}$$

Equation (4.31) is similar to the one described in Sheng and Villaret (1989) and Parchure (1984) for a "deposited bed", i.e., a bed made of sediments with density which increases with depth and works well for kaolinite in laboratory experiments.

The determination of erosion rate requires the knowledge of the bed structure. For well consolidated bed, the bed structure can be treated as vertically homogeneous, and the critical shear stress can be assumed constant over the depth. For a soft bed, the vertical variation of the critical shear stress should be known before the application of the erosion model. Since both the bulk density and the bed strength increase as consolidation goes on, the quantity τ_{ce} is often expressed in terms of density. On the other hand, the erosion rate constant E_o appears decrease with the depth. In other words, E_o decreases with the density or bed strength. For example, Villaret and Paulic (1986) found the following expression for San Francisco Bay mud:

$$\tau_{ce} = \beta(\rho_b - 1) \tag{4.32}$$

$$E_o = \gamma\exp(-\alpha_1\tau_{ce}) \tag{4.33}$$

wherein β, γ, and α_1 are constants and ρ_b is the wet bulk density. If ρ_b is in gcm^{-3} and τ_{ce} is in Nm^{-2}, $\beta = 1$. γ and α_1 were found to be 1.06×10^{-3} and 2.33, respectively.

Table 4.1: Values of ρ_B, ε_M, and τ_{ce} determined by Hwang and Mebta (1989). * indicates that these values were obtained by combining the erosion rate data resulting from tests 1, 2 and 3.

Test No.	ρ_b $(g\,cm^{-3})$	E_o $(mg\,cm^{-2}\,hr^{-1})$	τ_{ce} $(N\,m^{-2})$
1	1.10	2.82*	0.43*
2	1.12		
3	1.09		
4	1.19	2.37	0.64
5	1.07	57.61	0.34
6	1.09	14.61	0.55

Experiments conducted by Hwang and Mebta (1989) also show that τ_{ce} and E_o are very well correlated with the bed density. In fact, as shown in Table 4.1, a slight variation of ρ from 1.09 to 1.07 results in a 30-fold increase of E_o and a slight change in τ_{ce}. They fitted the relationship between E_o and the bed density to an an exponential curve:

$$ln\, E_o \,=\, s_1 \exp\left(\frac{s_2}{\rho_b - \rho_3}\right) \tag{4.34}$$

where $s_1 = 0.23, s_2 = 0.198$ and ρ_3 is the bulk density at the upper level of the fluid mud zone selected to be $1.0023\,g\,cm^{-3}$.

A major problem in developing and applying the erosion models in a field or laboratory situation is associated with the difficulty to determine the precise density structure of the bed. The bed density changes with time and space, but cannot be easily measured. A typical bed density profile (Hwang and Mehta, 1989) from Lake Okeechobee in the vicinity of Station C (see Figure 6.1 for location) is shown in Figure 4.1.

This study assumes that the bed structures in Lake Okeechobee and Tampa Bay are vertically homogeneous and uses Equation (4.30) with $T_d = 1$ for the calculation of the erosion rate. E_o and τ_{ce} are determined by the best fitting of simulated suspended sediment concentrations to measured data using the vertical one-dimensional sediment model (see Section 7.2).

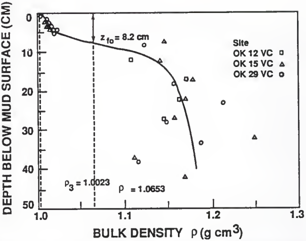

Figure 4.1: A typical bed density profile from Lake Okeechobee in the vicinity of Station C (after Hwang and Mehta, 1989).

4.3.5 Bottom Stress τ_b

Because of the fact that waves can induce very large bottom shear stresses (Section 3.2), τ_b in the equations for erosion rate, should be the bottom stress due to both currents and waves. Since τ_b cannot be readily measured in the field and laboratory, it is essential to be able to compute τ_b accurately via a numerical model. Wind-driven currents and tidal currents vary with periods of hours or longer, while wind waves produce orbital currents with a period of a few seconds. Thus, as pointed out in Section 3.2.2, bottom stresses due to waves can be very important for sediment transport. In the Lake Okeechobee study, Sheng *et al.* (1991) found that resuspension of sediments is primarily caused by wave-induced bottom stress. The current-induced bottom stress is generally insufficient to cause significant resuspension of sediments. Only during very windy conditions are both the wave-induced bottom stress and the current-induced bottom stress equally important.

To calculate the combined bottom shear stresses due to waves and currents, Sheng and Lick (1979) used a algorithm which kinematically combined the separately computed wave-induced bottom stress and current-induced bottom stress. Here, the current-induced bottom shear stress can be calculated by the quadratic formula (Equations (4.21) and (4.22)), and the bottom shear stress induced by the wave action can be calculated by Kajiura's model discussed in Section 3.2. Although this method lacks interaction between waves and current, it is used in the three-dimensional model because of its simplicity and the generally weak wind-driven currents.

Alternatively, Grant and Madsen's model of wave-current interaction can also be used for the computation of bottom shear stresses. This model is also relatively simple to use, but only for small currents. Moreover, the assumption made in the model that maximum bottom shear stress occurs when the oscillatory velocity at the water surface reaches maximum is not accurate.

An more sophisticated method to consider the nonlinear interaction of waves and current is to use a vertical one-dimensional numerical model to simulate the combined wave-current motion:

$$\frac{\partial u}{\partial t} = -\frac{1}{\rho}\frac{\partial p}{\partial x} + \frac{\partial}{\partial z}(A_v \frac{\partial u}{\partial z}) \tag{4.35}$$

$$\frac{\partial v}{\partial t} = -\frac{1}{\rho}\frac{\partial p}{\partial y} + \frac{\partial}{\partial z}(A_v \frac{\partial y}{\partial z}) \tag{4.36}$$

where the eddy viscosity in Equations (4.35) and (4.36) can be calculated by either the equilibrium second-order closure model or the TKE closure model discussed in Section 4.3.1. The time step used in solving Equations (4.35) and (4.36) should be very small, generally 1/60 to 1/20 of the wave period. The pressure gradient terms include two parts: one is the oscillatory part and the other is the one which drives currents. The oscillatory pressure gradient terms are

$$(\frac{\partial p}{\partial x})_w = \rho \frac{\partial u_w}{\partial t} \tag{4.37}$$

$$(\frac{\partial p}{\partial y})_w = \rho \frac{\partial v_w}{\partial t} \tag{4.38}$$

where u_w and v_w are oscillatory velocities in x and y directions, respectively.

If current data at a depth z_1 are available, the pressure gradient for current motion can be estimated as follow:

$$(\frac{\partial p}{\partial x})_c = \rho(\frac{\partial u_c}{\partial t})_{z_1} - \rho\frac{\partial}{\partial z}(A_v\frac{\partial u_c}{\partial z}) \tag{4.39}$$

$$(\frac{\partial p}{\partial y})_c = \rho(\frac{\partial v_c}{\partial t})_{z_1} - \rho\frac{\partial}{\partial z}(A_v\frac{\partial v_c}{\partial z}) \tag{4.40}$$

wherein u_c and v_c are measured velocities at depth z_1. The eddy viscous terms can be estimated using known A_v and velocity distributions at the old time step or can he treated as part of the solution implicitly. If current data at more than one depths are availahle, the horizontal pressure terms over the entire water column can be estimated more precisely. More details about using current data to calculate the horizontal pressure terms are presented in Appendix A.

4.4 Numerical Solution Algorithm

A finite difference method was used to estahlish the three-dimensional as well as the one-dimensional numerical model systems of hydrodynamics and sediment transport in this study. Details about the numerical solution algorithms used in the 3-D and 1-D models of hydrodynamics and sediment transport are documented in Sheng and Chen (1992) and Sheng *et al.* (1993a). For completeness, a brief description of the solution algorithm used in the 3-D and the 1-D model systems for hydrodynamics and sediment transport is presented in Appendix C. A flow chart for the 3-D model systems are presented in Appendix B. The 1-D model flow chart is similar to the 3-D model flow chart except for the horizontal advective and diffusive terms.

CHAPTER 5
MODELING NUTRIENT DYNAMICS

After describing numerical models for hydrodynamics and sediment transport in the last chapter, this chapter presents a three-dimensional model and a one-dimensional model model of nutrient dynamics for shallow lakes and estuaries. Nutrient species in the 1-D and the 3-D models consist of phosphorus components and nitrogen components. In the following, assumptions for nutrient models are discussed before presenting the governing equations for different nutrient species. The boundary and initial conditions are then specified, followed by a discussion of the reaction terms in the model and the model parameters. At the end of the chapter, the solution algorithm used in the 3-D and the 1-D models are described.

5.1 Governing Equations

Because the processes in nutrient cycles are very complicated and not fully understood, many assumptions have to be made in a numerical model of nutrient dynamics. The assumptions used in the present phosphorus model and the nitrogen model are as follows:

1. Phosphorus and nitrogen species follow the fluid motion in the water column, except that the particulate species are additionally influenced by the gravitational settling;
2. Particulate nutrient concentration in the water column is so low that the hydrodynamics and sediment transport processes are unaffected;
3. Molecular viscosity is much smaller than the eddy viscosity in the water column, such that it can be neglected;

4. Because of the lack of field data, all algal species (green, blue-green, and diatom) are aggregated to one algal species;
5. Phosphorus and nitrogen are limiting nutrients for algal growth in lakes and estuaries, respectively;
6. Temperature is a limiting factor for the growth of algae and zooplankton;
7. Light intensity is a limiting factor for algal growth,
8. The precipitation process and the complexing reaction are treated as adsorption reaction, and
9. The dissolution reaction is treated as the desorption reaction.

5.1.1 Phosphorus Equations in the Water Column

The phosphorus species simulated in the model are soluble reactive phosphorus (SRP), dissolved organic phosphorus (DOP), algal particulate phosphorus (Alg-P), zooplankton particulate phosphorus(Zoo-P), particulate organic phosphorus (POP), and particulate inorganic phosphorus (PIP). Mathematical descriptions of the dynamics of these phosphorus components in lakes and estuaries are essentially equations of mass balance for these species. Under the above assumptions, the three-dimensional governing equations for phosphorus species in the water column of lakes and estuaries are

SRP:

$$\frac{\partial P_1}{\partial t} + \frac{\partial u_j P_1}{\partial x_j} = \frac{\partial \mathcal{F}_j(P_1)}{\partial x_j} + R_1 \tag{5.1}$$

DOP:

$$\frac{\partial P_2}{\partial t} + \frac{\partial u_j P_2}{\partial x_j} = \frac{\partial \mathcal{F}_j(P_2)}{\partial x_j} + R_2 \tag{5.2}$$

Alg-P:

$$\frac{\partial P_3}{\partial t} + \frac{\partial (u_j - \delta_{j3} w_s^a) P_3}{\partial x_j} = \frac{\partial \mathcal{F}_j(P_3)}{\partial x_j} + R_3 \tag{5.3}$$

Zoo-P :

$$\frac{\partial P_4}{\partial t} + \frac{\partial u_j P_4}{\partial x_j} = \frac{\partial \mathcal{F}_j(P_4)}{\partial x_j} + R_4 \tag{5.4}$$

POP:

$$\frac{\partial (P_5)}{\partial t} + \frac{\partial (u_j - \delta_{j3} w_s) P_5}{\partial x_j} = \frac{\partial \mathcal{F}_j(P_5)}{\partial x_j} + R_5 \tag{5.5}$$

PIP:

$$\frac{\partial (P_6)}{\partial t} + \frac{\partial (u_j - \delta_{j3} w_s) P_6}{\partial x_j} = \frac{\partial \mathcal{F}_j(P_6)}{\partial x_j} + R_6 \tag{5.6}$$

where u_j is the j-th component of velocity, δ_{jk} is the Kronecker delta, P_1 and P_2 are concentrations of SRP and DOP, respectively; P_3 and P_4 are algal particulate phosphorus concentration and zooplankton particulate phosphorus concentration, respectively; P_5 and P_6 are adsorbed organic and inorganic phosphorus concentrations, respectively; w_s and w_s^a are settling velocities of suspended sediments and algae, respectively; $R_i (i = 1, 2, 3, 4, 5,$ and $6)$ are reaction terms for SRP, DOP, algal particulate P, zooplankton particulate P, POP, and PIP, respectively, in the water column; and

$$\mathcal{F}_j = (\delta_{1j} B_H + \delta_{2j} B_H + \delta_{3j} B_v) \frac{\partial}{\partial x_j} \qquad \text{no summation} \tag{5.7}$$

If the advection and the horizontal diffusion are negligible compared to vertical diffusion and reactions, the above equations become a set of one-dimensional equations:

$$\frac{\partial P_i}{\partial t} = \frac{\partial}{\partial z}\left(B_v \frac{\partial P_i}{\partial z}\right) + R_i \qquad i = 1, 2 \tag{5.8}$$

$$\frac{\partial P_3}{\partial t} = \frac{\partial}{\partial z}\left(w_s^a P_3 + B_v \frac{\partial P_3}{\partial z}\right) + R_3 \tag{5.9}$$

$$\frac{\partial P_4}{\partial t} = \frac{\partial}{\partial z}(B_v \frac{\partial P_4}{\partial z}) + R_4 \tag{5.10}$$

$$\frac{\partial P_i}{\partial t} = \frac{\partial}{\partial z}(w_s P_i + B_v \frac{\partial P_i}{\partial z}) + R_i \qquad i = 5,6 \tag{5.11}$$

5.1.2 Phosphorus Equations in the Sediment Column

Because of the difference in partial pressures of oxygen, carbon and other physical, biochemical factors, the transformation processes of phosphorus in the water column and in the bed soil are different. Because there is no living algae and zooplankton in the sediment column, the sediment-column phosphorus components are SRP, DOP, POP, and PIP. When algae and zooplankton die, they are treated as POP. Since the horizontal transport is generally very weak in the sediment column, the mass flows of phosphorus components are mainly vertical, and the governing equations are

$$\frac{\partial P_i}{\partial t} = \frac{1}{\phi}\frac{\partial}{\partial z}(\phi M \frac{\partial P_i}{\partial z}) + R_i \qquad i = 1,2 \tag{5.12}$$

$$\frac{\partial P_i}{\partial t} = \frac{\partial}{\partial z}(w_c P_i + M \frac{\partial P_i}{\partial z}) + R_i \qquad i = 5,6 \tag{5.13}$$

where P_1 and P_2 are SRP and DOP concentrations (per unit volume of porewater), w_c is the consolidation velocity of sediments, M is the molecular diffusivity, and ϕ is the porosity.

5.1.3 Nitrogen Equations in the Water Column

The governing equations of nitrogen dynamics are similar to the governing equations of phosphorus components. The nitrogen components simulated in the model are soluble organic nitrogen (SON), soluble ammonium nitrogen, nitrate nitrogen (N3), ammonia nitrogen, particulate ammonium nitrogen, particulate organic nitrogen (PON), algal particulate nitrogen, and zooplankton particulate nitrogen. Under the assumptions mentioned at the beginning of this chapter, the three-dimensional governing equations for nitrogen species in the water column are as follows:

dissolved nitrogen components:

$$\frac{\partial N_i}{\partial t} + \frac{\partial u_j N_i}{\partial x_j} = \frac{\partial \mathcal{F}_j(N_i)}{\partial x_j} + r_i \qquad i = 1,2,3,4 \tag{5.14}$$

adsorbed nitrogen components:

$$\frac{\partial N_i}{\partial t} + \frac{\partial (u_j - \delta_{j3} w_s) N_i}{\partial x_j} = \frac{\partial \mathcal{F}_j(N_i)}{\partial x_j} + r_i \qquad i = 5,6 \tag{5.15}$$

algal particulate nitrogen:

$$\frac{\partial N_7}{\partial t} + \frac{\partial (u_j - \delta_{3j} w_s^a) N_7}{\partial x_j} = \frac{\partial \mathcal{F}_j(N_7)}{\partial x_j} + r_7 \tag{5.16}$$

zooplankton particulate nitrogen:

$$\frac{\partial N_8}{\partial t} + \frac{\partial u_j N_8}{\partial x_j} = \frac{\partial \mathcal{F}_j(N_8)}{\partial x_j} + r_8 \tag{5.17}$$

wherein $N_i(i = 1, ..., 8)$ are concentrations of soluble organic nitrogen, soluble ammonium nitrogen, nitrate nitrogen, and ammonia nitrogen, adsorbed organic nitrogen, adsorbed ammonium nitrogen, algal particulate nitrogen, and zooplankton particulate nitrogen, respectively; and $r_i(i = 1, ..., 8)$ are reaction terms associated with SON, soluble NH_4^+-N, N3, ammonia N, PON, adsorbed NH_4^+-N, algal particulate nitrogen, and zooplankton particulate nitrogen, respectively.

If the advection terms and the horizontal diffusion terms are much smaller than other terms, Equations (5.14) – (5.17) become vertically one-dimensional equations:

$$\frac{\partial N_i}{\partial t} = \frac{\partial}{\partial z}\left(B_v \frac{\partial N_i}{\partial z}\right) + r_i \qquad i = 1, ..., 4 \tag{5.18}$$

$$\frac{\partial N_i}{\partial t} = \frac{\partial}{\partial z}\left(w_s N_i + B_v \frac{\partial N_i}{\partial z}\right) + r_i \qquad i = 5,6 \tag{5.19}$$

$$\frac{\partial N_7}{\partial t} = \frac{\partial}{\partial z}\left(w_s^a N_7 + B_v \frac{\partial N_7}{\partial z}\right) + r_7 \tag{5.20}$$

$$\frac{\partial N_8}{\partial t} = \frac{\partial}{\partial z}\left(B_v \frac{\partial N_8}{\partial z}\right) + r_8 \tag{5.21}$$

5.1.4 Nitrogen Equations in the Sediment Column

Like phosphorus, nitrogen transformation processes in the sediment column can be very different from those in the water column due to the different redox potential and other physical and biochemical factors. In the bed soil, there exist two distinctive layers: an aerobic layer and an anaerobic layer within which the transformation processes are not the same. For example, in the anaerobic layer, there is no nitrification process due to the lack of oxygen, while in the aerobic layer, there is no denitrification process due to the availability of oxygen. In the sediment column, since the horizontal advection and diffusion are generally insignificant, the transport of nitrogen components is primarily vertical. The vertically one-dimensional governing equations for nitrogen components are

$$\frac{\partial N_i}{\partial t} = \frac{1}{\phi}\frac{\partial}{\partial z}(\phi M\frac{\partial N_i}{\partial z}) + r_i \qquad i = 1,...,4 \tag{5.22}$$

$$\frac{\partial N_i}{\partial t} = \frac{\partial}{\partial z}(w_c N_i + M\frac{\partial N_i}{\partial z}) + r_i \qquad i = 5,6 \tag{5.23}$$

5.2 Boundary and Initial Conditions

5.2.1 Lateral Boundaries

The lateral boundaries can be either open boundaries or solid boundaries. Along a solid boundary, the boundary conditions for phosphorus and nitrogen components are that the diffusive fluxes through the boundary and hence the normal concentration gradients are zero:

$$\frac{\partial P_i}{\partial n} = 0 \tag{5.24}$$

$$\frac{\partial N_i}{\partial n} = 0 \tag{5.25}$$

where n is in the direction normal to the boundary.

Along an open boundary, nutrient concentrations are calculated by the advective transport equations similar to Equation (4.26).

$$\frac{\partial P_i}{\partial t} = -\frac{\partial u P_i}{\partial x} - \frac{\partial v P_i}{\partial y} \tag{5.26}$$

$$\frac{\partial N_i}{\partial t} = -\frac{\partial u N_i}{\partial x} - \frac{\partial v N_i}{\partial y} \tag{5.27}$$

5.2.2 Free Surface

At the free surface, the boundary conditions for all phosphorus and nitrogen species, except for ammonia nitrogen, are that the diffusive fluxes are zero. Thus,

$$\frac{\partial P_i}{\partial z} = 0 \qquad i = 1,2,4 \tag{5.28}$$

$$w_s P_i + B_v \frac{\partial P_i}{\partial z} = 0 \qquad i = 5,6 \tag{5.29}$$

$$w_s^3 P_3 + B_v \frac{\partial P_3}{\partial z} = 0 \tag{5.30}$$

$$\frac{\partial N_i}{\partial z} = 0 \qquad i = 1,2,3,8 \tag{5.31}$$

$$w_s N_i + B_v \frac{\partial N_i}{\partial z} = 0 \qquad i = 5,6 \tag{5.32}$$

$$w_s^a N_7 + B_v \frac{\partial N_7}{\partial z} = 0 \tag{5.33}$$

The boundary condition for ammonia nitrogen at the water surface is determined by the volatilization rate:

$$B_v \frac{\partial N_4}{\partial z} = v_{an}(h_v N_4 - N_a^4) \tag{5.34}$$

where v_{an} is the rate constant of volatilization and N_4^a is the ammonia nitrogen concentration in the air.

5.2.3 Water-Sediment Interface

Except for P_3, P_4, N_7, and N_8 equations, all other P and N equations are solved continuously from the sediment column to the water column in this study. Therefore, only boundary conditions for P_3, P_4, N_7, and N_8 need to be specified at the water-sediment interface. These boundary conditions are as follows:

$$w_s^a P_3 + B_v \frac{\partial P_3}{\partial z} = v_d P_3 \tag{5.35}$$

$$\frac{\partial P_4}{\partial z} = 0 \tag{5.36}$$

$$w_s^a N_7 + B_v \frac{\partial N_7}{\partial z} = v_d N_7 \tag{5.37}$$

$$\frac{\partial N_8}{\partial z} = 0 \tag{5.38}$$

5.2.4 Bottom of Simulated Sediment Column

The boundary conditions at the bottom of the simulated sediment column are

$$\frac{\partial P_i}{\partial z} = 0 \tag{5.39}$$

$$\frac{\partial N_i}{\partial z} = 0 \tag{5.40}$$

5.2.5 Initial Conditions

The initial concentrations of phosphorus and nitrogen components can be determined by available measured data. For example, if the SRP concentrations at several stations were measured synoptically at the sometime, the initial SRP concentration in the entire model domain can be obtained by an interpolation scheme which uses distance-inverses as weighting factors. In the absence of any measured data, proper constant values may be assumed as initial concentrations.

5.3 Modeling Nutrient Transformation Processes

The phosphorus kinetic pathways shown in Figure 2.1 were expressed as reaction terms R_i ($i = 1, ..., 6$) in Equations (5.1) through (5.13), while nitrogen kinetic pathways shown in Figure 2.1 were expressed as reaction terms r_i ($i = 1, ..., 8$) in Equations (5.14) through (5.23). Like most of the existing water quality models, nutrient models developed in this study also used first-order formulations to describe most of the reactions, except for those associated with algal and zooplankton growth. For the growth rate of algae and zooplankton, Michaelis-Menten type formulations were used. This section is a brief description of the treatment of these reaction terms in the phosphorus model and the nitrogen model.

5.3.1 Transformation Processes in Phosphorus Cycle

5.3.1.1 SRP

The kinetic pathways of soluble reactive phosphors (SRP) include the uptake of SRP by algae, the excretions of SRP by algae and zooplankton, the desorption/adsorption of inorganic phosphorus from/onto sediment particles, and the release of SRP from dissolved organic phosphorus due to the mineralization process. Therefore R_1 has the following terms:

$$\begin{aligned} R_1 \;&=\; -\mu_a P_3 + K_{ax} P_3 + K_{zx} P_4 \qquad (5.41) \\ &\quad +d_{ip}(P_6 - p_{ip} \mathrm{c} P_1) + K_D P_2 \end{aligned}$$

where c is the sediment concentration K_{ax} and K_{zx} are the excretion rate of algae and zooplankton, K_D is the rate constant of the mineralization of DOP, d_{ip} is the desorption rate of PIP, p_{ip} is the partition coefficient between PIP and SRP, and

$$\mu_a = \mu_{a_{max}} f_a(T) g(I) \frac{P_1}{H_p + P_1} \frac{N_3 + N_4}{H_n + N_3 + N_4} \qquad (5.42)$$

is the growth rate of algae, where $\mu_{a_{max}}$ is the maximum growth rate of algae, $f_a(T)$ is the temperature limiting function for algal growth, and $g(I)$ is the light intensity limiting function for algal growth.

5.3.1.2 DOP

The kinetic pathways of dissolved organic phosphorus (DOP) are the mineralization of DOP, the release of DOP during the mortality of algae and zooplankton, and the adsorption/desorption of organic phosphorus from/onto sediment particles. If the release of DOP during the mortality of algae and zooplankton is included in the pathways from particulate plankton phosphorus to POP and then from POP to DOP, R_2 can be written as

$$R_2 = -K_D P_2 + d_{op}(P_5 - p_{op} c P_2) \tag{5.43}$$

where d_{op} is the desorption rate of particulate organic phosphorus, p_{op} is the partition coefficient between POP and DOP.

5.3.1.3 Alg-P

The kinetic pathways associated with algal particulate phosphorus include the uptake of SRP by algae, the conversion of algal phosphorus to zooplankton phosphorus due to the uptake of algae by zooplankton, the excretion of SRP by algae, and the release of DOP during the mortality of algae. Therefore, R_3 can be written as

$$R_3 = \mu_a P_3 - K_{ax} P_3 - K_{as} P_3 - \mu_z P_4 \tag{5.44}$$

where μ_z is the growth rate of zooplankton due to the uptake of algae:

$$\mu_z = \mu_{z_{max}} f_z(T) \frac{c_a}{H_a + c_a} \tag{5.45}$$

5.3.1.4 Zoo-P

The kinetic pathways associated with zooplankton particulate phosphorus are the uptakes of algae, the excretion of SRP by zooplankton, and the release of DOP during the mortality of zooplankton:

$$R_4 = \mu_z P_4 - K_{zs} P_4 - K_{zx} P_4 \tag{5.46}$$

5.3.1.5 POP

The kinetic pathways of POP include the POP increase due to the mortality of algae and zooplankton and the desorption/adsorption of organic phosphorus from/onto sediment particles:

$$R_5 = K_{as}P_3 + K_{zs}P_4 - d_{op}(P_5 - p_{op}cP_2) \tag{5.47}$$

wherein K_{as} and K_{zs} are mortality rates of algae and zooplankton, respectively. The first two terms in R_5 are zero in the sediment column.

5.3.1.6 PIP

The kinetic pathways of PIP are the desorption/adsorption processes of inorganic phosphorus from/onto sediment particles:

$$R_6 = -d_{ip}(P_6 - p_{ip}cP_1) \tag{5.48}$$

The above transformation terms are not the same as those in WASP model and Dickinson *et al.*'s model for phosphorus dynamics. While WASP and Dickinson *et al.*'s model used equilibrium model for desorption-adsorption reactions, this study used kinetics model for these reactions because of the small time step used in the present study. Unlike Dickinson *et al*'s model which simulates three algal groups (green, blue-green, and diatom), this study aggregates all algal groups into one group due to the lack of data on algae. This treatment is the same as that in WASP model.

5.3.2 Transformation Processes in Nitrogen Cycling

5.3.2.1 SON

The kinetic pathways of soluble organic nitrogen (SON) are similar to those of dissolved phosphorus (DOP). They include the ammonification of SON, the desorption/adsorption of organic nitrogen from/onto sediment particles, and the release of SON during the mortality of algae and zooplankton. If the last pathway is treated in the same way as in the phosphorus cycle, the reaction term r_1 reads

$$r_1 = d_{on}(N_5 - p_{on}cN_1) - K_4N_1 \tag{5.49}$$

where K_4 is the rate constant of ammonification, d_{on} is the desorption rate of particulate organic nitrogen, and p_{on} is the partition coefficient of organic nitrogen in soluble and adsorbed phases.

5.3.2.2 Soluble Ammonium N

The kinetic pathways of soluble ammonium nitrogen include the ammonification of SON, the nitrification of soluble NH_4^+-N, the adsorption/desorption of ammonium nitrogen, the transformation between NH_4^+-N and NH_3-N, the uptake of ammonium by algae, and the excretions by algae and zooplankton (N_2 in this chapter represents soluble ammonium nitrogen, not nitrogen gas):

$$\begin{aligned} r_2 &= K_4N_1 - K_3N_2 + d_{an}(N_6 - p_{an}\mathrm{c}N_2) \\ &+ d_{aa}(N_4 - p_{aa}N_2) - P_n\mu_a N_7 + K_{ax}N_7 + KzxN_8 \end{aligned} \tag{5.50}$$

wherein K_3 is the rate constant of nitrification (equals zero in the anaerobic layer of the sediment column), d_{an} is the desorption rate of adsorbed ammonium nitrogen, p_{an} is the partition coefficient between adsorbed NH_4^+-N and dissolved NH_4^+-N, d_{aa} is the rate constant of the transformation between dissolved ammonium and ammonia, p_{aa} is the partition coefficient between dissolved ammonium-N and ammonia-N, and P_n is a preference factor for the uptaking of nitrogen nutrient by algae (Ambrose *et al.*, 1991).

$$P_n = \frac{N_2 \cdot N_3}{(H_n + N_2)(H_n + N_3)} + \frac{H_n N_2}{(N_2 + N_3)(H_n + N_3)} \tag{5.51}$$

5.3.2.3 Nitrate N

The kinetic pathways associated with nitrate nitrogen are the ammonification of soluble NH_4^+-N, the denitrification of N3, and the uptake of nitrate by algae for the growth:

$$r_3 = K_3N_2 - K_2N_3 - (1 - P_n)\mu_a N_7 \tag{5.52}$$

wherein K_2 is the rate constant of denitrification (only in the anaerobic layer of the sediment column).

5.3.2.4 Ammonia N

The kinetic pathways associated with ammonia nitrogen include the conversion between NH_4^+-N and NH_3-N:

$$r_4 = d_{aa}(p_{aa}N_2 - N_4) \tag{5.53}$$

5.3.2.5 PON

The kinetic pathways of particulate organic nitrogen include the desorption/adsorption processes and the the PON increase due to the mortality of algae and zooplankton:

$$r_5 = K_{as}N_7 + K_{zs}P_4 - d_{on}(N_5 - p_{on}cN_1) \tag{5.54}$$

where K_{as} and K_{zs} are mortality rates of algae and zooplankton.

5.3.2.6 PIN

The kinetic pathways of particulate ammonium nitrogen include the desorption/adsorption processes:

$$r_6 = -d_{an}(N_6 - p_{an}cN_2) \tag{5.55}$$

5.3.2.7 Alg-N

The kinetic pathways associated with algal particulate nitrogen include the uptake of nitrate and ammonia by algae, the conversion of algal nitrogen to zooplankton nitrogen due to the uptake of algae by zooplankton, the excretion of nitrogen by algae, and the release of SON during the mortality of algae. r_7 can be written as

$$r_7 = (\mu_a - K_{ax} - K_{as})N_7 - \mu_z N_8 \tag{5.56}$$

5.3.2.8 Zoo-N

The kinetic pathways associated with zooplankton particulate nitrogen are the uptake of algae, the excretion of nitrogen by zooplankton, and the release of SON during the mortality of zooplankton:

$$r_8 = (\mu_z - K_{zx} - K_{zs})N_8 \tag{5.57}$$

The above transformation terms are not the same as those in WASP model for nitrogen dynamics. While WASP uses equilibrium model for desorption-adsorption reactions of inorganic/organic nitrogen species, this study uses kinetics model for these reactions because of the small time step used in the present study. Because ammonia and ammonium have different functions in the nitrogen cycling, this study treats these two species separately. However, in WASP model these two species are aggregated into one species.

5.3.3 Modeling the Growth of Algae and Zooplankton

Concentrations c_a and c_z in the forenamed equations are the concentrations of algae and zooplankton in the water column, respectively. The governing equations for c_a and c_z are

$$\begin{aligned} \frac{\partial c_a}{\partial t} + \frac{\partial (u_j - \delta_{j3} w_s^a) c_a}{\partial x_j} &= \frac{\partial \mathcal{F}_j(c_a)}{\partial x_j} \\ &+ \mu_{a_{max}} f_a(T) g(I) \frac{P_1}{H_p + P_1} \frac{N_3 + N_4}{H_n + N_3 + N_4} c_a \\ &- \mu_{z_{max}} f_z(T) \frac{c_a}{H_a + c_a} c_z - K_{as} c_a - K_{az} c_a \end{aligned} \tag{5.58}$$

and

$$\begin{aligned} \frac{\partial c_z}{\partial t} + \frac{\partial u_j c_z}{\partial x_j} &= \frac{\partial \mathcal{F}_j(c_z)}{\partial x_j} - K_{zs} c_z \\ &- K_{zz} c_z + \mu_{z_{max}} f_z(T) \frac{c_a}{H_a + c_a} c_z \end{aligned} \tag{5.59}$$

wherein $f_a(T)$ and $f_z(T)$ are temperature limiting functions for the growth of algae and zooplankton (see Chapter 2), H_p and H_n are half-saturation constants for the uptake of phosphorus and nitrogen by algae, respectively, and K_{as} and K_{zs} are non-predatory mortality rates of algae and zooplankton, respectively.

The boundary boundary conditions for the above two equations are as follows: At the free surface,

$$\frac{\partial}{\partial z}(c_a, c_z) = 0 \tag{5.60}$$

At the water-sediment interface,

$$w_s^a c_a + B_v \frac{\partial c_a}{\partial z} = v_d^a c_a \tag{5.61}$$

$$B_v \frac{\partial c_z}{\partial z} = 0 \tag{5.62}$$

where v_d^a is the deposition velocity of algae. v_d^a is assumed to be a fraction $(0 - 1)$ of the settling velocity of algae.

5.4 Model Parameters

Reaction terms described in the last section contain many model parameters which should be determined before using the models. The model parameters include

1. maximum growth rate of algae $\mu_{A_{max}}$ (1/day),
2. half-saturation constants for the algal growth H_p and H_n (μg/l),
3. maximum growth rate of zooplankton $\mu_{Z_{max}}$ (1/day),
4. half-saturation constant for the zooplankton growth H_a (μg/l),
5. excretion rate of SRP by algae K_{ax} (1/day),
6. excretion rate of SRP by zooplankton K_{zx} (1/day),
7. mortality rate of algae K_{as} (1/day),
8. mortality rate of zooplankton K_{zs} (1/day),
9. rate constant of mineralization of DOP K_D (1/day),
10. desorption rate of inorganic phosphorus from sediment particles d_{ip} (1/day),
11. partition coefficient of inorganic phosphorus p_{ip} (l/mg),
12. desorption rate of organic phosphorus from sediment particles d_{op} (1/day), and

13. partition coefficient of organic phosphorus p_{op} (l/mg).

14. ammonification rate constant K_4 (1/day),

15. nitrification rate constant K_3 (1/day),

16. denitrification rate K_2 (1/day),

17. desorption rate of adsorbed organic nitrogen d_{on} (1/day),

18. partition coefficient of organic nitrogen p_{on} (l/mg),

19. desorption rate of adsorbed ammonium nitrogen d_{an} (1/day),

20. partition coefficient of ammonium nitrogen p_{an} (l/mg),

21. rate constant for the transformation from ammonium–N to ammonia–N d_{aa} (1/day),

22. partition coefficient of dissolved NH_4^+–N and NH_3–N p_{aa} (unitless),

23. rate constant of volatilization of ammonia v_{an}, and

24. Henry's constant h_v.

Almost all the rate constants are functions of temperature. Except for the algal growth, the zooplankton growth, and the nitrification process, Van't Hoff-Arrhenius equation is used as the temperature limiting function for different reaction rates in this study. As for the algal growth, the zooplankton growth, and the nitrification process, Lassiter and Kearns' model (Equation (2.52)) is used. Equation (2.53) is used for the light intensity limiting function for the algal growth.

The determination of the model parameters listed above is generally very difficult because they are dependent on many physical and biochemical factors, such as the location of the lake or estuary, temperature and tide variations, point or non-point loadings of nutrients and other chemical materials etc.. Literature values of these parameters vary over a very large range and up to 3 orders of magnitude difference. This study uses typical literature values for most of the above parameters in model applications and adjusts these parameters in order to obtain the most reasonable model results.

5.4.1 Parameters Related to Algal and Zooplankton Growth

While Michaelis (half-saturation) constants H_p and H_n parameterize the dependence of algal growth on nutrients, H_a parameterize the dependence of zooplankton growth on algal concentration. The constant H_p for algal uptake of SRP is the SRP concentration at which the growth rate is one half of the maximum provided other factors affecting the the algal growth stay the same, while the constant H_n for algal uptake of nitrogen nutrient components is the sum of nitrate and ammonia concentrations at which the growth rate is one half of the maximum in case nitrogen is the only limiting factor. Similarly, the constant H_a for zooplankton uptake of algae is the algal concentration at which the growth rate of zooplankton is one half of its maximum value.

The sensitivity of the algal growth to phosphorus and nitrogen concentrations is represented by the ratio of SRP to H_p and the ratio of nitrate and ammonia to H_n, respectively. If the SRP concentration is much lower than H_p, the algal growth rate increases linearly with the increase of SRP. For SRP concentration much larger than H_p, the growth of algae will not depend on the concentration of SRP (in this case, phosphorus is saturated and not a limiting factor for algal growth). Likewise, H_n represents the dependence of algal growth on the concentrations of ammonia and nitrate in the ecosystem. As shown in Table 5.1, literature values of H_p and H_n vary from 2 to 50 $\mu g/l$ for H_p and from 15 to 400 $\mu g/l$ for H_n.

The half-saturation constant H_a represents the relative importance of the algal concentration to the growth rate of zooplankton in the ecosystem. Similar to the algal growth, the growth of zooplankton increases linearly with the increasing food (algae) concentration at small ($<< 1$) ratio of algal biomass to H_a, but becomes independent of the available food concentration at high ($>> 1$) ratio. Literature values of H_a vary over a very large range, depending on the types of zooplankton and algae of concern. Some literature values of H_a are shown in Table 5.2.

Table 5.1: Literature values for H_p and H_n.

H_p ($\mu g/l$)	H_n ($\mu g/l$)	Water body	Reference
4-20	60-90	Eau Galle Reservoir (Wisconsin)	Wolsinski and Collins (1985)
20	200	Glumsø Sø (Denmark)	Jørgensen (1981)
5	50	Lake Biwa	Ikeda and Adachi (1978)
2.5	15	Lake Michigan	Canale *et al.* (1976)
10	25	Lake Erie	Di Toro *et al.* (1975)
30–50	300–400	Lake Ontario	Chen and Orlob (1975)
10.0-12.8	108.6-108.8	East Seto Inland See (Japan)	Kishi (1986)

Table 5.2: Literature values for H_a.

$H_a (\mu g/l)$	Water body	Reference
500-2000	Glumsø Sø, Denmark	Jørgensen (1981)
510	Lake Biwa	Ikeda and Adachi (1978)
200	Lake Michigan	Canale *et al.* (1976)
500	Lake Ontario	Chen and Orlob (1975)

The settling velocity of algae, w_s^a, is another important parameter for computing algal biomass in the aquatic system. Depending on algal species, temperature, light intensity, nutrient concentrations etc., the algal settling velocity varies over a very large range. Table 5.3 presents some typical literature values of algal settling velocity.

Table 5.3: Literature values for w_s^a.

w_s^a (m/day)	Water body	Reference
0.0-0.10	Chesapeake Bay	Salas and Thomann (1978)
0.04	Glumsø Sø (Denmark)	Jørgensen (1981)
0.76	Lower Winooski River	van Benschoten and Walker (1984)
0.14	Lake Valencia (Venezuela)	Jaffe (1988)
0.03	Lake Näsiselkä (Finland)	Virtanen *et al.* (1986)
0.01-0.5	Lake Veluwe, (the Netherlands)	Keesman and van Stratten (1990)
0.23	Lake Okeechobee	Blosser (1986)
0.2-1.7 (Melosira)	Lake Kasumigaura (Japan)	Takamura and Yasuno (1988)
0.2-2.0 (Synedra)	Lake Kasumigaura	Takamura and Yasuno (1988)
0.0045-0.24 (Microcystis)	Lake Kasumigaura	Takamura and Yasuno (1988)
0.06 (Anabaena)	Lake Kasumigaura	Takamura and Yasuno (1988)

5.4.2 Parameters in the Phosphorus Model

One of the important parameters in the phosphorus model is the mineralization rate constant K_D. Typical values of this parameter varies from 0.1 day^{-1} to 1 day^{-1} (Keesman and Van Stratten, 1990), and is thus not a very sensitive parameter in modeling short-term phosphorus dynamics. Typical literature values for the rate coefficient K_D governing the mineralization of DOP to SRP are presented in Table 5.4.

Table 5.4: Literature values for DOP mineralization rate.

K_D $(1/day)$	Water body	Reference
0.10 - 0.20	Chesapeake Bay	Salas and Thomann (1978)
0.10	Lake Glumsø Sø, (Denmark)	Jørgensen (1981)
0.05	Saginaw Bay	Bierman *et al.* (1980)
0.1	Lower Winooski River	van Benschoten and Walker (1984)
0.0176	Lake Valencia (Venezuela)	Jaffe (1988)
0.1-1.0	Lake Veluwe (the Netherlands)	Keesman and van Stratten (1990)
0.5	Lake Wolderwijd (the Netherlands)	Boers *et al.* (1991)

The most important parameters in phosphorus model are the desorption rates d_{op} and d_{ip} and the partition coefficients p_{op} and p_{ip}, which parameterize the release of the organic and inorganic phosphorus from sediments. In a episodic event, the desorption of organic and inorganic phosphorus from the sediment particles is major pathway of internal loading of phosphorus into the water column, because POP and PIP concentrations in the bottom sediments are generally much higher than those in the water column.

The release of organic and inorganic phosphorus from sediment particles is generally dependent of water temperature, pH value, dissolved oxygen concentration, sediment particle size, and the equilibrium condition between the dissolved forms and adsorbed forms of phosphorus components. Previous water quality models (e.g., WASP model) assumed that the equilibrium between the dissolved and the adsorbed forms of phosphorus species is reached instantaneously. In other words, the speeds of the desorption/adsorption reactions were assumed to be infinity in these models, although the final equilibrium between the dissolved and the adsorbed forms may take a long time to establish, depending on the temperature, pH, and dissolved oxygen concentration.

5.4.3 Parameters in the Nitrogen Model

The mineralization process of SON is consisted of the ammonification process and the subsequent nitrification process. The rate constants K_4 and K_3 represent the speeds of these two transformation processes. The rate of ammonification in lakes and estuaries is dependent on temperature, pH value, C/N ratio of the residue, available nutrients, and soil texture and structure. K_4 generally increases with increasing temperature. The rate of aerobic ammonification can double with a temperature increase of 10^oC (Reddy and Patrick, 1984). Cho and Ponnamperuma (1971) found that ammonia production increased 100% when the temperature of anaerobic soil was raised from 15 to 40^oC. The optimum pH range for ammonification process is between 6.5 and 8.5

Nitrification takes place as a result of the activity of chemoautotrophic bacteria of genera Nitrosomonas and Nitrobacter. It is affected by temperature, pH value, alkalinity of water, inorganic carbon source, microbial population and ammonium-nitrogen concentration. The ideal temperature for the nitrification process is about 25 to 40^0C (Reddy and Patrick, 1984). Reddy and Graetz (1981) found that nitrification in a waste water column aerated with air containing CO_2 is faster than that in a water column aerated with CO_2 free air. Erh *et al.* (1967) reported that high concentrations of ammonium-nitrogen have the effect of retarding nitrification by inhibiting the activity of Nitrobacter, particularly at high pH values. Reddy and Patrick (1984) listed various values of K_3 for oxidation of ammonium in various soil-water systems.

While nitrification can only take place under aerobic condition, denitrification can only take place under anaerobic condition. Under oxygen-free condition and in the presence of available organic substrate, the denitrifying organisms use nitrate as an electron acceptor during respiration. The speed of this reaction is parameterized by the model parameter K_2, which is influenced by temperature, soil moisture, pH, presence of denitrifers, soil texture, and presence of readily available carbon (Reddy and Patrick, 1984). In general, the denitrification rate in coastal marine sediments is greater than that in lake or river sediments (Seitzinger, 1988). Table 5.5 presents some literature values for K_2, together with some K_3 and K_4 values.

Table 5.5: Literature values for K_2, K_3, and K_4.

K_2 $(1/day)$	K_3 $(1/day)$	K_4 $(1/day)$	Water body	Reference
0.003	0.25-0.6	0.003-0.006	Everglades	Reddy *et al.* (1990)
0.00155	0.001	0.000027-0.00834	Lake Apopka	Reddy *et al.* (1988)
	0.03		Lake Ontario	Chen and Orlob (1975)
0.002			Lake Glumsø Sø (Denmark)	Jørgensen (1981)
	0.16	0.024	Lake Michigan	Canale *et al.* (1976)

The parameters d_{on} and p_{on} parameterize the adsorption-desorption kinetics between soluble organic nitrogen and adsorbed organic nitrogen in sediments. Likewise, the parameters d_{an} and p_{an} parameterized the adsorption-desorption kinetics of ionic ammonium-nitrogen between sediment particles and water. While d_{on} and d_{an} parameterize the speeds of the kinetics, p_{on} and p_{an} parameterize the equilibrium conditions.

The kinetics of adsorption-desorption of ionic nitrogen species in estuaries are affected by temperature, salinity, cation exchange capacity, and texture and structure of soil. Gschwend *et al.* (1987) developed a model which is based on the physics of interparticle diffusion. Weber and Liu (1980) considered interparticle diffusion as one of the limiting mechanisms for sorption of organic compounds to activated carbon, synthetic resins, and some porous catalysts.

An important pathway in nitrogen cycling is the nitrogen volatilization. As mentioned in Section 2.3.5, this kinetic pathway is dependent on the pH value in the system. For the water column with alkaline pH value, ammonium nitrogen is predominantly in the gaseous form of NH_3, which changes back to the ionic form if pH value decreases to 7 or below. The kinetic pathway of nitrogen volatilization can be described by a first-order equation as follows:

$$\frac{\partial N_2}{\partial t} = k_+ N_4 - k_- N_2 \tag{5.63}$$

where $k_+ = d_{aa}$ is the rate constant of reaction (5.63) from left to right, and $k_- = d_{aa} p_{aa}$ is the rate constant of reaction (5.63) from right to left. At the equilibrium condition, the partition between NH_4^+ and NH_3 is given by

$$N_4 = p_{aa} N_2 \tag{5.64}$$

where p_{aa} is the partition coefficient, which can be calculated based on the ionization constants as discussed in Section 2.3.5. Rao *et al.* (1984) used

$$p_{aa} = 5.8 \times 10^{(pH-10)} \tag{5.65}$$

in their nitrogen model for flooded soils.

5.5 Numerical Solution Algorithm

The numerical algorithm used to solve the nutrient equations is similar to that in the sediment transport model except for the reaction terms. A flow chart for the 3-D submodel of nutrient dynamics is presented in Appendix B.

In the finite difference equations for the three-dimensional differential equations of algal biomass, zooplankton biomass, phosphorus species, and nitrogen species, the horizontal advection and diffusion terms are treated explicitly, while the vertical diffusion term as well as the reaction terms are treated implicitly. Because all the nutrient equations are coupled through reaction terms, fractional step method is used in both the 3-D and the 1-D models for simplicity and numerical stability. In the 3-D model, the horizontal diffusion and horizontal and vertical advection terms are solved first, followed by solution of the vertical diffusion term and some of the reaction terms, and finally the desorption/adsorption reaction terms are solved:

$$\frac{C^{n1} - C^{n}}{\Delta t} = H_A^n + H_D^n + V_A^n \tag{5.66}$$

$$\frac{C^{n2} - C^{n1}}{\Delta t} = V_D^{n2} + R_r^{n2} \tag{5.67}$$

$$\frac{C^{n+1} - C^{n2}}{\Delta t} = D_s^{n+1} + A_s^{n+1} \tag{5.68}$$

where H_A, H_D, and V_A are horizontal advection, horizontal diffusion, and vertical advection terms, respectively, R_r represents reaction terms other than the desorption and adsorption reactions, and D_s and A_s represent the desorption and adsorption, respectively.

The negative concentration is numerically possible for a first order reaction if an explicit method is used:

$$\frac{C^{n+1} - C^{n}}{\Delta t} = -KC^n \tag{5.69}$$

or

$$C^{n+1} = (1 - K\Delta t)C^n \tag{5.70}$$

where K is the reaction rate. If $\Delta t > 1/K$, the numerical solution for the concentration C will change its sign every time step.

An implicit treatment of the desorption and adsorption terms can guarantee the numerical stability and non-negative solutions. However, if the desorption/adsorption terms are solved together with the vertical diffusion term, a large full matrix must be solved because of the coupled difference equations for the dissolved and adsorbed nutrient species. By solving the desorption/adsorption terms separately from the other terms, it is possible to treat these terms implicitly. To illustrate this, the difference equations for the desorption/adsorption reactions of SRP are examined:

$$\frac{P_1^{n+1} - P_1^{n2}}{\Delta t} = d_{ip} P_6^{n+1} - d_{ip} p_{ip} c P_1^{n+1} \tag{5.71}$$

$$\frac{P_6^{n+1} - P_6^{n2}}{\Delta t} = -d_{ip}P_6^{n+1} + d_{ip}p_{ip}\mathrm{c}P_1^{n+1} \qquad (5.72)$$

where P_1 and P_6 are concentrations of SRP and PIP, respectively, and d_{ip} and p_{ip} are desorption rate and partition coefficient of inorganic phosphorus, respectively. Numerical solutions to the above two equation can be readily obtained.

Equation (5.67) can be written in the same form as that of Equation (C.10), in which $A_1(k)$ and $A_4(k)$ may consist of reaction terms. The Thomas Algorithm is used to inverse the tridiagonal matrix.

The finite-difference form for the horizontal diffusion terms in equation (5.66) is based on the standard second-order central difference formula. For the advection terms, three algorithms described in the sediment model could be used: (1) central difference (2) upwind difference, and (3) combined central and upwind differences.

To improve the stability of the nutrient model, the nutrient model treats all the reaction terms implicitly. However, this can only be done when a certain order is followed when solving for the nutrient equations. The proper order of solving nutrient equations is as follows:

1. zooplankton biomass c_z,
2. algal biomass c_a,
3. particulate zooplankton phosphorus P_4,
4. particulate algal phosphorus P_3,
5. dissolved organic phosphorus P_2,
6. soluble reactive phosphorus P_1,
7. particulate organic phosphorus P_5,
8. particulate inorganic phosphorus P_6,

9. particulate zooplankton nitrogen N_8,
10. particulate algal nitrogen N_7,
11. soluble organic nitrogen N_1
12. dissolved ammonium nitrogen N_2
13. nitrate nitrogen N_3
14. ammonia nitrogen N_4
15. particulate organic nitrogen N_5, and finally
16. particulate inorganic nitrogen N_6.

In solving Equation (5.67) for organic/inorganic P and N species, the difference equations for the entire water column and sediment column are solved simultaneously. The exchanges of adsorbed nutrient species between the sediment column and the water column are automatically included in the numerical solutions. On the other hand, the exchanges of adsorbed nutrients at the water-sediment interface are determined by the resuspension and deposition fluxes of sediments. In order to ensure that the nutrient models are consistent with the sediment models in terms of the bottom exchanges, a special treatment is needed to solve the difference equations for adsorbed nutrients. The basic idea of this treatment is to solve the adsorbed nutrient concentrations in unit of percentage ($\mu g/\mu g$) so that the erosion and deposition rates calculated in the sediment model can be imported into the governing equations for adsorbed nutrients. As an example, consider the vertical 1-D PIP equation (Equation (5.11)). Let p_6 be the inorganic phosphorus per unit mass of sediments, then,

$$P_6 = p_6 c \tag{5.73}$$

where c is the sediment concentration and P_6 is the PIP concentration. Substitute P_6 with p_6c into Equation (5.11):

$$\frac{\partial(p_6c)}{\partial t} = \frac{\partial}{\partial z}(w_sp_6c + B_v\frac{\partial(p_6c)}{\partial z}) + R_6 \tag{5.74}$$

or

$$p_6\frac{\partial c}{\partial t} + c\frac{\partial p_6}{\partial t} = \frac{\partial}{\partial z}(p_6(w_sc + B_v\frac{\partial c}{\partial z})) + \frac{\partial}{\partial z}(B_vc\frac{\partial p_6}{\partial z}) + R_6 \tag{5.75}$$

Since the vertical one-dimensional sediment equations reads

$$\frac{\partial c}{\partial t} = \frac{\partial}{\partial z}(w_sc + B_v\frac{\partial c}{\partial z}) \tag{5.76}$$

Equation (5.75) becomes

$$c\frac{\partial p_6}{\partial t} = (w_sc + B_v\frac{\partial c}{\partial z})\frac{\partial p_6}{\partial z} + \frac{\partial}{\partial z}(B_vc\frac{\partial p_6}{\partial z}) + R_6 \tag{5.77}$$

This equation allows us to import the erosion and deposition rates calculated in the sediment model into the PIP equation. Since the boundary condition used for sediment at the bottom is

$$w_sc + B_v\frac{\partial c}{\partial z} = D - E \tag{5.78}$$

Equation (5.77) at the water-sediment interface becomes

$$c\frac{\partial p_6}{\partial t} = (D - E)\frac{\partial p_6}{\partial z} + \frac{\partial}{\partial z}(B_vc\frac{\partial p_6}{\partial z}) + R_6 \tag{5.79}$$

Numerical tests show that this treatment for adsorbed nutrient species is necessary to yield accurate model results.

CHAPTER 6
FIELD DATA COLLECTED IN LAKE OKEECHOBEE

6.1 Physical Setting

Lake Okeechobee, located in south central Florida (Figure 6.1), is the largest freshwater body in the state of Florida. It is the largest freshwater lake in the U.S., second to the Great Lakes. The lake receives drainage from south central Florida's agricultural area, and provides freshwater to the populous areas of southeastern Florida. As can be seen from Figure 6.2, Lake Okeechobee is a shallow lake with a maximum depth of about 5 m. The bathymetric cross-section AA' in Figure 6.2 shows that the deep region of the lake is in the eastern central portion, and that the western portion is shallow with a mild slope of *ca.* 0.00016.

In Lake Okeechobee, as in most shallow lakes, momentum is imparted to the water primarily by the action of surface wind stress. Therefore, the circulation pattern in the lake is primarily wind-driven. Wind over Lake Okeechobee varies on a time scale of less than one hour, and a spatial scale of about 10 km.

Sediments in Lake Okeechobee are composed of mostly fine-grained (silt and clay-sized) material in the deep region, with sand and shell in the shallow region of the lake (Figure 6.3). The thickness of the fine-grained sediments (mud) in Lake Okeechobee varies as shown in Figure 6.4, with the thickest accumulation being in the eastern central part of the lake.

Lake Okeechobee is a naturally eutrophic lake with the annual mean total phosphorus (TP) concentration ranging from 50-100 $\mu g/l$ (Schelske, 1989). The lake received more and more phosphorus and moved towards hypereutrophic status (annual mean TP $\geq 100 \mu g/l$) in 1980s (Huber *et al.*, 1982). Phosphorus enters Lake Okeechobee in a variety of forms via various physical pathways. The sources of phosphorus to Lake Okeechobee include dissolved and sediment-bound phosphorus from tributaries and canals, resuspended sediment-bound inorganic and organic phosphorus, diffusive fluxes of dissolved inorganic and organic phosphorus from the lake bottom, atmospheric deposition of dry particulates, and scavenged SRP in the rainfall (Brezonik *et al.*, 1983). High phosphorus loadings were from an extensive dairy industry in the Taylor Creek – Nubbin Slough drainage. Although Lake Okeechobee is a shallow, wind-driven, mixing basin, the lake is not a homogeneous water mass. Strong spatial gradients in phosphorus and nitrogen existed in data collected by the South Florida Water Management District at 40 station in the lake in the 1980s (Schelske, 1989).

6.2 Field Measurements

Extensive field experiments in Lake Okeechobee were conducted by the Department of Coastal & Oceanographic Engineering under the direction of Dr. Y. P. Sheng between 1988 and 1993. In these field measurements, portable platforms (Figure 6.5) were deployed at selected stations (Figure 6.1) in Lake Okeechobee to collect data of (1)wind speed and wind direction, (2)water velocity, (3)suspended sediment concentration, and (4)water temperature. In some experiments, pH, dissolved oxygen, phosphorus, and chlorophyll *a* were also measured. In addition, five synoptic surveys were conducted in the fall of 1988 and the spring of 1989, respectively. Data collected in the synoptic surveys include suspended sediment concentration, SRP concentration, total dissolved phosphorus concentration, and total phosphorus concentration. Results of the field experiments were presented in several reports (Sheng *et al.*, 1991; Sheng *et al.*, 1993).

Instruments used in the field measurements of hydrodynamics and sediment concentrations consisted of data loggers, real time data units (RTDU), water temperature gauges, bi-directional current meters, optical back scatter (OBS) sensors, pressure

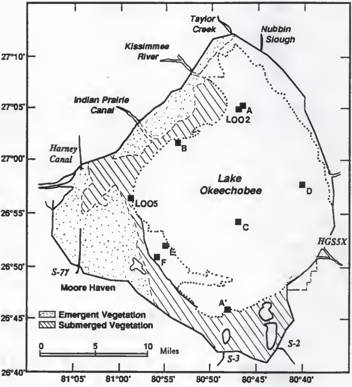

Figure 6.1: Major features of Lake Okeechobee (after Sheng *et al.*, 1989a).

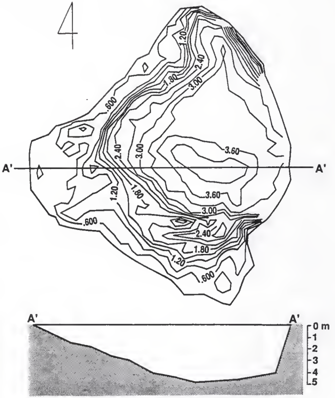

Figure 6.2: Bathymetry of Lake Okeechobee (after Sheng *et al.*, 1989a).

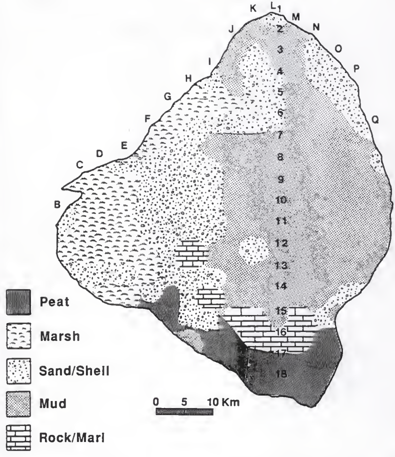

Figure 6.3: Bottom sediment types of Lake Okeechobee (after Reddy and Graetz, 1989).

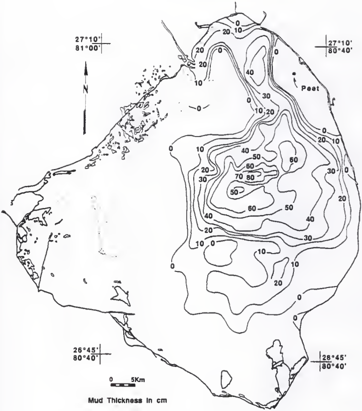

Figure 6.4: Mud Thickness in Lake Okeechobee (after Hwang and Mehta, 1989).

transducers, and wind anemometers. All these equipments were mounted on the portable platforms developed by Sheng et. al. (1989b) (Figure 6.5). Details of the instruments were described in Sheng *et al.* (1989). For completeness, a brief description of these instruments is given in the following.

The data logger was a SeaData models in the 1988 and 1989 field experiments and a Tattletale model 6 from Onset Corporation in 1993. The RTDU was programmed to collect data from each instrument for a 10 minute period, every 15 minutes, at a one second burst rate. The average for the 10 minute run was then calculated and stored for future retrieval. The power supply for the instrumentation was adequate for 12-13 days of continuous recording. Data were retrieved from the unit every 7-9 days. This allowed a three day window so no data would be lost between the weekly data retrievals. The instruments were mounted on two or three separate arms placed in the water at pre-selected heights from the bottom.

The water temperature gauges were model SBE-3 from Sea-Bird Electronics Inc. in the 1993 field experiment. The output from the temperature probes was a frequency between 5,000 and 13,000 Hertz corresponding to a temperature of -5 to $+35^\circ C$. The output of the temperature probes was connected to the RTDU's frequency input through the frequency multiplexer card.

The bi-directional current meters were Marsh-McBirney model 521 electromagnetic devices. These units measure water currents by using the Faraday principle of electromagnetic induction. A conductor passing through a magnetic field will produce a voltage proportional to the conductor velocity. The water acts as a conductor and four probes measure the electric potential developed as the water flows past the sensor. The current meters were set up to produce a voltage from $0.5v$ through $4.5v$ for a water current speed from -10 ft/sec to $+10$ ft/sec. These units have a demonstrated tendency to drift over time so frequent calibrations are necessary for absolute current

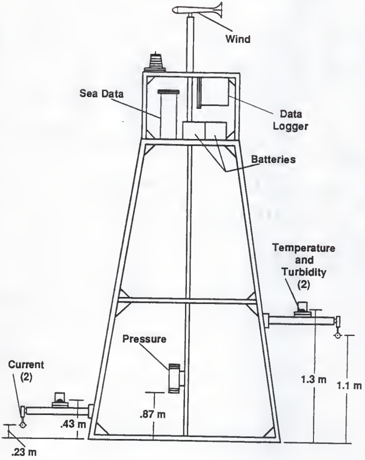

Figure 6.5: A portable platform for field measurements

measurements. The voltage produced by the current meters was sent to the RTDU's Analog input channels.

The total suspended solid (TSS) concentration was measured by OBS-2 instruments from D & A Instruments and Engineering. The Optical Back Scatter (OBS) sensors measure the amount of light reflected by the suspended particles in the water. The calibration of the OBS sensors is dependent on the type and size of particles in suspension. The OBS units were calibrated with a Formazin solution in units of NTU just prior to deployment. A mud sample was then taken from the deployment site and conversion coefficients were calculated to change the NTU units to mg/l.

The pressure transducer, a model P21L-A from Transmetrics provided a 0 – 5 v output corresponding to pressure from 0 PSIA – 50 PSIA. This unit was calibrated against a CEC primary pressure standard prior to placement in the field.

The anemometer from R.M. Young consists of a propeller wind speed sensor connected to an integral direction vane mounted about 3 meters above the water surface. This unit was calibrated in a wind tunnel prior to its deployment.

For water quality measurement, multi-parameter monitoring instruments manufactured by Hydrolab were used to record dissolved oxygen concentration and pH, and Sigma water samplers were deployed at the instrument tower arms every hour. The Sigma samplers contained 24 sample bottles with a 1000 ml capacity. Nutrient and chlorophyll *a* data were then obtained from the sampled water in laboratory experiments.

6.3 1989 Spring Survey

Two four-week long surveys were made by the UF Coastal and Oceanographic Department in lake Okeechobee in the fall of 1988 and the spring of 1989. Data collected in these two surveys include (1)time series of wind, current, temperature, and suspended sediment concentration at six pre-selected stations (in Figure 6.1, Stations A', B, C, D, E, and F in 1988, and Stations A, B, C, D, E, and F in

1989), and (2) synoptic surveys of suspended sediment concentration (SSC), total phosphorus concentration (TP), SRP concentration, and total dissolved phosphorus concentration (TDP). For the purpose of comparing model results to data, only the 1989 survey is briefly presented here.

The 1989 spring survey began on May 21, and ended on June 16. The entire survey period was divided into four short periods, or weeks. Week 1 was from May 21 to May 27, week 2 was from May 27 to June 3, week 3 was from June 3 to June 10, and week 4 was from June 10 to June 16. (Table 6.1). The five synoptic surveys were conducted at the beginning and the end of each week at about 25 locations in the lake (see Figure 6.6 for the locations of the synoptic survey in the spring of 1989).

Table 6.1: The synoptic surveys conducted in the spring of 1989 in Lake Okeechobee.

Week	Julian days	Starting date & time		Ending date & time	
1	141.50 – 147.49	5/21	12:00	5/27	11:45
2	147.50 – 154.49	5/27	12:00	6/03	11:45
3	154.50 – 161.49	6/03	12:00	6/10	11:45
4	161.50 – 167.49	6/10	12:00	6/16	11:45

Table 6.2 presents the location and the water depth of the six stations in the spring 1989 survey. Table 6.3 lists the elevations of underwater instrument arms and the elevation of wind sensors above the mean water surface. It should be noted that the current meters were deployed at depths different from these of the temperature gauges and OBS sensors.

Table 6.2: Locations and depths of the stations in Lake Okeechobee.

Station	Latitude	Longitude	Mean water depth (cm)
A	26°45.67'	80°47.83'	183
B	27°02.78'	80°54.31'	152
C	26°54.1'	80°47.36'	366
D	26°58.47'	80°40.34'	335
E	26°52.81'	80°55.96'	152
F	26°52.3 '	80°56.91'	91

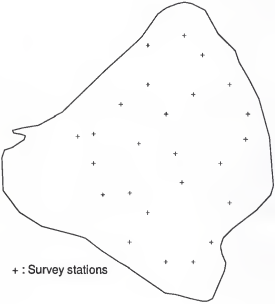

Figure 6.6: Locations of synoptic stations in Lake Okeechobee during the 1989 Spring Survey.

Table 6.3: Elevations (above lake bottom) of the instruments arms at the six stations.

Station	Current arm elevations (cm)			Temp./Sed. arm elevations (cm)			Wind sensor above mean water surf.(cm)
	Arm 1	Arm2	Arm 3	Arm 1	Arm 2	Arm 3	
A	71			86			487
B	25	114		43	132		366
C	61	123	284	79	140	302	518
D	79	241		97	259		548
E	36	116		53	135		366
F	25			43			

Figures D.1 through D.5 in Appendix D present the measured wind at Stations A, B, C, D, and E (because Station F was very close to Station E, wind at Station F was not measured). Figures D.6 through D.11 show measured u-velocities, v-velocities, and suspended sediment concentrations at the six stations during the four-week period, where the positive u-velocity is from west to east and the positive v-velocity is from south to north.

Figures D.12 through D.26 in Appendix D are results of the synoptic survey in the spring of 1989. The measured SSC, SRP, and TP are presented in Figures D.12 through D.16, D.17 through D.21, and D.22 through D.26, respectively. The top layer is at 20% of the water depth below the water surface, while the bottom layer is at 20% of the water depth above the bed.

Wind data presented in Figures D.1 to D.5 show that although hardware failures caused some missing wind data at all of the five stations in the lake during this survey, two distinct periodic events can be clearly seen in the data. One is the diurnal fluctuation related to land breeze effect (Sheng *et. al.*, 1991), while the other is a long time scale variation with the time scale of one to two weeks. The mean wind speed over the lake is on the order of 4 – 5 m/sec, and the amplitude of the diurnal fluctuation is about 3 – 4 m/sec. The maximum wind speed was about 12 m/sec. Seldom was the maximum wind speed in excess of 15 m/sec. Generally, wind over the lake was relatively weak in the morning but began to pick up speed in the afternoon, and reached the maximum speed at night. The wind direction was mostly from southeast to northwest.

Corresponding to the diurnal and the longer period fluctuations of the wind, measured currents shown in Figures D.6 through D.11 also exhibited the same periods of fluctuation, suggesting that the current in the lake was mainly wind-driven. The measured suspended sediment concentrations shown in these figures also correlated well with the wind data in terms of the diurnal and the longer period fluctuations. Comparing the current data to the wind data, it is evident that a decrease of wind speed was often followed by a current oscillation, which was generally damped out within 8 to 10 hours. This is the seiche motion caused by a sudden change in wind speed over the lake. FFT (Fast Fourier Transform) analysis of the measured velocity at the top layer of Station C (Figure 6.7) proved that currents contained a distinctive periodic motion with the period of 4 to 6 hours, which is almost the same as the logest eigenperiod of the lake.

However, FFT analysis of the suspended sediment concentration measured at the same place (Station C) did not show the corresponding periodic variation, indicating that the seiche motion was not able to cause resuspension of the bottom sediments even though the seiche current was sometimes higher than 20 cm/sec in the lake. The fact is that the wind-driven current in the lake is generally not responsible for the bottom sediment resuspension, but the wind-induced waves are the major causes for sediment resuspension. As can be seen in Figure 6.7, the wind speed spectrum and the SSC spectrum have almost the same shape except that SSC spectrum has a peak at zero frequency. This peak is because of a background SSC concentration in the water column probably due to the presence of plankton.

In Figure 6.7, the spectrum is defined as followed:

$$S_{XX}(f) = \lim_{T \to \infty} \frac{1}{T} |X(f)|^2 \tag{6.1}$$

where f is frequency, $X(f)$ is the Fourier Transform of a time series (wind, current, or SSC in Figure 6.7).

The synoptic data were presented in terms of concentration contours in Figures D.12 through D.26. In plotting the contours of these synoptic data, SSC, SRP, TP and TDP values at all grid points (see Figure 7.15 for the grid system) were estimated by an interpolation scheme which uses the distance-inverses from three nearest synoptic stations as weighting factors. Because all the synoptic stations were rather far away from the lake shore, some sharp concentration gradients which could exist near riverine inputs might be missing in Figures D.12 through D.26. Despite this, all these synoptic plots showed that the high SSC, SRP, TDP, and TP concentrations were found over the mud zone of the lake, suggesting (1) the importance of bottom sediment types to the suspended sediment concentrations and phosphorus concentrations in the water column, and (2) the weak horizontal transport in the lake.

6.4 1993 Spring Short-Term Survey

A 3-day intensive field experiment during a storm event from February 2 to 4, 1993 was conducted by the UF Coastal & Oceanographic Engineering Department (Sheng *et al.*, 1993). The field work included the continuous measurement of horizontal currents, temperature and OBS (Optical Back Scatter) at three vertical levels in addition to wind and underwater pressure. The monitoring of the storm event commenced with simultaneous nutrient and chlorophyll sampling, to provide further data for understanding and modeling of important processes in phosphorus dynamics.

Currents and suspended sediment concentrations were measured at three depths (30cm, 127cm, and 295cm above the bed, respectively). However, due to limitation of the measurement platform and drifting of the OBS data at the bottom arm, measured current and SSC at the bottom layer can not be used. Figure E.2 in Appendix E shows the measured u-velocities (from west to east), v-velocities (from south to north), and suspended sediment concentrations at the middle and the top arms during the three-

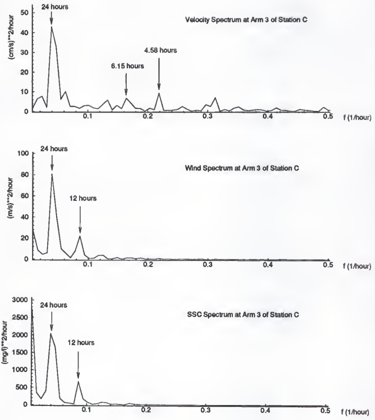

Figure 6.7: Spectra of measured current, wind speed, and SSC at Station C in Lake Okeechobee.

day survey. Measured wind speed and wind direction during these three days are shown in Figure E.1 in Appendix E.

The Sigma samplers were set up to collect 1000 ml of water every hour. In order to preserve nutrient characteristics and the parameters to be analyzed, the sample container (which has an insulated double walled base section) was filled with ice. The water sampling with the Sigma samplers was started on February 2, 1993 at 16:30 with a sampling interval of 1 hour. At the start of sampling, the winds were 7.5-10 m/sec from NE with seas at 30 to 100 cm. The first set of water samples was collected at 23:00. The wind at this time had begun to decrease to 5-7.5 m/sec, with seas decreasing to 30 to 65 cm.

The next set of samples was collected at 7:30 a.m. on February 3, 1993 when the winds shifted to the east at 5 m/sec, with seas of 30 to 60 cm. At 16:30 on February 3, the next set of samples were collected. The sampling interval was changed to 2 hours at this time. Winds and seas at this time were similar to the conditions at 23:00 on February 2. At 6:00 a.m. on February 4, the next set of water samples was collected. At this time the RTDU data were downloaded. The wind was from the east at 2.5-5 m/sec with seas of about 30 cm. After 9:00 on February 4, the winds were calm with seas less than 30 cm. At 17:30, the last set of water samples was collected. The water sampling was stopped on February 5, 1993 at 8:30 a.m.

Figure E.3 in Appendix E presents the field data of total phosphorus, total dissolved phosphorus, and soluble reactive phosphorus during the storm event. In each of the figure boxes, dotted lines show data measured at 296 cm above the bottom (top arm height), dashed lines show data measured at 127 cm above the bottom (middle arm height), and solid lines indicate data measured at 30 cm above the bottom (bottom arm height). All the chemical analyses were done by the chemistry lab of the South Florida Water Management District. Good correlations among TP, TDP, and SRP can be seen from Figure E.3. As shown in this figure, the data at all depths show the similar pattern and peak values throughout the measurement period. The DO and pH data collected at 30 cm above the bottom during the 3-day storm event are presented in Figure E.4. While pH values showed only little variation during the three days, the dissolved oxygen concentration was rather dynamic because DO concentration could be affected by many factors including reduction and oxidization reactions, photosynthesis, wind speed, and hydrodynamics.

CHAPTER 7

MODEL APPLICATIONS TO LAKE OKEECHOBEE

Numerical models of hydrodynamics, sediment transport, and nutrient dynamics described in the last Chapter 4 and 5 were applied to Lake Okeechobee, a large shallow lake in south Florida. Model applications include a one-dimensional simulation of hydrodynamics, sediment transport, and phosphorus dynamics during a storm event in February, 1993 and 1-D and 3-D simulations of current, sediment transport, and phosphorus dynamics for the 1989 Spring Survey discussed in Chapter 6.

7.1 Modeling of the 1993 Storm Event

The one-dimensional modeling system was used to simulate the hydrodynamics, sediment transport processes, and phosphorus dynamics for the 1993 spring storm event in Lake Okeechobee (Sheng, em et al., 1993a). The phosphorus species simulated are soluble reactive phosphorus (SRP), dissolved organic phosphorus (DOP), algal particulate phosphorus (Alg-P), zooplankton particulate phosphorus (Zoo-P), particulate organic phosphorus (POP), and particulate inorganic phosphorus (PIP).

Before using the one-dimensional model, a SMB wave model (U.S. Army Coastal Engineering Research Center, 1984) was used to calculate the significant wave heights and periods at various locations in the lake by using realistic wind and bathymetry data. Application of the SMB wave model to Lake Okeechobee by Ahn and Sheng (1989) showed reasonable agreement with the 1988 data.

In the 1-D model simulation, at every time step, results of the SMB model are first used to calculate the bottom shear stresses due to waves or wave-current interactions, before the sediment dynamics are calculated. In calculating the bottom shear stress due to waves or wave-current interactions, a very small time step (1/60 to 1/20 of the wave period) was used over a simulation period of at least four wave cycles. Also calculated during this process are the wave-cycle-averaged eddy viscosity/diffusivity, which represents the combined turbulence mixing due to waves and currents in the wave boundary layer. This wave-cycle-averaged eddy viscosity/diffusivity is used in calculating currents, sediment concentration and phosphorus dynamics at the new time step.

The simulated of currents and the suspended sediment concentrations for this storm event are presented in Figure 7.1, in the same order as in Figure E.2. From these two figures, we see that the simulated and measured currents agree very well. This should not be a surprise because the measured currents were used in the model to estimate the horizontal pressure gradient terms. The simulated sediment concentrations at arms 2 and 3 have the same trend and comparable magnitude as measured data. The model parameters used in the sediment model are: the critical shear stress for erosion $\tau_{cr} = 1 dyn/cm^2$ and the erosion rate constant $E_o = 2.5 \times 10^{-7} g/cm^2 sec$.

Since the field data of TDP and SRP indicate that dissolved organic phosphorus is less than 10 percents of the total dissolved phosphorus, the desorption kinetics of organic phosphorus is not a key mechanism for phosphorus budget in Lake Okeechobee. On the other hand, experience in modeling the phosphorus dynamics of Lake Okeechobee during the storm event suggests that the desorption of inorganic phosphorus from sediment particles is the major mechanism controlling the concentrations of phosphorus components, and the partition coefficient (p_{ip}) for inorganic phosphorus is the most sensitive parameter in the phosphorus model. Generally, the release of SRP from sediment particles is affected by temperature, pH value, and the dissolved oxygen concentration (DO). Because temperature did not change much during the storm event, and because temperature has little effect on desorption of SRP if temperature exceeds 17°C (Jensen and Anderson, 1992), pH and DO were considered to be the dominant factors affecting the release of SRP from sediments.

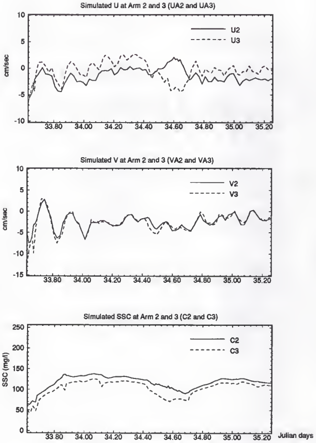

Figure 7.1: Model results of u-velocities, v-velocities, and suspended sediment concentrations at the middle layer (Layer 2) and the top layer (Layer 3) at Station L002 in Lake Okeechobee during the storm event in February, 1993.

Figures F.1 through F.9 in Appendix F present the results of three model runs along with the field data. The first run (Figures F.1 through F.3) considered only the effect of pH on the desorption of SRP; the second run (Figures F.4 through F.6) considered only the effect of DO on the desorption of SRP; and the third run (Figures F.7 through F.9) considered both effects.

In the first model run, the effect of pH on SRP desorption is represented by an empirical equation, which is obtained by fitting the laboratory data of Olila and Reddy (1993) for Lake Okeechobee sediments:

$$P_{ip}(pH) = P_{ip}(10.5)\frac{(pH - 7.5)^3}{64} \tag{7.1}$$

where $P_{ip}(10.5)$ is the partition coefficient at pH of 10.5.

From Figures F.1 through F.3, we see that pH value has some effect on phosphorus cycling, but in the range from 8.2 to 8.5 (the measured pH range during the storm event) the effect is not very significant. The more important factor controlling the SRP release from sediments may be the DO concentration in the water column. Although few studies have examined this effect, it has been widely acknowledged that DO could suppress phosphate release from sediments (e.g., Pomeroy *et al.*, 1965; Fillos and Molof, 1972; Holdren and Armstrong, 1980; Nakajiura, 1983; Ishikawa and Nishimura, 1989). Ishikawa and Nishimura assumed a linear distribution of DO in the oxygenation layer of sediment and found that phosphate release flux from bottom sediment is a linearly decreasing function of DO in the water column, and the critical DO at which phosphate release is stopped is dependent upon the dynamics of ferrous iron in the system. In the model, since there is no ferrous iron information, the following empirical formula is proposed to account for the effect of DO on SRP desorption:

$$P_{ip}(DO) = \left(\frac{DO_m}{DO_m - DO}\right)^n P_{ip}(0) \tag{7.2}$$

where DO_m is a model parameter having the same unit as DO and $P_{ip}(0)$ is the partition coefficient at anaerobic condition (DO=0).

Equation (7.2) is quite empirical. If n=1, it is similar to the result of Ishikawa and Nishimura. However, modeling experience indicates that only when n=2 can the model results best fit the field data. By fitting model results with data, the model parameter DO_m was found to be 10.5 mg/l.

From the results of model run 2 (Figures F.4 through F.6), which considered only the effect of DO on SRP desorption, it can be seen that by using Equation (7.2) (DO_m = 10.5 mg/l, n=2), model results are better than those of the first run (Figures F.1 through F.3). The model results are further improved by including both Equations (7.1) and (7.2) in the model, as can be seen in Figures F.7 through F.9.

In order to examine the correlation between SRP release and DO, correlation coefficients among phosphorus data and DO data were calculated. Figure 7.2 shows correlation coefficients between DO and SRP, DO and TDP, and DO and TP:

$$\rho_{DO-SRP} = \frac{Cov[SRP(t), DO(t-h)]}{\sqrt{Var[SRP(t)]Var[DO(t-h)]}} \tag{7.3}$$

$$\rho_{DO-TDP} = \frac{Cov[TDP(t), DO(t-h)]}{\sqrt{Var[TDP(t)]Var[DO(t-h)]}} \tag{7.4}$$

$$\rho_{DO-TP} = \frac{Cov[TP(t), DO(t-h)]}{\sqrt{Var[TP(t)]Var[DO(t-h)]}} \tag{7.5}$$

where $\rho_{DO-SRP}, \rho_{DO-TDP}$, and ρ_{DO-TP} are correlation coefficients in the top plot, the middle plot, and the bottom plot of Figure 7.2, respectively. $Cov[x,y]$ is the covariance between x and y, $Var[x], Var[y]$ are variances of x and y, respectively.

The horizontal axes in Figure 7.2 are h in Equations (7.3), (7.4), and (7.5). At about 8 hours, ρ_{DO-SRP} and ρ_{DO-TDP} are about -0.7. In other words, SRP and TDP data are well inversely-correlated with DO data at about 8 hours before. Or, the decrease of DO corresponds to the increase of SRP and TDP at eight hours later. If

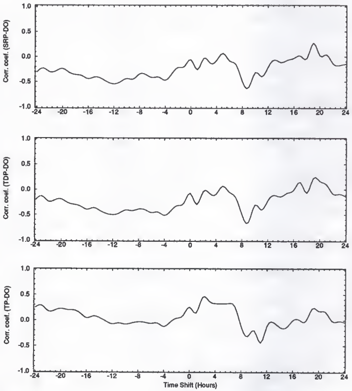

Figure 7.2: Correlation coefficients between DO and SRP, DO and TDP, and DO and TP measured at Station L002 in Lake Okeechobee during the storm event in February, 1993.

the argument is true that the release of SRP is due to the decrease of DO, then Figure 7.2 also indicates that the desorption of SRP from sediments during a release event takes about eight hours to complete. Since there are insufficient data of DO, pH, and ferrous iron in the entire water column and also the DO at the bottom arm varied only in a small range, the above discussion may be questionable. However, the model shows that without considering the DO effect on the SRP release, it is impossible to get good model results.

In conclusion, sediment resuspension and desorption kinetics of inorganic phosphorus play important roles in phosphorus dynamics in Lake Okeechobee. During the first few hours, the high SRP and TDP values at the bottom and the middle arms were obviously due to the resuspension because DO was high and pH was low then. At relatively calm weather conditions, the desorption of SRP from sediments plays an important role in phosphorus dynamics in Lake Okeechobee. Unfortunately, because insufficient data of DO and pH during the storm event were available, some questions remain at present time. For example, the continuous increase of SRP and TDP at the top arm during Julian day 24.0 through 34.4 may be due to a drop of DO, an increase of pH, or both. Since DO and pH data are not available there, model results cannot agree well during that period in the three runs described above (DO and pH data at the bottom arm were used for the entire water column in these three runs). However, the pH at the top layer was adjusted slightly, i.e., pH value from Julian day 34.0 to 34.4 was assumed to have a linear increase of 0.5 so that good model results of SRP and TDP at the top layer could be obtained (Figures 7.3 through 7.5). In future research, pH and DO should be measured in the entire water column and at least at three layers.

In order to examine effects of various transformation processes on nutrient concentrations in the lake, this study did some sensitivity tests. Baseline values of the model parameters were these used for the best simulation shown in Figures 7.3 through 7.5.

For each sensitivity model run, one model parameter was changed within a certain range. Results of these sensitivity runs are shown in terms of root-mean-square errors between data and model results of SRP and TDP in Table H.1 of Appendix H.

7.2 1-D Simulations of 1989 Spring Survey

Using the 1-D sediment transport model, numerical model simulation of the Spring 1989 Survey were conducted. Model simulation reveled that critical erosion shear stress (τ_{ce}) and erosion rate constant (E_o) are the most sensitive parameters in the sediment model. These two parameters are dependent on the bottom sediment type and the consolidation and fluidization processes in the sediment column. As shown in Figure 6.3, there are various types of sediments over the bottom of various part of Lake Okeechobee. Simulation of the sediment dynamics in the lake requires different τ_{ce}'s and E_o's for different areas. However, the determination of these two parameters in the field in not easy. Although they can be measured in laboratory, τ_{ce} and E_o determined in laboratory experiments may not necessary reflect their true values in the field because of some limitations of lab experiments. One of such limitations is the difficulty in creating laboratory wave conditions that resemble the field conditions.

An alternative and probably the best method to determine the sediment parameters τ_{ce} and E_o is to obtain them from field data of SSC with help of numerical models. By adjusting the two parameters to achieve the best fit between simulated and measured SSC, τ_{ce} and E_o can be determined. In this study, prior to three-dimensional simulation of sediment dynamics in Lake Okeechobee, a one-dimensional sediment model was first used to determine the parameters τ_{ce} and E_o in the lake from the field data. Data from three representative stations (Stations C, D, and E) were used to determine τ_{ce}'s and E_o's in muddy and sandy zones, respectively. Only data obtained during the second week were used because there were some missing data of current, wind, and SSC during other weeks.

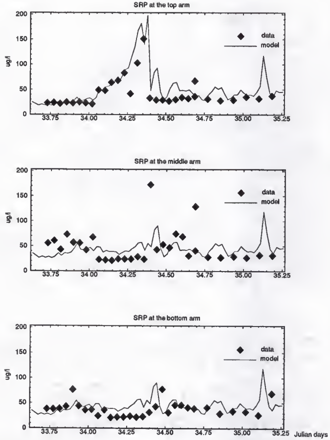

Figure 7.3: Measured and simulated SRP of a run with adjusted pH at the top layer at Station L002 in Lake Okeechobee during the storm event in February, 1993.

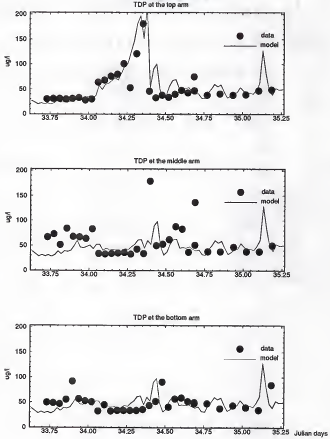

Figure 7.4: Measured and simulated TDP of a run with adjusted pH at the top layer at Station L002 in Lake Okeechobee during the storm event in February, 1993.

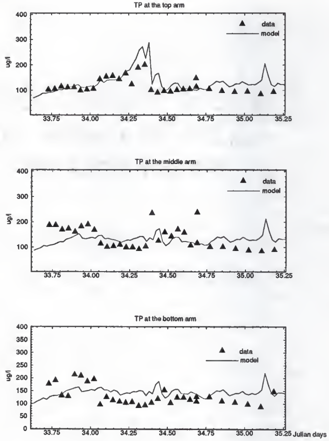

Figure 7.5: Measured and simulated TP of a run with adjusted pH at the top layer at Station L002 in Lake Okeechobee during the storm event in February, 1993.

Figures 7.6, 7.7 and 7.8 present the best model results at Stations C, D, and E, respectively. In all these runs, Sheng's deposition model was used for the deposition velocity and the power law was used for the erosion rate. Equation (4.27) with a cutoff of $w_{s_{min}} = 0.01 cm/sec$ was used to calculate the settling velocity at muddy zone (Stations C and D). For the sandy zone (Station D), a constant settling velocity of $0.02 cm/sec$ was used. In Figures 7.6 through 7.8, the solid lines represent measured or simulated SSC's at the bottom layers, the dashed lines represent the SSC's at the middle layers, and the dotted lines (if exist) represent the SSC's at the top layers. τ_{ce}'s and E_o used at these three runs are listed in Table 7.1. These values are believed to be the best sets of τ_{ce} and E_o determined by the 1-D sediment model and were used in the preliminary 3-D model simulations. The final values of τ_{ce} and E_o in the final 3-D simulations were slightly adjusted to take into account the effect of three-dimensional transport. Nevertheless, the 1-D sediment simulations provided a guideline for the selection of τ_{ce} and E_o.

Table 7.1: τ_{ce} and E_o values determined by the 1-D sediment model.

Station	τ_{ce} (dyn/cm^2)	E_o (g/cm^2 sec)
C	1.2	2×10^{-7}
D	1.0	2×10^{-7}
E	10.	1×10^{-8}

Hwang and Mehta (1989) used Equation (3.60) to present their laboratory measurements of settling velocity of Lake Okeechobee fine sediments. They obtained a set of values for the parameters a, b, m, and n. Previous simulations of Lake Okeechobee sediment dynamics (Sheng *et al.*, 1991) used the formula of settling velocity obtained by Hwang and Mehta (1989) (Figure 3.2). However, since Hwang and Mehta measured the settling velocity in laboratory, the direct usage of their results for Lake Okeechobee simulation has at least 3 problems: (1) Unlike in the field, there is no shearing in the laboratory settling tube; (2) It is easy for particle flocculation and breaking to reach equilibrium in the settling tube but not in the filed where there

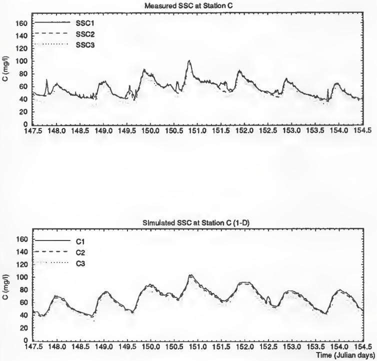

Figure 7.6: Measured and simulated SSC at Station C during week 2 of the 1989 Spring Survey in Lake Okeechobee.

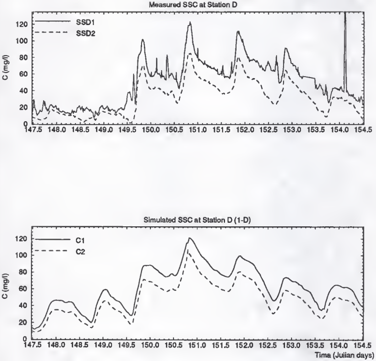

Figure 7.7: Measured and simulated SSC at Station D during week 2 of the 1989 Spring Survey in Lake Okeechobee.

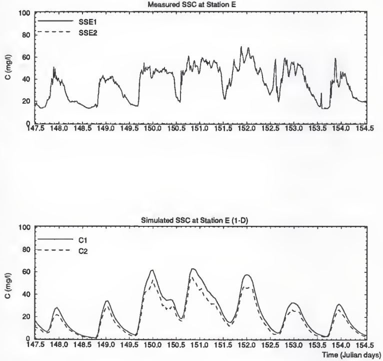

Figure 7.8: Measured and simulated SSC at Station E during week 2 of the 1989 Spring Survey in Lake Okeechobee.

is rapid change in shear stress and mixing; and (3) Even if turbulence is introduced in the settling tube by shaking the tube, sediment concentration in the settling tube does not change. However, in the field, an increase of shear stress can result in an increase of suspended sediment concentration due to erosion of the bed and turbulent mixing in the water column. In order to more accurately take account the settling process in the model, the effect of shear on settling velocity should be considered. In other words, the parameters a, b, m, and n should be functions of shear.

As mentioned before, some flocculation models have been developed (e.g., Burban *et al.*, 1989) based on Smoluchowski's equation for collision and laboratory experiments. However, since these models did not consider the differences between laboratory condition and field condition, they can not used for the purpose of modeling here. Le Hir (1993) proposed an empirical settling velocity formula considering the effect of shear stress as follows:

$$w_s = k_1(\log \mathrm{c} - k_2)\left[1 - \cos[\frac{\pi}{2}(\frac{u^*}{k_5(1 - k_6 \log \mathrm{c})} + k_3 \log \mathrm{c})^{k_4}]\right] \tag{7.6}$$

where k_1, k_2, k_3, k_4, k_5, and k_6 are model parameters, and u^* is the frictional velocity.

Equation (7.6) contains too many empirical model parameters which are difficult to quantify for new applications. It also does not consider the fact that a certain time period is needed for the settling velocity to respond to a change in the shear. Moreover, from the plot of Equation (7.6) shown in Figure 7(b) of Le Hir (1993), it is clear that this equation is not applicable at high shear, because it gives a wrong relationship between sediment concentration and settling velocity (settling velocity decreases as sediment concentration increases even for sediment concentration lower than 1000 mg/l.)

Because an increase in shear can result in an increase in suspended sediment concentration some time later in the field, it is probably better to parameterize the effect of shear on settling velocity through suspended sediment concentration (instead of shear) if the time lag for suspended sediment concentration in the water column to respond to a change in shear is of the same order as that for the settling velocity to respond to the same change. Therefore, it is possible to include the effect of shear in Equation (3.60) by considering the parameters a, b, m, and n to be functions of suspended sediment concentration. In other words, settling velocity can be expressed as a function of suspended sediment concentration only, although the physical meaning of the dependence of settling velocity on suspended sediment concentration now is different from that indicated in Equation (3.60). The final settling velocity as a function of suspended sediment concentration can also be written in the same form as that of Equation (3.60), but with different values for a, b, m, and n. Figure 7.9 shows the new settling velocity formula (or modified formula). The original formula obtained by Hwang and Mehta (1989) from laboratory experiment (Hwang and Mehta's formula) is also shown in this figure. The new values for the parameters a, b, m, and n are $20.0, 2.5, 1.2$, and 0.9, respectively, and the original values are $33.38, 4.39, 1.48$, and 1.3, respectively. It can be seen that the curve for settling velocity obtained by Hwang and Mehta has been shifted and the new settling velocity at low sediment concentration ($< 1000 mg/l$) is higher than the old one because of the flocculation of sediment particles caused by shearing.

Figure 7.10 shows model (1-D) results of suspended sediment concentration of two runs: one run used the original settling velocity formula obtained in the laboratory by Hwang and Mehta (1989) and the other used the modified settling velocity formula. Significant improvement has been achieved because the new formula empirically take into account the effect of shear on flocculation.

In order to test the uncertainty of the sediment model, the Monte Carlo technique was used to randomly choose τ_{ce} and E_o during the process of determining the sediment parameters. A random generator was used to pick up τ_{ce} and E_o with a uniform probability distribution:

$$\tau_{ce} = \tau_{ce}^1 + S_1 \times (\tau_{ce}^2 - \tau_{ce}^1) \tag{7.7}$$

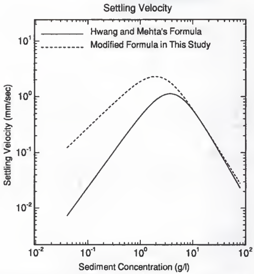

Figure 7.9: Settling velocity obtained from laboratory by Hwang and Mehta (1989) and the modified settling velocity considering the shear stress effect.

$$E_o \;=\; E_o^1 + S_2 \times (E_o^2 - E_o^1) \tag{7.8}$$

wherein τ_{ce}^1 and τ_{ce}^2 are the lower and the upper bounds of τ_{ce}, E_o^1 and E_o^2 are the lower and the upper bounds of E_o, and S_1 and S_2 are two random variables, which are uniformly distributed within 0 and 1.

Figures 7.11 and 7.12 are the results of 200 Monte Carlo simulations. Figure 7.11 shows the mean and the 99 percent bounds of the simulations, i.e., 99 percents of the model results were within the range bounded by the dashed lines. Figure 7.12 shows the contours of root-mean-square error between the SSC data and the model results, where the root-mean-square error is defined as

$$r = \sqrt{\frac{1}{N_a N_t} \sum_{i=1}^{N_a} \sum_{j=1}^{N_t} \left(\frac{c_{ij}^d - c_{ij}^m}{c_{ij}^d} \right)^2} \tag{7.9}$$

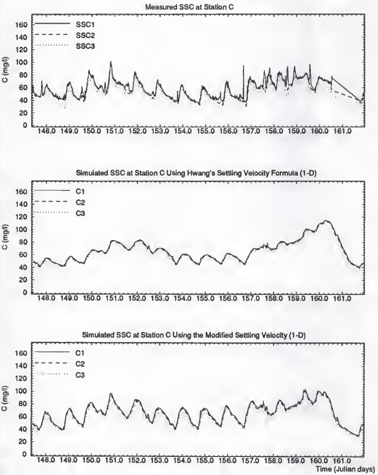

Figure 7.10: Comparison of model results of suspended sediment concentration using two different settling velocity formula.

where N_a is the number of the measurement arms, N_t is the total time steps of simulation, c^d_{ij} and c^m_{ij} are measured and simulated SSC's, respectively, at layer i and time step j.

The sediment dynamics at the sediment-water interface (the so-called lutocline) can significant affect the sediment budget in the water column. The 1-D sediment transport model was used to simulate lutocline dynamics. By including the effect of suspended sediment on fluid density and using the second-order closure turbulence model to calculate the eddy diffusivity, the 1-D sediment model does incorporate the effect of vertical stratification on the reduction of turbulent mixing near the lutocline (Sheng and Villaret, 1989 . Sheng's formulation for the deposition velocity was combined with Krone's probability function for the calculation of the deposition rate. Model simulations show that Krone's probability function is necessary for lutocline simulation. Otherwise, although the predicted SSC's at the three layers agree well with data, the sharp gradient in suspended sediment concentration disappears because of the infinite critical shear stress in Sheng's deposition model. In the modified version of Sheng's model (Equation (4.28)), the critical shear stress for deposition was about 6 times of the critical shear stress for erosion.

Figure 7.13 shows the results of the lutocline simulation for a 3-day event at Station C. Although there were no data of sediment concentration very near the mud-water interface, simulated sediment concentrations at three water depths agree well with the data. The lutocline elevation above the bottom of the computational domain shows a rather dynamic nature. It can be clearly seen that a higher wave height resulted in a higher lutocline elevation. Here, the lutocline is defined as the elevation where the SSC gradient is larger than 100 $mgl^{-1}cm^{-1}$. The predicted suspended sediment concentration profiles of this simulation are presented in Figure 7.14.

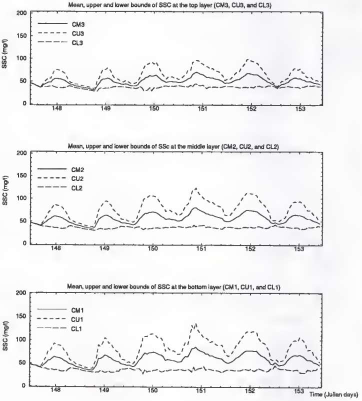

Figure 7.11: Results of Monte Carlo simulations of SSC at Station C during Week 2 of the 1989 Spring Survey in Lake Okeechobee.

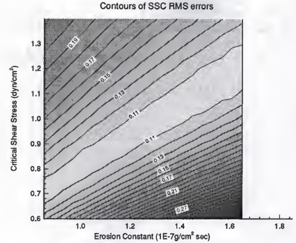

Figure 7.12: Contours of the root-mean-square error of the Monte Carlo simulations of SSC at Station C during week 2 of the 1989 Spring Survey in Lake Okeechobee.

7.3 3-D Simulations of 1989 Spring Survey

The three-dimensional models of hydrodynamics, sediment transport, and nutrient dynamics were used to simulate the four-week period in the 1989 Spring Survey in Lake Okeechobee. The nutrients simulated were phosphorus concentrations: SRP, DOP, PIP, POP, algal particulate phosphorus, and zooplankton particulate phosphorus. A Cartesian grid size of $\Delta x = \Delta y = 2km$ was used for the three-month simulation. A total of 25 × 28 grids were used for the entire lake (Figure 7.15).

7.3.1 Model Implementation

From the field data of currents and wind, it can be seen that the circulation of Lake Okeechobee is primarily wind-driven. Before the simulation of the four-week survey, the flow was allowed to spin-up from rest for a few days, during which period the simulation of sediment and phosphorus was not included. For the spin-up run, the wind data collected by the South Florida Water Management District at Station

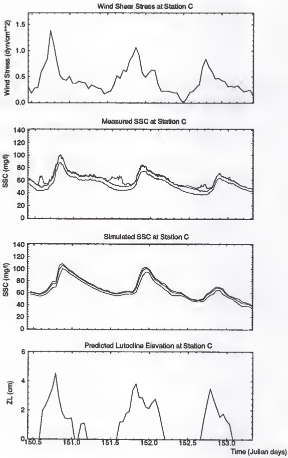

Figure 7.13: Results of the lutocline simulation at Station C during a three-day event in the 1989 Spring Survey in Lake Okeechobee.

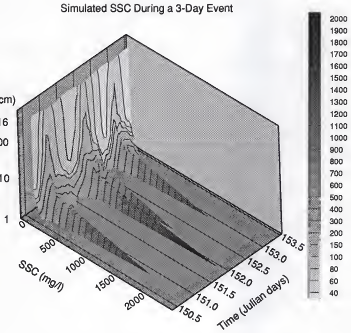

Figure 7.14: SSC profiles in the lutocline simulation at Station C during a 3-day event in Week 2 of the 1989 Spring Survey in Lake Okeechobee.

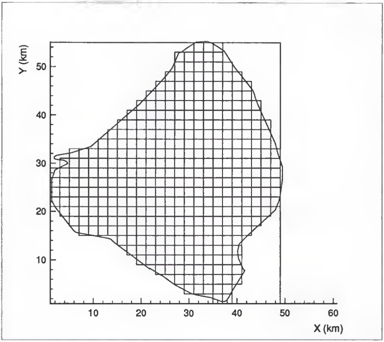

Figure 7.15: A Cartesian grid system for the 3-D simulation of Lake Okeechobee hydrodynamics, sediment, and nutrient dynamics.

L005 were used, and a uniform and time-dependent wind was assumed over the entire lake.

After the spin-up run, the hydrodynamics portion of the model first computed the circulation of Lake Okeechobee during the four-week period as a result of forcing by wind stress. The wind stresses over the lake were calculated from the wind data. The two-dimensional wind field was calculated from the wind data measureed at Stations A, B, C, D, and E using the inverses of the distances from the measurement platforms as weighting factors. The same 2-D wind field which was used to compute the wind stress was also used to compute the waves using the SMB model.

The measured data of river discharges of flow, sediments, and phosphorus were incorporated into the model as boundary conditions. The tributary inflows were from the Kissimee River, Taylor Creek/Nubbin Slough, Harney Canal and Indian Creek Canal, while outflows from Lake Okeechobee were at canals S-2, S-3, HGS5X, and S-77 (Figure 6.1).

Six sources of phosphorus to Lake Okeechobee are tributary dissolved and sediment phosphorus, resuspended bottom sediment, diffusion of dissolved phosphorus from lake sediments, internal recycling of pelagic phosphorus, atmospheric deposition of dry particulates, and SRP and DOP in the rainfall. The tributary boundary conditions for SRP and DOP are the tributary concentrations and flows to and from the lake. The SRP and TP loads are calculated from the daily flow in the tributary, multiplied by either the semi-monthly or monthly average tributary concentration of SRP and TP. DOP is the difference between the concentration of TP and SRP in the tributary. All other phosphorus components are assumed to have a zero concentration in the inflow tributaries. The outflow tributary fluxes are based on the currents and the simulated concentrations in canal cells.

Sediment dynamics parameters τ_{ce} and E_o determined in the last section (from the field data by the 1-D sediment model) were used in the sediment simulation.

According to the bottom sediment types shown in Figure 6.3, there were three distinct regions in the model. The first is the thin muddy region ($< 20cm$, represented by Station C), the second is the thick muddy region ($\geq 20cm$, represented by Station D), and the third is the sandy region (represented by Station E). τ_{ce} and E_o results at Stations C, D, and E listed in Table 7.1 were used for the three regions in the simulation.

SMB model was used to calculate the wind-induced waves over the entire lake. This wave model has been successfully used to predict significant wave height and period (modal wave period) by Ahn and Sheng (1989) in Lake Okeechobee for the fall of 1988 survey. However, it overpredicts the significant wave height and period for the 1989 Spring Survey by about 40%, because the mean water level in the lake in the spring of 1989 was about 1 meter lower than the mean water level in the fall of 1988 and the wave energy dissipation was larger. Nevertheless, SMB model can still be used to predict the waves in the lake in the spring of 1989 as long as an adjustment of model parameters was made. Figure 7.16 compares the predicted significant wave heights and periods by SMB model to those calculated from measured data by FFT analysis at Station C. Except for some underestimation, the results of SMB model after the adjustment agree well with data.

Previous 3-D simulations of sediment transport in Lake Okeechobee by Sheng *et al.* (1991) used Kajiura's model to calculate bottom shear stresses due to waves. Before doing 3-D simulations, wave-induced bottom shear stresses were first calculated based on the significant wave height, wave period, and the local mean water depth. The calculated wave-induced bottom shear stresses over the entire lake at each hour were saved in a file. During the 3-D simulation, the sediment model then read the calculated wave-induced bottom shear stresses saved on the file. However, this procedure contained error, because wave-induced bottom shear stress is also a function of water depth and the water surface variation in the lake. This study incorporate the

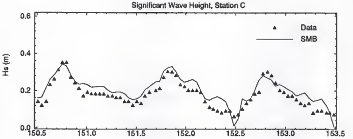

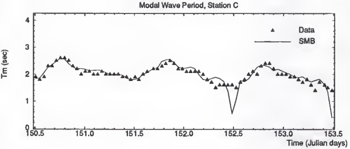

Figure 7.16: Measured and predicted significant wave height and period at Station C in Lake Okeechobee. Model parameters in SMB model has been adjusted.

effect of water surface elevation on wave-induced bottom shear stress by first creating a table of wave-induced bottom shear stress using the 1-D TKE (Turbulent Kinetic Energy) model. Three variables (wave height, wave period, and water depth) were included in the table. During the 3-D simulation of sediment transport, the model then searched the table for the correct wave-induced bottom shear stress based on the significant wave height and period calculated from the SMB model and the local water depth calculated by the 3-D circulation model at the new time step.

To illustrate the sensitivity of wave-induced bottom shear stress to wave height, wave period, and water depth, two contour plots of wave-induced bottom shear stress are presented in Figure 7.17. The upper one, with a constant water depth of 3 meters, shows the dependence of wave-induced bottom shear stress on wave parameters. The lower one, with a constant wave period of 2 seconds, shows the effect of water depth on wave-induced bottom shear stress. It can be seen that lowering the water depth can cause a significant increase in wave-induced bottom shear stress, especially when the wave height is large.

The above calculation of bottom shear stresses induced by waves considered only one single wave with the wave height of H_s. In reality, wind-generated sea consists of a group of waves with different wave heights. Therefore, a more precise prediction of wave-induced bottom shear stresses should consider group waves (Schoellhammer, 1993).

In order to see the importance of considering group waves in calculating wave-induced bottom shear stresses, this study also used the 1-D TKE to compute bottom shear stresses induced by 10 waves. The distribution of wave energy among the 10 waves are calculated based upon the Two-Parameter Spectra (Bretschneider, 1959) as followed:

$$S(\omega) = \frac{1.25}{4}\frac{\omega_m^4}{\omega^5}H_s^2 e^{-1.25(\frac{\omega_m}{\omega})^4} \tag{7.10}$$

where $\omega_m (= \frac{2\pi}{T_m})$ is the modal frequency.

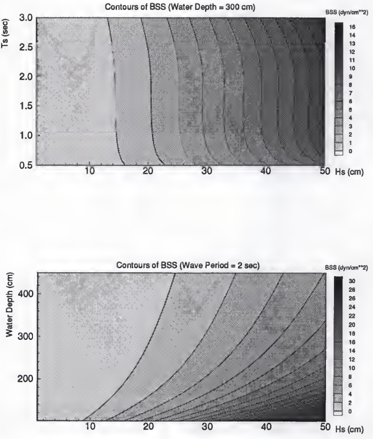

Figure 7.17: Contours of wave-induced bottom shear stress from the 1-D TKE model.

Figure 7.18 is a comparison of model results of bottom shear stresses induced by a single wave with those induced by group waves. The significant wave height (H_s) and the modal wave period (T_m) used in this comparison are measured data (see Figure 7.16). This figure shows that wave-induced bottom shear stresses induced by a single wave is not the same as those by group waves. The former seem to be proportional to the square of significant wave heights (or linear relationship with wave energy), while the later have a more or less linear relationship with H_s'. The reason for the second order relationship with H_s in the case of a single wave is obvious because the bottom shear stress for fully developed turbulence is proportional to the square of the orbital velocity, which, in turn, is proportional to the wave height. The more or less linear relationship with H_s in the case of group waves can be explained by considering the effect of wave period on wave-induced bottom shear stress (see Figure 7.17) and the fact that the modal wave period increases as the significant wave height increases (see Figure 7.16).

Although Figure 7.18 shows different relationships between wave-induced bottom shear stress and significant wave height, the absolute differences between two sets of model results are nevertheless not very significant. On the other hand, the calculation of bottom shear stresses induced by group waves using the 1-D TKE model is much more time-consuming than that induced by only one single wave, because the time step used should be much smaller (1/60 to 1/20 of the smallest wave period) and the number of time step is much larger (the wave with the largest wave period should be repeated at least 3 to 4 times). Therefore, this study still used a single wave to calculate the wave-induced bottom shear stress.

7.3.2 Model Results

The results of the combined circulation, sediment transport, and nutrient dynamics of the four-week simulation for Lake Okeechobee are discussed in the following. Time series of simulated currents and suspended sediment concentrations at Stations

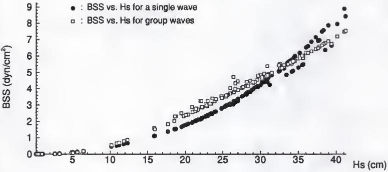

Figure 7.18: Comparison of model (1-D TKE) results of bottom shear stresses induced by a single wave to those induced by group waves.

A, B, C, D, and E are presented and discussed, and the 3-D fields of simulated SSC, SRP, and TP concentrations are shown in terms of flooded contours and compared to the synoptic data shown in Appendix D. Values for various model parameters used in the simulations are presented in Table H.2 of Appendix H.

Figures 7.19 through 7.21 show time series of currents and suspended sediment concentrations at Stations C, D, and E, respectively. Corresponding to the longer period fluctuations in wind data, simulated velocity results also exhibit these longer period fluctuations. For example, during the 1989 Spring Survey a persistent east wind was blowing from Julian day 147 to 161, with a resulting flow at Station C toward the east (a "return current") in both the measured data and model results. Another important point about the velocity results is that the short-term fluctuations (i.e., at period of about 3-4 hours, corresponding to the lake's natural seiche period) are in agreement with the 1989 Spring Survey data. For example, in response to a large wind event during Julian day 158, the measured u-velocity data showed a peak value exceeding 15 cm/sec, with a model response in the present simulation of about 12 cm/sec.

Similar to the measured SSC presented in Figures D.8 through D.10, simulated SSC presented in Figures 7.19 through 7.21 show both diurnal events and long-term events with periods of about one week. For example, during the period from Julian day 148 to 154, an event with the wind stress which peaked at Julain day 151 resulted (by wind wave-induced bottom shear stress) in a corresponding event in both measured and simulated SSC. The long-term fluctuations of measured and predicted SSC's were due to the long-term fluctuations of wind. For example, the mean wind speed at Station C in Week 2 first increased continuously during the first 3.5 days (from Julian days 147.5 to 151) and then decreased continuously during the second 3.5 day (from Julian days 151 to 154.5). As a result, the measured and predicted mean SSC's also respectively increased and decreased continuously in the corresponding time periods. The simulated SSC during this event agree very well with data.

Some simulated spatial distributions of SSC are presented in Figures 7.22 to 7.25, corresponding to Synoptic Surveys 2 to 5 shown in Figures D.14 to D.17, respectively. Comparison among contour plots of simulated and measured SSC spatial distributions shows that the three-dimensional sediment transport model can produce reasonable SSC results as long as reliable wind data are available. For example, comparison of the synoptic SSC data at the end of the week 1 (Figure D.14) to the simulated SSC at the same time (Figure 7.23) shows that at both the 20% the 80% depth levels, simulated SSC and measured SSC have similar contour lines with the comparable peak values. The high value of about $50\,\mathrm{mg}\,\ell^{-1}$ in the simulated SSC in the southeastern portion of the lake is in good agreement with the high value of about $51\,\mathrm{mg}\,\ell^{-1}$ located in the same area in the synoptic data. The agreement between simulated SSC and observed synoptic SSC seems especially good when it is considered that the precision of the calibration of the OBS meters used to measure SSC was $\sim 7\,\mathrm{mg}\,\ell^{-1}$.

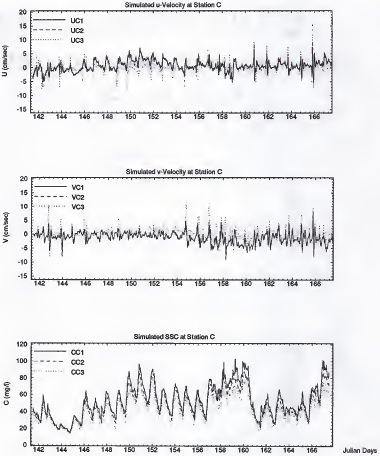

Figure 7.19: Simulated u-velocities, v-velocities, and suspended sediment concentrations at Station C of Lake Okeechobee form May 21 to June 16, 1989.

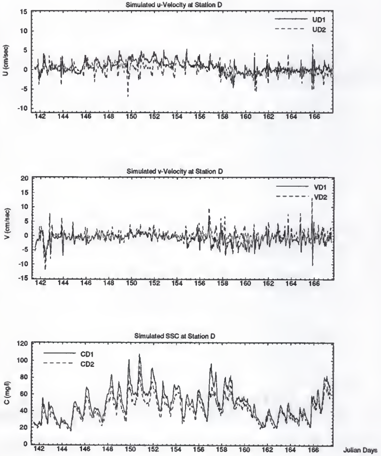

Figure 7.20: Simulated u-velocities, v-velocities, and suspended sediment concentrations at Station D of Lake Okeechobee form May 21 to June 16, 1989.

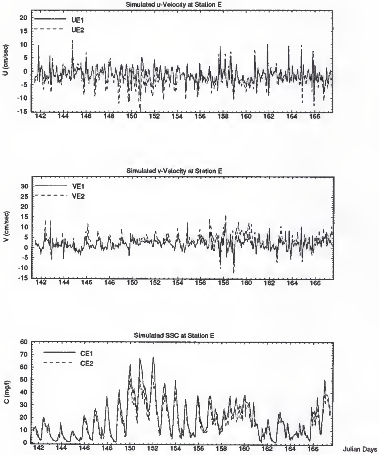

Figure 7.21: Simulated u-velocities, v-velocities, and suspended sediment concentrations at Station E of Lake Okeechobee form May 21 to June 16, 1989.

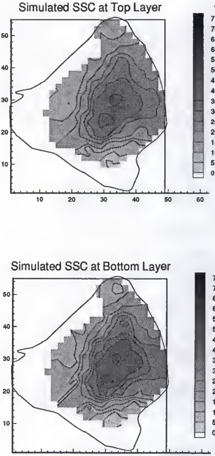

Figure 7.22: Spatial distribution of simulated suspended sediment concentration at the top and the bottom layers of Lake Okeechobee at noon of May 27, 1989.

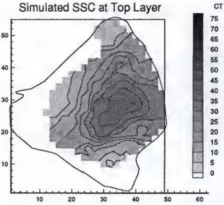

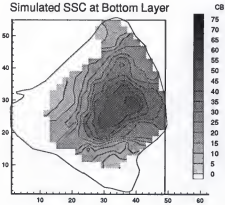

Figure 7.23: Spatial distribution of simulated suspended sediment concentration at the top and the bottom layers of Lake Okeechobee at noon of June 3, 1989.

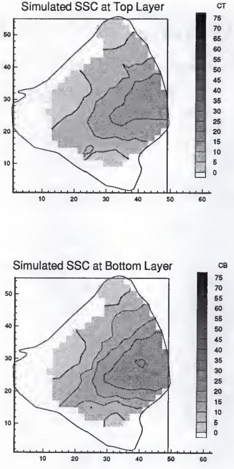

Simulated SSC at Top Layer

Simulated SSC at Bottom Layer

Figure 7.24: Spatial distribution of simulated suspended sediment concentration at the top and the bottom layers of Lake Okeechobee at noon of June 10, 1989.

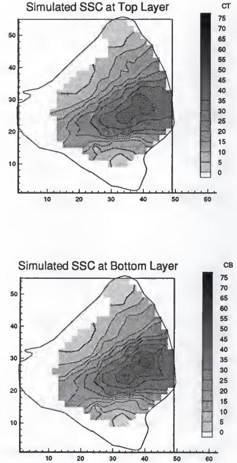

Figure 7.25: Spatial distribution of simulated suspended sediment concentration at the top and the bottom layers of Lake Okeechobee at noon of June 16, 1989.

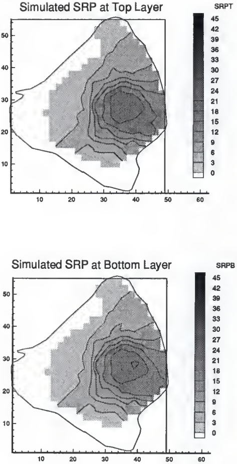

Figure 7.26: Spatial distribution of simulated SRP concentration at the top and the bottom layers of Lake Okeechobee at noon of May 27, 1989.

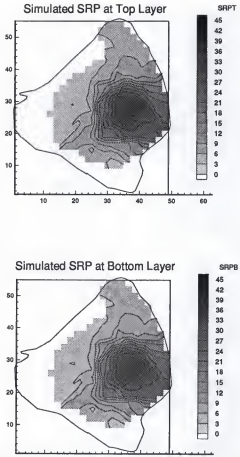

Figure 7.27: Spatial distribution of simulated SRP concentration at the top and the bottom layers of Lake Okeechobee at noon of June 3, 1989.

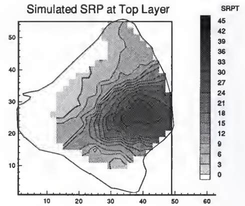

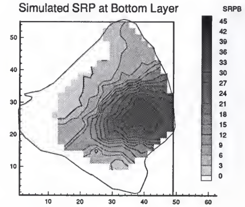

Figure 7.28: Spatial distribution of simulated SRP concentration at the top and the bottom layers of Lake Okeechobee at noon of June 10, 1989.

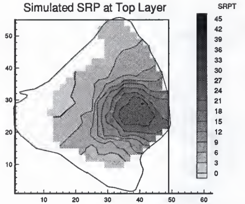

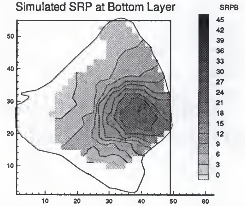

Figure 7.29: Spatial distribution of simulated SRP concentration at the top and the bottom layers of Lake Okeechobee at noon of June 16, 1989.

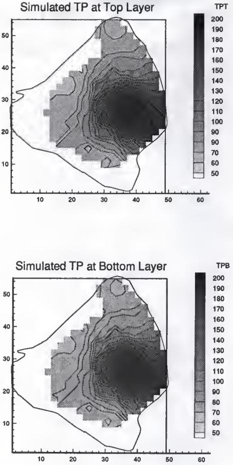

Figure 7.30: Spatial distribution of simulated TP concentration at the top and the bottom layers of Lake Okeechobee at noon of May 27, 1989.

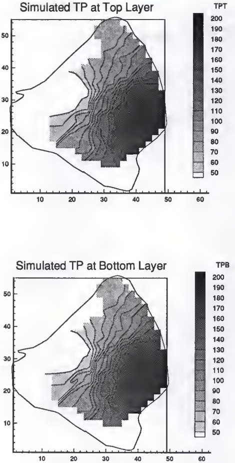

Figure 7.31: Spatial distribution of simulated TP concentration at the top and the bottom layers of Lake Okeechobee at noon of June 3, 1989.

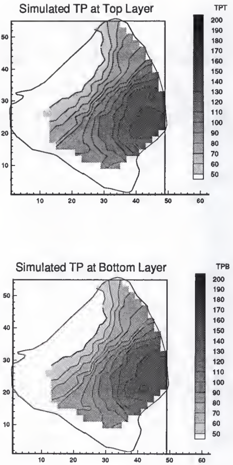

Figure 7.32: Spatial distribution of simulated TP concentration at the top and the bottom layers of Lake Okeechobee at noon of June 10, 1989.

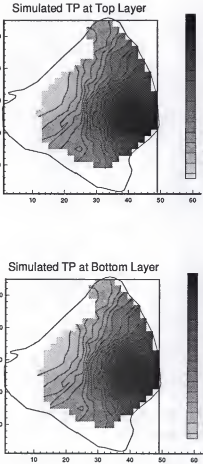

Figure 7.33: Spatial distribution of simulated TP concentration at the top and the bottom layers of Lake Okeechobee at noon of June 16, 1989.

Figures 7.26 to 7.29 present the spatial distributions of simulated SRP, while Figures 7.30 to 7.33 present the spatial distributions of simulated total phosphorus. The total phosphorus presented here include SRP, DOP, PIP, POP, algal and zooplankton particulate phosphorus. Model results of both SRP and TP at the ends of the four weeks are in good agreement with measured data. In modeling the phosphorus dynamics, model parameters (the desorption rate of PIP, the partitioning coefficients between SRP and PIP, the rate constant for the mineralization of DOP etc.) were determined by adjusting them to achieve the best fit between model results and the synoptic data in the first week run. The thus determined model parameters were then used in the model runs for the rest three weeks. Comparison of simulated SRP and TP results in Figures 7.26 to 7.29 to measured SRP and TP in Appendix D shows that model results agree well with data. For example, the contours of simulated SRP and measured SRP at both the top and the bottom layers are almost the same at the end of Week 1 (the second synoptic survey).

In order to quantitatively measured the agreement of the model results with the measured data, correlation coefficients between simulated and measured SSC, SRP, and TP (r_{SSC}, r_{SRP}, and r_{TP}) were calculated at the ends of Weeks 1, 2, 3, and 4. Table 7.2 shows the these correlation coefficients. One of the differences between this study and the study presented in Sheng and Chen (1992) for Lake Okeechobee sediment dynamics and phosphorus dynamics is that this study took into account the effect of temporal variation in water depth on wave-induced bottom shear stress by using a bottom shear stress table. Other modifications included the correction of SMB model results for the low water stage in 1991 in Lake Okeechobee and the new nutrient dynamics model. Model results have been improved by considering the effect of temporal water depth change on the wave-induced bottom shear stress. Correlation coefficients of measured data and model results without considering such effect are shown in Table 7.3.

Table 7.2: Correlation coefficients between measured and simulated SSC, SRP, and TP. The effect of water depth variation with time on wave-induced bottom shear stress was considered.

Survey	r_{SSC}	r_{SRP}	r_{TP}
Synoptic 2	0.73	0.90	0.91
Synoptic 3	0.72	0.71	0.72
Synoptic 4	0.80	0.61	0.78
Synoptic 5	0.87	0.58	0.80

Table 7.3: Correlation coefficients between measured and simulated SSC, SRP, and TP. The effect of water depth variation with time on wave-induced bottom shear stress was not considered.

Survey	r_{SSC}	r_{SRP}	r_{TP}
Synoptic 2	0.51	0.61	0.70
Synoptic 3	0.45	0.58	0.60
Synoptic 4	0.46	0.55	0.47
Synoptic 5	0.63	0.50	0.58

Sheng (1993) analyzed the 1989 synoptic data of SSC, SRP, and TP measured in Lake Okeechobee. He found that the synoptic TP data were well correlated with the synoptic SSC data, while the correlation between measured SSC and SRP was very poor. Model results of this study also indicated that TP was better correlated with SSC than SRP was. In Figures 7.34(a) and (b), the 1989 synoptic data of SSC are plotted vs. the 1989 synoptic data of SRP and TP, respectively, and the simulated results of SSC are plotted vs. the simulated results of SRP and TP in Figures 7.34(c) and (d), respectively. The model results plotted here are simulated SSC, SRP, and TP at locations near the 25 synoptic stations at the same times as the synoptic surveys. The correlation coefficient in in each of the plots was calculated and shown. While correlation coefficients between SSC and TP in measured data and model results are 0.87 and 0.78, respectively, correlation coefficients between SSC and SRP in measured data and model results are only 0.46 and 0.60, respectively.

The better correlation between SSC and TP can also be seen in the time series of simulated SSC and TP at any locations in the lake. For example, Figure 7.35 shows

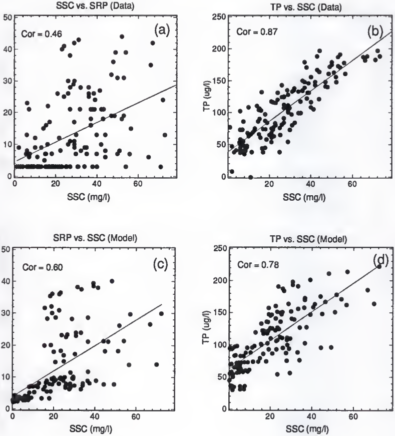

Figure 7.34: Correlations among SSC, SRP, and TP in the synoptic data and the 3-D model results for the 1989 synoptic survey in Lake Okeechobee.

the time series of simulated SSC, SRP, and TP at Station C in the lake. It can be seen from this figure that although SRP and TP do not have the diurnal fluctuation of SSC, they have the same longer period fluctuation as that of SSC. However, because TP's longer period fluctuation does not lag SSC's longer period fluctuation as SRP does, TP is better correlated with SSC than SRP is. The reason for the time lag between TP (or SSC) and SRP is that the desorption/adsorption reactions of SRP from/onto sediment particles take a certain period of time to reach the equilibrium.

Good correlation between SSC and TP in both measured data and model results indicates that resuspension and deposition of bottom sediments play important roles in controlling the TP level in the lake because SSC in the water column is mainly determined by resuspension and deposition processes. Time series of simulated resuspension and erosion rates of sediments over the entire lake are shown in Figure 7.36, together with the series of simulated resuspension/deposition rates of PIP and the total SRP mass (integration of SRP over the entire lake) . This figure shows that the average PIP resuspension rate in Lake Okeechobee is on the order of 1 kg/sec, or the average PIP resuspension flux is on the order of 66.7 mg/m^2day, which is much larger than the molecular diffusion flux of 0.045 to 1.9 mg/m^2day (Sheng, 1993).

In order to understand the relative effects of river loading, advection and horizontal diffusion, and biochemical reaction (other than desorption/adsorption reactions) on SRP budget and net PIP resuspension in Lake Okeechobee, this study made a few sensitivity runs of the 3-D model. The time period for these runs were about one month. Table 7.4 lists results of these runs, where

$$\Delta SRP = \oint P_1 dxdydz \tag{7.11}$$

$$PIP_{net} = \oint (E\left[\frac{P_6}{c}\right]_- - D\left[\frac{P_6}{c}\right]_+)dxdy \tag{7.12}$$

In Equations (7.11) and (7.12), the first intergration is made over the entire lake, and the second over the entire lake bottom. + and − represent the layers above

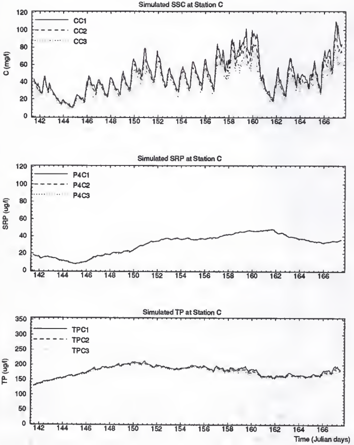

Figure 7.35: Time series of simulated SSC, SRP, and TP at Station C of Lake Okeechobee during the 1989 Spring Survey.

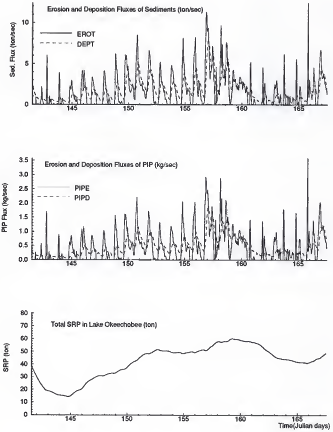

Figure 7.36: Model results of time series of sediment and PIP resuspension/deposition fluxes and SRP mass in Lake Okeechobee during the 1989 Spring Survey.

Table 7.4: Results of some sensitivity runs of the 3-D nutrient model.

Run No.	Advection and Horiz. Diffusion	River Discharge	Reaction Terms	ΔSRP (ton)	PIP_{net} (ton)
1	on	off	all on	8.71	33.17
2	on	off	only ads-des	59.29	-30.26
3	on	on	all on	8.85	27.27
4	on	on	only ads-des	55.57	-44.42
5	off	off	all on	27.35	7.02
6	off	off	only ads-des	36.31	-25.97
7	off	on	all on	26.26	-1.1
8	off	on	only ads-des	32.84	-40.0

and below the water-sediment interface, respectively; c is the sediment concentration, P_1 and P_6 are the SRP and PIP concentrations, respectively; and E and D are the erosion and deposition rates, respectively.

From Table 7.4, the following three conclusions can be drawn:

1. Advection and horizontal diffusion have significant effects on the release of SRP from sediments. Advection and horizontal diffusion can transport PIP from high concentration regions (mud zone) to low concentration regions (sand zone), and thus promote the desorption of SRP.
2. River discharges have very little effect on total SRP mass in the lake over one month period.
3. Algal uptake plays an important role in the SRP budget in the lake. Algal uptake can reduce the total SRP in the water column very dramatically, and therefore promote the release of SRP from the sediments.

7.3.3 Comparison with Other Water Quality Models

Disregarding the differences in hydrodynamics, sediment transport, and the treatment of sediment and nutrient fluxes across the water-sediment interface, the basic differences between the nutrient models developed in this study and the EPA WASP model in phosphorus cycling are in the kinetics/transformation processes: (1) While instantaneous equilibrium model is used in the WASP model, kinetics model is used in this study; and (2) Zooplankton is simulated in this study, but not in the WASP model. If one lets the desorption rate coefficients d_{ip} and d_{op} be very large values (e.g., $10^{50} day^{-1}$) and all the model parameters related to zooplankton ($\mu_{z_{max}}, K_{zx}$, and K_{zs}) be zero, then the transformation processes of this study are the same as those in the WASP model. To examine the effect of this difference, this study performed a simulation of Week 1 by using the same transformation processes as those in the WASP model. The model results of SRP are shown in Figure 7.37.

Compared to measured SRP data in Figure D.18, we see that model results with the same transformation processes as those of the WASP model (Figure 7.37) is not as good as the model results in this study (Figure 7.26). Simulated SRP results in Figure 7.37 are higher than data, and the maximum SRP location is closer to the maximum SSC location in model results than in the data because of the instantaneous equilibrium assumption used in WASP model for the adsorption-desorption reactions.

The differences between the 3-D model developed by Dickinson *et al.* (1992) for Lake Okeechobee phosphorus dynamics and the 3-D model developed in this study are: (1) While this study calculated nutrient concentrations simultaneously in the sediment column and in the water column, Dickinson's model calculated nutrient concentrations in the water column and sediment column in sequence; (2) While instantaneous equilibrium model is used in Dickinson's model, kinetics model is used in this study; and (3) While three algal groups are simulated in Dickinson's model, all algal groups are aggregated into one group in this study.

Huber and Dickinson (1991) used the 3-D model developed by Dickinson *et al.* (1992) to simulate phosphorus dynamics in Lake Okeechobee during the time period of Week 1. To compare the 3-D nutrient model developed in this study with Dickinson's 3-D phosphorus model, this study also used Dickinson's model to simulate phosphorus dynamics in Lake Okeechobee. The simulated SRP results at the end of Week 1 from

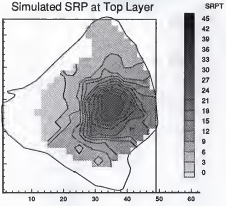

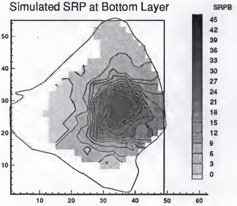

Figure 7.37: Spatial distribution of simulated (with the WASP transformations) SRP concentration at the top and the bottom layers of Lake Okeechobee at noon of May 27, 1989.

Dickinson's model are presented in Figure 7.38. From this figure, it can be seen that SRP predicted by Dickinson's model is generally higher than measured SRP in most of the lake and the shapes of the simulated SRP concentration contours are different from that of data. Similar to model results presented in Figure 7.37, the maximum SRP location is also closer to the maximum SSC location in Figure 7.38 than in the data because of the instantaneous equilibrium assumption used in Dickinson's model for the adsorption-desorption reactions. The differences in the shapes of SRP concentration contours in Figures 7.38 and 7.37 are due to the different treatment of nutrient fluxes across the water-sediment interface. The differentiation of algae into three groups does not make any significant difference in model results.

7.4 Summary

The 1-D and the 3-D model systems of hydrodynamics, sediment dynamics, and nutrient dynamics have been applied to a long-term survey conducted in the spring of 1989 and a short-term survey conducted in the spring of 1993 in Lake Okeechobee. All the simulations incorporated time-varying measurements of wind. The three-dimensional simulations used the measurements of riverine flow, sediment, and phosphorus components as boundary conditions and the first synoptic survey as initial conditions.

Model applications to the both surveys have quantitatively demonstrated that both the short-term and the long-term simulations using the 1-D and the 3-D modeling systems yields realistic results. The results of the four-week simulation show that simulated SSC, SRP, and TP agree reasonably well with the synoptic data measured during the Spring 1989 Survey. Long-term model predictions illustrate the importance of good wind data in the generation of reasonable model results, as shown by the nearly complete sinking out of sediment from the water columns following a long period of low wind.

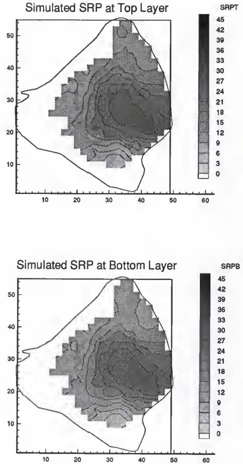

Figure 7.38: Spatial distribution of simulated SRP concentration (by the 3-D model developed by Dickinson *et al*, 1992) at the top and the bottom layers of Lake Okeechobee at noon of May 27, 1989.

In the short-term simulations, emphases was placed more or less on the short-term dynamics of phosphorus cycling. Both field data and model results suggest that the dissolved oxygen concentration in the water column is a key factor controlling the desorption of SRP from sediments in the lake. During an episodic event, the resuspension of bottom sediments can causes a drop of DO in the water column due to the increase of CBOD. The decrease of DO will catalyze the desorption reaction of SRP in the presence of iron ions. Therefore, during a resuspension event, the increase of SRP concentration in the water column is not solely due to the high inorganic phosphorus adsorbed in sediments, but also due to the decrease of DO caused by the resuspension. On the other hand, for an aquatic system with very high DO concentration, the resuspension of sediments may have little effect on DO concentration in the water column, and the desorption of SRP may very small. This might be the reason for no significant increase of SRP during a storm event captured in Tampa Bay in 1993, as will be discussed in the next chapter.

Model simulations have shown that settling velocity measured by using a settling tube may be not accurate and can not be directly used in a numerical model because of the reduction (or lack) of turbulence in the tube. This study first used the settling velocity formula obtained by Hwang and Mehta (1989) based on the laboratory measurements of Lake Okeechobee mud. Unfortunately, model results of SSC did not agree very well with data. By modifying their settling velocity formula to consider the effect of turbulent shearing on flocculation, model results have been much improved.

Both measured data and 3-D model results show that TP is well correlated with SSC in Lake Okeechobee, while the correlation between SRP and SSC in the lake is low. The 3-D simulations for the 1989 Spring Survey confirms the conclusion drawn by Sheng (1993) that the resuspension flux of phosphorus in Lake Okeechobee is two orders of magnitude larger than the molecular diffusive flux of phosphorus.

The 3-D nutrient model developed in this study covers all of the phosphorus transformations in the EPA WASP model. Model simulation with the WASP transformations shows that the instantaneous equilibrium model for adsorption-desorption reactions can not be used in real-time simulations such as these in this study because the time period for adsorption-desorption reactions to reach equilibrium can be larger than the time step used in the simulations (15 minutes).

CHAPTER 8
FIELD DATA COLLECTED IN TAMPA BAY

As part of a Sea Grant project entitled "Quantifying Sediment Resuspension Flux of Nutrient and Contaminants in Estuaries Due to Episodic Events", field data were collected during two storm events in February, 1992 and March, 1993 in Tampa Bay (Sheng *et al.*, 1993b). The field data included wind, current, water temperature, salinity, suspended sediment concentration, pH, DO, and nutrient concentrations at two stations (Figure 8.1). The main purpose of project was to develop a reliable method to quantify the resuspension fluxes of nutrients during episodic events in a shallow estuaries.

8.1 Physical Setting

Tampa Bay is located in the western central part of the Florida peninsula (Figure 8.1). The northwestern and northeastern compartments of the bay are known as Old Tampa Bay and Hillsborough Bay, respectively. The center part is referred to as middle Tampa Bay and the region adjacent to the West Florida shelf is called lower Tampa Bay. The bay extends about 60 km northeastward from the 8 km wide mouth that connects it to the Gulf of Mexico. The width of Tampa Bay is about 15 km and the total water open area is about 1,030 m^2.

Tampa Bay is a relatively wide and shallow estuary, with an average depth of about 4 meters. The depth generally does not exceed 10 meters except within the navigational channel, which has been dredged from the mouth to the upper reaches of the lower Tampa Bay where it spilts into two branches, one entering the Old Tampa Bay and the other going into Hillsborough Bay.

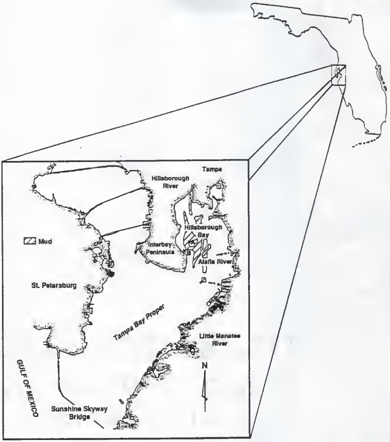

Figure 8.1: Location of Tampa Bay and the experiment stations (after Sheng *et al.*, 1993b)

The watershed area of Tampa bay covers about 4,600 square kilometers, and delivers a total annual mean fresh water runoff of ahout 63 m^3/sec into the estuary. The major fresh water runoff into the Tampa Bay are the four rivers on the right bank: Manatee river, Little Manatee river, Alafia river and Hillsborough river. The annual mean fresh water discharges by them are 15, 13, 6, and 10 m^3/sec, respectively, which comprise about 70% of the total fresh water discharge (Lewis and Estevez, 1988).

Bottom sediments are sandy in most of Tampa Bay. Muddy sediments only exist in Hillsborough Bay (see Figure 8.1 for mud areas in Tampa Bay).

Available data indicate that Tampa Bay has high phosphate levels, especially in Hillsboruogh Bay (Spaulding *et al.*, 1989). The mean annual phosphate concentration in Tampa Bay can be as high as 1.28 mg/l (Fanning and Bell, 1985). The major source of phosphorus for Tampa Bay is the Alafia River which passes through areas of high phosphate and phosphate mining, processing and handling activities (Lewis and Estevez, 1988). This is the primary reason for high phosphorus levels in Hillsborough Bay hecause the Alafia River discharges into Hillshorough Bay. Johansson and Squires (1989) found that the Alafia River loading rate is sufficient to meet 51% of the phosphate uptake estimated for phytoplankton growth and sediment flux rates are sufficient to meet 140% of the uptake. Therefore, phosphorus levels in Hillshorough Bay is much higher than what is needed for phytoplankton production and phosphorus is not a limiting factor to plant growth in the bay.

On the other hand, nitrogenous nutrient may limit phytoplankton production in Tampa Bay. Generally, the mean ratio of nitrogen to phosphorus (N:P, as atoms) is used to determine if the system is nitrogen limiting or phosphorus limiting to phytoplankton production. The commonly accepted value in marine system is 16. If N:P is higher than 16, then the system is primary phosphorus limiting. Otherwise, the system is considered to be nitrogen limiting. Fanning and Bell (1985) calculated that the N:P ratio in Tampa Bay ranged from 0.3-1.3 in 1981, indicating that nitrogen is limiting phytoplankton production in the bay.

Nitrogenous nutrient levels in Tampa Bay range from 1-280 $\mu g/l$ nitrate plus nitrite and 10-280 $\mu g/l$ ammonia (Fanning and Bell, 1985). Fanning and Bell found that a relatively high ammonia to total inorganic nitrogen ratio of 0.84 in Tampa Bay. This ratio did not show clear seasonal trend. Fanning and Bell suggested that among other causes, ammonia recycling in the sediment (resuspension flux) may be more important in Tampa Bay than in some other estuaries because of the shallowness of the bay. No available measurements of denitrification or nitrogen fixation exist (Spaulding *et al.*, 1989).

8.2 Field Measurements

In February,1992 and March 1993, field measurements were conducted at two locations (Stations A and B in Figure 8.1) in Hillsborough Bay by the Department of Coastal & Oceanographic Engineering and the Water and Soil Science Department of the University of Florida. Station A is in the muddy zone with a mean depth aof bout 4 meters, and Station B is in the sandy zone with a depth of about 2 meters. Data measured at both stations include wind, tide, current, suspended sediment, salinity, and water temperature. In addition, pH, DO, and nutrients at Station A were also measured. Basic equipments used in the measurement were almost the same as those used in the field experiments in Lake Okeechobee described in Chapter 6: (1) wind anemometer (model 05103) by R.M. Young Company for the measurement of wind speed and wind direction, (2) electromagnetic current meter by Marsh-McBirney Inc. for current measurement, (3) optical back scatter (OBS) sensor of D & A Instruments and Engineering for suspended sediment concentration sampling, (4) oceanographic thermometer by Sea-Bird Electronics, Inc. (SBE) for the temperature, (5) conductivity meter by Sea-Bird Electronics, Inc. for the salinity, and (6) Data Sonds 3 (DS3) package of Hydrolab, Corp. for the measurement of pH and dissolved oxygen. Nutrient data were measured by first collecting water samples using the Sigma sampler at the field, and then measuring SRP, TSP, TP, and ammonium concentrations in the laboratory. A porewater equlibrator (peeper) was placed at Station A to measure nutrient profiles in the sediment column.

8.3 A Storm Event in February, 1992

The 1992 field measurement was carried out for ten days, from Julian day 30 to Julian day 40 (January 31 to February 9) in 1992. During these ten days, wind, current, tide, salinity and temperature were successfully measured. But for suspended sediment and nutrients, data were collected for only 24 hours (form Julian day 35.6 to Julian day 36.6).

For current, temperature, salinity and suspended sediment concentration, values at two vertical levels of Stations A and B were measured. The upper level is near the water surface (about 2.4 and 1.6 meters above the bottom for Station A and B, respectively), and the lower level is near the bottom (about 0.7 and 0.4 meters above the bottom for Station A and B, respectively). The wind was measured at about 2.5 meters above the mean water surface.

Figures G.2 to G.1 in Appendix G are plots of measured wind, surface elevation, salinity, temperature, and water velocities from Julian day 30 to Julian day 40. Figure show G.4, measured wind, current, and suspended sediment concentration during a storm event (from Julian days 35.6 to 36.6).

From Figure G.3, we see that the water level dynamics show a very strong semi-diurnal variation at Station A. This is caused by the astronomical M_2 and S_2 constituents. Beside the tidal effect on the water level, wind can also causes setup of water level. Figures G.2 and G.3(a) show a clear correlation between the wind speed (from south) and mean water level rise.

Figure G.3(b) indicates that, due to the heat exchange at the water surface, the temperature variation at Station A was more dynamic than the salinity variation.

Because Station A is far away from the estuary mouth, the salinity variation was not high (only within 1 ppt). Both salinity and temperature show little stratification at Station A. The mean value of salinity at the bottom arm was about 27.5 ppt, and the mean salinity at the top arm was about 26.5 ppt. For temperature, the mean value at the bottom arm was about 16 ^oC, and the mean value at the top arm was about 16.5 ^oC. The small stratification of salinity and temperature at Station A indicates that the vertical mixing was strong at this station. This agrees with early investigations carried by Palmer and McClelland (1988) and Goodwin (1987). Flow velocities in the x-direction (from west to east) at both the bottom and top layers of Station A were much smaller than those in the y-direction (from south to north) as shown in Figure G.1 because of the geometry and the direction of tide propagation.

Measured total N and C were ca. 0.31% and 4%, respectively of the total bottom sediments at Station A. Sediments were enriched with N and C in the surface and decreased with depth, suggesting recent deposits of organic matter. This was evidenced by lower bulk density of surficial sediments. The total inorganic carbon in the surface sediments was about 40 presents of the total C in the surface sediments, as compared to more than 80% of the total C in the lower sediment column. Redox potential (Figure G.6 in Appendix G) of the sediments show decrease with depth, with the sediment-water interface oxidized. Redox potential in the top 1 cm of the sediment column was about 300 mV indicating oxidized surficial sediments.

Data on SRP, TP, and ammonium N collected during storm event at Station A are presented in Figure G.5 in Appendix G. Dissolved N and P species showed no clear trend during the diel sampling event. Total phosphorus did shown some correlation with the wind event. The increase was likely due to entrained sediment particles. Since there was not a concurrent increase in SRP, it is likely that the dissolved P is strongly sorbed onto suspended particles. No significant relationship was observed between suspended solids and dissolved SRP, ammonium N and TP.

Results of average concentration profiles of SRP and ammonium N are presented in Figure G.6 in Appendix G. We see that NH_4^+-N and SRP concentrations in the sediment column were much higher than those in the water column (average ammonium N and SRP concentrations in the upper sediment layer were 200 and 20, respectively, times larger than those in the water column).

8.4 A Storm Event in March, 1993

The second field measurement was conducted during the "Storm of the Century" in 1993. Data of current, salinity, temperature, wind, waves, dissolved oxygen, pH, as well as nutrients were collected at the same two locations as in 1992.

Figure G.7 in Appendix G are plots of measured salinity, temperature, pH, and dissolved oxygen at Station A before the storm arrived. Figures G.8 to G.11 in Appendix G are plots of the measured data of wind, current, and suspended sediment concentration at Station A and B, respectively. Because of the collapse of the measurement platform caused by the very strong wind and current in the deep water region during the storm, hydrodynamic and suspended sediment data were collected only for less than one day at Station A (Figure G.9), while at Station B data for about one week were obtained. The nutrient species measured were ammonium nitrogen and soluble reactive phosphorus (SRP) at Station A. Because of the danger of collecting data during the storm, nutrient data were measured for only a few hours just before the wind became too strong. The measured nutrient data are shown in Figure G.12 in Appendix G.

The measured salinity, temperature, pH, and DO in Figure G.7 show small variation during Julian day 70.5 to 71.1. Before the storm arrived, both salinity and temperature were stratified. When wind speed started to pick up at Julian day 70.95, salinity and temperature became well-mixed. The measured suspended sediment concentration measured during this time period correlated well with the wind. The increase in wind speed caused the sediment resuspension, and thus caused the increase in suspended sediment concentration in the water column from Julian day 70.8 on.

The SRP data shown in Figure G.12 indicate that the SRP concentration at Station A was at a very high level. The storm event had almost no significant effect on the SRP concentration in the water column. However, the ammonium nitrogen concentration in the water column did increase with the increasing sediment concentration, although the reason for the peak values at the middle and the bottom layers around Julian day 70.6 is still not clear because of the lack of pH, DO, and other biochemical data. The fact that SRP concentration did increase with the sediment concentration increase in the water column indicates that there was no significant desorption of SRP at Station A, probably due to the high DO concentration in the bay.

CHAPTER 9
MODEL APPLICATIONS TO TAMPA BAY

The vertically one-dimensional models of hydrodynamics, sediment transport, and nitrogen dynamics described in Chapter 4 and 5 have been used to simulate the storm events observed in February, 1992 and in March, 1993 in Tampa Bay. Details of the study are described in a See Grant report (Sheng *et al.*, 1993). Some simulation results are presented in the following.

9.1 Modeling the 1992 Storm Event

The 1992 storm event in Tampa Bay were simulated using the one-dimensional model. Before running the model, the SMB model was employed to compute the significant wave height and period using the measured wind data and bay geometry and bathymetry. The simulated significant wave height and period are shown in Figure 9.1. In solving the hydrodynamic equations, the combined flow due to oscillatory wave and wind mixing was first solved using the combined pressure gradient associated with the oscillatory wave orbital current and wind-driven current (Equations (4.37) – (4.40)). The following parameters are then calculated: (1) bottom shear stress due to the combined action of wave and current, and (2) the wave-averaged eddy viscosity and eddy diffusivity which represent the turbulent mixing induced by the combined action of wave and current (Section 7.1). Similar to the 1-D model application to Lake Okeechobee described in the previous chapter, the calculated wave-averaged eddy viscosity and diffusivity are used in the computation of current, sediment concentration, and nitrogen concentrations in the new time step. The calculated bottom shear stress due to the combined wave and current actions is used in the computation of the erosion and deposition rates.

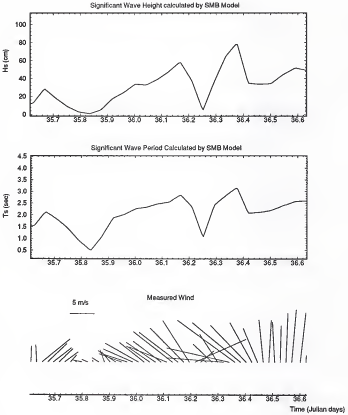
Significant Wave Height calculated by SMB Model

Significant Wave Period Calculated by SMB Model

Measured Wind

Figure 9.1: Significant wave heights calculated from SMB model for the time period of the 1992 storm event.

Figure 9.1 presents the significant wave height and period predicted by the SMB model at Station A in Tampa Bay during the 1992 storm event. Measured wind is also shown in the figure in terms of a stick diagram. The SMB model results show that the significant wave height at Station A was very high during the storm event. It reached about 80 cm, when the wind speed reached about 16 m/sec.

Figure 9.2 shows the simulated flow velocities and sediment concentrations at the same two vertical levels as the measurement arms. Compared to the measured data in Figure G.4, we see that the model results compare well with data. Again, the good agreement between simulated and measured currents should not be a surprise, because the measured currents at the two arms were used to calculated the pressure gradient terms in the model. The aim of this one-dimensional simulation is not to predict current, but to obtain a reasonable velocity profile so that the turbulent mixing can be calculated accurately.

In the simulation of suspended sediment dynamics, the resuspension rate was calculated using the Power Law with $T_d = 1$ and $p = 1$, the deposition velocity was calculated using Sheng's model, the settling velocity is calculated using Equation (4.27), and the vertical mixing was calculated using the TKE model. The simulated significant wave height and the measured (or simulated) suspended sediment concentration appear to be significantly correlated. However, high suspended sediment concentration at the upper layer of the water column cannot be caused by the action of a purely oscillatory current due to an oscillatory wave alone. In the absence of slowly varying current, the turbulent mixing due to a pure wave motion is very small outside the wave boundary layer. Thus, the suspended sediment concentration in the water column is affected by the current through vertical mixing, though the current does not contribute much to the resuspension of bottom sediment. In the presence of large waves and currents, the suspended sediment concentration can be very high through the water column.

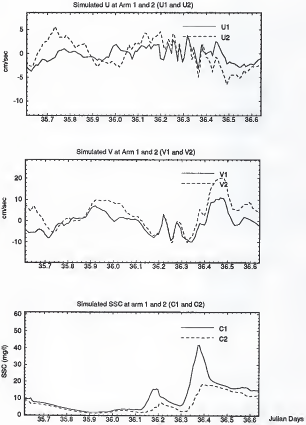

Figure 9.2: Model results of u-velocity, v-velocity, and sediment concentration at Station A during the storm event of 1992.

The equations for algal biomass, zooplankton and nitrogen dynamics are solved after solving the current and sediment equations in the model. Measured temperature data are used in the model for calculating the temperature effects on algal growth rate, zooplankton growth rate, and other reaction rates. Literature values of the model coefficients were first used to run the nitrogen model, and then tuned to fit the measured data. Table H.3 in Appendix H lists the values of model coefficients used in the simulation. Model results of ammonium nitrogen are presented in Figure 9.3, together with the measured data. We see that the simulated ammonium N at the bottom layer agrees well with the measured data. Performing sensitivity runs by adjusting the model coefficients, we learned that the decrease in ammonium N concentration at the beginning of the measurement was most likely due to the volatilization process and the increase in ammonium N concentration near the end of the measurement was due to the resuspension. The model results of bottom resuspension fluxes of sediment and ammonium N are shown in Figure 9.4.

9.2 Modeling the 1993 Storm Event

The one-dimensional model used for the 1992 storm event was also used to simulate the hydrodynamics, sediment concentration, and nitrogen concentrations during the 1993 field measurement. Model results of currents and sediment concentrations at Stations A and B are presented in Figures 9.5 and 9.6, respectively. Again, model results of current are almost the same as data because the pressure gradient terms were calculated from the measured current data. At both stations, the simulated sediment concentrations agree well with data.

The model results of ammonium N at the top layer and the bottom layer are shown in Figure 9.7. Due to the lack of the pH and DO data at the beginning of the measurement and also due to the lack of other biochemical data, it is not clear what caused the peak value of ammonium N concentration. Because the wind speed was not very high and the sediment concentration in the water column did not have

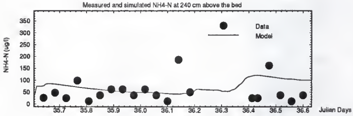

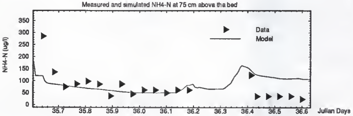

Figure 9.3: Comparison of model results of NH_4^+-N and measured data during the storm event of 1992 at Station A.

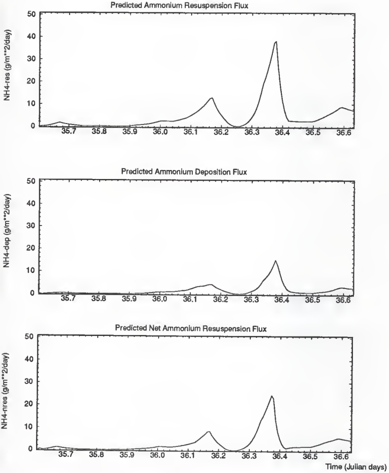

Figure 9.4: Model results of resuspension fluxes of (a) sediments and (b) NH_4^+-N during the storm event of 1992 at Station A.

a high peak around Julian day 70.6, the ammonium N increase at that time was definitely not caused by the resuspension. It might be because of a sudden increase of dissolved oxygen, or due to the advective transport. The increase in ammonium N concentration at the bottom layer after Julian day 70.8 was well correlated with the increase in sediment concentration, hence suggesting that increased ammonium N concentration was caused by the sediment resuspension and the desorption process afterwards. The resuspension fluxes of sediment and ammonium nitrogen are shown in Figure 9.8.

9.3 Conclusions

It can be concluded from the Tampa Bay field data and the model results that sediment resuspension in the bay is mainly caused by the wind-induced wave action. Measured data during the two measured storm events have clearly shown an increase in suspended sediment concentration and dissolved ammonium N concentration. On the other hand, SRP concentrations during the storm events did not show an obvious increase. The reason might be the very slow desorption of SRP during the storm events.

Model applications show that desorption processes play a very important role in the internal loading of nutrients during episodic events. While fast desorption can result in a very high nutrient level in the water column, very slow desorption may yield very small net nutrient resuspension during an episodic event. To illustrate this, a test run with zero desorption rate of ammonium nitrogen was made for the 1992 survey. The results are shown in Figure 9.9. As can be seen, ammonium N concentration did not respond to storm event, even though sediment resuspension took place. As a result, the net input of nutrients from the bottom over the resuspension event becomes zero because the adsorbed nutrient species will fall to the bottom with deposited sediments again when the wind calms down.

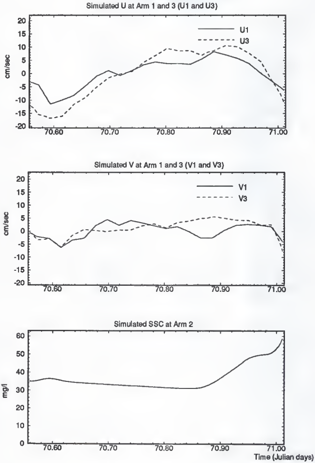

Figure 9.5: Model results of u-velocity, v-velocity, and sediment concentration at Station A during the storm event of 1993.

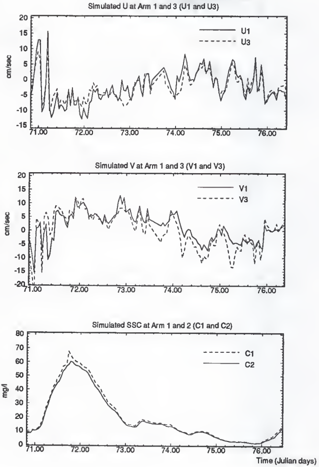

Simulated U at Arm 1 and 3 (U1 and U3)

Simulated V at Arm 1 and 3 (V1 and V3)

Simulated SSC at Arm 1 and 2 (C1 and C2)

Figure 9.6: Model results of u-velocity, v-velocity, and sediment concentration at Station B during the storm event of 1993.

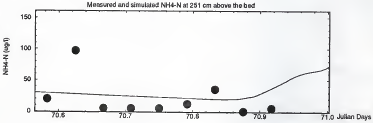

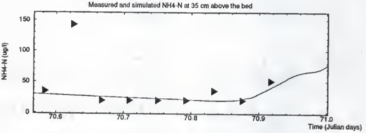

Figure 9.7: Comparison of model results of NH_4^+–N and measured data during the storm event of 1993 at Station A.

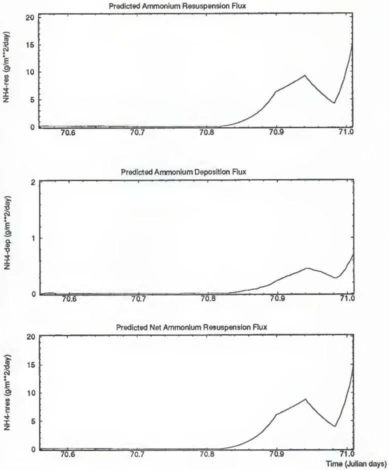

Figure 9.8: Model results of resuspension fluxes of (a) sediments and (b) NH_4^+–N during the storm event of 1993 at Station A.

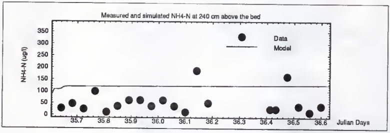

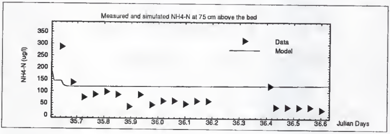

Figure 9.9: A test run with zero desorption rate of ammonium N at Station A during the storm event of 1992.

CHAPTER 10
CONCLUSIONS AND RECOMMENDATIONS

10.1 Conclusions

From the field data and the model results carried out in this study, the following conclusions can be drawn:

1. Lake Okeechobee circulation is driven by wind. Significant seiche oscillation appears in the lake after the decrease in wind speed.
2. Sediment resuspension in shallow lakes and estuaries is mainly caused by wind-generated waves. The wave-induced bottom shear stress is much higher than the current induced bottom shear stress in Lake Okeechobee and Tampa Bay.
3. Advection and horizontal diffusion have significant effects on phosphorus release in Lake Okeechobee. The horizontal transport of phosphorus species from one region to another region can enhance the desorption of SRP from suspended sediments.
4. The horizontal distribution of suspended sediment concentration (SSC) in shallow lakes such as Lake Okeechobee is determined by the wave field (which is in turn determined by the wind field) and the bottom sediment type. The maximum SSC in Lake Okeechobee always occurs over the muddy zone.
5. Vertical mixing and settling are more important than horizontal transport processes to sediment dynamics in Lake Okeechobee due to its shallowness and relatively week currents (on the order of $10cm/sec$) in it. The horizontal advective transport during one hour, for example, is only about 360 meters which is less then 1% of the lake dimension. Strong currents only occur during seiche oscillation, which causes only small net horizontal transport.

6. Although horizontal transport processes are not very important to sediment dynamics in Lake Okeechobee, they can significantly affect the release of SRP from sediments. Advection and horizontal diffusion can transport PIP from high concentration regions (mud zone) to low concentration regions (sand zone), and thus promote the desorption of SRP.
7. The sediment transport in Tampa Bay is also mainly determined by the vertical mixing, at least in Hillsborough Bay where the horizontal current is not strong (on the order of $10cm/sec$). The vertical one-dimensional sediment model has given fairly good results.
8. The total phosphorus concentration in Lake Okeechobee correlated much better with the suspended sediment concentration than soluble reactive phosphorus concentration did. This suggests that the release of SRP and DOP in the lake is not instantaneous. Previous water quality models assuming instantaneous equilibrium between dissolved and adsorbed nutrients are thus unable to simulate nutrient dynamics in the lake correctly.
9. The three-dimensional model system for hydrodynamics and sediment transport originally developed by Sheng was used to simulate the hydrodynamics and sediment transport processes in Lake Okeechobee. Model results showed that this model system could simulate the wind-driven circulation and SSC distribution in shallow lakes such as Lake Okeechobee fairly well. Although the present model simulation did not include the temperature effect, model results of currents agreed well with data, especially in terms of the long term (on the order of one week or more) trend of currents. The model results can be further improved by including the temperature effect as was done in Lee and Sheng (1993).
10. The 3-D model results of suspended sediment concentration of the 1989 Spring Survey in Lake Okeechobee (Sheng, *et al.*, 1991) have been improved by incorporating the effect of surface elevation on wave-induced bottom shear stress.

This shows that the precise estimation of wave-induced bottom shear stress is very important to model applications.

11. Comprehensive turbulence closure models have been used to calculate the vertical mixing in this study. In the lutocline simulation, the second-order closure model used includes the effect of sediment stratification automatically. The predicted lutocline elevation indicates that lutocline level varies with the wind.
12. The three-dimensional nutrient model developed in this study has been applied to Lake Okeechobee. Model results of SRP and TP agreed well with the synoptic data. Compared to Dickinson *et al.*'s model of phosphorus dynamics for Lake Okeechobee, the nutrient model developed in this study was able to better simulate the phosphorus dynamics in the lake because kinetic models for adsorption-desorption reactions were used and the exchange of nutrients between the water column and the sediment column was better simulated.
13. The one-dimensional model system for hydrodynamics, sediment transport, and nutrient dynamics has been applied to Lake Okeechobee and Tampa Bay. Results of model applications to both water bodies agreed well with data, thus confirming the dominance of the vertical transport in these two water bodies.
14. The erosion rate determined from the field data in Lake Okeechobee was found to be much larger than that determined from laboratory experiments, primarily due to the presence of waves and wave-induced fluidization of mud.
15. Many factors can affect nutrient dynamics. Field data and model results have shown the effect of dissolved oxygen and pH on the release of SRP in Lake Okeechobee. A decrease of DO and an increase of pH (from 7.5) most likely caused a significant release of SRP in the lake.
16. The resuspension flux of nutrients during an episodic event was much larger than the diffusive flux. Model results showed that the resuspension flux in Tampa Bay was about 1000 times larger than the diffusive flux (Sheng *et al.*, 1993b).

To quantify nutrient budget in lakes and estuaries, it is essential to estimate the resuspension flux of nutrients from the bottom.

10.2 Recommendations

Although numerical models used or developed in this study have performed well in simulating hydrodynamics, sediment transport, and nutrient dynamics in Lake Okeechobee and Tampa Bay, some shortcomings still exist in these models. These shortcomings include, for example: (1) no temperature effect on currents, (2) no vegetation effects on currents and nutrient dynamics, (3) no multiple sediment groups (although the 3-D model can treat sandy sediments and fine sediments differently) (3) no wave-current interaction in the 3-D model, (5) no consideration of the change of shoreline due to the surface fluctuation, and (6) no DO dynamics simulation in the models. Model improvements can be made in future studies. For example, the effect of temperature on currents can be included in the hydrodynamics part of the models, and DO equation can be solved in the nutrient part of the models.

Because of the importance of internal loading of nutrients in affecting nutrient dynamics in shallow lakes and estuaries, future modeling effort should also focus on physical and biochemical processes taking place in the top sediment layer. For example, it has been hypothesized that processes associated with the fluidization of mud could affect nutrient exchange rate between the sediment column and the water column by wave-induced pumping of water into the sediment column to cause porewater movement and/or alter the dissolved oxygen level in the sediment column, which in turn affects the release of SRP from sediments and the decomposition process of algae. Laboratory experiments need to be conducted to examine such hypotheses. However, because of the lack of complete understanding of the fluidization process, it is still impossible to include fluidization in the sediment model at this time. Future laboratory studies and field experiments are needed for the development of a predictive model of fluidization, before such process could be included into a nutrient model.

BIBLIOGRAPHY

Ahn, K., 1989: Wind-wave hindcasting and estimation of hottom shear stress in Lake Okeechohee, M.S. Thesis, Univ. of Florida, Gainesville.

Alldrdge, A.L. and C.C. Gotschalk, 1988: Direct observation of the mass flocculation of diatom blooms: Characteristics, settling velocities and formation of diatom aggregates, *Deep-Sea Res.*, **36:** 159-171.

Alexander, M., 1965: Nitrification, in (W.V. Bartholomew and F.E. Clark, eds.), *Soil Nitrogen*, Am. Soc. Agron., Madison, Wisconsin, pp. 307-343.

Alexis, A., P. Bassoullet, P. Le Hir, and C. Teisson: 1992 Consolidation of soft marine soils: Unifying theories, numerical modelling and in situ experiments, *Proc. of 23th International Conference on Coastal Engineering.*, Venice, Italy, Oct.

Ambrose, R. A., T. A. Wool, J. P. Connolly, and R. W. Schanz, 1991: WASP5.x, A hydrodynamic and water quality model — Model theory, User's manual, and programmer's guide, EPA/600/3-87/039, U.S. Environmental Protection Agency, Athens, GA.

Ariathurai, R., and R. B. Krone, 1976: Finite element model of cohesive sediment transport, *J. Hyd. Div.*, American Society of Civil Engineers, **HY4**: 323–338.

Bakker, W.T., 1974: Sand concentration in oscillatory flow, *Proc. of the 14th Conf. on Coast. Eng., Copenhagen*, ASCE, New York, pp. 1129-1148.

Barica, J. and R.J. Allan, 1988: Utility of soluble reactive phosphorus measurements in Great Lakes surveillance programs: A Summary, *J. Great Lakes Research,* **14**(3): 377-379.

Beck, M.B. and L. Somlyody, 1982: Identification of a model for wind induced sediment-water interactions in Lake Balaton, IIASA Working Paper, Laxenhurg, Austria.

Bedford, K.W., O. Wai, C. Lihicki, and R. VanEvra III, 1987: Sediment entrainment and deposition measurements at a spoil disposal site, *J. Hyd. Engineering*, ASCE, **113**: 1325-1342.

Berkheiser, V.E., J.J. Street, P.S.C. Rao, and T.L. Yuan, 1980: Partitioning of inorganic orthophosphate in soil-water systems, *CRC Critical Review in Environmental Control*, Volumn 10.

Bierman, V.J., D.M. Dolan, E.F. Stoermer, J.F. Gannon, and V.E. Smith, 1980: The development and calibration of a spatially simplified multi-class phytoplankton model for Saginaw Bay, Lake Huron, *Great Lakes Environmental Planning Study*, Contribution No. 33.

Blosser, M.C., 1986: Phosphorus models for Lake Okeechobee, Florida, M.E. Thesis, Dept. of Environmental Engineering Sciences, University of Florida, Gainesville.

Blumberg, A. F., 1975: A numerical investigation into the dynamics of estuarine circulation, Chesapeake Bay Institute Report No. 91, Baltimore, MD.

Blumberg, A. F., and G. L. Mellor, 1987: A description of a three-dimensional coastal ocean circulation model, in (Heaps, N. S., ed.), *Three-Dimensional Coastal Ocean Models*, American Geophysical Union, Washington, DC, pp. 1-16.

Boers, P., L. Van Ballegooijen, and J. Uunk, 1991: Changes in phosphorus cycling in a shallow lake due to food web manipulations, *Freshwater Biology*, **25:** 9-20.

Bostrom, B., Persson, G. and B. Broberg, 1988: Bioavaiability of different phosphorus forms in freshwater systems, *Hydrobiologia*, **170:** 133-155.

Bowden, K. F., and P. Hamilton, 1975: Some experiments with a numerical model of circulation and mixing in a tidal estuary, *Est. Coastal Mar. Sci* **3:** 281.

Bowman, R.A. and D.D. Focht, 1974: The influence of glucose and nitrate concentrations upon denitrification rate in sandy soil, *Soil Biol. Biochem.*, **6**(5): 297-301.

Bretschneider, C.L., 1959: Wave variabilty and wave spectra for wind-generated waves, Tech. Memo. No. 118, Beach Erosion Board, U.S. Army Corps of Engineers, Washington, DC, 1959.

Brevik, I., 1981: Oscillatory rough turbulent boundary layers, *Journal of Waterway Port Coastal Ocean Division, ASCE*, **107:** 175-188.

Brezonik, P.L., W.C. Huber, C. Pollman, M. Blosser, S. Zoltewicz, C. Miles and L. Lane, 1983: Evaluation and modeling of internal nutrient cycling processes in Lake Okeechobee, Florida, Completion Report, Dept. of Environmental Engineering Sciences, University of Florida, to South Florida Water Management District, West Palm Beach, March.

Broadbend, F.E. and R.E. Clark, 1965: Denitrification, in (W.V. Bartholomew and F.E. Clark, eds.), *Soil Nitrogen*, Am. Soc. Agron., Madison, Wisconsin, pp. 344-359.

Burban, P.-Y., W. Lick, and J. Lick, 1989: The flocculation of fine-grained sediments in estuarine waters, *J. Geophys. Res.* **94:** 8323-8330.

Burt, T.N., 1986: Field settling velocities of estuary muds, in (A. J. Mehta, ed.), *Estuarine Cohesive Sediment Dynamics*, Springer-Verlag, Berlin, pp. 126-150.

Canale, R.P., L.M. DePalma, and A.H. Vogel, 1976: A plankton-based food web model for Lake Michigan, in (R.P. Canale, ed.), *Modeling Biochemical Processes in Aquatic Ecosystem*, Ann Arhor Science Publishers Inc., Ann Arhor, MI, pp. 33-74.

Casulli V. and R.T. Cheng, 1992: Semi-implicit finite difference methods for free-dimensional shallow water flow, *International Journal for Numerical Methods in Fluids*, **15**: 629–648.

Cerco, C.F. and T. Cole, 1992: Application of the three-dimensional eutrophication model CE-QUAL-ICM to Chesapeake Bay, Technical Report, U.S. Army Engineer Waterways Experiment Station, Vickshurg, MS.

Chen, C.W. and G.T. Orloh, 1975: Ecology simulation of aquatic environments, in (B.C. Patten, ed.), *System Analysis and Simulation in Ecology*, **3**, Academic Press, New York, pp. 476-588.

Cho, D.Y. and F.N. Ponnamperuma, 1971: The influence of soil temperature on the chemical kinetics of flooded soils and growth of rice, *Soil Sci.*, **112**(3): 184-194.

Choi, J.-K., 1992: Three-dimensional curvilinear-grid modeling of baroclinic circulation and mixing in a partially-mixed estuary, Ph.D. Dissertation, University of Florida, Gainesville.

Chou, H.-T., 1989: Rheological response of cohesive sediments to water waves, Ph.D. Dissertation, University of California, Berkeley.

Chou, H.-T., A.M Foda, and J.R. Hunt, 1993: Rheological response of cohesive sediments to oscillatory forcing, in (A.J. Mehta, ed.), *Coastal and Estuarine Studies 42: Nearshore and Estuarine Cohesive Sediment Transport*, American Geophysical Union, Washington, DC, pp. 126-147.

Clukey, E.C., F.H. Kulhawy, and P.L.-F., 1983: Laboratory and field investigation of wave-sediment interaction, Joseph H. DeFrees Hydraulics Laboratory, Report 83-1, School of Civil and Environmental Engineering, Cornell University, Ithaca, New York.

Cole, J.J., 1982: Interactions between bacteria and algae in aquatic ecosystems, *Ann. Rev. Ecol. Syst.*, **13**: 291-314.

Day, J.W., Jr., C.A.S. Hall, W.M. Kemp, and Y.-A. Alejandro, 1989: *Estuarine Ecology*, John Wiley & Sons, Inc., New York.

Davies, A.G., R.L. Soulshy, and H.L. King, 1988: A numerical model of the combined wave and current bottom boundary layer, *Journal of Geophysical Research*, **93**(C1): 491-508.

Dawson, R.W. and K.L. Murphy, 1972: The temperature dependency of biological denitrification, *Water Res.*, **6**(1): 71-83.

Devol, A.H., 1979: Zooplankton respiration and its relation to plankton dynamics in two lakes of contrasting trophic state, *Limnology and Oceanography*, **24**(5): 893-905.

DePinto, J.V., T.C. Young, and D.K. Salisburg, 1986: Impact of phosphrus availability on modelling phytoplankton dynamics, *Hydrobiological Bulletin*, HY-BUD 9, **20**(1/2): 225-243.

Dickinson, R.E., W.C. Huber, and C.D. Pollman, 1992: Modeling of phosphorus dynamics of Lake Okeechobee, Subtasks Report to South Florida Water Management District, Department of Environmental Engineering Sciences, University of Florida, Gainesville.

Di Toro, D.M., 1980: Applicability of cellular equilibrium and Monod theory to phytoplankton growth kinetics, *Ecological Modelling*, **8:** 201-218.

Di Toro, D.M., O'Connor, D.M., R.V. Thomann, and J.L. Mancini, 1975: Phytoplankton-zooplankton-nutrient interaction model for western Lake Erie, in (B.C. Patten, ed.), *System Analysis and Simulation in Ecology*, **3**, Chapter 11, Academic Press, New York, pp. 423-474.

Di Toro, D.M., R.V. Thomann, D.J. O'Connor and J.L. Mancini, 1977: Estuarine phytoplankton biomass models – Verification analyses and preliminary applications, in (E.D. Goldberg, I.N. McCave, J.J. O'Brien, and J.H. Steele, eds.), *The Sea*, **6**, *Marine Modeling*, Wiley, New York, pp. 969-1020.

Dyer, K.R., 1973: *A Physical Introduction*, Wiley, New York.

Eckart, C, 1958: Properties of water, Part II. The equation of state of water and sea water at low temperatures and pressures, *Amer. J. Sci.* **256**: 225-240.

Eidsvik, K.J., 1990: Parameterization of wave effects upon large scale bottom boundary layer flow, Technical Report, Dept. of Coastal and Oceanographic Engineering, University of Florida, Gainesville.

Erh, K.T., D.E. Elrick, R.L. Thomas and C.T. Corke, 1967: Dynamics of nitrification in soils using a miscible displacement technique, *Soil Sci. Soc. Am. Proc.*, **31**(4): 585-592.

Fanning, K.A. and L.M. Bell, 1985: Nutrient in Tampa Bay, in (S.F. Treat, J.L. Simon, R.R. Lewis, III, and R.L. Whitman, Jr., eds.), *Proceedings, Tampa Bay Area Scientific Information Symposium*, Burgess Publishing CO., Minneapolis, MN.

Farley, K. J., and F. M. Morel, 1986: Role of coagulation in the kinetics of sedimentation, *Environ. Sci. Technol.* **20**: 187–195.

Feng, J., A. Mehta, D.J.A. Williams, and P.R. Williams, 1992: Laboratory experiments on cohesive soil bed fluidization by water waves, UFL/COEL-92/015, Coastal and Oceanographic Engineering Department, University of Florida, Gainesville.

Fillos, J. and A.H. Molof, 1972: Effect of benthal deposits on oxygen and nutrient economy of flowing waters, *J. Wat. Pollut. Control Fed.*, **44**: 644-662.

Fogg, G.E., 1978: Nitrogen fixation in the oceans, environmetal role of nitrogen-fixing blue-green algae and a symbiotic bacteria, *Ecol. Bull.* (Stockholm), **26**: 11-19.

Gargas, E., 1976: A three-box eutrophication model of a mesotrophic Danish lake, Water Quality Institute, Horsholm, Denmark.

Garland, J.H.N., 1978: Nitrification in the River Trent, in (A. James, ed.), *Mathematical Models in Water Pollution Control*, John Wiley & Sons, New York, pp. 167-191.

Garratt, J.R., 1977: Review of drag coefficients over oceans and continents, *Monthly Weather Review* **105**: 915-929.

Gibbs, R. D, 1983: Coagulation rates of clay minerals and natural sediments, *J. Sed. Petro.* **53**: 1193–1203.

Gibbs, R. D., 1985: Settling velocity, diameter, and density for flocs of illite, kaolinite, and montmorillonite, *J. Sed. Petro.*, **55**: 65-68.

Golterman, H.L., 1973: Vertical movement of phosphorus in freshwater, in (E.J. Griffith, A. Beeton, J.M. Spencer, and D.T. Mitchell, eds.), *Environmental Phosphorus Handbook*, John Wiley & Sons, New York.

Golterman, H.L., 1975: *Developments in Water Science – Physiological Limnology*, Elsevier Scientific Publishing Company, Amsterdam.

Goodwin, C.R., 1987: Tidal flow, circulation, and flushing changes caused by dredge and fill in Tampa Bay, Florida. U.S. Geological Survey, Water Supply Paper 2282, Tampa, FL, 88p.

Grant, W. D. and O. S. Madsen, 1979: Combined wave and current interaction with a rough bottom, *J. Geophys. Res.* **84**: 1797-1808.

Grobbelaar, J.U., 1985: Carbon flow in the pelagic zone of a shallow turbid impoundment, *Wuras Dam, Arch. Hydrobiol.*, **103**(1): 1-24.

Gschwend, P. M., S. Wu, O. S. Madsen, J. L. Wilken, R. B. Ambrose, and S. C. McCutcheon, 1987: Modeling the benthos-water column exchange of hydrophobic chemicals, Environmental Research Laboratory, Office of Research and Development, EPA, Athens, GA.

Hall, E.R. and K.L. Murphy, 1980: Estimation of nitrifying biomass and kinetics in wastewater, *Water Research*, **14:** 297–304.

Hansen, D. V. and M. Rattray, 1966: New dimensions in estuary classification, *Limnology and Oceanography*, **11:** 319–325.

Hayter, E.J. and Pakala, C.V., 1989: Transport of inorganic contaminants in estuarial waters, *Journal of Coastal Research*, Special Issue No. 5, pp. 217-230.

Harleman, D.R.F., 1977: Real-time models for salinity and water-quality analysis in estuaries, *Studies in Geophysics: Estuaries, Geophysics, and the Environment*, National Academy of Sciences, Washington, DC.

Harleman, D.R.F. and P. Shanahan, 1983: Hydrodynamic and mass transport aspects of the Lake Balaton models, in (L. Somlyody, S. Herodek, and J.

Fischer, eds.), *Eutrophication of Shallow Lakes: Modeling and Management*, IIASA Collaborative Proceedings Series, CP-81-S3, Laxenhurg, Austria.

Heath, R.T., 1992: Nutrient dynamics in Great Lakes coastal wetlands: Future directions, *Journal of Great Lakes Research*, **18**(4): 590-602.

Holdren, G.C., Jr. and D.E. Armstrong, 1980: Factors affecting phosphorus release from intact lake sediment cores, *Environmental Science & Technology*, **14**(1): 79-87.

Hooper, F.F., 1972: Origin and fate of organic phosphorus compounds in aquatic systems. in (E.J. Griffith, A. Beeton, J.M. Spencer, and D.T. Mitchell, eds.), *Environmental Phosphorus Handbook*, John Wiley & Sons, New York, pp. 179-201.

Horikawa, K. and A. Watanahe, 1968: Laboratory study on oscillatory boundary layer flow. *Coastal Engineering Japan*, **8:** 85-103.

Horne, A.J., 1978: Nitrogen fixation in eutrophic lakes, in (R. Mitchell, ed.), *Water Pollution Microbiology*, **2:**, John Wiley & Sons, New York, pp. 1-30.

Howarth, R.W. and J. Cole, 1985: Molybdenum availability, nitrogen limitation, and phytoplankton growth in natural waters, *Science*, **229:** 653-656.

Hsiao, S.V. and O.H. Shemdin, 1980: Interaction of ocean waves with a soft bottom, *J. Phys. Oceanogr.*, **10:** 605-610.

Huher, W.C., P.L. Brezonik, J.P. Heaney, R.E. Dickinson, S.D. Preston, D.S. Dwornikand, and M.A. DeMaio, 1982: A classification of Florida lakes, Publication No. 72, Florida Water Resources Research Center, University of Florida, Gainesville.

Huher, W.C. and R.E. Dickinson, 1991: Modeling of phosphorus dynamics in Lake Okeechohee, Florida, in (C. Maksimovic, ed.), *New Technologies in Urban Drainage, UDT '91*, Elsevier Applied Science, London and New York, pp. 203-215.

Hunt, J. R, 1982: Self-similar particle-size distributions during coagulations: theory and experimental verification, *J. Fluid Mechanics* **122:** 169–185.

Hwang, K. N., 1989: Erodibility of fine sediment in wave-dominated environments, M.S. Thesis, University of Florida, Gainesville.

Hwang, K.-N., and A. J. Mehta, 1989: Fine sediment erodibility in Lake Okeechohee, Florida. UFL/COEL-89/019, Coastal and Oceanographic Engineering Department, University of Florida, Gainesville.

HydroQual, 1987: A steady-state coupled hydrodynamic/water quality model of eutrophication and anoxia process in Chesapeake Bay, T.R. 40 under EPA Contract No. 68-03-3319, Princeton, NJ, August 31.

Ikeda, S. and N. Adachi, 1978: A dynamic water quality model of Lake Biwa, *Ecological Modelling*, **4:** 151-172.

Ishikawa, M. and H. Nishimura, 1989: Mathematical model of phosphorus release rate from sediments considering the effect of dissolved oxygen in overlying water, *Water Research*, **23**(3):351-359.

Jackson, G.A. and S.E. Lochmann, 1992: Effect of coagulation on nutrient and light limitation of an algal bloom, *Limnology and Oceanography*, **37**(1): 77-89.

Jaffe, P.R., 1988: Tropical eutrophic lake modeling and parameter discrimination, *Water Resources Bulletin*, **24**(3): 585-592.

Jansson, M., 1988: Phosphate uptake and utilization by bacteria and algae, *Hydrobiologia*, **170:** 177-189.

Jensen, H.S. and F.O. Andersen, 1992: Importance of temperature, nitrate, and pH for phosphorus release from aerobic sediments of four shallow eutrophic lakes, *Limnology and Oceanography*, **37**(3): 577-589.

Johansson, J.O.R. and A.P. Squires, 1989: Surface sediments and their relationship to water quality in Hillsborough Bay, a highly impacted subdivision of Tampa Bay, Florida, in (E. D. Estevez, ed.), *Tampa and Sarasota Bays: Issues, Resources, Status, and Management*, Proc. Seminar, NOAA Estuary-of-the Month, Seminar Ser. No. 11. NOAA Estuarine Programs Office, Washington, DC, pp. 129-143.

Johnson, B.H., K.W. Kim, Y.P. Sheng, and R.E. Heath, 1989. Development of a three-dimensional hydrodynamic model of Chesapeake Bay, in (M.L. Spaulding, ed.), *Estuarine and Coastal Modelling*, ASCE, Newport, RI, pp. 162-171.

Jonsson, I.G., 1966: Wave boundary layers and friction factors, *Proc. 10th Int. Conf. Coastal Eng.*, Tokyo, pp. 127-148.

Jonsson, I.G. and N.A. Carlsen, 1976: Experimental and theoretical investigations in an oscillatory turbulent boundary layer, *J. Hydraulic Res.*. **14:** 45-60.

Jørgensen, S.E., 1976: A eutrophication model for a lake, *Ecological Modelling*, **2:** 147-165.

Jørgensen, S.E., 1981: Model for Lake Glumsø Sø, Denmark, in (A.E. Biswas, ed.), *Models for Water Quality Management*, McGraw-Hill, New York.

Jørgensen, S.E., 1983a: Modeling the ecological processes, in (G.T. Orlob, ed.), *Mathematical Modeling of Water Quality: Streams, Lakes and Reservoirs*, John Wiley and Sons, New York, pp. 116-149.

Jørgensen, S.E., 1983b: Ecological modeling of lakes, in (G.T. Orlob, ed.), *Mathematical Modeling of Water Quality: Streams, Lakes and Reservoirs*, John Wiley and Sons, New York, pp. 337-394.

Jørgensen, S.E., 1983c: Modeling the distribution and effect of toxic substances in rivers and lakes. in (G.T. Orlob, ed.), *Mathematical Modeling of Water Quality: Streams, Lakes and Reservoirs*, John Wiley and Sons, New York, pp. 395-424.

Jørgensen, S.E., 1989: Volatilization, in (S.E. Jørgensen and M.J. Gromiec, eds.), *Mathematical Submodels in Water Quality Systems*, Elsevier Science Publishing Company Inc., New York, pp. 19-32.

Jørgensen, S.E. and Gromiec (eds.), 1989: *Mathematical Submodels in Water Quality Systems*, Elsevier Science Publishing Company Inc., New York.

Kajiura, K, 1968: A model of the bottom boundary layer in water waves, *Bull. Earthquake Res. Inst.* **46**: 75–123.

Kamphuis, J.W., 1975: Fiction factors under oscillatory waves, *J. Waterway Harbours Coastal Enginerring Division, ASCE*, **101**: 135-144.

Keesman, K. and G. van Straten, 1990: Set membership approach to identification and prediction of lake eutrophication, *Water Resources Research*, **26**(11): 2643-2652.

Kemp, W.M., R.L. Wetzel, W.R. Boynton, C.F. D'Elia, and J.C. Stevenson, 1982: Nitrogen cycling and estuarine interfaces: some current concept and research directions, in (V.S. Kennedy, ed.), *Estuarine Comparisons*, Academic Press, New York, pp. 209-230.

Kent, R. E., and D. W. Pritchard, 1959: A test of mixing length theories in a coastal plains estuary, *J. Mar. Res.*, **18**: 62–72.

Kirhy, R. and Parker, W. R., 1984: Distribution and behavior of fine sediment in the Severn Estuary and Inner Bristol Channel, UK, *Can. J. Fish. Aquat. Sci.*, hf 40(suppl. 1): 83-95.

Kishi, M., 1986: Population dynamics of 'red tide' organisms in eutrophicated coastal waters – Numerical experiment of phytoplankton bloom in the East Seto Inland Sea, Japan, *Ecological Modelling*, **31**: 145-174.

Kjerfve, B. and J.A. Proehl, 1979: Velocity variability in a cross section of a well-mixed estuary, *J. Mar. Res.*, **37**: 409-418.

Krone, R.B, 1962: Flume studies of the transport of sediment in estuarial shoaling processes, Final Report, Hydraulic Engineering Laboratory and Sanitary Engineering Research Laboratory, University of California, Berkeley.

Krone, R.B, 1993: Sediment revisited, in (A.J. Mehta, ed.), *Coastal and Estuarine Studies 42: Nearshore and Estuarine Cohesive Sediment Transport.* American Geophysical Union, Washington, DC, pp. 108-125.

Lam, D.C.L. and J.M. Jaquet, 1976: Computations of physical transport and regeneration of phosphorus in Lake Erie, fall 1970. *J. Fish. Res. Bd. Can.*, **33**: 550-563.

Lam, D.C.L., W.M. Schertzer, and A.S. Fraser, 1983: Simulation of Lake Erie water quality responses to loading and weather variations, *I. W.D. Scientific Series*, **134**, Environment Canada, Ottawa, 299p.

Lang, G., R. Schuhert, M. Markofsky, H.-U. Fanger, I. Grahemann, H. L. Krasemann, L. J. R. Neumann, and R. Riethmüller, 1989: Data interpretation and numerical modeling of the mud and suspended sediment experiment 1985, *J. Geophys. Res.* **94**: 381–393.

Lassiter, R.R. and DK. Kearns, 1974: Phytoplankton population changes and nutrient flucuIations in a simple aquatic ecosystem model, in (E.J. Middlebrooks, D.H. Falkenberg, and T.E. Maloney, eds.), *Modeling the Eutrophication Process*, Ann Arbor Science, Ann Arbor, MI, pp. 131-138.

Lavelle, J. W., H. O. Mofjeld, and E. T. Baker, 1984: An *in situ* erosion rate for a fine-grained marine sediment, NOAA/ERL PMEL Contribution No. 654, National Oceanic and Atmospheric Administration, Washington, DC.

Lee, H.-K., 1993: Wind-driven circulation in Lake Okeechobee, Florida: The effect of thermal stratification and aquatic vegetation, Ph.D. Dissertation, University of Florida, Gainesville.

Leenderste, J. J., and S.-K. Liu, 1975: A three-dimensional model for estuaries and coastal seas, Vol. II: Aspects of computation, The RAND Corporation Report R-1764-OWRT, 123p.

Lehfeldt, R. and S. Bloß, 1988: Algebraic turbulence model for stratified tidal flows, in (J. Dronkers and W. van Leussen, eds.), *Physical Processes in Estuaries*, Springer-Verlag, Berlin, pp. 278-291.

Le Hir, P., P. Bassoullet and J. L'Yavance, 1993: Applications of a multivariate transport model for understanding cohesive sediment dynamics, in (A.J. Mehta, ed.), *Coastal and Estuarine Studies 42: Nearshore and Estuarine Cohesive Sediment Transport.* American Geophysical Union, Washington, DC, pp. 467-485.

Lewellen, W. S., 1977: Use of invariant modeling, in (W. Frost, ed.), *Handbook of Turbulence*, Vol. 1, Plenum Publishing Corp., New York, pp. 237-280.

Lewis, R.R., III and E. Estevez, 1988: Ecology of Tampa Bay, Florida, an estaurine profile, U.S. Department of Interior Fish and Wildlife Service, National Wetland Research Center, Washington, DC.

Maa, P.-Y., 1986: Erosion of soft muds by waves, Ph.D. Dissertation, University of Florida, Gainesville.

Maa, P.-Y. and A.J. Mehta, 1988: Soft mud properties: Voigt model, *J. Wtrway., Port, Coast., Oc. Engrg.*, **114**(6): 765-770.

Mallard, W.W. and R.A. Dalrymple, 1977: Water waves propagating over a deformable bottom, *Proc. 9th Offshore Tech. Conf.*, OTC 2895, pp. 141-146.

Markofshy, M., G. Lang, and R. Schubert, 1986: Numerische Simulation des Schwebstofftransport auf der Basis der Messkapagne MESEX '83, *Die Kuenste*, **44:** 171-189.

Martin, J.H., 1968: Phytoplankton-zooplankton relationships in Narragansett Bay. III. Seasonal chances in zooplankton excretion rates in relation to phytoplankton abundance, *Limnology and Oceanography*, **13:** 63-71.

McClelland, S., 1984: Draft Tampa Bay 205 (j) Water quality impact study, Bureau of Water Analysis, Florida Dept. of Envirnonmental Regulation, Tallahassee.

McElroy, M.B., J.W. Elkins, S.C. Wofsy, C.E. Kolh, A.P. Duran, and W.A. Kaplan, 1978: Production and release of N_2O from the Potomac Estuary, *Limnology and Oceanography*, **23**(6): 1168-1182.

McPherson, H., 1980: The attenuation of water waves over a non-rigid bed, *J. Fluid Mechanics* **97**: 721–742.

Mei, C.C. and K.F. Liu, 1987: A Bingham-plastic model for a muddy seabed under long waves, *J. Geophys. Res.*, **92**(C13): 14,581-14,594.

Mellor, G. L. and T. Yamada, 1982: Development of a turbulence closure model for geophysical fluid problems, *Reviews of Geophysics and Space Physics* **20**: 851-875.

Mesinger, F., and A. Arakawa, 1976: Numerical methods used in atmospheric models, GARP publications ser., No. 17, 64p.

Mimura, N., 1993: Rates of erosion and deposition of cohesive sediments under wave action, in (A.J. Mehta, ed.), *Coastal and Estuarine Studies 42: Nearshore and Estuarine Cohesive Sediment Transport*, American Geophysical Union, Washington, DC, pp. 247-264.

Monod, J., 1949: The growth of bacterial cultures, *Ann. Rev. Microbiol.*, **371**, 1949.

Munk, W. H. and E. R. Anderson, 1948: Notes on a theory of the thermocline, *J. Mar. Res.* **7**: 276–295.

Nakajiura, M., 1983: Nutrient cycle in eutrophic waters–processes on sediments and gas exchange, Ph.D. Thesis, University of Tokyo.

Nalewajko, C., K. Leeand, and H. Shear, 1981: Phosphorus kinetics in Lake Superior: Light intensity and phosphate uptake in algae, *Can. J. Fish. Aquat. Sci.*, **38**: 224-232.

NEDECO, 1965: *A Study of the Siltation of the Bangkok Port Channel, Vol II, The Fiels Investigation*, Netherlands Engineering Consultants, The Hague, Holland, 474p.

Nezu, I. and W. Rodi, 1986: Open-channel flow measurements with a laser Doppler anemometer, *J. Hydraul. Eng.*, **112**(5): 335-355.

OECD, 1982: Eutrophication of waters. Monitoring, assessment and control, Paris

Olila, O.G. and K.R. Reddy, 1993: Influence of pH on phosphorus sorption in Lake Okeechohee, Unpublished manuscript, Soil and Water Science Department, University of Florida, Gainesville.

Onishi, Y., H.C. Graher, and D.S. Trent, 1993: Preliminary modeling of wave-enhanced sediment and comtaminant transport in New Bedford Harbor, in

(A.J. Mehta, ed.), *Coastal and Estuarine Studies 42: Nearshore and Estuarine Cohesive Sediment Transport.* American Geophysical Union, Washington, DC, pp. 126-147.

Owen, M.W., 1970: A detailed study of the settling velocities of an estuary mud, *Hydraulics Res. Rep.*, No. INT 78.

Palmer, S.L. and S.I. McClelland, 1988: Tampa Bay water quality assessment (205(j) water quality study), Florida Department of Environmental Regulation, Water Quality Technical Series, Vol. 3, No. 17, Tallahassee.

Parchure, T. M, 1984: Erosional behavior of deposited cohesive sediments, Ph.D. dissertation, University of Florida, Gainesville.

Parchure, T. M. and A. J. Mehta, 1985: Erosion of soft cohesive sediment deposits, *J. Hyd. Engineering*, **111**: 1308–1326.

Partheniades, E, 1962: A study of erosion and deposition of cohesive soils in salt water, Ph.D. Dissertation, University of California, Berkeley.

Pomeroy, L.R., E.E. Smith, and C.M. Grant, 1965: The exchange of phosphorus between estuarine water and sediments, *Limnology and Oceanography*, **10:** 167-172.

Pritchard, D.W., 1956: The dynamic structure of a coastal plain estuary, *J. Mar. Res.*, **15:** 33-42.

Puls, W. and H. Kuehl, 1986: Field measurements of the settling velocities of estuarine flocs, in (S.Y. Wang, H.W. Shen, and L.Z. Ding, eds.), *Proc. Int. Symp. on River Sedimentation*, School of Engineering, Univ. of Mississippi, Oxford, pp. 525-536.

Puls, W., H. Kuehl, and K.Heymann, 1986: Settling velocity mud flocs: Results of field measurements in the Elbe and the Weser estuary, *Proc. Int. Symp. Physical Processes in Estuaries*, Springer-Verlag, Berlin.

Rao, P.S.C., R.E. Jessup and K.R. Reddy, 1984: Simulation of nitrogen dynamics in flooded soil, *Soil Science*, **138:** 54-62.

Reddy, K.R. and D.A. Graetz, 1981: Use of shallow reservoirs and flooded soil systems for waste water treatment: nitrogen and phosphorus transformations, *J. Environ. Qual.,* **10:** 113-120.

Reddy, K.R. and D.A. Graetz, 1989: Lake okeechobee phosphorus dynamics study: Biogeochemical processes in sediments, Semi-Annual Reports to the South Florida Water Management District, Soil Science Dept., University of Florida, Gainesville.

Reddy, K.R., R.E. Jessup, and P.S.C. Rao, 1988: Nitrogen dynamics in a eutrophic lake sediment, *Hydrobiologia*, **159**: 177-188.

Reddy, K.R. and W.H. Patrick, 1984: Nitrogen transformation and loss in flooded soil and sediments, *CRC Critical Reviews in Environmental Control*, **13**(4), 273-309.

Reddy, K.R., W.H. Patrick, and R.E. Phillips, 1978: The role of nitrate diffusion in determining the order and rate of denitrification in flooded soil. 1. Experimental results, *Soil Sci. Soc. Am. J.*, **42**(2): 268-272.

Reddy, K.R., P.S.C. Rao, and R.E. Jessup, 1990: Transformation and transport of ammonium nitrogen in a flooded soil, *Ecological Modelling*, **51**: 205-216.

Riebesell, U., 1991: Particle aggregation during a diatom bloom. 1. Physical aspects. 2. Biological aspects, *Marine Ecol. Prog. Ser.* **69**: 273-280, 281-291.

Riley, M.J. and H.G. Stefan, 1988: MINLAKE: A dynamic lake water quality simulation model, *Ecological Modelling*, **43**: 155-182.

Rodi, W, 1980: *Turbulence Models and Their Application in Hydraulics*, International Association of Hydraulic Research, Delft, The Netherlands.

Ross, M. A., 1988: Vertical structure of estuarine fine sediment suspension, Ph.D. Dissertation, University of Florida, Gainesville.

Ross, M. A. and A. J. Mehta, 1989: On the mechanics of lutoclines and fluid mud, *J. of Coastal Res.*, Special Issue **5**: 51–61.

Roache, P. J, 1982: *Computational Fluid Dynamics*, Hermosa Publishers, Albuquerque, NM. 446p.

Sakai, T, H. Mase, D.T. Cox, and Y. Ueda, 1992: Field observation of wave-induced transient porewater pressure in seabed, *Proc. of 23th International Conference on Coastal Engineering.*, Venice, Italy, Oct.

Salas, H.S. and R.V. Thoman, 1978: The Chesapeake Bay waste load allocation study, Hydroscience, Inc. for the Maryland Dept. of Natural Resources Administration, Annapolis, MD.

Schelske, C.L., 1989: Assessment of nutrient effects and nutrient limitation in Lake Okeechobee, *Water Resources Bulltin*, **25**(6): 1119-1130.

Schnoor, J.L. and D.J. O'Connor, 1980: A steady state eutrophication model for lakes, *Water Research*, **14**: 1651-1665.

Schoellhamer, D.H., 1993: Simulation and analysis of sediment resuspension observed in Old Tampa Bay, Ph.D. Dissertation, University of Florida, Gainesville.

Seitzinger, S.P., 1988: Denitrification in freshwater and coastal marine ecosystems: Ecological and geochemical significance, *Limnology and Oceanography*, **33**(4): 702-724.

Sheng, Y. P., 1982: Hydraulic applications of a second-order closure model of turbulent transport, in (P. Smith, ed.), *Proceedings 1982 ASCE Hydraulic Division Specialty Conference on Applying Research to Hydraulic Practice*, American Society of Civil Engineers, Jackson, MS, pp. 106-119.

Sheng, Y. P., 1983: Mathematical modeling of three-dimensional coastal currents and sediment dispersion: Model development and application, Coastal Engineering Research Center Technical Report CERC-TR-83-2 DACW39-80-C-0087, Vicksburg, MS.

Sheng, Y. P., 1984: A turbulent transport model of coastal processes, in *Proceedings 19th International Conference on Coastal Engineering*, American Society of Civil Engineers, Houston, TX, pp. 2380-2396.

Sheng, Y. P., 1985: A new one-dimensional ocean current model. Tech. Rep. No. 566, Aeronautical Research Associates of Princeton, Princeton, NJ.

Sheng, Y. P., 1986: Modeling bottom boundary layers and cohesive sediment dynamics, in (A. J. Mehta, ed.), *Estuarine Cohesive Sediment Dynamics*, Springer-Verlag, Berlin, pp. 360-400.

Sheng, Y. P., 1989: Predicting the dispersion and fate of contaminated marine sediments. in *Contaminated Marine Sediments – Assessment and Remediation*, Marine Board, National Research Council, National Academy Press, Washington, DC, pp. 166-177.

Sheng, Y.P., 1993: Hydrodynamics, sediment transport and their effects on phosphorus dynamics in Lake Okeechobee, in (A.J. Mehta, ed.), *Coastal and Estuarine Studies 42: Nearshore and Estuarine Cohesive Sediment Transport*, American Geophysical Union, Washington, DC, pp. 558-571.

Sheng, Y. P., and H. L. Butler, 1982: A three-dimensional numerical model of coastal, estuarine, and lake currents, in *Proc. 1982 Army Num. Anal. and Comp. Conf.*, U. S. Army Research Office Report No. 82–3, Washington, DC, pp. 531–574.

Sheng, Y. P. and X. J. Chen, 1992: A three-dimensional numerical model of hydrodynamics, sediment transport and phosphorus dynamics in Lake Okeechobee: theory, model development, and documentation, Spring 1989, Final report to the South Florida Water Management District, Coastal and Oceanographic Engineering Department, University of Florida, Gainesville.

Sheng, Y.P., X.-J. Chen, S. Schofield, and E. Yassuda, 1993a: Hydrodynamics and sediment and phosphorus dynamics in Lake Okeechobee during an episodic event, Technical Report, Coastal & Oceanographic Engineering Department, University of Florida, Gainesville.

Sheng, Y.P., X.-J. Chen, E. Yassuda, K.R. Reddy and M.M. Fisher, 1993b: Quantifying sediment resuspension flux of nutrients and contaminants in estuaries due to episodic events, Technical Report, Coastal & Oceanographic Engineering Department, University of Florida, Gainesville.

Sheng, Y. P., J. K. Choi, and A. Y. Kuo, 1989d: Three-dimensional numerical modeling of tidal circulation and salinity transport in James River Estuary, in (M. L. Spaulding, ed.), *Estuarine and Coastal Modeling*, ASCE, Newport, RI, pp. 200-208.

Sheng, Y.P., and S.S. Chiu, 1986: Tropical cyclone generated currents, in *Proc. of the 20th International Conference on Coastal Engineering*, ASCE, Capetown, South Aferica, pp. 737-751.

Sheng, Y. P., V. Cook, S. Peene, D. Eliason, P. F. Wang, and S. Schofield, 1989b: A field and modeling study of fine sediment transport in shallow waters, in (M. L. Spaulding, ed.), *Estuarine and Coastal Modeling*, ASCE, Newport, RI, pp. 113-122.

Sheng, Y. P., D. E. Eliason, J.-K. Choi, X. J. Chen, and H.-K. Lee, 1991: Numerical simulation of three-dimensional wind-driven circulation and sediment transport in Lake Okeechohee during Spring 1989, Final report to the South Florida Water Management District, Coastal and Oceanographic Engineering Dept., University of Florida, Gainesville.

Sheng, Y. P., H. K. Lee, and K. H. Wang, 1989c: On numerical strategies of estuarine and coastal modeling, in (M. L. Spaulding, ed.), *Estuarine and Coastal Modeling*, ASCE, Newport, RI, pp. 291-301.

Sheng, Y. P., and W. Lick, 1979: The transport and resuspension of sediments in a shallow lake, *J. Geophys. Res.* **84**: 1809–1826.

Sheng, Y. P., W. Lick, R. T. Gedney, and F. Molls, 1978: Numerical computation of three-dimensional circulation in Lake Erie: A comparison of a free-surface model and a rigid-lid model, *J. Phys. Oceanogr.* **8**: 713–727.

Sheng, Y. P., S. Peene, D. Eliason, and V. Cook. 1990: Wind- induced resuspension of sediments in shallow water. ICCE Paper 1, presented at the 22nd International Conference on Coastal Engineering, Delft, The Netherlands.

Sheng, Y. P., S. Schofield, S. Peene, V. Cook, K. M. Ahn, J. Capitao, P. F. Wang, J. K. Choi, D. Mueller, C. Broward, J. Joiner, and V. Sparkman, 1989a: Hydrodynamics, sediment transport, and their effects on phosphorus dynamics in Lake Okeechobee, Annual Report to South Florida Water Management District, UFL/COEL Report 89-021, Coastal and Oceanographic Engineering Dept., University of Florida, Gainesville.

Sheng, Y. P., and C. Villaret, 1989: Modeling the effect of suspended sediment stratification on bottom exchange processes, *J. Geophys. Res.* **94**: 14429–1444.

Simon, N.S., 1988: Nitrogen cycling between sediment and the shallow-water column in the transition zone of the Potomac River and Estuary. I. Nitrate and ammonium fluxes, *Estuarine, Coastal and Shelf Science*, **26**: 483-497.

Simon, N.S., 1989: Nitrogen cycling between sediment and the shallow-water column in the transition zone of the Potomac River and Estuary, II. The role of wind-driven resuspension and adsobed ammonium, *Estuarine, Coastal and Shelf Science*, **28**: 531-547.

Simons, T. J, 1974: Verification of numerical models of Lake Ontario. Part 1: Circulation in spring, early summer, *J. Phys. Oceanogr.* **4**: 507-523.

Sleath, J.F.A., 1991: Velocities and shear stresses in wave-current flows, *Journal of Geophysical Research*, **96**(C8): 15237-15244.

Smoluchowski, M. von, 1918: Versuch einer mathematischen Theorie der Koajulationskinetik kolloider Lösungen, *Zeitschrift für Physikalische Chemie*, **92**: 129–168.

Somlyody, L., 1983: Major features of the Lake Balaton eutrophication problem: Approach to the analysis, in (L. Somlyody, S. Herodek, and J. Fischer, eds.), *Eutrophication of Shallow Lakes: Modeling and Management*, IIASA Collaborative Proceedings Series, CP-81-S3, Laxenburg, Austria.

Spaulding, M.L., D.P. French, and H. Rines, 1989: A review of Tampa Bay water quality model system, Applied Science Associates, Inc., Narragansett, RI.

Spencer, C.N. and D.L. King, 1989: Role of light, carbon dioxide and nitrogen in regulation of buoyancy, growth and bloom formation of anabaena flos-aquae, *Journal of Plankton Research*, **11**(2): 283-296.

Srinath, E.G. R.C. Loehr, and T.B.S. Prakasam, 1976: Nitrifying organism concentration and activity, *J. Environ. Eng. Div., ASCE*, **102**: 449-463.

Stanford, G., R.A. VanderPol, and S. Dzienia, 1975: Denitrification rates in relation to total and extractable soil carbon, *Soil Sci. Soc. Am. Proc.*, **39**(2): 284-289.

Steele, J.A., 1974: *The Structure of Marine Ecosystem,* Blackwell, Oxford.

Stratton, E.E and McCarty, P.L., 1969: Discussion to paper by Werzernak and Gannon, Evaluation of nitrification in stream, *Journal of the Sanitary Engineering Division, ASCE*, **95**: 952–955.

Streeter H.W. and E.B. Phelps, 1925: A study of the pollution and natural purification of the Ohio River, III. Factors concerned in the phenomena oxidation and reaeration, US Public Health Service, Washington, DC Bulletin, **146**, 75p.

Takamura, N and M. Yasuno, 1988: Sedimentation of phytoplankton populations dominated by microcystis in a shallow lake, *Journal of Plankton Research*, **10**(2): 283-299.

Tee, K.T., 1976: Tide-induced residual current, A 2-D nonlinear, numerical model, *J. Mar. Res.*, **34:** 603-628.

Thompson, L.M., C.A. Black, and J.A. Zoellner, 1954: Occurrence and mineralization of organic phosphorus in soil with particular reference to association with nitrogen, carbon, and pH, *Soil Sci.*, **77:** 185-196

Thorn, M. F. C., 1981: Physical processes of siltation in tidal channels, in *Proceedings of Hydraulic Modeling Applications to Marine Engineering Problems*, ICE, London, pp. 47-55.

Toorman, E.A. and J.E. Berlamont, 1993: Mathematical modeling of cohesive sediment settling and consolidation, in (A.J. Mehta, ed.), *Coastal and Estuarine*

Studies 42: Nearshore and Estuarine Cohesive Sediment Transport, American Geophysical Union, Washington, DC, pp. 167-184.

Toetz, D. and B. Cole, 1980: Ammonia mineralization and cycling in Chagawa Lake Minnesota, *Arch. Hydrobiol., 88(9)*.

Tsai, C.-H., S. Iacobellis and W. Lick, 1987: The flocculation of fine-grained lake sediments due to a uniform shear stress, *J. Great Lakes Res.* **13**: 135–146.

Tzang, S.Y., J.R. Hunt, and M.A. Foda, 1992: Resuspension of seabed sediments by water waves, *Proc. of 23th International Conference on Coastal Engineering.*, Venice, Italy, Oct.

U. S. Army Coastal Engineering Research Center, 1984: Shore protection manual, Vol. 1. Coastal Engineering Research Center, Department of the Army, Waterways Experiment Station, Corps of Engineers, Vickshurg, MS.

Valiela, Ivan, 1984: *Marine Ecological Processes*, Springer Advanced Texts in Life Science, Springer-Verlag, New York.

van Benschoten, J.E. and W.W. Walker, 1984: Calibration and application of Qual-II to the lower Winooski River, *Water Resources Bulletin*, **20**(1): 109-117.

van Leussen, W. and J.M. Cornelisse, 1993: The role of large aggregates in estuarine fine-grained sediment dynamics, in (A.J. Mehta, ed.), *Coastal and Estuarine Studies 42: Nearshore and Estuarine Cohesive Sediment Transport*. American Geophysical Union, Washington, DC, pp. 75-91.

Villaret, C. and M. Paulic, 1986: Experiments on the erosion of deposited and and placed cohesive sediments in an annular flume and a rocking flume, UFL/COEL-86/007, Coastal and Oceanographic Engineering Dept., University of Florida, Gainesville.

Virtanen, M., J. Koponen, K. Dahlbo, and J. Sarkkula, 1986: Three-dimensional water-quality-transport model compared with field observations, *Ecological Modelling*, **31**: 185-199.

Voinov A.A. and A.A. Akhremenkov, 1990: Simulation modeling system for aquatic bodies, *Ecological Modelling*, **52**: 181-205.

Watanabe, C.T., Ishiguro, M, and Nisaidome, K., 1980: Nitrification kinetics in a rotating biological disk reactor, *Progress in Water Technology*, **12**: 233–251.

Weber, W.J., Jr., and K.T. Liu, 1980: Determination of mass transport parameters of fixed bed adsorbers, *Chem. Eng. Comm.*, **6**: 49-60.

Witkowski, P.J. and P.R. Jaffe, 1987: Kinetic and equlibrium formulations in modelling of hydrophobic organic chemicals in surface and ground waters, in (M.B. Beck, ed.), *System Analysis in Water Quality Management*, Advances in Water Pollution Control – A Series of Conferences Sponsored hy IAW-PRC, Pergamon Press, Oxford, England, pp. 333-338.

Wlosinski, J. and C.D. Collins, 1985: Evaluation of a water quality model (CE-QUAL-R1) using data from a small Wisconsin reservoir, *Ecological Modelling*, **29**: 303-313.

Wolanski, E., T. Aseda, and J. Imberger, 1989: Mixing across a lutocline, *Limnology and Oceanography*, **31**: 931–938.

Wolanski, E., J. Chappell, P. Ridd and R. Vertessy, 1988: Fluidization of mud in estuaries, *J. Geophys. Res.*, **93**: 2351-2362.

Wu, S-C and P.M. Gschwend, 1988: Numerical modeling of sorption kinetics of organic compounds to soil and sediment particles, *Water Resources Research*, **24**(8): 1373-1383.

Zalesak, S. T., 1979: Fully multi-dimensional flux-corrected transport algorithms for fluids, *J. Comp. Phys.* **31**: 375.

APPENDIX A
COMPUTING PRESSURE GRADIENTS FROM CURRENT DATA

If measured data of currents at two water depths are available, the horizontal pressure gradient $\frac{\partial p}{\partial x}$ and $\frac{\partial p}{\partial y}$ at these two depths can be computed through the following procedure (only x-direction is presented here, and the same procedure can also be applied to y-direction):

$$\begin{aligned} -\frac{1}{\rho}\left(\frac{\partial p}{\partial x}\right)_1^{n+1} &= \frac{u_{k1}^{n+1}-u_{k1}^{n}}{\Delta t} \\ &- \frac{1}{\Delta z_{k1}}\left(A_{v_{k1}}\frac{u_{k1+1}^{n+1}-u_{k1}^{n+1}}{\Delta z_{k1_t}} - A_{v_{k1-1}}\frac{u_{k1}^{n+1}-u_{k1-1}^{n+1}}{\Delta z_{k1_b}}\right) \end{aligned} \tag{A.1}$$

$$\begin{aligned} -\frac{1}{\rho}\left(\frac{\partial p}{\partial x}\right)_2^{n+1} &= \frac{u_{k2}^{n+1}-u_{k2}^{n}}{\Delta t} \\ &- \frac{1}{\Delta z_{k2}}\left(A_{v_{k2}}\frac{u_{k2+1}^{n+1}-u_{k2}^{n+1}}{\Delta z_{k2_t}} - A_{v_{k2-1}}\frac{u_{k2}^{n+1}-u_{k2-1}^{n+1}}{\Delta z_{k2_b}}\right) \end{aligned} \tag{A.2}$$

wherein, u, v are velocities, A_v is the vertical eddy diffusivity, Δz is the grid spacing, p is the pressure, n is the time step number, $k1$ and $k2$ are indexes of the two water depths where measurements were made, and Δz_{k_t} and Δz_{k_b} are:

$$\begin{aligned} \Delta z_{k_t} &= \frac{\Delta z_{k+1}+\Delta z_k}{2} \\ \Delta z_{k_b} &= \frac{\Delta z_k+\Delta z_{k-1}}{2} \end{aligned}$$

Once the pressure gradients at the two depths are known, $\frac{\partial p}{\partial x}$ over the entire water column can be estimated as follows:

$$\begin{aligned} \frac{\partial p}{\partial x} &= \left(\frac{\partial p}{\partial x}\right)_1 , & k \le k1 \\ \frac{\partial p}{\partial x} &= \left(\frac{\partial p}{\partial x}\right)_2 , & k \ge k2 \\ \frac{\partial p}{\partial x} &= a_1\left(\frac{\partial p}{\partial x}\right)_1 + a_2\left(\frac{\partial p}{\partial x}\right)_2 , & k1 \le k \le k2 \end{aligned}$$

where

$$\begin{aligned} a_1 &= \frac{z - z_2}{z_2 - z_1}, \\ a_2 &= 1. - a_1, \end{aligned}$$

and z, z_1, and z_2 are the vertical coordinates of cells $k1, k2$, and k, respectively.

Finally, the difference equations of the 1-D model take the following form:

for $k \leq k1$:

$$\begin{aligned} \frac{u_k^{n+1} - u_k^n}{\Delta t} &= \frac{u_{k1}^{n+1} - u_{k1}^n}{\Delta t} \\ &- \frac{1}{\Delta z_{k1}} \left(A_{v_{k1}} \frac{u_{k1+1}^{n+1} - u_{k1}^{n+1}}{\Delta z_{k1_t}} - A_{v_{k1-1}} \frac{u_{k1}^{n+1} - u_{k1-1}^{n+1}}{\Delta z_{k1_b}} \right) \\ &+ \frac{1}{\Delta z_k} \left(A_{v_k} \frac{u_{k+1}^{n+1} - u_k^{n+1}}{\Delta z_{k_t}} - A_{v_{k-1}} \frac{u_k^{n+1} - u_{k-1}^{n+1}}{\Delta z_{k_b}} \right) \end{aligned} \tag{A.3}$$

for $k \geq k2$:

$$\begin{aligned} \frac{u_k^{n+1} - u_k^n}{\Delta t} &= \frac{u_{k2}^{n+1} - u_{k2}^n}{\Delta t} \\ &- \frac{1}{\Delta z_{k2}} \left(A_{v_{k2}} \frac{u_{k2+1}^{n+1} - u_{k2}^{n+1}}{\Delta z_{k2_t}} - A_{v_{k2-1}} \frac{u_{k2}^{n+1} - u_{k2-1}^{n+1}}{\Delta z_{k2_b}} \right) \\ &+ \frac{1}{\Delta z_k} \left(A_{v_k} \frac{u_{k+1}^{n+1} - u_k^{n+1}}{\Delta z_{k_t}} - A_{v_{k-1}} \frac{u_k^{n+1} - u_{k-1}^{n+1}}{\Delta z_{k_b}} \right) \end{aligned} \tag{A.4}$$

for $k1 \leq k \leq k2$:

$$\begin{aligned} \frac{u_k^{n+1} - u_k^n}{\Delta t} &= a_1 \frac{u_{k1}^{n+1} - u_{k2}^n}{\Delta t} a_2 \frac{u_{k2}^{n+1} - u_{k2}^n}{\Delta t} \\ &- \frac{a_1}{\Delta z_{k1}} \left(A_{v_{k1}} \frac{u_{k1+1}^{n+1} - u_{k1}^{n+1}}{\Delta z_{k1_t}} - A_{v_{k1-1}} \frac{u_{k1}^{n+1} - u_{k1-1}^{n+1}}{\Delta z_{k1_b}} \right) \\ &- \frac{a_2}{\Delta z_{k2}} \left(A_{v_{k2}} \frac{u_{k2+1}^{n+1} - u_{k2}^{n+1}}{\Delta z_{k2_t}} - A_{v_{k2-1}} \frac{u_{k2}^{n+1} - u_{k2-1}^{n+1}}{\Delta z_{k2_b}} \right) \\ &+ \frac{1}{\Delta z_k} \left(A_{v_k} \frac{u_{k+1}^{n+1} - u_k^{n+1}}{\Delta z_{k_t}} - A_{v_{k-1}} \frac{u_k^{n+1} - u_{k-1}^{n+1}}{\Delta z_{k_b}} \right) \end{aligned} \tag{A.5}$$

The above difference equations result in a full matrix. Gaussian Elimination Method was used to inverse the matrix.

APPENDIX B
FLOW CHARTS OF THE 3-D MODEL SYSTEM

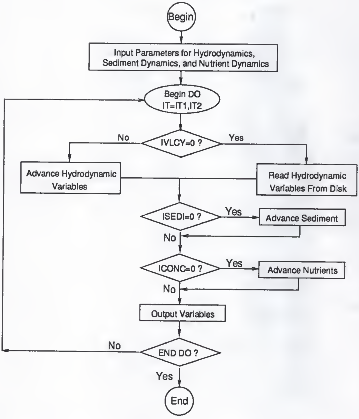
Begin
Input Parameters for Hydrodynamics, Sediment Dynamics, and Nutrient Dynamics
Begin DO IT=IT1,IT2
No
IVLCY=0 ?
Yes
Advance Hydrodynamic Variables
Read Hydrodynamic Variables From Disk
ISEDI=0 ?
Yes
Advance Sediment
No
ICONC=0 ?
Yes
Advance Nutrients
No
Output Variables
No
END DO ?
Yes
End

Figure B.1: Flow chart of the 3-D model system of hydrodynamics, sediment transport, and nutrient dynamics in lakes and estuaries.

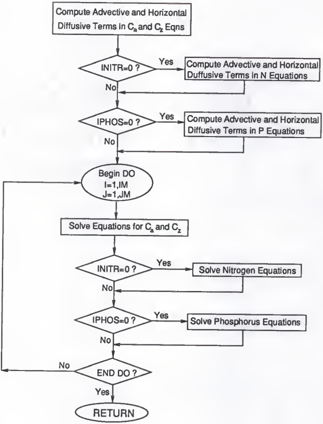
Compute Advective and Horizontal Diffusive Terms in C_a and C_z Eqns
INITR=0 ?
Yes
Compute Advective and Horizontal Duffusive Terms in N Equations
No
IPHOS=0 ?
Yes
Compute Advective and Horizontal Diffusive Terms in P Equations
No
Begin DO I=1,IM J=1,JM
Solve Equations for C_a and C_z
INITR=0 ?
Yes
Solve Nitrogen Equations
No
IPHOS=0 ?
Yes
Solve Phosphorus Equations
No
No
END DO ?
Yes
RETURN

Figure B.2: Flow chart of the 3-D submodel for nutrient dynamics.

APPENDIX C
NUMERICAL SOLUTION ALGORITHMS IN HYDRODYNAMIC AND SEDIMENT TRANSPORT MODELS

C.1 3-D Hydrodynamics Model

Because the computational requirements of three-dimensional, time-dependent, free-surface hydrodynamics models can be intense, the numerical solution algorithm must be designed for efficient computation. To properly resolve the dynamic response of water bodies such as lakes and estuaries to forcing by wind, the classical three-dimensional, free-surface model (e.g., Leenderste and Liu, 1975) requires exceedingly small time-steps (on the order of 10 seconds). As mentioned in Section 3.1, separation of the computation into an internal mode (the three-dimensional velocities), which is governed by slower dynamics, and an external mode (surface elevation and vertically integrated velocities), which is governed by fast surface gravity waves, results in a more efficient three-dimensional model (e.g., Simons, 1974; Sheng *et al.*, 1978). The separation of internal mode and the external model is physically allowed because the dynamics of the internal mode are slower than those of the external mode. Internal mode computations allow the three-dimensional flow field to be advanced to the present time-step by using the results from the external mode computations.

For external computation, an alternating direction implicit (ADI) method can further increase the efficiency of the model (Sheng and Butler, 1982). The basic idea of the ADI method is to compute first in one direction (e.g. x-direction) and then in the other direction (e.g. y-direction). At the next time step, the computation order in the two directions is switched (first y-direction and then x-direction).

The external mode solves the vertically integrated forms of the governing equations of hydrodynamics (in dimensionless forms):

$$\frac{\partial \zeta}{\partial t} + \beta \left(\frac{\partial U}{\partial x} + \frac{\partial V}{\partial y} \right) = 0 \tag{C.1}$$

$$\begin{aligned}
\frac{\partial U}{\partial t} = & - H\frac{\partial \zeta}{\partial x} + \tau_{sx} - \tau_{bx} + V \\
& - \left[\frac{\partial}{\partial x}\left(\frac{UU}{H}\right) + \frac{\partial}{\partial y}\left(\frac{UV}{H}\right) \right] \\
& + \left[\frac{\partial}{\partial x}\left(A_H \frac{\partial U}{\partial x}\right) + \frac{\partial}{\partial y}\left(A_H \frac{\partial U}{\partial y}\right) \right] \\
& - \frac{Ro}{{Fr_D}^2}\frac{H^2}{2}\frac{\partial \rho}{\partial x} \\
\equiv & - H\frac{\partial \zeta}{\partial x} + D_x
\end{aligned} \tag{C.2}$$

$$\begin{aligned}
\frac{\partial V}{\partial t} = & - H\frac{\partial \zeta}{\partial y} + \tau_{sy} - \tau_{by} - U \\
& - Ro\left[\frac{\partial}{\partial x}\left(\frac{UV}{H}\right) + \frac{\partial}{\partial y}\left(\frac{VV}{H}\right) \right] \\
& + E_H\left[\frac{\partial}{\partial x}\left(A_H \frac{\partial V}{\partial x}\right) + \frac{\partial}{\partial y}\left(A_H \frac{\partial V}{\partial y}\right) \right] \\
& - \frac{Ro}{{Fr_D}^2}\frac{H^2}{2}\frac{\partial \rho}{\partial y} \\
\equiv & - H\frac{\partial \zeta}{\partial y} + D_y
\end{aligned} \tag{C.3}$$

where U and V are the vertically integrated velocities, ζ is the water surface displacement, $\zeta = gD/L^2f^2$ (D and L are reference length scales in vertical and horizontal directions, respectively), H is the water depth, and Ro, E_H, and Fr_D are Rossby number, horizontal Ekman number, ad Froude number, respectively (Sheng, 1983). the nonlinear inertia, lateral diffusion, and baroclinic pressure gradient terms in Equations (C.3) and (C.4) are obtained by vertically integrating the corresponding terms in Equations (4.3) and (4.4), respectively. However, these terms contain assumptions about the vertical profiles of horizontal velocities and density and are not exact, i.e., the horizontal velocities and density are assumed to be uniform in the vertical direction.

Once U and V of the external mode are computed, the internal mode can be proceeded. Defining perturbation velocities as $\tilde{u} = u - \overline{u}$ and $\tilde{v} = v - \overline{v}$, where $\bar{u}$ and $\overline{v}$ represent the vertically-averaged velocities, the differential equations for the internal mode are obtained by subtracting the vertically averaged momentum equations from the three-dimensional momentum equations multiplied by H:

$$\frac{1}{H}\frac{\partial H\tilde{u}}{\partial t} = B_x - \frac{D_x}{H} + \frac{E_v}{H^2}\frac{\partial}{\partial \sigma}\left[A_v \frac{\partial}{\partial \sigma}(\overline{u} + \tilde{u})\right] \tag{C.4}$$

$$\frac{1}{H}\frac{\partial H\tilde{v}}{\partial t} = B_y - \frac{D_y}{H} + \frac{E_v}{H^2}\frac{\partial}{\partial \sigma}\left[A_v \frac{\partial}{\partial \sigma}(\overline{v} + \tilde{v})\right] \tag{C.5}$$

It is also important to ensure that the vertically integrated perturbation velocities always equal zero such that the internal computations are consistent with the external computations:

$$\sum_{k=1}^{k_{max}} \tilde{u}_{i,j,k} = 0 \tag{C.6}$$

$$\sum_{k=1}^{k_{max}} \tilde{v}_{i,j,k} = 0 \tag{C.7}$$

Once $\tilde{u}^{n+1}$ and $\tilde{v}^{n+1}$ are obtained, u and v can be obtained at the present $(n+1)$ time-level from:

$$u^{n+1} = \tilde{u}^{n+1} + U^{n+1}/H^{n+1} \tag{C.8}$$

$$v^{n+1} = \tilde{v}^{n+1} + V^{n+1}/H^{n+1} \tag{C.9}$$

and the vertical velocity is computed from the continuity equation. More about the algorithm of the three-dimensional model can be found in Sheng and Chen (1992).

C.2 1-D Hydrodynamics Model

Compared to the three-dimensional model, the algorithm in the one-dimensional model is relatively simple. Except for the eddy viscosity and the bottom shear stress, all the other tems are treated implicitly in the difference equation. The final difference equations for u and v have the common form as follows:

$$A_1(k)g_{k-1}^{n+1} + A_2(k)g_k^{n+1} + A_3(k)g_{k+1}^{n+1} = A_4(k) \qquad k = 1, ..., k_{max} \qquad \text{(C.10)}$$

where, g can be either u or v.

The Thomas Algorithm is used solve Equation (C.10). More details about the one-dimensional difference equations can be found in Sheng *et al.* (1993).

C.3 3-D Sediment Transport Model

In writing the finite difference equation for the three-dimensional sediment transport equation, only the vertical diffusion term was treated implicitly. All the other terms were written in the explicit forms. The final difference equation for sediment transport had the same form as that of Equation (C.10), in which $A_4(k)$ consists of advection terms and horizontal diffusion terms at time step n. The Thomas Algorithm is also used for inversing the matrix.

The finite-difference form used for the horizontal diffusion terms is the standard second-order divided difference:

$$\frac{\partial^2 c}{\partial x^2} = \frac{c_{i+1,j,k}^n - 2c_{i,j,k}^n + c_{i-1,j,k}^n}{(\Delta x)^2} \qquad \text{(C.11)}$$

There is no need to treat the horizontal diffusion terms implicitly because the time step constraint associated with them is usually much larger than that allowed by the advection terms.

As for advection terms, three options are available in the model code for treatment of the advection terms in the sediment transport model: (1) central difference (2) upwind difference, and (3) combined central and upwind difference (see Roache, 1982 for a discussion of central versus upwind differencing, and for descriptions of accuracy, dispersion, and diffusion of numerical schemes). The central difference option has the advantage of second-order accuracy, but a disadvantage of numerical dispersion. When a large concentration gradient exists in the model domain with insufficient grid points across the gradient, negative concentrations may sometimes develop in the simulation. The upwind difference option has the advantage of increased stability versus the central difference option, but at a cost of increased numerical diffusion. The upwind difference option guarantees positivity of suspended sediment concentrations. The combined central and upwind option gives the advantages of central and upwind options together, but minimizes the disadvantages. The combined option is, however, more computationally demanding. More about the treatment of the advection terms are reported elsewhere (e.g. Sheng, 1991).

To improve the accuracy of advective terms in the numerical model, it is possible to use higher order advective schemes which have formal truncation errors that are third order or fourth order in Δx. For example, Sheng (1983) applied the Flux-Corrected-Transport (FCT) scheme (Zalesak, 1979) to simulate the advection and diffusion of salinity and suspended sediments by wind-driven currents, and compared the performance of the FCT scheme versus the three advective schemes discussed above. The performance of the combined central upwind option was found to be quite comparable to that of the FCT scheme. Sheng *et al.* (1989d) found that, when a σ-grid model is used, higher-order advective scheme should be avoided in regions of sharp bathymetric gradient when insufficient grid points exist to resolve the sharp gradient.

C.4 Numerical Stability

Since the model does not use fully implicit numerical schemes, the time step of numerical computation cannot exceed the limits associated with the advection terms, the Coriolis terms, the baroclinic pressure gradient terms, and the horizontal diffusion terms:

$$\begin{aligned}
(\Delta t)_{\text{advection}} &\leq \frac{1}{\left(\frac{|u|}{\Delta x}\right)+\frac{|v|}{\Delta y}+\left(\frac{|w|}{\Delta z}\right)} \\
(\Delta t)_{\text{Coriolis}} &\leq 1/f \\
(\Delta t)_{\text{baroclinic}} &\leq \frac{1}{\sqrt{\frac{\Delta\rho}{\rho} g H_{max}} \left(\frac{1}{\Delta x}+\frac{1}{\Delta y}\right)_{max}} \\
(\Delta t)_{\text{diffusion}} &\leq \frac{1}{2A_H \left[\frac{1}{(\Delta x)^2}+\frac{1}{(\Delta y)^2}\right]_{max}}
\end{aligned} \tag{C.12}$$

If the allowable internal time step according to the above equations is much (10 to 100 times) larger than the Δt allowed by the surface gravity wave as shown in Equation (C.12), then it is feasible to use a small time step for the internal mode (Δt_i). We have used $\Delta t_i/\Delta t_e$ between 1 and 6, depending on the particular problems of interest. If the difference between the allowable internal time step is only a few factors larger than the external step, then it is better to simply use the same Δt_e and Δt_i. The selection of time step is still very much an "art" because all the time step limits are based on stability analysis which is strictly valid only in a linear system without considering the effects of nonlinearity and boundary conditions. Because of this, a variable time-step option is built in. The simulation starts with a fairly small step, which can grow if the evolution of the flow field is sufficiently small, but decreases if the evolution is too fast.

APPENDIX D
FIELD DATA OF 1989 SPRING SURVEY IN LAKE OKEECHOBEE

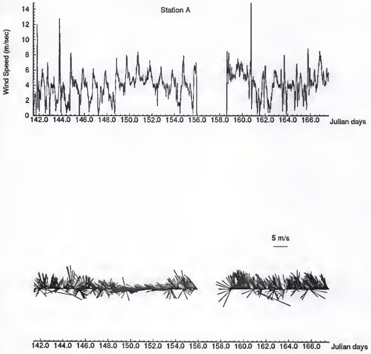

Figure D.1: Measured wind at Station A in Lake Okeechobee from May 21 to June 16, 1989.

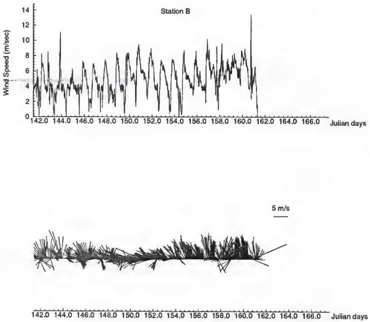

Figure D.2: Measured wind at Station B in Lake Okeechobee from May 21 to June 16, 1989.

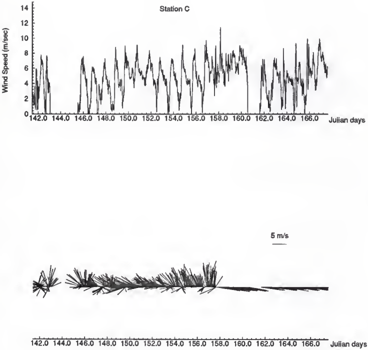

Figure D.3: Measured wind at Station C in Lake Okeechobee from May 21 to June 16, 1989.

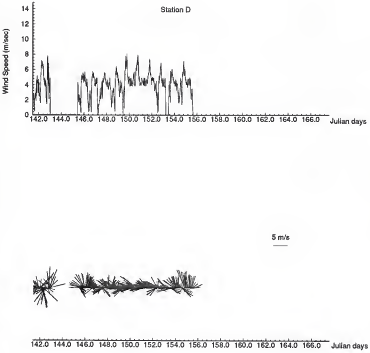

Figure D.4: Measured wind at Station D in Lake Okeechobee from May 21 to June 16, 1989.

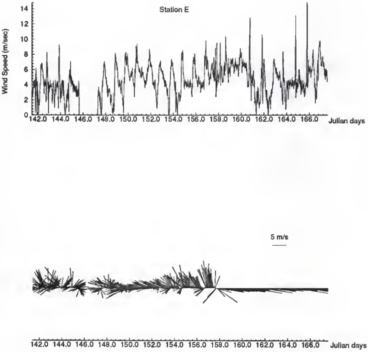

Figure D.5: Measured wind at Station E in Lake Okeechobee from May 21 to June 16, 1989.

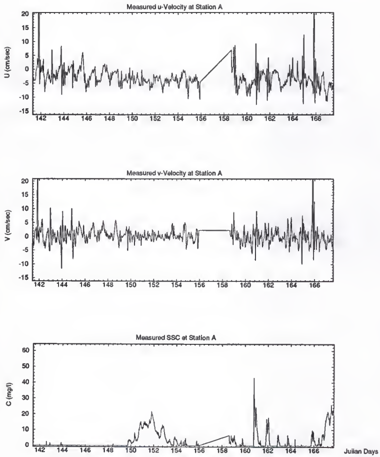

Figure D.6: Measured u-velocities, v-velocities, and suspended sediment concentrations at Station A from May 21 to June 16, 1989.

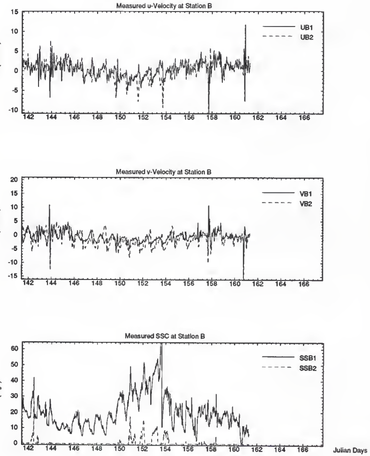

Figure D.7: Measured u-velocities, v-velocities, and suspended sediment concentrations at Station B from May 21 to June 16, 1989.

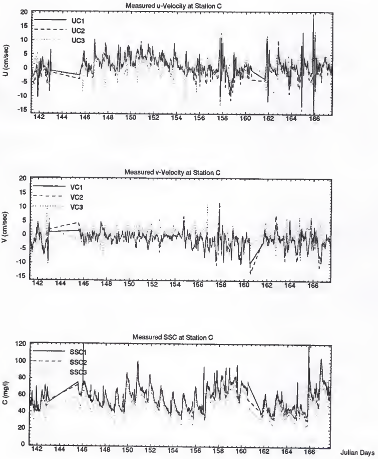

Figure D.8: Measured u-velocities, v-velocities, and suspended sediment concentrations at Station C from May 21 to June 16, 1989.

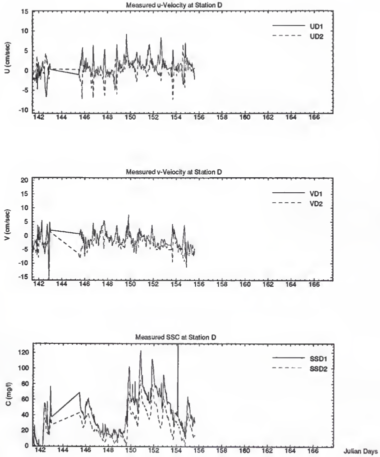

Figure D.9: Measured u-velocities, v-velocities, and suspended sediment concentrations at Station D from May 21 to June 16, 1989.

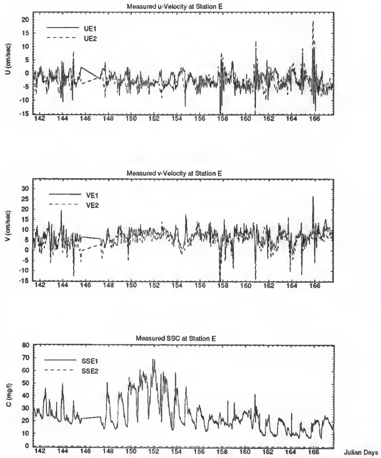

Figure D.10: Measured u-velocities, v-velocities, and suspended sediment concentrations at Station E from May 21 to June 16, 1989.

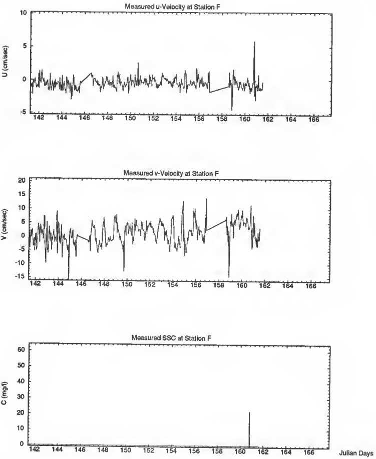

Figure D.11: Measured u-velocities, v-velocities, and suspended sediment concentrations at Station F from May 21 to June 16, 1989.

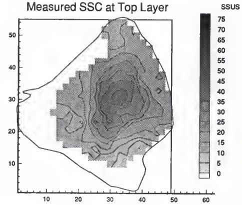

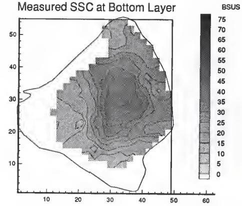

Figure D.12: Contours of synoptic data of suspended sediment concentrations at the top and the bottom layers of Lake Okeechobee at noon of May 21, 1989.

Measured SSC at Top Layer

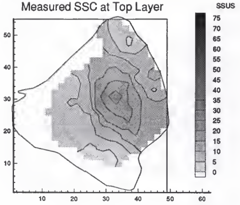

Measured SSC at Bottom Layer

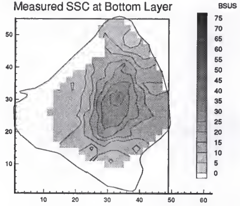

Figure D.13: Contours of synoptic data of suspended sediment concentrations at the top and the bottom layers of Lake Okeechobee at noon of May 27, 1989.

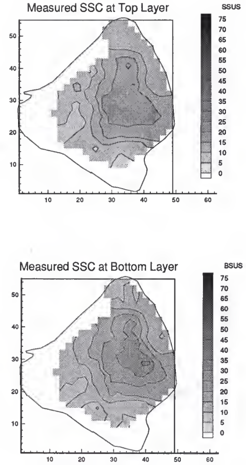

Figure D.14: Contours of synoptic data of suspended sediment concentrations at the top and the bottom layers of Lake Okeechobee at noon of June 3, 1989.

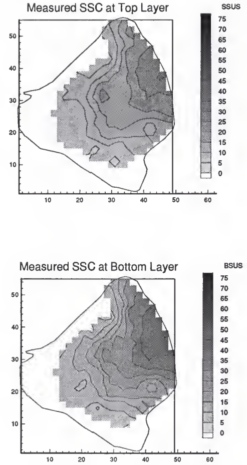

Figure D.15: Contours of synoptic data of suspended sediment concentrations at the top and the bottom layers of Lake Okeechobee at noon of June 10, 1989.

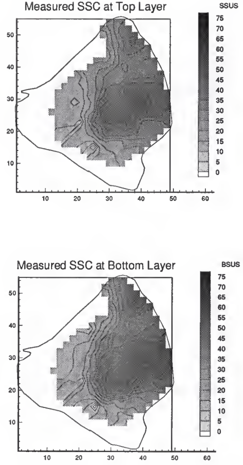

Figure D.16: Contours of synoptic data of suspended sediment concentrations at the top and the bottom layers of Lake Okeechobee at noon of June 16, 1989.

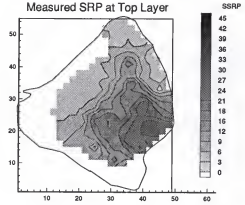

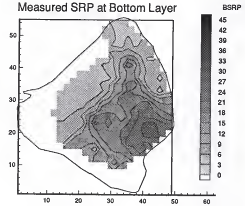

Figure D.17: Contours of synoptic data of SRP concentrations at the top and the bottom layers of Lake Okeechobee at noon of May 21, 1989.

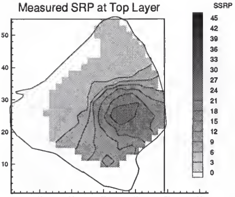

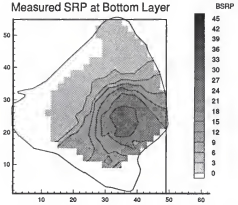

Figure D.18: Contours of synoptic data of SRP concentrations at the top and the bottom layers of Lake Okeechobee at noon of May 27, 1989.

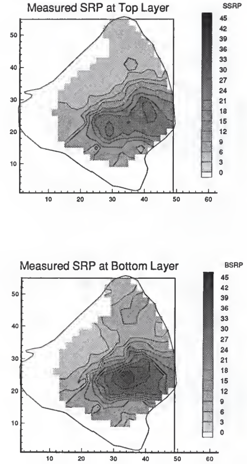

Figure D.19: Contours of synoptic data of SRP concentrations at the top and the bottom layers of Lake Okeechobee at noon of June 3, 1989.

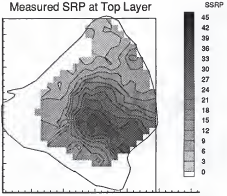

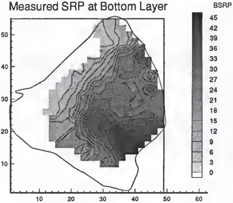

Figure D.20: Contours of synoptic data of SRP concentrations at the top and the bottom layers of Lake Okeechobee at noon of June 10, 1989.

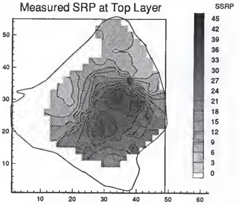

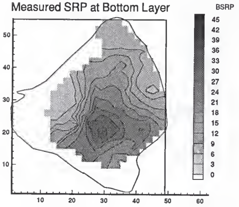

Figure D.21: Contours of synoptic data of SRP concentrations at the top and the bottom layers of Lake Okeechobee at noon of June 16, 1989.

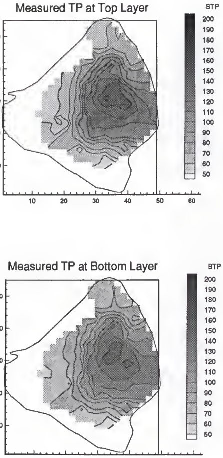

Figure D.22: Contours of synoptic data of TP concentrations at the top and the bottom layers of Lake Okeechobee at noon of May 21, 1989.

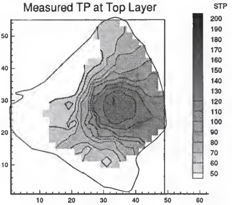

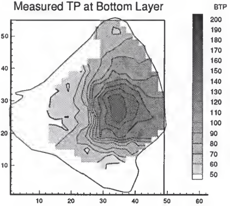

Figure D.23: Contours of synoptic data of TP concentrations at the top and the bottom layers of Lake Okeechobee at noon of May 27, 1989.

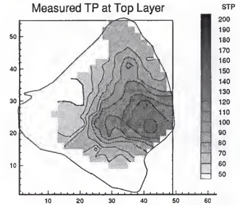

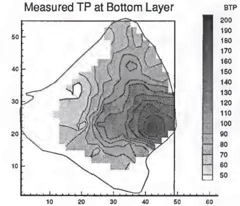

Figure D.24: Contours of synoptic data of TP concentrations at the top and the bottom layers of Lake Okeechobee at noon of June 3, 1989.

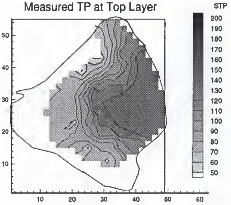

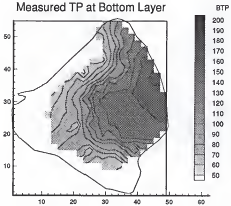

Figure D.25: Contours of synoptic data of TP concentrations at the top and the bottom layers of Lake Okeechobee at noon of June 10, 1989.

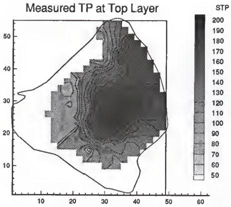

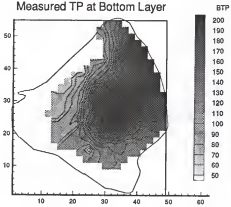

Figure D.26: Contours of synoptic data of TP concentrations at the top and the bottom layers of Lake Okeechobee at noon of June 16, 1989.

APPENDIX E
FIELD DATA OF 1993 SPRING STORM EVENT IN LAKE OKEECHOBEE

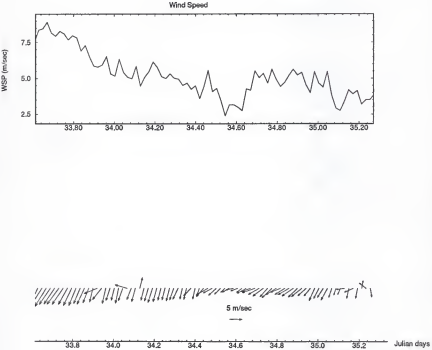

Figure E.1: Measured wind during a storm event at Station L002 in Lake Okeechobee in February, 1993.

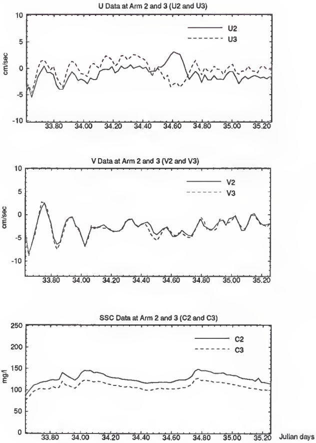

Figure E.2: Measured u-velocities, v-velocities, and suspended sediment concentrations at the middle and the bottom arms at Station L002 in Lake Okeechobee in February, 1993.

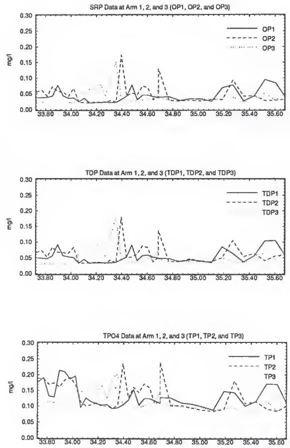

Figure E.3: Measured total phosphorus (TP), total dissolved phosphorus (TDP), and soluble reactive phosphorus (SRP) at Station L002 in Lake Okeechobee in February, 1993.

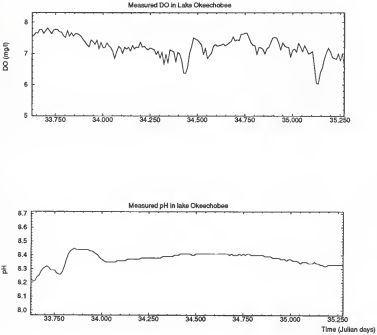

Figure E.4: Measured DO and pH at the bottom layer at Station L002 in Lake Okeechobee in February, 1993.

APPENDIX F
3 RUNS FOR 1993 SPRING STORM EVENT IN LAKE OKEECHOBEE

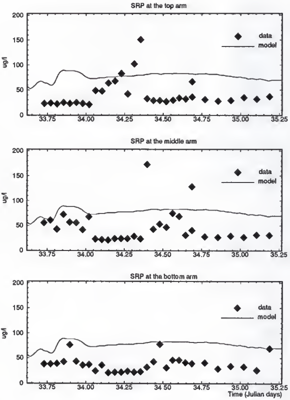

Figure F.1: Measured and simulated SRP of the first run at Station L002 in Lake Okeechobee during the storm event in February, 1993.

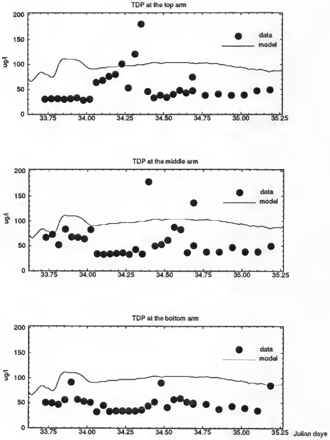

Figure F.2: Measured and simulated TDP of the first run at Station L002 in Lake Okeechobee during the storm event in February, 1993.

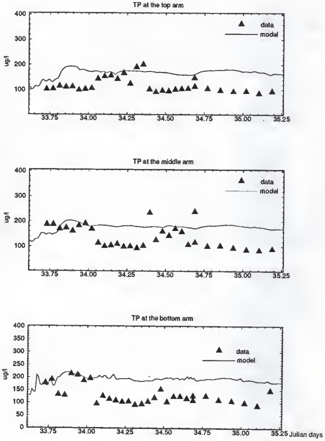

Figure F.3: Measured and simulated TP of the first run at Station L002 in Lake Okeechobee during the storm event in February, 1993.

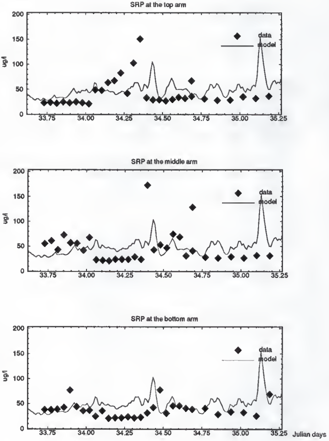

Figure F.4: Measured and simulated SRP of the second run at Station L002 in Lake Okeechobee during the storm event in February, 1993.

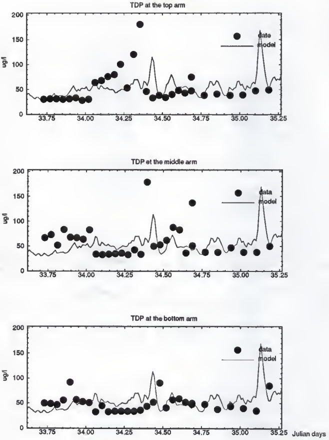

Figure F.5: Measured and simulated TDP of the second run at Station L002 in Lake Okeechobee during the storm event in February, 1993.

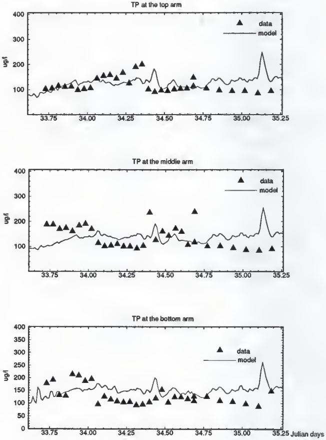

Figure F.6: Measured and simulated TP of the second run at Station L002 in Lake Okeechobee during the storm event in February, 1993.

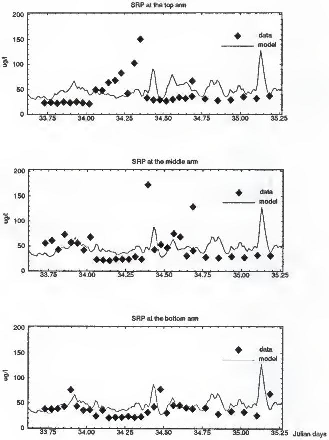

Figure F.7: Measured and simulated SRP of the third run at Station L002 in Lake Okeechobee during the storm event in February, 1993.

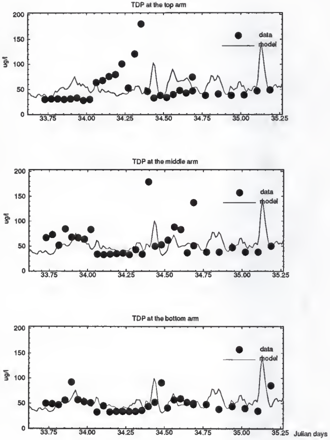
TDP at the top arm

TDP at the middle arm

TDP at the bottom arm

Figure F.8: Measured and simulated TDP of the third run at Station L002 in Lake Okeechobee during the storm event in February, 1993.

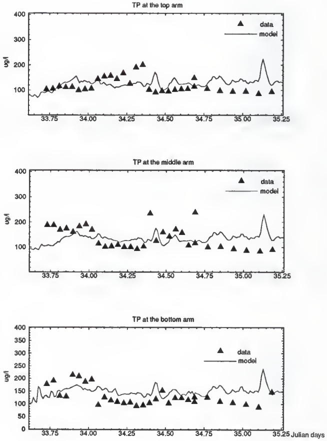

Figure F.9: Measured and simulated TP of the third run at Station L002 in Lake Okeechobee during the storm event in February, 1993.

APPENDIX G
FIELD DATA COLLECTED IN TAMPA BAY

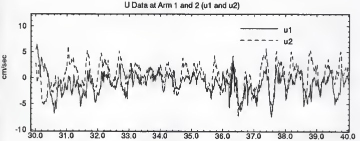

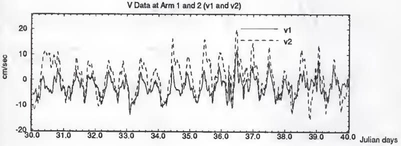

Figure G.1: Measured u-velocites and v-velocities at Station A in Tampa Bay during Julian days 30 to 40, 1992.

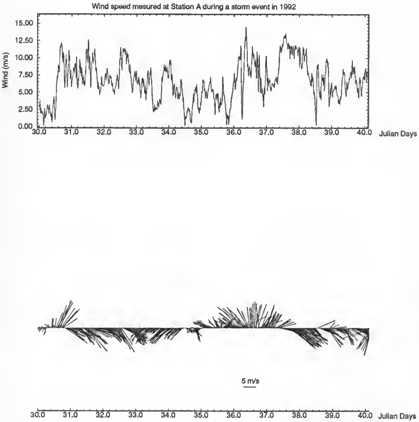

Figure G.2: Measured wind at Station A in Tampa Bay during Julian days 30 to 40, 1992.

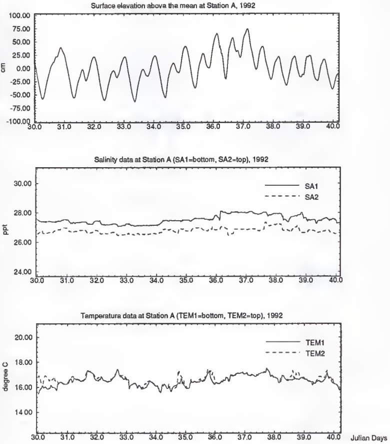

Figure G.3: Measured free surface variation about the mean water level, salinity, and temperature at Station A in Tampa Bay during Julian days 30 to 40, 1992.

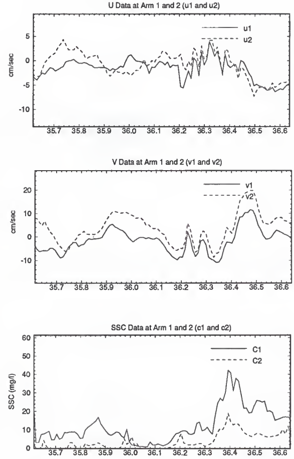
U Data at Arm 1 and 2 (u1 and u2)

V Data at Arm 1 and 2 (v1 and v2)

SSC Data at Arm 1 and 2 (c1 and c2)

Figure G.4: Measured u-velocity, v-velocity, and suspended sediment on the storm day at Station A of Tampa Bay during Julian day 35.6 to 36.6, 1992.

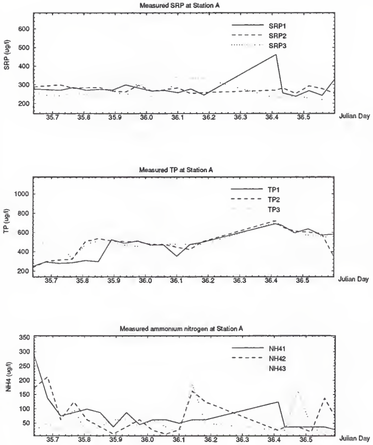

Figure G.5: Measured SRP, TP, and ammonium N concentrations at Station A in Tampa Bay during Julian days 35.6 to 36.6, 1992.

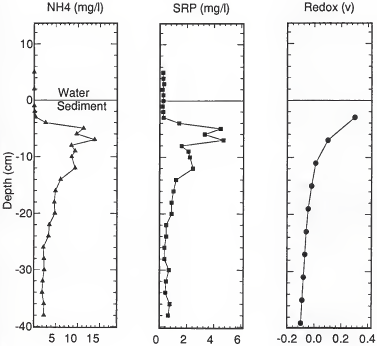

Figure G.6: Measured SRP, NH_4^+-N, and redox profiles in Tampa Bay.

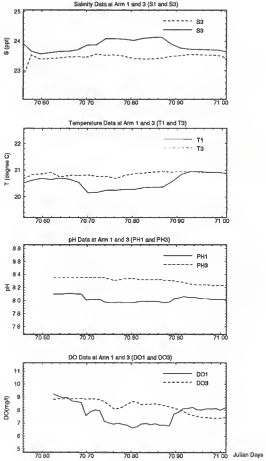

Figure G.7: Measured salinity, temperature, pH, and dissolved oxygen concentration at Station A in Tampa Bay during Julian days 70.59 to 71.1, 1993.

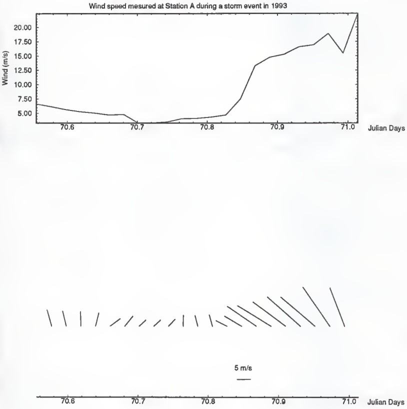

Figure G.8: Measured wind at Station A in Tampa Bay during Julian days 70.59 to 71.1, 1993.

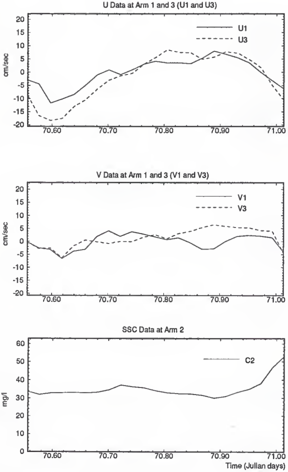

Figure G.9: Measured u-velocity, v-velocity, and suspended sediment concentration at Station A in Tampa Bay during Julian days 70.59 to 71.1, 1993.

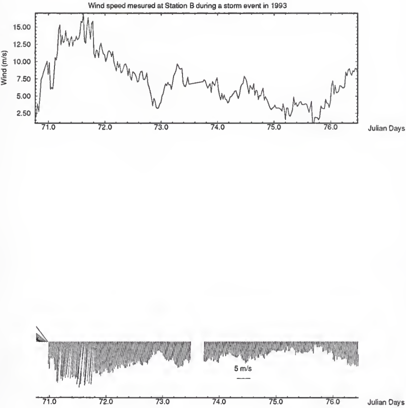

Figure G.10: Measured wind at Station A in Tampa Bay during Julian days 70.5 to 76.3, 1993.

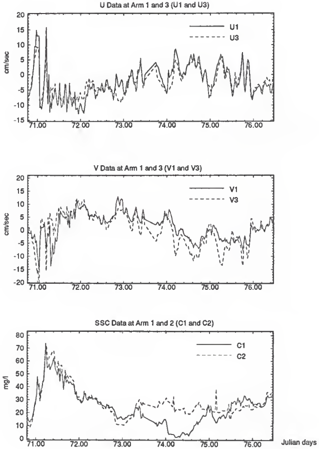

Figure G.11: Measured u-velocity, v-velocity, and suspended sediment concentration at Station B in Tampa Bay during Julian days 70.5 to 76.3, 1993.

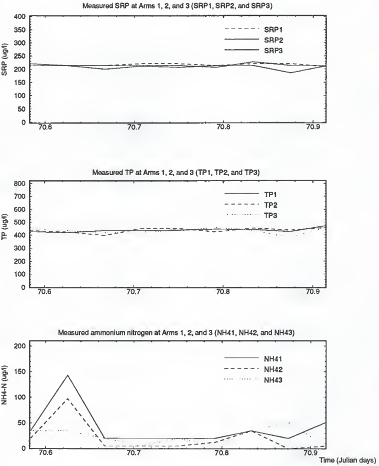

Figure G.12: Measured ammonium N and SRP concentrations at Station A in Tampa Bay during Julian days 70.5 to 71.1, 1993.

APPENDIX H
DETERMINING MODEL COEFFICIENTS

H.1 1-D Simulation of Lake Okeechohee Phosphorus Dynamics

After obtaining the best fit between the model results and the measured data by tuning the model coefficients, the 1-D phosphorus model was used to examine the sensitivities of SRP and TDP concentrations in the water column to various transformation processes in Lake Okeechobee. The model coefficient values which produce the best fit between model results and measured data (Figures 7.3 through 7.5) were used as baseline values and are shown in Table H.1. In each sensitivity model run, only one model coefficient was changed within a certain range. Results of these sensitivity runs are presented in terms of RMS (root-mean-square) errors between the measured SRP and TDP data and model results in Table H.1. The RMS errors are defined as followed:

$$r_s = \sqrt{\frac{1}{N_a N_t} \sum_{i=1}^{N_a} \sum_{j=1}^{N_t} \left(\frac{SRP_{ij}^d - SRP_{ij}^m}{SRP_{ij}^d} \right)^2} \tag{H.1}$$

$$r_d = \sqrt{\frac{1}{N_a N_t} \sum_{i=1}^{N_a} \sum_{j=1}^{N_t} \left(\frac{TDP_{ij}^d - TDP_{ij}^m}{TDP_{ij}^d} \right)^2} \tag{H.2}$$

where N_a is the number of the measurement arms, N_t is the number of SRP and TDP data, SRP_{ij}^d and SRP_{ij}^m are measured and simulated SRP's, respectively, at layer i and time step j, and TDP_{ij}^d and TDP_{ij}^m are measured and simulated SRP's, respectively, at layer i and time step j.

The p_{ip} and p_{op} values in Table H.1 are those at DO of $5.5 mg/l$. The RMS errors, r_s and r_d, are 0.382 and 0.357, respectively, for the baseline simulation shown in Figures 7.3 through 7.5. From Table H.1, it can be seen that the most sensitive

Table H.1: Results of some sensitivity tests for Lake Okeechobee phosphorus dynamics.

Model Parameter	Baseline Value	Range	Low Bound		Upper Bound	
			r_s	r_d	r_s	r_d
p_{ip} (l/mg)	2.2×10^{-7}	0.5–10.0×10^{-7}	2.164	1.495	0.759	0.692
p_{op} (l/mg)	1.0×10^{-6}	$0.1 - 10.0 \times 10^{-6}$	0.398	0.905	0.380	0.386
$\mu_{a_{max}}$ (day^{-1})	2.0	1.0–2.5	0.386	0.357	0.382	0.359
$\mu_{z_{max}}$ (day^{-1})	0.6	0.3–0.9	0.383	0.358	0.383	0.358
w_s^a (cm/sec)	0.0015	0.0001–0.0025	0.382	0.358	0.383	0.357
K_D (day^{-1})	0.5	0.1–1.0	0.381	0.358	0.386	0.357
H_p $(\mu g/l)$	20	5–40	0.381	0.360	0.384	0.357
H_a $(\mu g/l)$	1000.	500–1500	0.383	0.358	0.383	0.358
K_{as} (day^{-1})	0.3	0.01–0.5	0.382	0.358	0.383	0.357
K_{ax} (day^{-1})	0.2	0.01–0.5	0.382	0.358	0.384	0.357
K_{zs} (day^{-1})	0.2	0.01–0.5	0.383	0.358	0.383	0.358
K_{zx} (day^{-1})	0.2	0.01–0.5	0.383	0.358	0.383	0.358

model coefficients are the partition coefficients, p_{ip} and p_{op}. The maximum growth rate of algae, $\mu_{a_{max}}$, is the next most sensitive model coefficient.

H.2 3-D Simulation of Lake Okeechobee Phosphorus Dynamics

Model coefficients in the 3-D Lake Okeechobee simulations were first obtained from literature and the 1-D simulations of the 1993 storm event, and then tuned to fit the data of the second synoptic survey. The final values the 3-D simulations of Lake Okeechobee phosphorus dynamics are shown in Table H.2. The ranges within which the coefficients were tuned are also presented in this table.

H.3 1-D Simulation of Tampa Bay Nitrogen Dynamics

Model coefficients in the 1-D Tampa Bay nitrogen dynamics simulations were first obtained from literature, and then tuned to fit the data collected during the 1992 storm event. The final values used for the 1-D simulation of Tampa Bay nitrogen dynamics are shown in Table H.2, together with the ranges the coefficients were tuned.

Table H.2: Model coefficients used in the 3-D simulations of Lake Okeechobee phosphorus dynamics.

Model Parameter	Muddy Zone		Sandy Zone		Unit
	Value	Range	Value	Range	
p_{ip}	1.0×10^{-5}	0.5– 5.0×10^{-5}	6.0×10^{-6}	1.0–10.0×10^{-6}	l/mg
p_{op}	6.0×10^{-6}	1.0–10.0×10^{-6}	5.0×10^{-5}	0.3– 10.0×10^{-5}	l/mg
$\mu_{a_{max}}$	2.0	1.0 – 2.5	2.0	1.0 – 2.5	day^{-1}
$\mu_{z_{max}}$	0.5	0.3 – 0.9	0.5	0.3 – 0.9	day^{-1}
w_s^a	0.0005	0.0001–0.0015	0.0005	0.0001 – 0.0015	cm/sec
K_D	0.5	0.1 – 1.0	0.5	0.1 – 1.0	day^{-1}
H_p	10	5 – 30	10	5 – 30	$\mu g/l$
H_a	1000	600 – 1500	1000	600 – 1500	$\mu g/l$
K_{as}	0.2	0.01 - 0.5	0.2	0.01 – 0.5	day^{-1}
K_{ax}	0.05	0.01 - 0.2	0.05	0.01 – 0.2	day^{-1}
K_{zs}	0.3	0.05 - 0.5	0.3	0.05 – 0.5	day^{-1}
K_{zx}	0.05	0.01 - 0.2	0.05	0.01 – 0.2	day^{-1}

Table H.3: Model coefficients used in the 1-D simulations of Tampa Bay nitrogen dynamics.

Model Parameter	Final Value	Range	Unit
p_{an}	5.0×10^{-7}	2.0–10.0×10^{-7}	l/mg
p_{on}	1.0×10^{-5}	0.1 –3.0×10^{-5}	l/mg
p_{aa}	1.5	1.0 – 2.0	–
$\mu_{a_{max}}$	1.2	0.9 – 2.0	day^{-1}
$\mu_{z_{max}}$	0.95	0.4 – 1.2	day^{-1}
w_s^a	0.0005	0.0001 – 0.001	cm/sec
K_2	0.05	0.01 – 1.0	day^{-1}
K_3	0.05	0.01 – 1.0	day^{-1}
K_4	0.1	0.01 – 1.0	day^{-1}
v_{an}	48.0	1.0 – 100.	day^{-1}
h_v	45.0	30.0 – 50.0	–
H_n	50	10 – 200	$\mu g/l$
H_a	1000	600 – 1500	$\mu g/l$
K_{as}	0.2	0.05 - 1.0	day^{-1}
K_{ax}	0.2	0.05 - 1.0	day^{-1}
K_{zs}	0.2	0.05 - 1.0	day^{-1}
K_{zx}	0.2	0.05 - 1.0	day^{-1}

BIOGRAPHICAL SKETCH

The author was born on November 7, 1962, in Jiangsu, China. He spent his childhood in Wuxi, a beautiful city near Taihu (lake of the greatest – actually it is not even the biggest lake in China and it has almost the same size and average water depth as those of Lake Okeechobee). In 1978, he left his hometown for college in Nanjing (Southern Capital). He entered the East China University of Water Resources (now Hohai University), which is well-known for its programs in hydroelectrical engineering and water resources. He received his B.S. degree in hydroelectrical engineering in July 1982, and his M.S. degree in civil engineering in June 1985 from the East China University of Water Resources. Right after obtaining his M.S. degree, the author was offered a teaching/research assistant position at the same university. In 1986, he was awarded a scholarship to study at the Institute of Fluid Mechanics of the University of Hannover, West Germany. At an international conference held in Hamburg, Germany, he met Professor Y.P. Sheng of the University of Florida. Impressed by Dr. Sheng's research activities in numerical modeling of hydrodynamics and sediment transport in estuaries and lakes, he came to the United States to joined Professor Sheng's group in June 1990.

The author wishes to use his knowledge obtained at the University of Florida to help his hometown to preserve water qualities in Taihu.

I certify that I have read this study and that in my opinion it conforms to acceptable standards of scholarly presentation and is fully adequate, in scope and quality, as a dissertation for the degree of Doctor of Philosophy.

Y. Peter Sheng, Chairman
Professor of Coastal and Oceanographic
Engineering

I certify that I have read this study and that in my opinion it conforms to acceptable standards of scholarly presentation and is fully adequate, in scope and quality, as a dissertation for the degree of Doctor of Philosophy.

Ashish J. Mehta

Ashish J. Mehta
Professor of Coastal and Oceanographic
Engineering

I certify that I have read this study and that in my opinion it conforms to acceptable standards of scholarly presentation and is fully adequate, in scope and quality, as a dissertation for the degree of Doctor of Philosophy.

D. Max Sheppard

D. Max Sheppard
Professor of Coastal and Oceanographic
Engineering

I certify that I have read this study and that in my opinion it conforms to acceptable standards of scholarly presentation and is fully adequate, in scope and quality, as a dissertation for the degree of Doctor of Philosophy.

Robert J. Thieke
Assistant Professor of Coastal and
Oceanographic Engineering

I certify that I have read this study and that in my opinion it conforms to acceptable standards of scholarly presentation and is fully adequate, in scope and quality, as a dissertation for the degree of Doctor of Philosophy.

K. Ramesh Reddy
Graduate Research Professor of Soil and
Water Science

This dissertation was submitted to the Graduate Faculty of the College of Engineering and to the Graduate School and was accepted as partial fulfillment of the requirements for the degree of Doctor of Philosophy.

April, 1994

Winfred M. Phillips
Dean, College of Engineering

Karen A. Holbrook
Dean, Graduate School

LD
1780
1994
.C51891

UNIVERSITY OF FLORIDA
3 1262 08554 8884